Francisco de Castro Sobral

Licenciado

Towards the development of a 3D cell model to study interactions between glioma cells and microglia

Dissertação para obtenção do Grau de Mestre em

Bioquímica para a Saúde

Orientador: Giacomo Domenici, PhD, Investigador, IBET e ITQB-NOVA

Coorientadora: Catarina Brito, PhD, Investigadora Principal, IBET e ITQB-NOVA

Fevereiro, 2023

Francisco de Castro Sobral

Licenciado

Towards the development of a 3D cell model to study interactions between glioma cells and microglia

Dissertação para obtenção do Grau de Mestre em

Bioquímica para a Saúde

Orientador: Giacomo Domenici, PhD, Investigador, IBET e ITQB-NOVA

Coorientadora: Catarina Brito, PhD, Investigadora Principal, IBET, ITQB-NOVA

Júri:

Presidente: Prof. Doutor Pedro Manuel Henriques Marques Matias

Arguente: Doutora Flávia Raquel Teixeira de Castro

Vogal: Prof. Doutor Ana Maria de Jesus Bispo Varela Coelho

Instituto de Tecnologia Química e Biológica António Xavier,

Universidade NOVA de Lisboa

Fevereiro, 2023

Towards the development of a 3D cell model to study interactions between glioma cells and microglia

Acknowledgments

Neste ano turbulento, e no alcanço de uma nova etapa, há inúmeras pessoas a quem devo agradecer por este sucesso. Tive um grande desenvolvimento intra/inter-pessoal, ganhei imensa experiência e foi um dos acontecimentos que sem dúvida marcou-me.

Ao meu orientador Giacomo Domenici, uma pessoa brilhante, que tanto me ensinou e apoiou nesta etapa. Muito do que sei hoje sobre a minha área de estudo se deve a si. Pude contar consigo, não só como supervisor, mas também como amigo.

À minha co-orientadora, Catarina Brito, uma cientista brilhante e compreensiva. Esteve sempre disponível para qualquer questão, dúvida ou dificuldade. Apesar de ser uma pessoa exigente, não deixa ter um coração enorme, e isso sobressaiu-se durante toda a tese.

Queira também agradecer à professora Paula Alves e ao professor Manuel Carrondo, sem dúvida que as aulas inspiradoras que lecionaram na disciplina de biofármacos me incentivaram a escolher o iBET para fazer a tese de mestrado.

Aos meus colegas do Advanced Cell Model Group, que tiveram, sem dúvida um impacto no meu percurso académico. Ao meu colega Gonçalo, uma pessoa impecável, independentemente da situação esteve sempre disponível para ajudar. Desejo a melhor sorte para o teu doutoramento. À Catarina Gomes, não só por ter disponibilizado a microglia derivada de hiPSCs, mas também nas imunofluorescências, agradeço imenso por todo o apoio que deste nesta tese. To Isabella, one of the nicest people I met at iBET, for helping me in confocal imaging, as well as listening to me in the most difficult moments. You are a very intelligent girl and I wish you all the best in your PhD. Um obrigado à Inês Correia, por seres uma pessoa descontraída e fácil de falar. Apesar de teres chegado relativamente há pouco tempo, apoiaste-me nos momentos mais chatos da tese. À Francisca, obrigada por toda a ajuda nos momentos mais desesperantes da tese, especialmente quando estava mais stressado e desmotivado. Ao Nuno Lopes, uma pessoa super descontraída e sempre disponível para ajudar, por me fazeres sentir incluído no grupo. À Gabriela Silva, uma pessoa com quem aprendi imenso e sempre ajudou nos troubleshootings quando não conseguia arranjar uma solução. À Sofia, por todas as suas críticas construtivas. E por fim, à Inês Sá, uma rapariga super simpática, desejo-te a melhor sorte na tua tese de mestrado, e poderás sempre contar com a minha ajuda.

Ao José Escandell e à Filipa pela presença nos 3D meetings, o vosso feedback foi sem dúvida crucial para este trabalho.

A todas as pessoas da unidade de tecnologia de células animais, pela vossa simpatia e boa vontade.

Ao meu amigo Francis, uma pessoa espetacular e genuína. Apesar de nos últimos anos não termos convivido muito, sei que pude sempre contar contigo. Sempre te mostraste interessado e preocupado comigo. És das poucas pessoas em quem eu realmente confio. Obrigado por tudo.

Um grande agradecimento à minha família, que teve um peso considerável nesta minha etapa. À minha mãe, por estar sempre disponível para ajudar, apoiar e dar carinho. Ao meu pai, obrigada por todo apoio que me deste, e por estares sempre disponível para o que precisasse. Tenho pena de não conseguires assistir ao fim desta etapa, e só quero que saibas que irei sentir sempre a tua falta. À minha tia e prima Micá, que foram sempre carinhosas e super acessíveis em qualquer situação, e pelo incansável apoio. Ao meu irmão, por todo o apoio que me deu, desculpa por não ter mostrado muita disponibilidade estes últimos meses para falarmos e convivermos, prometo que te irei visitar e fazer imensas sessões de escalada num futuro próximo. Sempre tive saudades tuas.

Um grande agradecimento à pessoa mais importante para mim, à minha namorada Inês. És sem dúvida a pessoa que mais admiro. Tens dado um apoio incansável, independente da situação sempre estiveste disponível para me ajudar. Nunca conheci uma pessoa tão bondosa querida e simpática como tu. Apesar de todas as situações nunca me senti sozinho, e isso é graças a ti. Fizeste-me ser uma pessoa melhor, e sem dúvida que irei aprender muito contigo. Sei que não te tenho dado tanta atenção quanto gostarias, mas prometo que no fim desta etapa, serás uma das minhas prioridades, independentemente de qualquer obstáculo que terei à frente.

E por fim queria agradecer a todos os meus amigos. Obrigado a todos.

Abstract

Gliomas are central nervous system tumors with glial origin. A subset of aggressive, high-grade gliomas, which includes glioblastoma (GBM) and several pediatric gliomas, is characterized by immunosuppressive tumor microenvironments (TMEs). These immunosuppressive TMEs were recently associated with increased tumorigenicity and reduced effectiveness of immunotherapies. The molecular crosstalk between cancer and non-cancer cells (e.g., microglia, astrocytes) establishes and sustains the immunosuppressive TME. However, the molecular mechanisms underlying immunosuppression in different glioma subtypes are not well described, mainly due to the lack of adequate experimental models to address them. Most glioma cell models fail to include the different cell types of the TME.

This master thesis aim was to select 3D culture methodologies for co-culture of glioma cells and microglia. First, different human microglia-like cell (MLC) sources were considered: monocytes (MLC-Mo), human induced pluripotent stem cells (MLC-hiPSCs), and microglia cell lines (HMC3 and C20). MLC-Mos and MLC-hiPSCs expressed key microglia genes *AIF1*, *P2RY12/3,* and *CD68*, negligibly detected in C20 and HMC3. MLC-Mo also responded to pro- and anti-inflammatory stimuli, upregulating the response genes *CD86*, *IL1B* and *TGFB1* and was therefore selected as microglia cell source. Secondly, 3D culture methodologies were implemented for a GBM cell line - neurospheres and agitation-based spheroids. Preliminary analysis suggested that neurospheres were enriched in CD133- and SOX2-positive cancer stem cells and immunosuppressive markers were upregulated, compared to spheroids. Finally, we performed a preliminary experiment of co-culture of MLC-Mos with neurospheres, observing high cell viability, MLC-Mo adhesion to the neurospheres, as well as the expression of microglia genes.

This work established methodologies to be employed in the development of more complex 3D models of glioma immunosuppressive TME, incorporating the brain resident cell types. In the long term, we expect it to be useful to discover immunosuppressive mechanisms and development of novel therapies for high grade gliomas.

Key words: gliomas, microglia, tumor microenvironment, immunosuppression; 3D cell models

Resumo

Gliomas são tumores do sistema nervoso central que provêm da glia. O subconjunto de gliomas de alto grau (GAG), onde inclui glioblastoma e outros gliomas pediátricos, são caracterizados por um microambiente tumoral (MAT) imunossupressivo. Este MAT imunossupressivo está associado a uma maior tumorigenicidade e baixa eficácia imunoterapêutica. A interação estabelecida entre células tumorais e não-neoplásicas (microglia, astrócitos, etc.) promovem este MAT imunossupressivo. Porém, os mecanismos moleculares responsáveis pela imunossupressão em diferentes subtipos de gliomas não estão bem descritos, por falta de modelos experimentais adequados. A maior parte dos modelos celulares não incluem componentes celulares relevantes para a recapitulação MAT.

Este trabalho tem como objetivo selecionar várias metodologias de culturas 3D para a implementação de co-culturas entre células de glioma e microglia. Inicialmente, diferentes fontes miméticas de microglia humana foram utilizadas: monócitos (MLC-Mo), células estaminais pluripotentes induzidas (MLC-hiPSCs), e linhas celulares de microglia. MLC-Mos e MLC-hiPSC expressaram genes de microglia *AIF1, P2RY12/3* e *CD68* os quais estavam ausentes nas linhas celulares. Adicionalmente, MLC-Mo responderam a estímulos pro- e anti-inflamatórios, aumentando de expressão de *CD86*, *IL1B* e *TGFB1*. Como resultado, MLC-Mo foi a fonte de microglia escolhida. De seguida foram implementadas metodologias de culturas 3D para uma linha celular de glioblastoma – neurosferas e esferóides gerados por agitação. Os resultados sugerem que as neurosferas são enriquecidas em células estaminais com CD133 e SOX2 comparativamente aos esferóides. Por último, foi realizada uma co-cultura entre MLC-Mo e neurosferas onde se observou uma alta viabilidade celular, adesão de MLC-Mos nas neurosferas e expressão de genes provenientes de microglia.

Neste trabalho implementaram-se metedologias que irão ser empregues para o desenvolvimento de um modelo 3D onde se recapitula o MAT de gliomas, incorporando células residentes do cérbero. A longo prazo, espera-se que este modelo seja vantajoso na descoberta de novos mecanismos imunosupressivos e no desenvolvimento de novas terapias para GAG.

Palavras-chaves: Glioma, microglia, microambiente tumoral, imunossupressão, modelos celulares 3D

Table of Contents

List of Figures

List of Tables

Abbreviations

36B4	60S Ribosomal Phosphoprotein P0
2D	Two Dimensional
3D	Three Dimensional
2-HG	2-hydroxyglutarate
α-KG	Alpha Ketoglutarate
ADC	Antibody-Drug Conjugated
AIF1	Allograft Inflammatory Factor 1
AKT	Protein Kinase b
APC	Antigen-Presenting Cell
ATM	Ataxia Telangiectasia Mutated
ATR	Ataxia Telangiectasia and Rad3-related protein
ARF	Alternative Reading Frame protein
BAD	BCL2 Associated Agonist of Cell Death
BCL-xL	B-cell lymphoma-extra large
BDNF	Brain-Derived Neurotrophic Factor
B-NGF	Beta-Nerve growth factor
BFGF	Basic Fibroblast Growth Factor
BMDM	Bone Marrow derived Macrophage
BT	Brain Tumor
CCR	C-C Motif Chemokine Receptor
CCL	C-C Motif Chemokine Ligand
CD	Cluster of Differentiation
CDKN2A	Cyclin Dependent Kinase Inhibitor 2A
CHK1/2	Checkpoint kinase-1/2 protein
CM	Conditioned Medium
CNS	Central Nervous System
CO	Cerebral Organoids
CSC	Cancer Stem Cell
CSF1	Colony Stimulating Factor 1
CSF1R	Colony Stimulating Factor 1 Receptor
Ct	Cycle Threshold
CTLA4	Cytotoxic T-lymphocyte–associated antigen 4
CX3CL1	C-X3-C Motif Ligand 1
CX3CR1	CX3C motif chemokine receptor 1
DAMP	Damage-Associated Molecular Patterns
DAPI	4′,6-diamidino-2-phenylindole
DC	Dendritic Cell
ddH_2O	Double-distilled water
DM1	Mertansine

DMEM	Dulbecco’s Modified Eagle Medium
DIPG	Diffuse Intrinsic Pontine Glioma
DMG	Diffuse Midline Glioma
DNA	Desoxyribonucleic Acid
DPBS	Dulbecco's Phosphate-Buffered Saline
ECM	Extracelular Matrix
EDTA	Ethylenediamine Tetraacetic Acid
EGF	Epidermal Growth Factor
EGFR	Epidermal Growth Factor Receptor
EHS	Engelbreth-Holm-Swarm
ErbB	erythroblastic leukemia viral oncogene homologue
ERK	Extracellular Signal-regulated Kinase
EZH2	Enhancer of Zeste Homolog 2
FAS	Fas Cell Surface Death Receptor
FASL	FAS Ligand
FBS	Fetal Bovine Serum
FC	Flow Cytometry
FDA	Fluorescein Diacetate
FGF	Fibroblast Growth Factor
GAM	Glioma-associated microglia/macrophages
GBM	Glioblastoma
GEPIA	Gene expression profiling interactive analysis
GFAP	Glial Fibrillary Acidic Protein
GLICO	Organoids co-cultured with tumour spheroids
GM-CSF	Granulocyte-Macrophage Colony-Stimulating Factor
GMEM	Genetically Modified Engineered Mice
GP34	G-Protein Coupled Receptor 34
GRB2	Growth Factor receptor-Bound protein
GzmB	Granzyme B
H3K9	Histone H3 Lysine at position 9
HGF	Hepatocyte Growth Factor
hiPSC	Human induced Pluripotent Stem Cells
HSC	Hematopoietic Stem Cell
IBA1	Ionized calcium-Binding Adapter molecule 1
IDH	Isocitrate Dehydrogenase
IF	Immunofluorescence
IFN-γ	Interferon Gamma
IGF-1	Insulin Growth Factor 1
IL	Interleukin
ITGAM	Integrin Subunit Alpha M

KDM4B	Lysine Demethylase 4B
KOH	Potassium Hydroxide
LPS	Lipopolysaccharide
Mϕ	Macrophages
M0	Resting Macrophages/Microglia
M1	Inflammatory Macrophages/Microglia
M2	Anti-inflammatory Macrophages/Microglia
MAFB	V-maf Musculoaponeurotic Fibrosarcoma oncogene homolog B
MCC	maleimidomethyl cyclohexane-1-carboxylate
MDM2	E3 ubiquitin-protein ligase Mdm2 protein
MGMT	O6 -methylguanine-DNA methyltransferase
MLC-Mo	Microglia like cells derived from Monocytes
MLC-hiPSC	Microglia like cells derived from human induced pluripotent stem cells
MHC	Major histocompatibility complex
MIC-1	Macrophage Inhibitory Cytokine 1
MMP	Matrix metalloproteinase
MRC1	Macrophage Mannose Receptor 1
mTOR	Mammalian target of rapamycin
mTORC1	Mammalian target of rapamycin complex 1
mTORC2	Mammalian target of rapamycin complex 2
NADPH	Nicotinamide adenine dinucleotide phosphate
Nanog	Nanog homeobox 1
NeoCOR	Genetically engineered cerebral organoids
NF	Neurosphere Medium
NGF	Nerve Growth Factor
NO	Nitric Oxide
NS	Neurospheres
NTC	Non template control
OLIG2	Oligodendrocyte transcription factor 2
OV	Oncolytic viruses
P	Phosphate
P27	Cyclin-dependent kinase inhibitor 1B
P53	Cellular tumor antigen p53
P2RY12	Purinergic Receptor P2Y12
P2RY13	Purinergic Receptor P2Y13
PA	Polylactic acid
PAGE	Polyacrylamide gel electrophoresis
PAMP	Pathogen-associated molecular patterns
PBMC	Peripheral Blood Mononuclear Cells
PD1	Programmed Cell Death Protein 1

PDGF	Platelet-Derived Growth Factor
PDGFR	Platelet-Derived Growth Factor Receptor
PD-L1	Programmed Cell Death-Ligand 1
PDMS	polydimethylsiloxane
PDO	Patient-derived organoids
PDX	Patient Derived Xenograft
PEG	Polyethylene glycol
PenStrep	Penicillin-Streptomycin
PFN	Perforin
PFS	Progression free survival
PGA	Polyglycolic acid
PI3K	Phosphoinositide 3-kinase
Postn	Perostin
POU5F1	POU Class 5 Homeobox 1
PRR	Pattern recognition receptor
pSTAT3	Phosphorylated signal transducer, and activator of the transcription 3
PTPRC	Protein Tyrosine Phosphatase Receptor Type C
PTEN	Phosphatase and Tensin Homolog Deleted on chromosome 10
PVDF	Polyvinylidene difluoride
SALL1	Spalt Like Transcription Factor 1
SDS	Sodium dodecyl-sulfate
SGK	Serum/Glucocorticoid Regulated Kinase 1
siRNA	Small interferring RNA
SOS	Son of sevenless
SOX2	SRY-Box Transcription Factor 2
STAT3	Signal transducer, and activator of the transcription 3
R132H	Substitution of arginine at position 132 to a histidine
RAS	Rat Sarcoma Virus protein
RPL22	Ribossomal Protein L22
RPM	Rotations per minute
RPMI	Roswell Park Memorial Institute
RT-qPCR	Real time quantitative polymerase chain reaction
SSEA4	Stage-specific embryonic antigen 4
SV40	Simian vacuolating virus 40
TAA	Tumor-associated astrocytes
TAE	Tris-acetate-EDTA
TBST	Tris Buffered Saline Tween
TCA	Tricarboxylic Acid
TERT	Telomerase Reverse Transcriptase
TF	Transcription Factors

TGF-β	Transforming Growth Factor β
TIP60	Histone acetyltransferase Tip60
TLR	Toll-Like Receptor
TME	Tumor microenvironment
TMEM119	Transmembrane Protein 119
TMZ	Temozolomide
TNF-α	Tumor necrosis factor alpha
TO-PRO™-3	TO-PRO™-3 Iodide
TPM	Transcripts per million
TRA-1-60	Podocalyxin
TRA-1-81	Podocalyxin-like
TREM2	Triggering receptor-expressed on myeloid cells 2
ULA	Ultra-Low Attach
VEGF	Vascular Endothelial Growth Factor
VEGFR	Vascular Endothelial Growth Factor Receptor
WB	Western Blot
WHO	World Health Organization
WNT	Wingless-related integration site

Chapter 1. Introduction

1.1. Gliomas

Brain tumors (BT) are malignant cells that arise in the central nervous system (CNS). CNS neoplastic cells are cancer cells that develop directly in the brain parenchyma (primary BT) or cancer cells that metastasize into the brain, deriving from peripheral tumors like skin, breast, or lung cancer (secondary or metastatic BT) [1–4]. Common symptoms of BT include persistent headaches, seizures, nausea, vomiting, neurocognitive symptoms, and personality changes [5]. BT are classified into two main groups: glial/glioneuronal tumors and non-glial tumors [1–4]. Non-glial tumors are composed of neoplastic cells that do not have a glial or neuronal origin. They include a diversity of tumors like meningioma, primary CNS lymphoma, medulloblastoma, and craniopharyngioma[3]. Neuronal tumors are a group of CNS tumors derived from cells with neuronal differentiation. These tumors may arise from neuronal origin or have mixed neuronal and glial components that comprise the glioneuronal subset [6].

Glial tumors are called gliomas and include the astrocytomas - tumors derived from astrocytes, the oligodendrogliomas - tumors derived from oligodendrocytes, the ependymomas - tumors derived from ependymal cells, and the brain stem gliomas - derived from glial cells in the brain stem [3]. Gliomas can be further classified based on the location of the tumor, characteristic differentiation patterns, mitotic activity, necrosis, microvascular proliferation, and anaplasia. Anaplasia is the cytologic term that describes features of cells that are considered characteristic of malignant neoplasms such as: high nuclear to cytoplasmic ratios, hyperchromatic nuclei, abnormal nuclear contours, nuclear pleiomorphism, and loss of normal polarity [7]. These anaplasia characteristics are used by the world health organization (WHO) to classify the malignancy grade of gliomas. The classification includes grades I to IV, where IV has the highest degree of malignancy and is identified as glioblastoma (GBM) [3,8].

1.1.1. Epidemiology

In 2020 an estimated 19.3 million individuals were diagnosed with cancer worldwide [5], and every year, 100 000 individuals are diagnosed with gliomas (accounting for around 0.5% of all cancer cases) [6]. Although this comprises a small number of individuals, substantial mortality and morbidity are associated with this type of tumor. Additionally, a regional variation was observed, the occurrence in Japan being less than half that in Northern Europe and the United States. The underlying reasons for this are currently unknown [2]. Around 75-80% of the gliomas are classified as glioblastomas, with overall survival of 14-17 months [9].

This work will focus on GBM, the most common type of glioma, and the one with the most well-characterized immunosuppression mechanisms. It will also focus on diffuse midline glioma (DMG), a rare and deadly pediatric brain tumor, whose immunosuppression mechanisms differ from GBM, and is not so well described in the literature.

1.2. Glioblastoma

GBM is one of the most common, malignant, and aggressive forms of glioma. Patients generally have a poor prognosis, with an overall 4-5% 5-year patient survival rate. During the last

20 years, no significant improvements in overall survival were observed [10]. Diagnosis and molecular biology of GBM will be discussed in the following chapters.

1.2.1. Diagnosis

Magnetic resonance imaging (MRI) has been the standard tool for over 20 years in GBM detection, location, and overall anatomical characterization. Despite its usefulness, MRI cannot analyze the underlying cellular alterations [11,12].

Another technique used for GBM diagnosis is positron emission tomography (PET), which is considered a minimally invasive tool, that can quantify cerebral blood flow, metabolism, and receptor binding [11].

Overall, PET presents advantages over MRI, but cannot provide information about the tumor`s histological features, which only a biopsy can reveal. Unfortunately, in some GBM cases, a biopsy may not be possible because of the high risk associated with damaging the healthy surrounding nervous tissue [12]. Because of this, it is imperative to establish and validate new non/minimally invasive diagnostic tools which can give molecular insights important for the diagnosis and treatment of GBM.

In recent years, microvesicles secreted by GBM cells have been explored as a potential biomarker source, since they are detected in blood samples. Microvesicles are plasma membrane-enclosed structures released by cells through membrane fission. Those microvesicles carry a cargo composed of RNA, miRNA, proteins, and metabolites between cells [12]. Microvesicles are found in the peripheral blood, being easy to detect in plasma samples, potentially giving tumor molecular insights while being less invasive and accessible compared to a biopsy. Two examples of GBM-related molecules that are present in those microvesicles are the mutated form of the epidermal growth factor receptor (EGFR), EGFRvIII, and the U6 small non-coding nuclear RNA (RNU-6-1), both found to be related with a malignant GBM phenotype [13,14].

1.2.2. GBM mutations

A large panel of mutations has been reported in GBM tumor cells, influencing cancer cell behavior through the inhibition of apoptosis, uncontrolled proliferation, and survival [15–18]. Among the numerous mutations that alter the phenotype of glioblastoma cells, the most common are in the genes coding for: epidermal growth factor receptor (EGFR), cellular tumor antigen p53 (p53), phosphatase and tensin homolog deleted on chromosome 10 (PTEN) and isocitrate dehydrogenase (IDH) [2,3,8].

1.2.2.1. Epidermal growth factor receptor (EGFR)

EGFR belongs to a large family of erythroblastic leukemia viral oncogene homologue (ErbB) receptors with tyrosine kinase activity. Upon the binding of its natural ligand, EGF, the receptor dimerizes, auto-phosphorylates and activates downstream signaling cascades (Figure 1.1) [19].

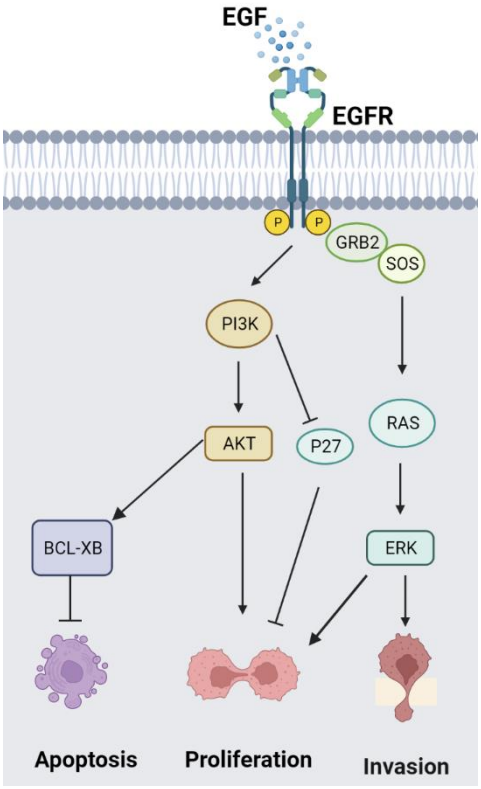

Figure 1.1 – The epidermal growth factor receptor (EGRF) pathway. EGFR is activated by epidermal growth Factor **(**EGF), which leads to autophosphorylation (P) of the receptor and activation of several proteins. EGFR signaling leads to inhibition of apoptosis by B-cell lymphoma-extralarge (Bcl-xL), increased proliferation by activation of protein kinase B (AKT) and inhibition of cyclin-dependent kinase inhibitor 1B (p27) nuclear translocation, and increased invasion by nuclear translocation of extracellular signal-regulated kinase 1/2 (ERK1/2), due to the rat sarcoma virus protein (RAS)-mediated phosphorylation cascade. Adapted from [15] and created in biorender.com.

The EGFR downstream signals involve protein kinase B (AKT), activated by phosphoinositide 3-kinase (PI3K), that phosphorylates BCL2 associated agonist of cell death (BAD), a pro-apoptotic protein. When BAD is phosphorylated, it fails to inhibit B-cell lymphoma-extra large (Bcl-xL), a protein with an anti-apoptotic effect [20,21]. Additionally, activation of AKT induces cell proliferation and prevents the nuclear translocation of cyclin-dependent kinase inhibitor 1B (p27). This prevents p27 from binding to cyclin E/CDK, activating transcription of genes required for the S phase [22,23]. Moreover, EGFR phosphorylation promotes rat sarcoma virus (RAS) protein activation, leading to extracellular signal-regulated kinase 1/2 (ERK1/2) phosphorylation and nuclear translocation, which induces cyclin D1 gene expression, promoting G1/S phase transition, and finally boosting the proliferation and invasion potential of GBM cells [24–26]. In nearly 40% of all GBM cases, EGFR gene amplification (EGFR gene copy number duplication) is observed [27] in which all cases are accompanied with EGFR overexpression (enhanced transcription and EGFR protein levels) [28].

Mutations are also observed in GBM patients [28]. A common mutation in GBM is EGFRvIII, found in 26% of all patients [12]. EGFRvIII mutation is characterized by a deletion in the EGFR N-terminal ligand-binding region between amino acids 6 and 273. This leads to the constitutive activation of EGFR downstream signaling, without the requirement of EGF binding [29].

1.2.2.2. Cellular tumor antigen p53 (p53)

The p53 protein is a well-known tumor suppressor. It is responsible for apoptotic induction, limiting tumor cell expansion. One of the particular features of p53 is the complexity of stimuli to which it responds, and a wide variety of downstream functions induced (Figure 1.2). Upon P53 activation caused by various cellular stress mechanisms (e.g., DNA damage, oxidative stress, hypoxia, etc.), specific pathways will be induced and lead to p53 phosphorylation. These phosphorylation events triggered by cell stress are initiated by numerous protein kinases such as ataxia-telangiectasia mutated (ATM) and ataxia telangiectasia, Rad3-related (ATR). Moreover, P53 can be negatively regulated by E3 ubiquitin-protein ligase Mdm2 protein **(**MDM2), activated due to hyperproliferative signals [30,31].

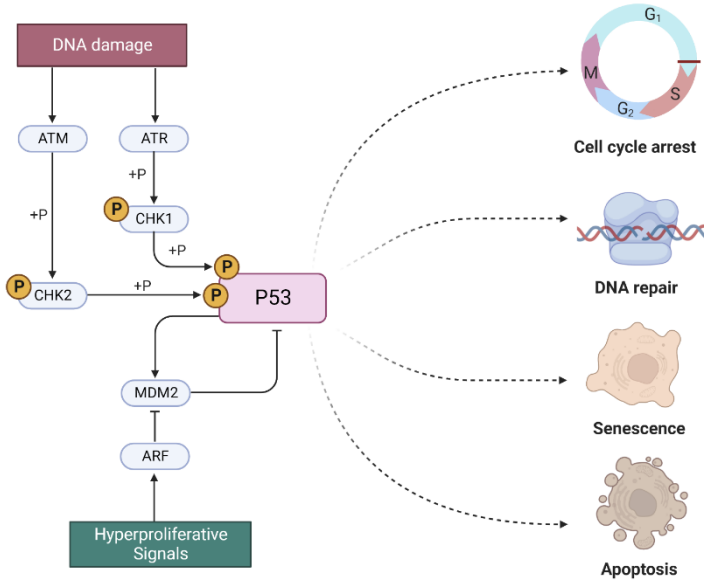

Figure 1.2- Cellular tumor antigen p53 (p53) activation pathway. In response to acute DNA damage, the ataxia-telangiectasia mutated (ATM) and ataxia telangiectasia and Rad3-related (ATR) protein kinases will phosphorylate the checkpoint protein kinase 1 or 2 (CHK1/2). CHK1/2 will phosphorylate p53 in serine 15 and 20, respectively, leading to p53 stabilization and oligomerization and binding to p53 response elements, responsible for cell cycle arrest, DNA repair apoptosis and senescence. The E3 ubiquitin-protein ligase Mdm2 protein (MDM2) is the main regulator of p53. MDM2 is transcriptionally regulated by p53, and promotes p53 ubiquitination and proteasome-mediated degradation, in a regulatory feedback loop. In response to hyperproliferative signals, the tumor suppressor protein p14 alternative reading frame (p14ARF) activates p53 by blocking the access of MDM2 to p53. Adapted from “p53 regulation and signaling” template, by biorender.com and [30, 31].

In GBM, the p53-ARF-MDM2 regulatory pathway is affected in 84% of patients and 94% of the cell lines. These pathway components impact GBM cell invasion, migration, proliferation, and evasion of apoptosis [32]. Moreover, a positive correlation between long-term GBM patient survival and nuclear localization of p53 has been reported: in 85% of long-term survivors (≥ 3 years after initial surgical diagnosis), tumors had high levels of nuclear p53, whereas in short-term survivors (< 1.5 years after initial surgical diagnosis) 56% of the tumors showed high nuclear p53 [33].

1.2.2.3. Phosphatase and tensin homolog deleted on chromosome 10 (PTEN)

PTEN is a tumor suppressor protein that acts as a phosphatase converting phosphatidylinositol-3,4,5-trisphosphate (PIP3) into phosphatidylinositol-4,5-bisphosphate

(PIP2). This impedes the activation of the (PI3K)/Akt/mammalian target of rapamycin (mTOR) pathway. In the latter, two complexes are activated, mTOR complex 1 and 2 (mTORC1/2)[34]. The mTORC1 activates ribosomal protein S6 kinase beta-1 (P70S6K), which regulates cell growth by inducing protein synthesis components [35,36]. The mTORC2 complex activates the AKT protein, which promotes proliferation and inhibits apoptosis, as described above (EGFR subsection). Additionally, mTORC2 activates serum/glucocorticoid regulated kinase 1 (SGK), an oncoprotein that promotes cell survival [35,37]. Distinct *PTEN* mutations are found in 5 to 40% of GBM cases [38]. Moreover, PTEN mutation is associated with a poorer prognosis in various types of gliomas, including GBM [39].

1.2.2.4. Isocitrate dehydrogenase (IDH-1)

Isocitrate dehydrogenase 1 (IDH-1) plays an important role in basal cell metabolism converting isocitrate into alpha-ketoglutarate (α-KG) in the tricarboxylic acid (TCA) cycle [40]. In 90% of GBM cases with IDH-1 mutation, in codon 132, the replacement of an arginine by a histidine is reported. This is a gain of function mutations, resulting in the ability of the enzyme to convert α-KG into 2-hydroxyglutarate (2-HG). Mutant IDH-1 takes advantage of the α-KG produced by the IDH codified by the wildtype allele to produce 2-HG (Figure 1.3) [41]. The 2-HG oncometabolite prevents DNA repair by hampering signals that recruit crucial DNA-repair factors, through competitively inhibiting the binding of α-KG to the active site of lysine demethylase 4B (KDM4B) [42].

The IDH-1^{R132H} gain of function mutation is found in approximately 83% of all secondary GBM cases but it is rare in primary GBM (present in around 5% of the tumors) [43].

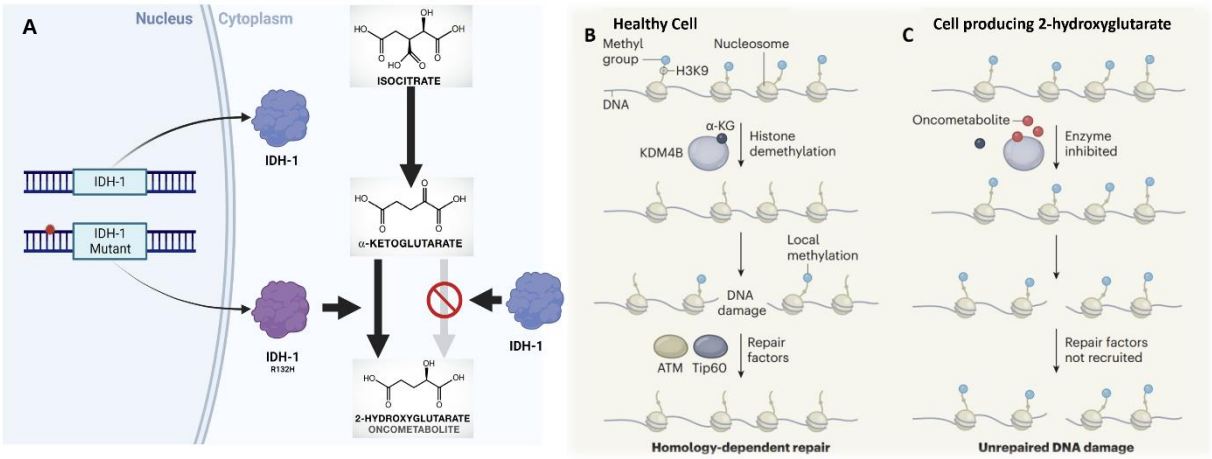

Figure 1.3 - Isocitrate dehydrogenase 1 (IDH-1) gain-of-function mutation affects the epigenetic landscape and inhibits repair of DNA damage. A – A mutation in the *IDH-1* gene results in the IDH-1^{R132H} gain of function mutant, which converts α-ketoglutarate (α-KG) into 2-hydroxyglutarate (2-HG), an oncometabolite. When the mutation is in a single allele, IDH-1 wildtype converts isocitrate into α-ketoglutarate, which is then converted to 2-HG by IDH-1^{R132H}. **B** – In healthy conditions, lysine demethylase 4B (KDM4B) removes methyl groups from lysine 9 (K9) of the protein histone 3 (H3K9) in the nucleosome. Upon DNA damage, local methylation of H3K9 at the damage site will recruit an essential repair factor, such as ataxia telangiectasia mutated (ATM) and histone acetyltransferase tat-interactive protein, 60 kD (Tip60). **C** – The *IDH-1* mutation leads to the accumulation of the oncometabolite 2-HG which inhibits the KDM4B enzyme. The global hypermethylation will impair the recruitment of repair factors to DNA damage sites. Adapted from [12, 41, 42]. Panel A created in biorender.com.

1.3. Diffuse midline glioma (DMG)

Diffuse midline glioma (DMG), previously named diffuse intrinsic pontine glioma (DIPG) [8], is a rare and aggressive subtype of glial tumors that occurs in the brainstem. DMG accounts for 75% of the brainstem tumors in children, with an occurrence of 1/18000 to 1/15000 newborns in both genders, and a 5-year survival rate of 1% [38].

1.3.1. The H3K27M mutation

DMG is characterized by the presence of a mutation in histone 3 - a substitution of lysine at position 27 by methionine (H3K27M) [44,45]. Interestingly, this mutation has been identified also in up to 22% of non-brainstem pediatric GBM [46–48].

H3K27M mutant inhibits the activity of the enhancer of zeste homolog 2 (EZH2) protein, a histone methyltransferase involved in cell cycle, proliferation, and differentiation [49]. This inhibition reduces global methylation, resulting in a hypo-methylated DNA and leading to a subsequent loss of the transcriptional repression of H3K27M loci [50]. Loss of transcriptional repression leads, for example, to the overexpression of known oncogenes, such as oligodendrocyte transcription factor 2 (*OLIG2*), which has been implicated in gliomagenesis through p53 inactivation [46,51].

1.4. Glioma therapies

1.4.1. Standard of care therapies

Current treatments for GBM are surgical resection of the tumor, followed by radiotherapy, chemotherapy, or a combination of both [12]. Maximal tumor resection is case-specific, based on the size and shape of the tumor, its location, and the presence of blood vessels. In the case of DMG, tumor resection is not feasible when there is diffuse infiltration within the midbrain parenchyma and/or involvement of a sensitive brain region. In these cases, the only possible treatment is radiotherapy [52].

Temozolomide (TMZ), first described in 1997, is the standard-of-care drug used against GBM. TMZ is a brain-penetrant alkylating agent that methylates purines (adenine or guanine) in DNA, inducing apoptosis [53,54]. Upon TMZ treatment in combination with radiotherapy, the median progression-free survival (PFS) increased for those who were only treated with radiotherapy (9.4 vs. 3.0 months, log-rank P = 0.0001) [55].

However, 35–50% of GBM cases express O6-methylguanine-DNA methyltransferase (MGMT). MGMT is a mediator of DNA mismatch repair that corrects TMZ-induced damage, leading to TMZ resistance [56,57]. It has been found that MGMT expression was significantly associated with shorter median PFS of patients upon TMZ treatment (5.6 vs. 9.9 months, log-rank P = 0.0032)) [55]. Nonetheless, even in patients that do not express MGMT, the overall long-term survival of GBM cases under TMZ and radiotherapy treatment is still low.

1.4.2. Novel therapeutic modalities

The overall survival of glioma patients did not improve over the past 20 years, claiming for the development and discovery of novel and more effective therapeutic modalities against this deadly

cancer [7,12,58]. Monoclonal antibodies, oncolytic viruses, and dendritic cell therapies are examples of novel therapies under development for which clinical trials are ongoing [12].

1.4.2.1. Monoclonal antibodies

Therapeutic anti-cancer monoclonal antibodies recognize and block relevant cancer cell surface receptors and/or their ligands, preventing oncogenic downstream receptor signaling activation [59]. An example is bevacizumab, an antibody that binds to the vascular endothelial growth factor (VEGF). This growth factor is secreted by GBM cells and promotes neoangiogenesis [12]. Upon binding to VEGF, bevacizumab prevents the interaction of the factor to the VEGF receptor, inhibiting neovascularization of the tumor (Figure 1.4A) and ultimately consequent reduction of the cancer mass in nude mice [60].

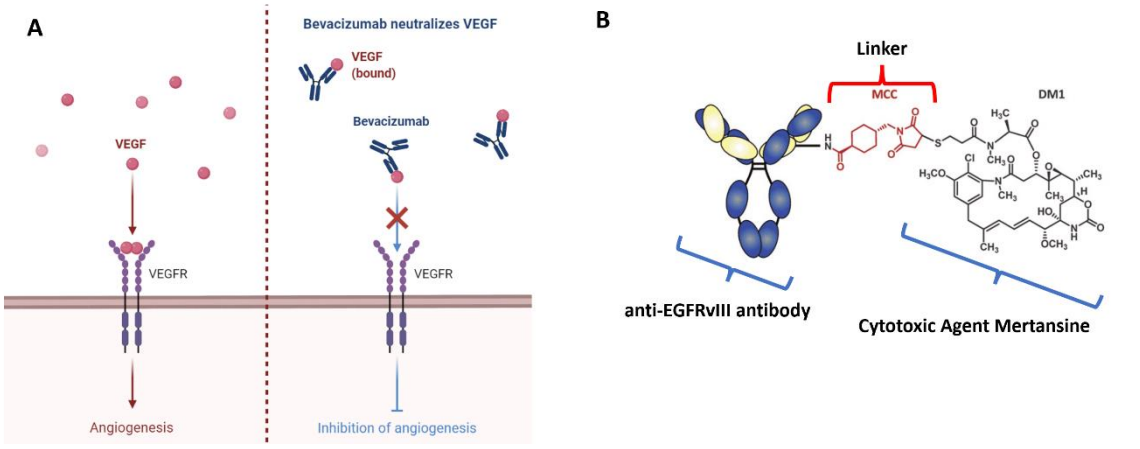

Figure 1.4 – Potential monoclonal antibody therapies for glioma. A – Vascular endothelial growth Factor (VEGF) binds to its receptor (VEGF receptor, VEGFR), eliciting downstream signals responsible for angiogenesis. Bevacizumab binds VEGF inhibiting the interaction of VEGF to its receptor and consequently inhibiting angiogenesis. **B** – The antibody-drug conjugate AMG595 is composed of an antibody specific for EGFR vIII, bound to the cytotoxic agent mertansine (DM1 compound) through a linker - maleimidomethyl cyclohexane-1-carboxylate (MCC). Figure A adopted from "Bevacizumab: Potential" template in biorender.com and [60, 62].

Although it appeared as a valuable treatment option, results from a randomized trial for the treatment of newly diagnosed GBM patients showed no significant difference between the overall survival of the bevacizumab and the placebo group [61].

Another potential treatment for gliomas is AMG595, an antibody-drug conjugated (ADC) that specifically targets the EGFRvIII. When receptor-mediated internalization of the ADC into the endo-lysosomal pathway occurs, the DM1 cytotoxic compound induces cancer cell death through mitotic arrest [62]. Nonetheless, the usage of this treatment is limited by the fact that only 26% of GBM cases present the EGFRvIII mutation (Figure 1.4B), and the blood-brain barrier may impair antibody diffusion to the brain [63].

1.4.2.2. Oncolytic viruses

Another promising class of new therapeutics against gliomas is the oncolytic viruses (OVs). These are engineered viral vectors that cannot replicate except in the tumor cells (Figure 1.5A). This tumor cell-specificity of OVs is achieved by vector specificity to tumor receptors or transcriptional targeting of tumor-specific promoters and abnormal signaling pathways present in

cancer cells (e.g., Ras/Akt/IFN). In the latter, OVs can enter healthy cells, although replication does not occur [64].

OVs present advantages over previous therapies mentioned besides tumor cell specificity [65]. OVs have immunostimulatory properties since, upon lysis of cancer cells, tumor antigens are released and can be uptaken by surrounding antigen-presenting cells (APC), like dendritic cells (DCs). This leads to the induction of tumor- and virus-specific T cells that will act exclusively on cancer cells, enhancing the anti-tumorigenic effect of OVs (Figure 1.5B) [66,67]. Furthermore, OVs can be used as platforms for intratumoral delivery of immunostimulatory cytokines and chemokines, enhancing antitumor responses [68].

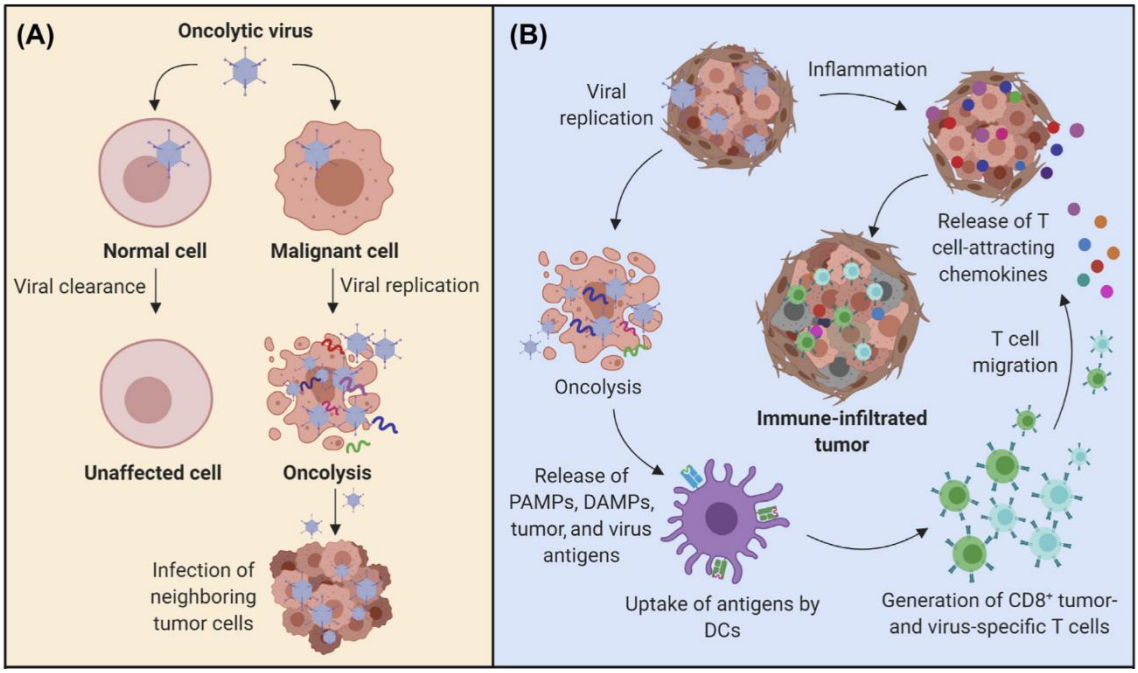

Figure 1.5 - Biological effects and properties of oncolytic viruses (OVs). A – One of the main properties of OVs is the ability to replicate only in malignant cells. B – Upon OV infection and oncoviral-mediated cancer cell lysis there is a massive release of tumor and virus antigens, besides pathogen-associated molecular patterns (PAMPs) and damage-associated molecular patterns (DAMPs) that will be uptaken by dendritic cells (DCs). Antigen presentation by DCs will elicit an adaptive immune response by generating $CD8^+$ cells with anti-tumor and virus-specific activities. $CD8^+$ will release chemokines that promote infiltration of other immune cells, enhancing the antitumor response. Adapted from [49].

Engineered OVs to target GBM are selectively tailored to bind to specific GBM receptors, like EGFRvIII, platelet-derived growth factor receptor (PDGFR), or the interleukin-13 receptor (IL-13R) [12]. DNX-2401, previously known as delta-24-RGD-4C, is an oncolytic adenovirus currently under development, showing promising results in clinical trials. In one of the studies, stabilization, partial or complete regression were reported in 52% of the 24 GBM patients that received the OV as first-line therapy [69]. DNX-240 was also employed in a dose escalation trial in patients recently diagnosed with DMG. The results of the study have been recently reported, showing that despite frequent adverse events, only two patients had a severe adverse effect. Promising results on median overall patient survival were reported, suggesting improvements when compared to historical data from DMG patients [70].

1.4.2.3. Dendritic cell (DC) therapy

DCs play a vital role in the innate and adaptive immune systems. DCs circulate in the peripheral tissues capturing non-self-antigens that are internalized, processed into small peptides, and exposed to naïve T-cells in the lymphoid organs. This process will induce a cellular immune response involving CD4+ T helper 1 (TH1) cells and cytolytic CD8+ T cells [71]. Altogether, this led to the belief that DCs could be used as immunotherapeutic treatments against cancer. A common DC immunotherapeutic protocol involves the isolation of monocytes from cancer patients' blood and converting them into immature DCs (iDCs). Then, patient-derived iDCs are pulsed with tumor- specific antigens or cancer cell lysates, and reintroduced into the patients, eliciting anti-tumor immunity induction through mechanisms described in figure 1.6 [72].

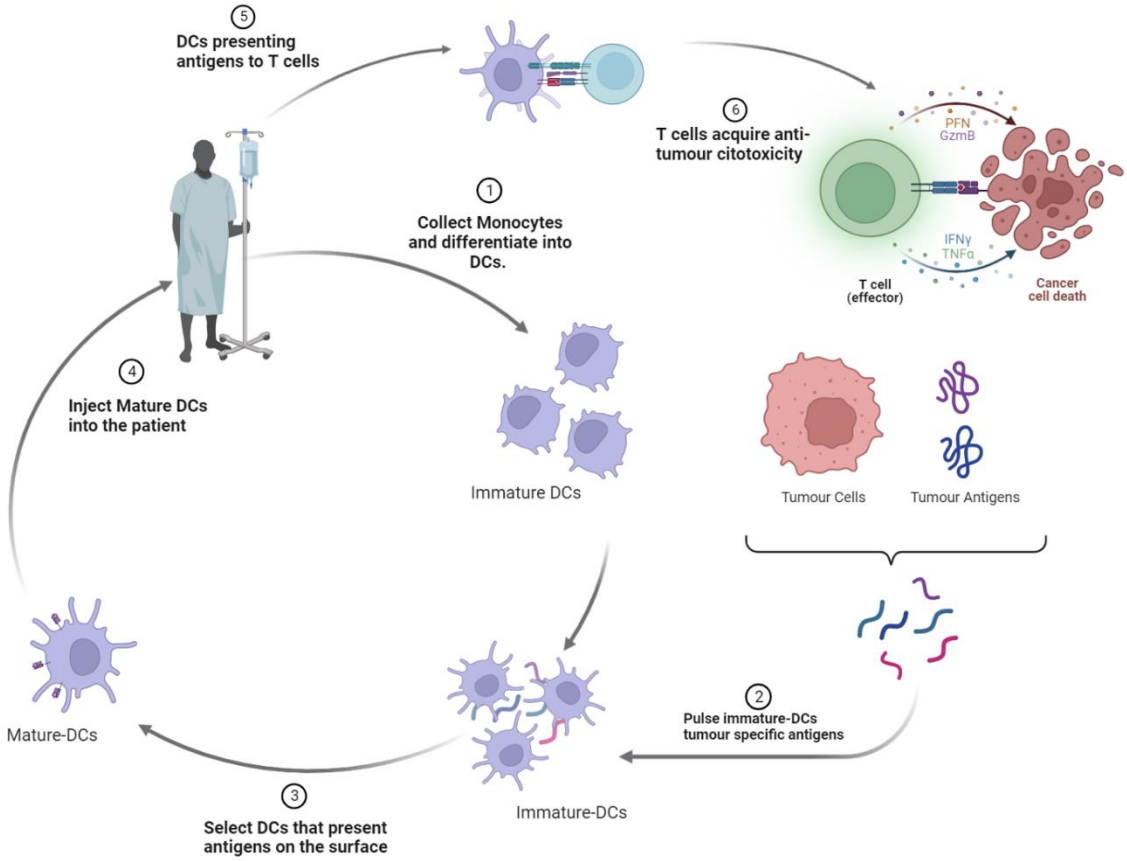

Figure 1.6 - Dendritic cell (DC) therapy. Immature DCs are differentiated from monocytes collected through a blood sample of the cancer patient and matured by stimulation with tumor-specific antigens. These mature DCs are then injected into the patient's blood stream and present these tumor antigens to CD8+ cells, eliciting an anti-tumor cellular response. T-cells educated by DCs specifically target tumor cells, causing apoptosis through release perforin (PFN) and granzyme B (GzmB), and sustaining a pro-inflammatory environment, through secretion of interferon gamma (IFN-γ) and tumor necrosis factor alpha (TNF-α). Created in biorender.com and adapted from [69, 70].

Currently, several DC therapies for GBM are currently in clinical trials: DCVax-L by Northwest Biotherapeutics and Prophage G100 from Agenus [12,73,74]. In a DCVax-L phase I/II trial, 33.0% of patients reached or exceeded a median survival of 2 years and 27.0% reached or exceeded a median survival of 3 years [74]. In DMG, DC therapies are also under phase I clinical trials. Preliminary results demonstrate a DMG-specific immune response in peripheral blood mononuclear cells (PBMC) and cerebrospinal fluid (CSF) [75].

Considering that gliomas are characterized as “cold” tumors, presenting an immunosuppressive tumor microenvironment (TME) [76–81], the development of immune-stimulating therapies could be a milestone in the treatment of these cancer types. The characterization and understanding of the TME are imperative for the development of immune-stimulating therapies.

1.5. The glioma microenvironment

The tumor microenvironment (TME) is the result of the heterotypic molecular and cellular interactions that occur within solid tumors, among cancer cells and non-cancer cells, such as immune cells, fibroblasts, and other cells in the tissue of origin, as represented in Figure 1.7 for gliomas.

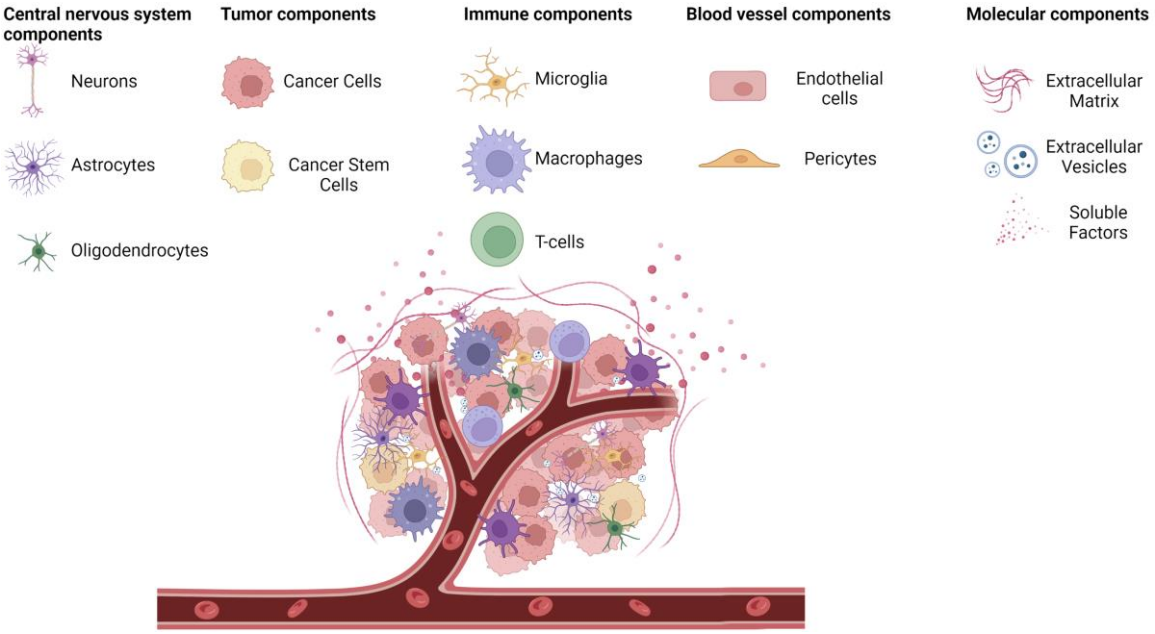

Figure 1.7 - Simplified representation of the tumor microenvironment (TME) of gliomas. Besides the presence of cancer cells and cancer stem cells, glioma TME is composed of a vast panel of non-neoplastic cells, such as central nervous system cells (neurons, astrocytes, and oligodendrocytes), immune cells (microglia and macrophages) and aberrant extracellular matrix and soluble proteins, as well as extracellular vesicles secreted, by cancer cells and other cells of TME. Created in biorender.com and adapted from [76-81].

The glioma TME it is characterized by normal brain resident cells, such as neurons, astrocytes, oligodendrocytes, microglia, as well as the specific brain vasculature that is part of the blood-brain barrier [76,82]. Additionally, there is typically high infiltration of blood-derived macrophages (Mφ) and low infiltration of T-cells, typical of a “cold” immune TME [78], which is detailed later (Section 1.5.2). Cancer cells are very heterogeneous. In fact, brain cancer cells show different degrees of differentiation, the so-called glioma cancer stem cells (CSCs) being the less differentiated [83]. Glioma GSCs not only serve as a critical regulator of tumor progression and recurrence but are also crucial players in the establishment of the immunosuppressive glioma TME [83]; they will be further described in the following section.

The GBM TME is characterized by an aberrant ECM deposition. It differs from the healthy brain since it contains collagen IV, low molecular weight hyaluronic acid, matrix metalloproteinases that enhance tumor cell invasion [84], and an overall high density and stiffness

[85,86]. This increased stiffness has been associated with therapeutic resistance, since it reduces the diffusion of drugs within the TME, as shown for therapeutical antibodies [87]. A plethora of immunosuppressive cytokines, growth factors, and altered metabolite accumulation, as well as hypoxia and acidic pH have also been reported. All components contribute to a typically immunosuppressive TME, which can inhibit immune cell activation and cell death, ultimately aiding tumor cells in escaping the immune surveillance [88–91].

1.5.1. Cancer stem cells

CSCs are a small cancer cell population that shares characteristics with normal stem cells, such as the ability to self-renew and differentiate into multiple lineages. Moreover, CSCs are oncogenic and give rise to a heterogeneous cell population [92]. CSCs are identified by a large panel of surface markers (e.g., CD133, CD44, CD70), transcription factors (e.g., SOX2 and NANOG), and intermediate filaments (e.g., NESTIN), among other molecular markers, and are characterized by chemo and radio-resistance [14].

The presence of CD133+ has been positively correlated with worse patient survival, highlighting the role of CSCs in patient outcomes [93]. Several studies reported that $CD133^{+}$ cells secrete multiple immunosuppressive cytokines such as tumor growth factor-β1 (TGF-β1), colony stimulating factor 1 (CSF-1), and macrophage inhibitory cytokine 1 (MIC-1). Furthermore, in human Mφ exposed to GBM CSC conditioned medium (CM), increased immunosuppressive protein detection (IL-10, TGF-β, and IL-23) and decreased phagocytic ability were reported [94]. *W. Zhou et al*. found that GBM CSCs secrete perostin, a potent microglia/ Mφ attractant, and by silencing the perostin gene (*postn*) tumor growth and tumor-associated microglia/ Mφ infiltration could be reduced in mice xenograft models [95].

In addition, GBM CSCs secrete exosomes that contain the phosphorylated signal transducer and activator of the transcription 3 (pSTAT3), which mediates an immunosuppressive switch [96]. These exosomes enter the peripheral blood and traverse the monocyte cytoplasm, transferring pSTAT3 to monocytes. This contributes to the overexpression of programmed death-ligand 1 (PD-L1), which inhibits CD8+ and CD4+ T cell activation, enhancing tumor immunosuppression [97,98].

1.5.2. The crosstalk of GBM cells with astrocytes, neurons, and oligodendrocytes

Astrocytes are the most abundant glial cells of the CNS, exerting metabolic and scavenger functions. They remove cell debris after injury, regulate ion concentration in the synaptic cleft, and guide the migration of neurons and the outgrowth of axons during development [99].

Recently, distinct populations of reactive astrocytes started to be uncovered. Two opposing phenotypes were identified, one in response to inflammatory stimuli, the other under ischemic conditions. They were named A1 and A2, respectively, to parallel the nomenclature of microglia states [100]. A1 astrocytes undergo upregulation of pathways related to antigen presentation, complement activation, and increased neurotoxicity, and are characterized by increased expression of GFAP and vimentin [101]. A2 astrocytes participate in scar formation and protect

neurons and synapses by releasing neurotrophic factors like brain-derived neurotrophic factor (BDNF) and nerve growth factor (NGF) [102].

In the GBM context, data suggest that astrocytes contribute to GBM progression and are classified as tumor-associated astrocytes (TAA) [103]. TAA secretes immunosuppressive cytokines like TGF-β, and pro-tumorigenic growth factors, such as insulin growth factor 1 (IGF-1), VEGF, fibroblast growth factor (FGF), hepatocyte growth factor (HGF) and EGF [104]. Additionally, Yu, T. *et al.* found that astrocytes deliver MGMT mRNA via exosomes to GBM cells, conferring the resistance to standard of care treatment, TMZ [105].

Neurons are the brain cells that convey information through electric and chemical signals, composed by a single axon and multiple dendrites [106]. In the glioma`s context, neurons release soluble neuroligin-3 that is uptaken by glioma cells. Venkatesh, H. S *et al*. reported that neuroligin-3 induces activation of the PI3K-mTOR pathway resulting in glioma progression [107]. Additionally, in the synaptic cleft, glioma cells secrete glutamate and uptake cystine via the cystine–glutamate transporter system. This results in excessive glutamate in the synaptic cleft causing hyperexcitation and originating an epileptic discharge and excitotoxicity [108].

Oligodendrocytes are cells responsible for myelin sheath formation, which enhances the conduction of electrical signals along the axons of neurons [99]. Although oligodendrocytes are not deeply studied in GBM TME, Asslaber, M. *et al.* findings suggest that oligodendrocytes might have a paracrine anti-tumor effect, inhibiting GBM growth via WNT inhibitory factor 1 [109]. On the other hand, oligodendrocyte progenitor cells were found to promote angiogenesis due to the enhanced expression of platelet-derived growth factor receptor-α (PDGFR-α) [110].

1.5.3. Immune cells in the TME

The glioma microenvironment contains a substantial portion of non-neoplastic cells, mainly resident microglia, and peripheral blood-derived Mφ, collectively known as glioma-associated microglia/ Mφ (GAMs) [76]. These cells present enormous plasticity depending on the stimuli of the surrounding microenvironment, and can polarize mainly towards the M1 inflammatory state, in the presence of pathogen or cell damage, or towards the M2 anti-inflammatory phenotype, during tissue healing and remodeling [76,111]. Although microglia/ Mφ are present as M1 and M2 phenotypes in BT [78,112], in gliomas, tumor cells promote the M2 anti-inflammatory phenotype, to escape the immune surveillance and promote cancer growth (figure 1.8) [76]. GAMs are further discussed in the next sections.

T-cell activity is also hijacked by glioma cells. TGF-β and IL-10 secreted by GBM cells induce differentiation of regulatory T- cells (Tregs) [113]. These are a subpopulation of T cells that act to suppress the immune response [114].

In the GBM TME, Tregs inhibit T-cell activation and cytokine production like IFN-γ and IL-2. In addition, Tregs interact with APC through CTLA-4 and with co-stimulatory molecules CD80/86, causing inhibition of antigen presentation to T cells. These interactions cause lower T cell effector proliferation and cytotoxicity towards cancer cells, which further inhibit APC induction, and enhance Treg activation. These mechanisms, as represented in figure 1.8, are hijacked by tumors, preventing an effective antitumor immune response [76,113].

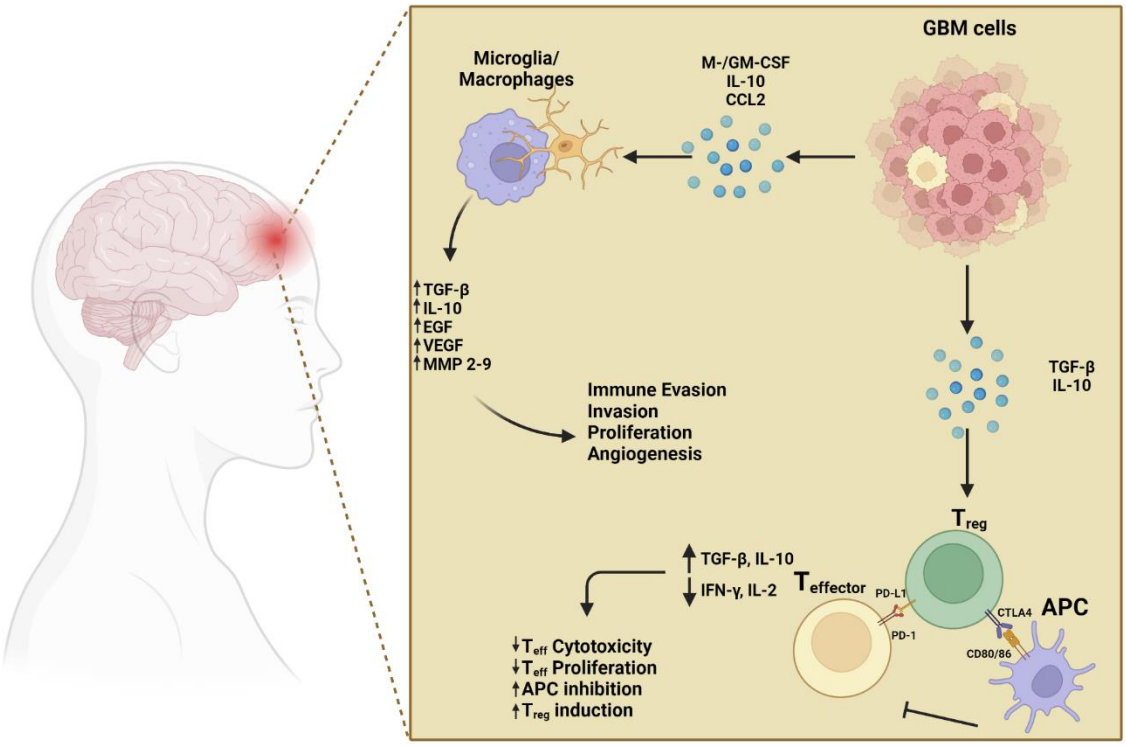

Figure 1.8 – Immunosuppressive mechanisms in the GBM microenvironment. Glioma cells secrete a variety of cytokines that modulate immune cells such as macrophage and granulocyte macrophage colony stimulating factor (M-CSF and GM-CSF respectively), C-C motif chemokine 2 (CCL2), C-C motif chemokine 11 (CCL11), and C-X3-C motif ligand 1 (CX3CL10), leading to infiltration Mφ and polarization of M2 tumor associated microglia/ Mφ (GAM). These M2 GAMs secrete multiple factors like transforming growth factor beta (TGF-β), interleukin 10 (IL-10), epidermal growth factor (EGF), vascular endothelial growth factor (VEGF) and matrix metalloproteinase 2 and 9 (MMP2-9) that elicit immune evasion, cancer cell proliferation and invasion, and angiogenesis. Additionally, GBM-secreted factors induce peripheral T cells into regulatory T cells (T_{regs}), which have immunosuppressive properties. T_{regs} present programmed cell death-ligand 1 (PD-L1) that binds to programmed cell death protein 1 (PD-1) on effector T cells (T_{eff}) cells inducing apoptosis. They also present cytotoxic T-lymphocyte–associated antigen 4 (CTLA4) that binds to the co-stimulatory molecules T-lymphocyte activation antigen 80 and 86 (CD80/86) on antigen presenting cells (APCs), inducing inhibitory signals. The inhibitory signals cause an increase in TGF-β and IL-10 levels and a decrease in Interferon Gamma (IFN-γ) and Interleukin 2 (IL-2) resulting in lower T_{eff} Cytotoxicity and proliferation, and higher antigen presenting cell (APC) inhibition and T_{reg} induction. Adapted from [76, 113] and created in biorender.com.

1.5.3.1. Microglia

Microglia are the resident innate immune cells of the CNS. Microglia cells have an origin different from Mφ, which are developed from bone-marrow-derived monocytes [115]. Microglia cells are originated from erythromyeloid progenitors in the yolk sac, migrating into the developing CNS at an early embryonic stage and differentiating in the CNS [116]. Transcription factors (TF), such as PU.1 and interferon regulatory factor 8 (IRF8), are required for the maturation of microglia precursors. The key transcriptional regulators, spalt like transcription factor 1 (SALL1), and V-maf musculoaponeurotic fibrosarcoma oncogene homolog B (MAFB), are essential for maintaining

microglial homeostasis and identity [115]. This process accompanies a gradual acquisition of microglia markers such as transmembrane protein 119 (TMEM119) and purinergic receptor 12 (P2RY12) [117]. Additionally, the survival, proliferation and differentiation of microglia are sustained by a series of cytokines such as colony stimulating factor-1 (M-CSF), granulocyte-macrophage colony-stimulating factor (GM-CSF), beta-nerve growth factor (β-NGF) as well as interleukin-34 (IL-34) that bind to the M-CSF receptor (CSF1R) [115,118].

Microglia cells influence brain development and homeostasis of the neural environment by phagocyting apoptotic cells and supporting neurogenesis, synaptic pruning, and axonal growth. Moreover, microglia cells are involved in immune surveillance and are a critical component of the first line of defense against CNS pathogens. In the absence of anti- or inflammatory stimulus, microglia are termed microglia M0 [119,120].

CNS infections by bacteria and viruses lead to the activation of inflammatory microglia, due to the detection of bacterial and viral pathogen-associated molecular patterns (PAMPs), such as lipopolysaccharides (LPS), viral DNA, or RNA. These PAMPs bind to pattern recognition receptors (PRRs) such as toll-like receptors (TLRs). TLR-mediated signaling leads to a variety of events, such as the induction of Mφ infiltration through the microglia-derived secretion of chemo-attractants (e.g., MCP-1/CCL2); an increase in redox molecules (NADPH oxidase, phagocytic oxidase); and anti-bacterial nitric oxide (NO) production, to support the phagocytic process. Additionally, upon inflammation, microglia upregulate T-lymphocyte activation antigen 80 and 86 (CD80 and CD86), and the antigen-presenting markers major histocompatibility complex (MHC) Class I A, B and C and MHC class II (MHCII) DR that trigger adaptive immune responses. Moreover, microglia secrete pro-inflammatory interleukins, such as IL-1β and IL-6, to promote inflammatory reactions, crucial for pathogen clearance. The inflammatory phenotype of microglia is termed M1 [76,121].

Although inflammation is essential for the pathogenic response, it is tightly regulated through a subsequent polarity transition into an anti-inflammatory phenotype. This phenotype is commonly termed M2 microglia, and it is associated with the downregulation of immune responses, preventing tissue damage and supporting the tissue healing processes, by the secretion of anti-inflammatory cytokines and immune regulators [76,122]. This anti-inflammatory phenotype is characterized by different markers, such as the scavenger receptor cysteine-rich type 1 protein M130 (CD163), responsible for clearing oxidative hemoglobin in tissues. The process involves hemoglobin uptake by microglia/ Mφ and subsequent heme degradation by heme oxygenase 1 in anti-inflammatory heme metabolites (e.g., bilirubin) [123]. Another M2 marker is the Mφ mannose receptor 1 (*MRC1* that codes CD206), which is responsible for endocytosis, phagocytosis, and scavenging high mannose N-linked glycoproteins [119]. Moreover, M2 microglia/ Mφ secrete anti-inflammatory cytokines such as TGF-β, VEGF, IL-4, IL-10, and the enzyme arginase-1, to further enhance the wound healing process, angiogenesis, and downregulation of inflammatory response [76,121].

1.5.3.1.1. Microglia markers

Microglia express a large panel of molecular markers that distinguish them from other cell types and provide unique functions. Common microglia clusters of differentiation (CD) represent a group of surface markers that identify a particular differentiation lineage of hematopoietic cells [124]. Protein tyrosine phosphatase receptor type C (*PTPRT*), known as CD45 protein, integrin subunit alpha M **(**ITGAM/ CD11B), and the scavenger receptor class D, member 1 (CD 68) are the markers commonly used to identify human microglia, although they are not specific for this cell type. CD45 is expressed on most hematopoietic lineages, being involved in the regulation of numerous processes, including cell division and differentiation, as well as lymphocyte activation [125,126]. CD11B is usually expressed in leukocytes, including monocytes, Mφ, neutrophils, natural killer cells and granulocytes, modulating biological functions key for innate immune cells, including cell adhesion, migration, and phagocytosis [127]. CD68 is usually expressed in the mononuclear phagocyte lineage, including Mφ, microglia, osteoclasts, and myeloid DCs. It is preferentially located within late endosomes, cycling through the plasma membrane. Being described as a scavenger receptor, recent data suggest a role in peptide transport/antigen processing [128].

Apart from CDs, other microglia markers have been identified. Among those, it is important to mention: the ionized calcium-binding adapter molecule 1 (IBA1), also known as the allograft inflammatory factor 1 (*AIF1*) gene product, triggering receptor-expressed on myeloid cells 2 (TREM2); the purinergic receptors P2RY12 and P2RY13; G-protein coupled receptor 34 (GPR34); TMEM119; and a variety of chemokine receptors such as chemokine receptor 1 (CX3CR1) [76,121].

IBA1 is responsible for reorganization of the cytoskeleton, required for phagocytosis [129]. TREM 2 is a transmembrane protein, proposed to bind to a variety of ligands: lipids, lipoproteins, and ligands associated with PAMPs, leading to downstream signals of cell proliferation and differentiation, survival, phagocytosis, chemotaxis, and inflammation [130]. P2RY12 and P2RY13 belong to the purinergic receptor family of plasma membrane molecules, responsible for the detection of nucleotides that are released upon injury, promoting phagocytic clearance of dead cells and tissue debris via oriented migration of microglia [131]. GPR34 is an orphan receptor whose endogenous ligand has not been identified. GPR34 knockout in microglia has been associated with altered cell morphology, motility, and phagocytosis, highlighting its relevance in microglia function and identity [132].

TMEM119 is a transmembrane protein, with unknown function in microglia, although there are data showing an important role in bone formation and normal bone mineralization, as well as in promoting differentiation of myoblasts into osteoblasts [89,102].

Chemokine (C-X3-C motif) receptor 1 (CX3CR1) has a unique ligand, the chemokine C-X3-C motif ligand 1 (CX3CL1 or fractalkine), which can promote inflammation [133]. Microglia are activated through CX3CL1/CX3CR1 signaling by neurons, which consequently activate inflammatory transcription factors, like NF-κB and cyclic adenosine monophosphate (cAMP)

[133,134]. Nevertheless, the administration of recombinant CX3CL1 in neurodegenerative mice models attenuated inflammatory response by downregulating IL-1β and tumor necrosis factor alpha (TNF-α). In addition, microglia secreted neuroprotective factors, like adenosine and phagocyted amyloid beta peptides [135].

As most of these microglia markers are also expressed in Mφ, discriminating these two cell populations and studying them independently becomes exceedingly difficult. Microglia cells are traditionally defined by flow cytometry as $CD11B^{+}/CD45^{low}$, whereas Mφ are $CD11B^{high}/CD45^{high}$. However, upon inflammation, CD45 expression is upregulated in microglia [136,137]. Current markers that are considered exclusively expressed by microglia within the brain parenchyma are TMEM119 and P2RY12/13 [60].

1.5.3.2. Glioma-associated microglia/macrophages (GAMs)

GAMs contribute to an immunosuppressive TME by secreting anti-inflammatory cytokines, chemokines, and growth factors [76]. Moreover, GAMs trigger inhibitory immune checkpoint blockage in T cells, such as PD-1 or CTLA4, augmenting the pro-tumorigenic milieu. GAMs can comprise up to a third of the tumor mass and are positively correlated with disease progression [76,138,139].

In GBM, tumor cells secrete several immune modulators such as the monocyte/ Mφ chemoattractants C-C Motif Chemokine Ligand 2 (CCL2), and 11 (CCL11); M-CSF and GM-CSF, that promote GAM differentiation and proliferation. Additionally, GBM cells secrete TGF-β, particularly the TGF-β1 isoform [140,141]. TGF-β is an immunosuppressive cytokine that induces M2 microglia/Mφ polarization, by downregulating MHC class II and co-stimulatory molecules, and lowering microglia phagocytic ability. Additionally, TGF-β downregulates perforin, granzyme A, granzyme B, and IFN-γ expression, which is responsible for T lymphocyte (CTL)-mediated tumor cytotoxicity [142]. Furthermore, it inhibits the differentiation of Th1/Th2 cells, which are modulators of anti-tumor responses, promotes immunosuppressive Treg T-cell polarization, and dampens the antigen presentation ability of DCs [143]. Knock-out in adult mice microglia of *Tgfbr2* (the gene that codes for the TGF-β receptor) led to the induction of genes responsible for microglia activation like CD86, MHCII, CCL2, and CXCL10 [144]. These results could indicate that the TGF-β signaling pathway is a promising target to revert microglia polarization in GBM. Additionally, GBM cells secrete IL-10, which promotes a shift in phenotype towards M2-GAM [113].

1.5.3.3. GAMs sustain the immunosuppressive GBM and DMG microenvironment.

Immunosuppressive GAMs are collectively indicated as M2-GAMs and secrete pro-tumorigenic molecules reported to induce GBM tumorigenicity and progression. One example is EGF, which promotes anti-apoptotic activity, proliferation, and growth [76,145]. Other factors secreted by GAMs are VEGF [76,146,147], which induces neoangiogenesis; and TGF-β, which promotes glioma cell stemness and invasion [76,93,141]. Additionally, GAMs secrete IL-10, a pleiotropic cytokine that inhibits pro-inflammatory cytokine synthesis, and antigen presentation in activated microglia/ Mφ and dendritic cells. It also impairs T-cell activation and proliferation by

activating the JAK1-TYK2-STAT3 pathway, leading to STAT3-mediated transcription genes that limit the inflammatory response [76,148–152]. Additionally, GAMs secrete metalloprotein matrix 2 and 9 (MMP2/9), which are associated with GBM invasion due to their matrix-degrading function [153].

GAMs can also modulate the immune TME through cell-to-cell interactions [149,154,155]. GAMs express the membrane-bound Fas ligand (FASL), a transmembrane protein that belongs to the TNF family and binds to the Fas receptor (FAS) expressed in T cells, ultimately inducing T-cell apoptosis [156]. This mechanism, along with the secretion of immunosuppressive cytokines by GAMs, causes a low content of T cells within the TME [76]. In addition, these limited T cells presented in the TME are dysfunctional due to the PD1 and CTLA4 immune checkpoint blockage, mainly by the action of GAMs, limiting the cytotoxic effect of T cell against GBM [97]. This outcome contributes to the establishment of a highly immunosuppressive TME (named “cold”), with the addition of a high content of M2 microglia/ Mφ [76].

In pediatric high-grade gliomas, including DMG, very low levels of infiltrated T cells have also been reported [78,157,158]. Lin *et al.* reported a negligible percentage of CD3+ cells in DMG (1.72–2.65% of the total CD45+ leukocytes), compared to 7.09–50.2% in adult GBM [78]. In fact, the authors reported that 94.80% ± 0.92% of the CD45+ cells in DMG were CD11B+ myeloid cells (compared to 70.34% ± 7.20% in adult GBM).

However, in DMG, the paradigm of immunosuppression may differ from adult GBM. The secretome of cultured DMG cells (derived from DMG biopsy samples) was found to be very poor in cytokines and chemokines, when compared to adult GBM [78] which was later confirmed by Lieberman *et al* [159]. The only cytokine secreted by tumor cells that could be detected was TGF-β. These results were corroborated in RNAseq data of freshly isolated DMG biopsies [78]. TGF-β is known to contribute to the immunosuppressive TME, enhancing a pro-tumorigenic milieu as previously mentioned (Section 1.5.3.2). In conclusion, DMG “cold” TME paradigm is characterized by a low intrinsic inflammatory signature, a higher non-inflammatory Mφ, and a lower T-cell infiltration, when compared to GBM [78,157,158], and reviewed by Casper J. *et al.* [160].

1.5.4. GAMs as a potential immunotherapeutic target

Since M2-like GAMs are one of the key players of immunosuppression in GBM, it was hypothesized that re-polarizing them to a pro-inflammatory phenotype would present a therapeutical benefit. By allowing the immune system to better recognize and attack tumor cells, it could contribute to reduce GBM progression [161]. It has been shown that blocking CSF1R through a chemical inhibitor (BLZ945) leads to a decrease in M2 Mφ polarization in patient-derived GBM xenografts, resulting in a significantly slower tumor growth rate [124].

Moreover, BLZ945 in combination with an anti-PDL1 antibody, is currently in phase I clinical trials in advanced solid tumors, including GBM [162].

Another target for GAM modulation is STAT3. It has been shown that GL261 GBM murine cells CM induced STAT3 activation in N9 microglia cells. This stimulated the expression of IL-10

and IL-6, which are cytokines involved with GAM polarization toward the M2 phenotype. Upon siRNA-mediated silencing of STAT3, N9 cells showed reduced M2 markers and increased M1 marker expression, such as TNF-α [163]. Currently, there are several STAT3 chemical inhibitors in distinctive phases of clinical trials, for various cancer types, including GBM. However, none of these inhibitors have been approved yet by the Food and Drug Administration for clinical use [164].

Another potential therapeutical target against GAMs is P-selectin, a 140kDa glycoprotein expressed in endothelial cells and platelets [165], recently found to be highly expressed in GBM [166]. Through the inhibition of P-selectin with neutralizing antibodies, small compound inhibitors, and shRNA, it was observed a decrease in M2 markers (*ARG1, IL10, TGFB1*), an increase in M1 marker (*iNOS*) and phagocytic ability in GAMs [167].

Although GAMs are heavily studied, further research is required to discover novel molecular mechanisms of immunosuppression and develop potential drug candidates to polarize GAMs into an inflammatory state. Currently, known immunosuppressive mechanisms are ineffective targets, since blocking a single pathway does not result in significant survival outcomes in clinical trials [97]. This could be due to the existence of other active mechanisms that assist TME immunosuppression, described in section 1.5.2. For example, anti-PD1 antibody (nivolumab) did not improve significantly the median overall survival in phase III clinical trials when compared to patients treated with an Anti-VEGF antibody (bevacizumab) [168]. Also, it was already stated in section 1.4.2.1, that GBM treatment with bevacizumab is not effective [61].

This claims for the usage and development of cell models that can properly sustain cell-to-cell interactions between microglia and glioma cells. The models currently used will be the focus of the next paragraphs.

1.6. Current models to study GBM tumor biology

The vast number of mutations involved, the broad heterogeneity, and the aggressiveness of GBM render this type of cancer particularly difficult to investigate. Over the last few decades, *in vitro* and *in vivo* preclinical models were generated, to study the mechanisms that lead to GBM onset and progression (Figure 1.9). Nevertheless, it is important to point out that novel methodologies are required, especially to better recapitulate heterotypic cell- to-cell interactions that occur in vitro, and that are important for brain tumor biology, cancer progression, and response to therapy.

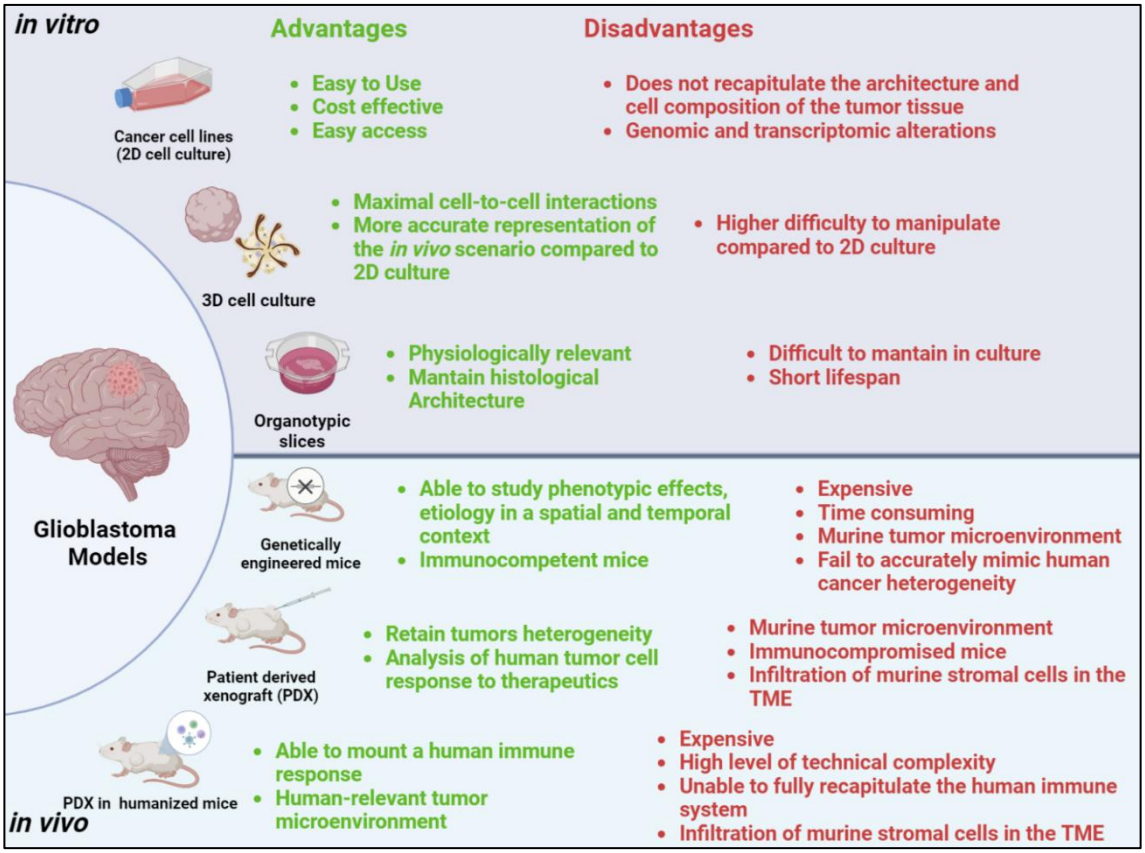

Figure 1.9 - Schematic representation of different glioblastoma (GBM) models. GBM models can be divided into two main groups: *in vitro* and *in vivo*. *In vitro* models are cancer cells lines in 2D cultures, 3D cell cultures and organotypic tissue slices. *In vivo* models include genetically engineered mice, patient-derived xenografts (PDXs), and PDXs in humanized mice. Adapted from [163-182] and created in biorender.com.

1.6.1. Animal models (*in vivo*)

1.6.1.1. Genetically engineered mouse models (GEMMs)

GEMMs are mice that undergo genetic alterations intending to induce a specific phenotype. Among all the available models, GEMMs have been exploited to study the etiology of GBM, the molecular basis and phenotypic aspects, in a spatial and temporal context [169]. Importantly, GEMMs are used to assess tumor progression, in a microenvironment that resembles the conditions for endogenous cancer onset. Generally, GEMMs do not require immunosuppressed mice, therefore they are good models to study interactions between GBM and the immune system. However, their applications are limited because GEMM establishment is very expensive and time-consuming, and it cannot recapitulate human tumor heterogeneity. Differential features between human and rodent GBM may lead to misleading data interpretation when investigating genetic drivers and treatment responses [170].

1.6.1.2. Patient-derived xenografts (PDXs)

PDXs are based on transplantation of patient-derived cancer cells into immunodeficient mice. These models became the gold standard for preclinical anti-cancer drug testing [171,172] because they present numerous advantages: the heterogeneity of tumor cells is retained and allows for analysis of human tumor cell response to a therapeutic regime. Although PDXs provide additional advantages over previous models, mice are immunosuppressed to allow patient-

derived cell engraftment, resulting in a less realistic tumor microenvironment. Additionally, human tissues engrafted in mice show infiltration of mice stromal cells within the tumor, that gradually substitute the original stromal components [173].

1.6.1.3. PDX in humanized mice

In recent years, humanized mouse models have been developed to overcome the major downsides of PDXs. Humanized mice are engrafted with human cells and tissues, such as human peripheral blood mononuclear cells (PBMCs), hematopoietic stem cells (HSCs) or even human bone marrow, and human fetal tissues (thymus and liver). Adding the human components along with the patient-derived tumor cells allows to mount a human immune response. With this model, the use of patient-derived tumor tissue to feature the genetic and epigenetic abnormalities aids the development of potential therapeutic approaches, that translate realistically to tumor patients [174,175]. Although humanized mice models present a breakthrough in cancer research, ethical issues are still a drawback, due to the high number of animals required. Additionally, humanized mice still lack key elements of a complete human immune system. For example, human T cells developing in these humanized mice do not recognize antigens in an MHC-restricted manner, impeding the investigation of human T cell responses against therapeutic proteins [176,177]. In addition, these models are expensive, and require a high level of technical expertise and cost [173].

1.6.2. Cell models (*in vitro*)

1.6.2.1. 2D cultures of GBM cell lines

The culture of established cell lines on plastic surfaces is the most accessible, straightforward, and easier model to study GBM. Several human GBM cell lines, including U87, U251, T98G, and A172, have been established in the past years to investigate the mechanisms underlying GBM biology [178,179]. Cell lines cultured as 2D monolayers have contributed to the discovery and characterization of cell signaling in cancer cells and represent a convenient model for high throughput screening of drug candidates [170]. The major downfall of 2D culture of cell lines is that a high number of passages leads to a high amount of genotypic and transcriptomic alterations resulting often in little resemblance with the tumor of origin [180]. In addition, 2D cell cultures lack cell-cell and cell-ECM interactions in three dimensions typical of the tissue. Additionally, transplantation of GBM cell lines into nude mice showed tumor homogeneity, limited necrosis, and microvascular alterations, that do not recapitulate *in vivo* GBM microenvironment [181].

1.6.2.2. 3D GBM cell models

3D cell cultures are based on cell aggregation and/or cell adhesion to a scaffold in three dimensions (3D), promoting maximal cell-to-cell interactions that resemble the *in vivo* dynamics. 3D cell cultures are a very useful tool to study molecular mechanisms, cell-to-cell interactions, and drug screening/development. When compared to *in vivo* models, 3D cell models present a higher reproducibility and throughput potential, while better representing the *in vivo* cell-to-cell and cell-ECM interactions than 2D cell cultures [182].

Current 3D models can be divided into two major groups: scaffold-dependent, in which cells are cultured in physical and mechanical supportive structures, and scaffold-independent, where cells rely on self-aggregation capabilities [183].

1.6.2.3. Scaffold-free 3D cell cultures

1.6.2.3.1. Hanging drop, force floating, and agitation-based cell aggregation

Scaffold-free 3D cell cultures rely on the self-aggregation ability of cells. Cell-to-cell contacts can be achieved using a variety of methods, such as the hanging drop method, the forced floating method, and collision-based methods in agitation [183].

The hanging drop method is based on gravity. A small drop of culture medium with a suspension of cells hangs on an inverted petri dish or is generated using specialized plates developed in recent years [184]. Cells aggregate in the bottom of the drop, forming a spheroid. Another possibility is the force floating method, which requires a low adhesion surface, to prevent cells from attaching to the culture plate. Suspended cells are brought together by lower-speed centrifugation, forming spheroids [183].

Agitation-based aggregation relies on cell collisions promoted by the orbital shaking or stirring (in bioreactors or spinner flasks) The stirred-tank systems present numerous advantages, like large-scale production of spheroids, improved mass transfer that results in homogeneous nutrient and oxygen availability [182].

1.6.2.3.2. GBM neurospheres

The most used 3D cell culture approach for GBM modeling is the neurosphere method. It relies on the capacity of CSCs to self-renew and proliferate. A single-cell suspension of GBM cells is plated at a low cell density in ultra-low attach (ULA) plates, in serum-free medium conditions supplemented with stem cell growth factors. These conditions favor CSCs survival and proliferation in sphere-like structures, as these cells are more resistant to anoikis than differentiated cancer cells, and respond to the stem cell growth factors added to the culture medium (e.g., EGF, FGF) [185–187]. Anoikis is a form of programmed cell death induced by the loss of cell adhesion to the ECM [188]. Various reports show GBM-derived neurospheres to present stemness markers, such as NESTIN, MUSASHI-1, CD44, CD133, OCT4, and SOX2 [189–194]. The presence of CSCs features is crucial to recapitulate chemotherapeutic resistance, and the heterogeneity of the GBM cell population [195].

1.6.2.4. Scaffold-dependent 3D cell models

Scaffold-based culture technologies provide physical and chemical support for cells to grow. Scaffolds can have a biological or synthetic origin. The biological scaffold includes alginate, collagen I, fibrin, and matrigel [183]. Some beneficial aspects are the high biocompatibility and natural adhesive properties. Biological scaffolds can sustain physiological cell functions. These include controlled proliferation and/or differentiation, cell phenotype and functionality. One of the most used scaffolds in 3D cell cultures is Matrigel, a protein mixture secreted by Engelbreth-Holm-Swarm (EHS) mouse sarcoma cells that resemble basement membrane composition: laminin,

collagen IV, heparan sulfate proteoglycans, entactin/nidogen, enzymes like matrix metalloproteinases and several growth factors including EGF, basic fibroblast growth factor (BFGF), NGF, PDGF, IGF-1, and TGF-β [196]. Although there are numerous successful 3D cultures performed using matrigel, like the organoids described in the next section, there are major disadvantages associated with this scaffold, such as: the animal origin, the complex composition with numerous soluble factors with biological activity and the batch-to-batch variability [197], which may negatively impact experimental reproductivity. Moreover, matrigel cannot be manipulated biochemically or physically, making it difficult to fine-tune the matrix to promote intended cell behaviors and achieve specific biological outcomes [198].

Examples of synthetic hydrogels used in 3D cell models are polyethylene glycol (PEG), polylactic acid (PA), or polyglycolic acid (PGA). These scaffolds are relatively inert, inexpensive, usually easy to tune through synthesis or crosslinking, and reproducible, supporting the acquisition of consistent results [199–201]. On the other side, artificial polymers lack adhesive moieties found in natural ECM and require previous biological knowledge to define the biological peptides to be crosslinked, to improve scaffold functionality [183,202].

1.6.2.4.1. Organoids

Organoids are 3D cultures of stem cells within an ECM scaffold (typically matrigel) that proliferate and undergo multi-lineage differentiation. The distinct cell populations self-organize, mimicking structural features and functional properties of the organ of origin [203]. In the case of GBM research, two main types of organoids have been employed – patient-derived organoids (PDOs), generated from patient-derived tumor cells, and cerebral organoids (COs), derived from pluripotent stem cells, and reviewed in [170].

PDOs rely on culturing GBM cells directly derived from patients. The main advantage of PDOs is the expansion of GBM cells retaining tumor heterogeneity, which makes this a suitable model for precision medicine and to study immunotherapeutic modalities and allows biobanking [204]. Recently, Jacob *et al*. developed a protocol for generation of scaffold-free GBM organoids (named GBOs) from fresh tumor specimens, without single-cell dissociation. This method is scaffold-free, and the culture medium has a defined composition. GBOs were cultured under agitation to facilitate the organoid formation and to guarantee homogeneous diffusion of nutrients and oxygen. Although less time-consuming than previous PDO methodologies (1-2 weeks versus 1-2 months), there are still pitfalls to be overcome, such as the tendency to diverge genetically from the primary tumor over very large numbers of passages [170].

COs recapitulate early stages of human brain development and comprise diverse brain cell types, such as neural progenitors, neurons, astrocytes, and oligodendrocytes. Therefore, in these models, the GBM microenvironment neural cell components are represented. COs engineered using gene-editing tools have been employed to study GBM onset [170,205,206]. Amplification of oncogenes and mutations in tumor suppressor genes were introduced into neuroepithelial progenitors during CO differentiation. These included common GBM genetic alterations, such as *CDKN2A*$^{-}$, *PTEN*$^{-}$, *TP53*$^{-}$, *EGFR*^{OE} and *EGFRvIII*^{OE}, and their combinations typically presented

in patients [170,205]. The resulting COs, named neoplastic cerebral organoids (NeoCORs), recapitulated transcriptomics profiles and presented markers typically associated with GBM in the clinic. In another study, mutant *RAS* and *TP53* disruption were introduced in mature COs, leading to oncogenic transformation, Tumor cells showed an invasive phenotype when co-cultured with non-transformed COs and oncogenic potential when transplanted into mice [206].

Co-cultures of COs with GBM cells have also been proposed by other authors. Silva *et al* co-cultured early-stage COs with GBM CSC spheroids. CSCs adhered and migrated into the COs; Linkous *et al*. co-cultured COs with GSCs isolated from patient tumors, generating what the authors termed the cerebral organoid glioma (GLICO) model [206,207]. GLICO organoids generated with GSCs from different patients showed distinct invasive properties and sensitivities to chemotherapy and radiation therapy [206]. Nonetheless, this methodology comes with two main limitations: 1) the requirement for patient-derived GSCs, and 2) it is more time consuming then previous models due to spheroids derivation [170].

1.6.2.5. Organotypic tissue slices

Organotypic tissue slices represent a physiologically relevant model for studying the tumor microenvironment, since the methodology preserves the tumor histological architecture and contains other cell types, such as immune cells and endothelial cells [208]. This model requires a tumor resection from a patient/animal model, sliced into sections, and cultured in petri dishes. Some studies have used this model to study glioma cell signaling [209], invasion [210], and GBM-microglia interactions [211]. However, organotypic tissue slices have a short life span and it is challenging to maintain the viability of the different cell populations [212]. In addition, most studies are performed with mice organotypic slices due the low abundancy of human tissue samples [209,210,212].

1.6.3. *In vitro* microglia models

To study interactions between CNS immune cells and GBM *in vitro*, co-cultures of these two cell types appear as the best way to maximize heterotypic cell signaling, via soluble mediators and cell-to-cell contacts. To attain such a model, a microglia model that retains phenotype and functionality similar to the *in vivo* microglia is required. Currently, the cell sources available are immortalized microglia cell lines, microglia-like cells derived from monocytes (MLC-Mo) or human induced pluripotent stem cells (MLC-hiPSC), and primary cultures of freshly isolated human microglia [213]. In this section, each of these microglia models will be described.

1.6.3.1. Microglia cell lines

Human microglia cell lines are immortalized by viral transduction with oncogenes and derive from the brain or the spinal cord. One of the advantages of these *in vitro* models is the extensive proliferative capacity, easy maintenance, and high availability [213]. The most common human microglia cell lines used in CNS studies are HMC3 and C20. HMC3 (also reported as CHM3) is derived from the human spinal cord and cortical cells of 8 to 12-week embryos, which were transduced with a plasmid encoding for the large T antigen of SV40 (Figure 1.10) [214,215]. C20 originated from human cortical tissue, stably transduced with SV40 T antigen (SV40) and human

telomerase reverse transcriptase, to bypass senescence [216]. Both cell lines were successfully employed in multiple studies [216–220], and are reported to express some microglia markers [221]. However, due to immortalization and long-term culture, alteration of the cell phenotype may occur. Typically, higher cell passages lead to genomic and transcriptomic alterations. In addition, cell lines in general show high lab-to-lab cell genetical and phenotypical variability [222]. A recent transcriptomics study has in fact pointed out that microglia cell lines differ both genetically and functionally from freshly isolated microglia and microglia cultured *ex vivo* [213].

1.6.3.2. Microglia-like cells derived from monocytes (MLC-Mo)

A method for differentiation of monocytes into microglia-like cells was recently established by Etemad *et al*. Monocytes were isolated from PBMCs and cultured for 14 days in a serum-free medium, in the presence of M-CSF, GM-CSF, β-NGF, and CCL2 (Figure 1.10). The initial characterization of MLC-Mo showed that these cells presented low levels of CD45, CD14, MHCII, CD11B, and CD11c; undetectable levels of CD40, CD80, and CD83, and a distinct pattern of chemokine receptors (positive for CCR1, CCR2, CCR4, CCR5, CXCR1, CXCR3, CX3CR1; negative for CCR6 and CCR7). This resembles the profile of human microglia [118]. Variation on the methodology has been shown, using a combination of GM-CSF, M-CSF and IL-34 [223]. The MLC-Mo method has the advantage of generating MLCs with a gene expression that resembles human primary microglia. Additionally, easy access to PBMC makes this *in vitro* model very appealing. However, differentiation into functional MLC-Mos takes 14 days [118]. MLC-Mos have been employed in inflammatory response studies in schizophrenia [224], development of Alzheimer`s disease therapeutics under pre-clinical trials[225], human immunodeficiency virus (HIV) infection replication and pathogenesis [221].

1.6.3.3. Microglia-like cells derived from human induced pluripotent stem cells (MLC-hiPSCs)

Presently, there are multiple methods for differentiation of microglia-like cells from hiPSC, based on the exposure to defined factors and/or viral transfection [213,226]. Additionally, there are commercial kits available, such as the one from StemCell™ Technologies (Figure 1.10). The major downfalls of these models are that they are time-consuming and require expensive reagents for differentiation [213].

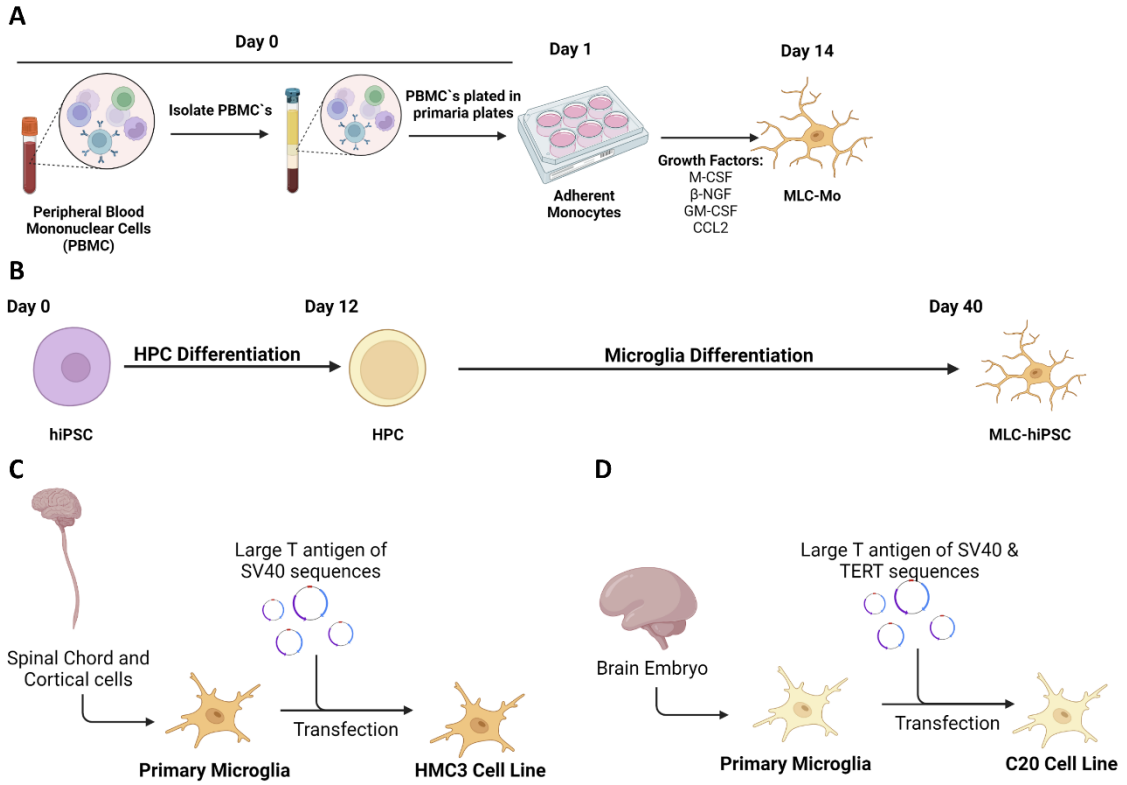

Figure 1.10 - Main microglia cell models. A – Peripheral blood monocytic cells plated in primaria plates to promote monocytes adherence. After 24 h, monocytes are cultured in serum free medium supplemented with microglia growth factors (macrophage colony stimulating factor, M-CSF; human beta-nerve growth factor, β-NGF**;** granulocyte macrophage colony stimulating factor, GM-CSF; C-C motif chemokine 2, CCL2) and kept in culture for 14 days to attain MLC-Mo. **B –** Human induced pluripotent stem cells (hiPSC) are firstly differentiated to hematopoietic progenitor cells (HPCs) and then to microglia-like cells (MLC-hiPSCs). **C –** The HMC3 cell line is derived from spinal cord and cortical cells that were transfected with simian vacuolating virus 40 (SV40) sequences. **D –** The HMC3 cell line is derived from cells from 8–12-week embryos that were transfected with SV40 and telomerase reverse transcriptase (TERT) sequences. Panel A adapted from [118]. Panel B adapted from [205], Panel C and D adapted from [206, 207] respectively. All figures were created in biorender.com.

1.6.3.4. Primary cultures of human microglia

Human microglia cells are normally obtained from post-mortem fetal or adult brain tissue (available from abortions and deceased donors, respectively). Primary cultures of human microglia is the cell source that better reflects the phenotype and genetic variability of the human population compared to cell line-derived microglia [227]. Limitations include the limited availability of (healthy) adult brain tissue, lack of control over the ante-mortem conditions, and variable post-mortem delay, which might affect the microglia phenotype [228,229].

1.7. Current GBM microenvironment *in vitro* models to study brain cancer and potentially GBM-GAMs interactions

Several models have been established in the literature to study interactions between non-neoplastic cells and GBM and/or to test the potential of novel pharmaceuticals. Recently, a bioprinting-based model proposed by Tang *et al.* was established employing as scaffold gelatin methacrylate (GelMA) and glycidyl methacrylate-HA (GMHA) hydrogels. Here, by using sequential cell printing in the hydrogel, human astrocytes, PDX-derived GBM neurospheres, Mφ

(derived from either hiPSC, PBMCs or THP1) and neural precursor cells (source of neurons) were progressively deposited on the hydrogel scaffold. By using this “3D tetra-culture cell model” authors observed recapitulation of patient transcriptional signatures similar to GBM tissues, maintenance of stemness, invasion, and drug resistance [230]. Moreover, the tetra 3D cell culture model showed increased expression of M2-related genes *IL-10* and *CD163* compared to 2D Mφ, which corroborates previous observations [76,139]. In addition, the authors observed that GBM cells displayed increased migratory ability when in presence of Mφ [230].

Although this model recapitulates several features of the GBM TME, it does not include microglia that is known to represent a large portion of the GBM TME along with blood-derived Mφ [231], oligodendrocytes, and differentiated neurons that are essential components that interact with GBM [76,107,109,110].

Leite *et al.* developed a co-culture GBM model with the microglia cell line HMC3. Here, microglia promoted tumor cell proliferation, migration, and TMZ resistance [232]. The authors showed a partial response of HMC3 microglia cells after inflammatory stimuli (LPS+IFN-γ), yet the effect of the presence of GBM cells toward microglia polarization was not investigated [232]. Chen *et al.* performed a similar 3D co-culture model approach by using patient derived GBM cells to study their paracrine interactions with primary murine microglia. In this study, a methacrylamide functionalized gelatin scaffold was employed to prevent GBM cells-microglia contact [233]. The authors described that GBM cells showed increased cell proliferation and decreased cell invasion when co-cultured with microglia, compared to 3D GBM monoculture. Although increased proliferation in GBM cells co-cultured with microglia has been reported in other studies [232,234] decreased GBM invasion capacity due to the presence of microglia is in contrast with other studies [211,232,234]. This disagreement in the literature could be technical since reports tested invasion in GBM co-cultures/organotypic slices in different scaffolds (matrigel, methacrylamide-functionalized gelatin). Additionally, matrigel batch-to-batch variability may also have an impact on the outcomes [197]. Another element is the diverse microglia sources used (e.g., mainly human, primary murine, HMC3 cell line) or primary GBM cells that could influence the results. Finally, secretome analysis in this model [233] showed CCL2 secretion, which is observed in patient-derived cells[78] and GBM cell lines (U-105 MG and U-251 MG) [235].

Relative to the co-culture model systems described [233], they lack several of the TME GBM components (e.g., astrocyte, neurons and oligodendrocytes). This limits the recapitulation of TME complexity necessary to study in a more detailed manner GBM oncobiology. In addition, Chen *et al.* [233] model studied only paracrine GBM-microglia interactions, without covering cell-to-cell interaction analysis.

Another model to recapitulate GBM-TME complexity is a co-culture system of patient-derived GBM cells, astrocytes, and murine microglia, assembled in a fibrin scaffold. In addition, the co-culture is set in a vascular mimicry with brain pericytes and endothelial cells [236]. This system presents a significant advantage over previously mentioned models [233,237,238], due to the presence of blood vessel mimicry, which features angiogenesis, one of the cancer hallmarks

[239]. This system, established by Neufeld *et al.,* shows similar growth curves, drug response, and genetic signature of this model platform compared to orthotopic cancer mouse models, as opposed to 2D static cultures [236]. This result confirmed previous observations on the fact that GBM cells cultured in 2D cell cultures are far from recapitulating GBM features [170]. However, this latter model, similarly to the previous ones [233,237,238], does not include CNS cells such as neurons and oligodendrocytes that interact with GBM cells [76,110]. Moreover, the use of a fibrin scaffold does not recapitulate GBM ECM, which is composed mainly of collagen IV and low molecular weight hyaluronic acid [85].

1.8. Aim and objectives

This thesis is integrated in a project that aims to decipher immunosuppressive events in rare brain gliomas by developing and interrogating recapitulative 3D cell models of the brain cancer microenvironment (Figure 1.11). To attain such models, the molecular crosstalk between tumor cells, microglia cells and astrocytes must be recapitulated. Another important aspect is that the system is amenable to challenge with advanced therapeutics. Such models can be instrumental in the study of immunosuppressive mechanisms in distinct brain cancer types and to advance immunotherapeutic approaches.

The strategy proposed for setting up of the 3D glioma microenvironment models is to establish co-cultures of CNS neurospheroids (3D structures composed of neurons, astrocytes, and oligodendrocytes) differentiated from hiPSC cultures, following a methodology established in the host laboratory [240]. These neurospheroids will be co-cultured with microglia and 3D spheroids of glioma cells, in stirred-tank bioreactors, in which environmental culture conditions can be tightly controlled [241].

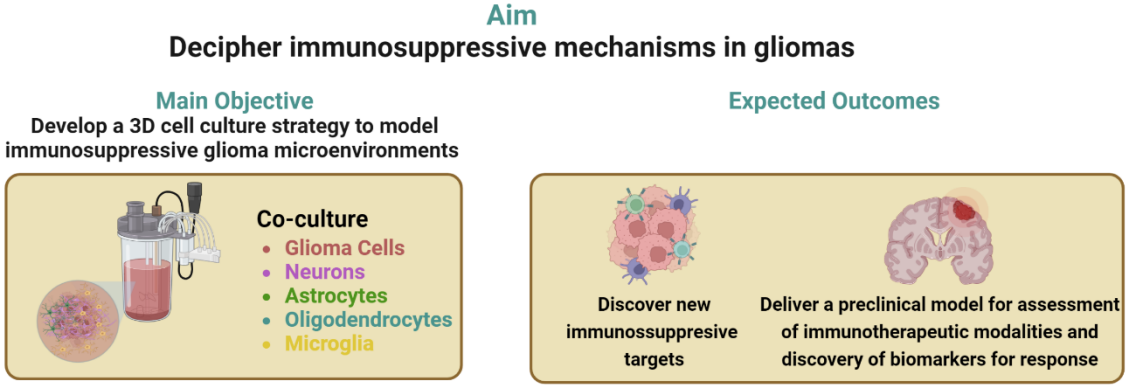

Figure 1.11 - Scheme of the project in which this thesis is integrated, that aims to decipher immunosuppressive events in rare brain gliomas.

In this thesis, the aim was to define methodologies for 3D co-culture of tumor and microglia cells and set-up analytical assays for their characterization, all to be latter employed in the development of the 3D models of immunosuppressive glioma microenvironments.

As such, three main objectives were set for this thesis:

1. Selection of a microglia cell source
2. Selection of a 3D GBM cell culture methodology
3. Proof of concept: Initial co-culture assessment

1 – Selection of a microglial cell source to be used in the co-culture studies (to be performed in the Objective 3), three microglia sources were evaluated: 1) microglia-like cells derived from monocytes (MLC-Mo), 2) immortalized microglia cell lines (HMC3 and C20), and 3) microglia-like cells derived from hiPSC (MLC-hiPSC) (Figure 1.12).

The microglial cells obtained from each of the cell sources were evaluated in terms of: 1) microglial phenotype: expression of microglial genes by quantitative reverse transcription polymerase chain reaction (RT-qPCR) and detection of microglia protein markers by immunofluorescence (IF), western blot and flow cytometry (FC) (Task 1.1); 2 – microglial functionality, through the evaluation of the ability to respond to prototypical pro- and anti-inflammatory stimuli through modulation of cytokine expression (RT-qPCR and IF) (Task 1.2).

2 - Selection of a 3D GBM cell culture methodology

To select a method for generation of 3D GBM cell cultures which resemble the *in vivo* phenotype, the human A172 GBM cell line was employed**.** This cell line was chosen due to the presence of the PTEN mutation which is one of the common alterations observed in GBM [12,160]. Moreover, the A172 cell line is classified within the GBM mesenchymal subtype [178], which is associated with worse prognosis and higher therapy resistance than other GBM subtypes [242]. In addition, several studies employed this cell line to perform 3D cell culture [243–245], which this task will rely on. Lastly, the A172 cell line was used among other cancer cell lines to study microglia-induced cancer cell migration [246,247].

To attain the objective, two tasks were defined: **Task 2.1** - Implementation of 3D cell cultures employing two methodologies and their characterization in terms of cell viability and morphology; **Task 2.2**- Evaluation of the expression of GSC marker genes and immunosuppressive cytokine genes by RT-qPCR, and protein detection by WB and IF (Figure 1.12).

In Task 2.1, two scaffold-independent methodologies were tested for the generation of 3D GBM cultures. One was the neurosphere formation assay, largely used in studies with GBM cell lines (A172, U251, TG98 and U118), and primary GBM cells [243,248,249], in which survival and aggregation of CSCs is favored by the culture conditions. Alternatively, an agitation-based method widely used in the host laboratory and implemented for a large panel of cancer cell lines [241,250,251] was also tested. Single cell suspensions of A172 cells were inoculated in spinner flasks, so that the continuous agitation could promote cell-to-cell collision, therefore inducing generalized cell aggregation and leading to spheroid formation. Despite being widely used in cancer research, this last methodology has never been reported for glioma cells.

3 - Proof of concept: Initial co-culture assessment

To attain this objective, two tasks were planned: **Task 1:** characterization of the phenotype of the microglia cell source chosen in objective 1 when cultured in neurosphere CM; **Task 2**: evaluate the feasibility for co-culture of microglia with GBM neurospheres generated by the method selected in objective 2. Cell viability and microglia gene expression were characterized in a preliminary assay (Figure 1.12).

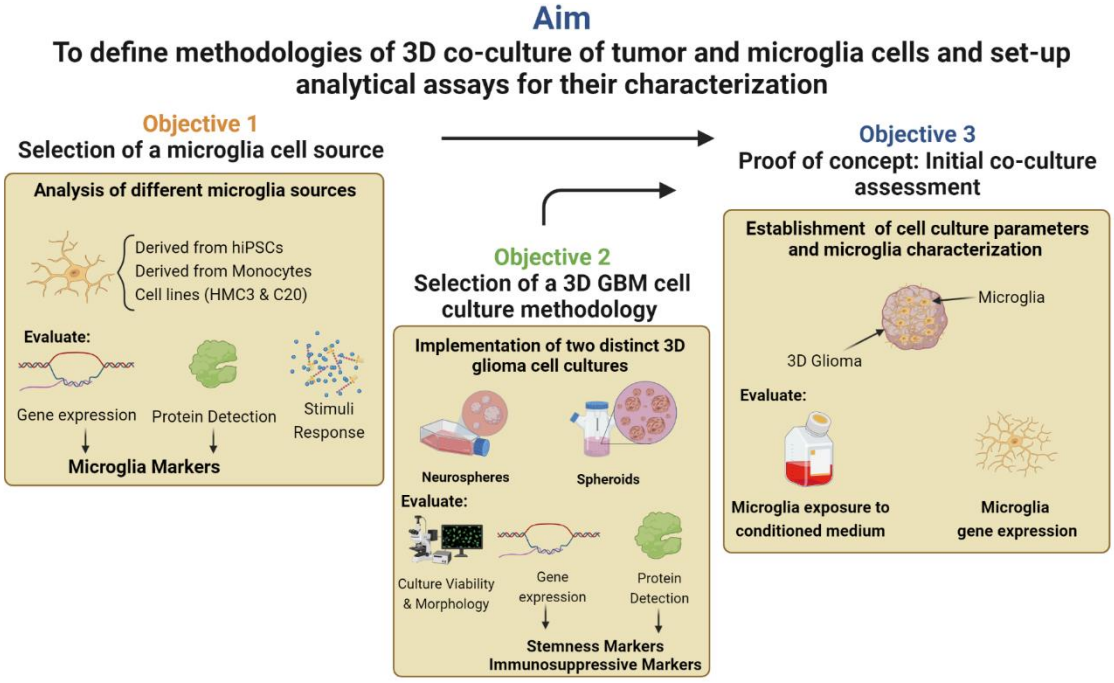

Figure 1.12 - Scheme representing the thesis aim, objectives and workplan. Three main objectives were defined: to select an appropriate microglia cell source, by analysing microglia derived from monocytes and microglia human cell lines, namely HMC3 and C20; to select the best 3D GBM cell culture strategy; and to develop a 3D co-culture of GBM cells and microglia cells that recapitulates the interactions between these two cell types.

Chapter 2. Materials and Methods

2.1. Cell culture

2.1.1. Cancer cell lines 2D cell culture

Established A172 GBM and C20 microglia cell lines were cultured with Dulbecco's modified eagle medium (DMEM) supplemented with 4.5 g/L of D-glucose, L-glutamine, and pyruvate (Gibco™ #41966052), 10% (v/v) fetal bovine serum (FBS) (Gibco™ #A3160801).

THP1 and MDA-MB-231 cells were cultured in Roswell Park Memorial Institute (RPMI) 1640 (Gibco™, #11875093) medium supplemented with 10% (v/v) FBS.

Cells were kept in a humified incubator at 37 ^{o}C and 5% CO_2. All cell lines were subcultured twice a week, at a seeding density of 0.8x10^4 cell/cm^2 (A172) and 1 x10^4 cell/cm^2 (MDA-MB-231), and a seeding concentration of 2 x10^5 cell/mL for THP1. For subculture, adherent cells were washed with Dulbecco's phosphate-buffered saline without Ca^{2+} and Mg^{2+} (DPBS (-/-), Gibco™, #141190144) followed by incubation with 0.05% (v/v) trypsin-ethylenediamine tetraacetic acid (EDTA) (Gibco™, #25300062) for cell detachment. Afterward, trypsin was inhibited by the addition of complete medium containing FBS. THP1 cells were sub-cultured twice a week; eventual adherent cells were trypsinized and maintained in culture, along with cells growing in suspension.

2.1.2. Microglia cell lines

The HMC3 microglia cell line was cultured in eagle´s minimum essential medium (EMEM) supplemented with 10% (v/v) of FBS. The C20 microglia cell line was cultured with DMEM containing 4.5 g/L of D-glucose, 42.0 mg/L of L-glutamine, 110 mg/L of sodium pyruvate, 15 mg/L of phenol red and supplemented with 10% (v/v) FBS. Cells were kept in a humified incubator at 37 ^{o}C and 5% CO_2. Microglia cell lines were subcultured twice a week, at a seeding density of 5 000 cell/cm^2 (HMC-3 and C20). For subculture, adherent cells were washed with DPBS (-/-), followed by incubation with 0.05% (v/v) trypsin-EDTA for cell detachment. Afterward, trypsin was inhibited by the addition of complete medium (containing 10% (v/v) FBS).

Cancer and microglia cell lines were maintained in culture for up to two months after thawing and regularly tested for *Mycoplasma* contamination. For the mycoplasma test, the culture supernatant was incubated at 95 ^{o}C for 10 min, spun down at 13 000 rpm and transferred into a new labeled microtube. Subsequently, the sample was sent to GATC biotech, the company providing the *Mycoplasma* test.

2.2. 3D GBM culture

2.2.1. A172 neurosphere cultures

A172 cells were dissociated by trypsinization and plated at a seeding density of 20 000 cell/mL in T25 ultra-low attachment (ULA) culture flasks (Corning, #4616) in a serum-free medium composed by DMEM containing 4.5 g/L of D-glucose, 42.0 mg/L of L-glutamine, 110 mg/L of sodium pyruvate, 15 mg/L of phenol red and supplemented with 20 ng/mL of BFGF and EGF, 2% (v/v) of B27, 1% (v/v) of N2 and 5 µg/mL of heparin, as described in Table 1. Neurospheres were kept in a humified incubator at 37 °C and 5% CO_2, for up to 2 weeks, with addition of fresh medium

(same volume as inoculated cells) after the first week (Figure 2.1). The condition for the establishment of the neurosphere cultures were implemented in the host Lab according to a previous publication [252].

Table 1 - Composition of the medium for culture of A172 neurospheres.

Medium components	Concentration	Brand	Catalogue number
DMEM [+] 4.5 g/L D-glucose [+] 42.0 mg/L L-glutamine [+] 110 mg/L Pyruvate [+] 15 mg/L Phenol red	[1X]	Gibco™	#11965092
Basic fibroblast growth factor	20 ng/mL	PeproTech	#100-18B
Epidermal growth factor	20 ng/mL	PeproTech	#AF-100-15
B27	2% (v/v)	Gibco™	#17504044
N2	1% (v/v)	Gibco™	#17502048
Heparin	5 µg/mL	Stem cell technologies	#07980

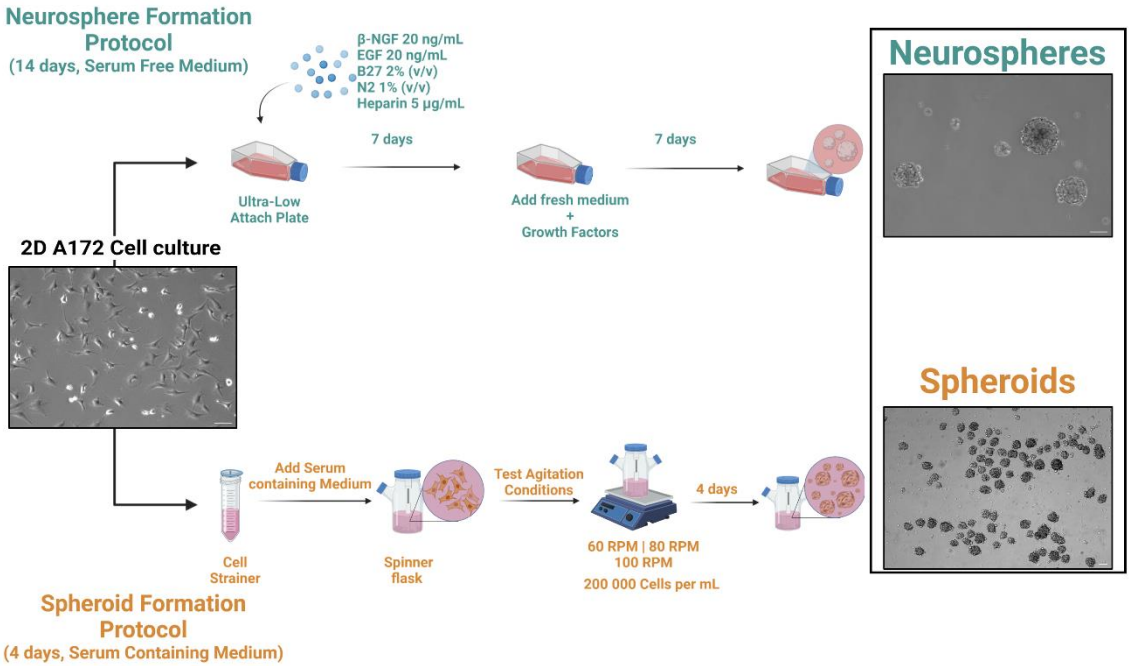

Figure 2.1 - Schematic representation of the implemented A172 3D cell culture strategies. Scale bar: 50 µm

2.2.2. Spheroid formation in agitation-based culture systems

2.2.2.1. Spinner flask preparation

The spinner vessels were silanized to reduce surface hydrophobicity, and consequently, reduce cell adherence to the glass. Silanization procedure required first a cleaning step with 1 M of potassium hydroxide (KOH) (Merck, #105033) in ddH_20 overnight. Afterward, spinner

vessels were submitted to dicloromethysilane (Merck, #803452) coating and excess solution removal with toluene (Merck, #108325).

The impeller of the spinner vessel was coated with polydimethylsiloxane (PDMS) to avoid cell infiltration into the impeller fenestrations, during culture. First, a two-component mixture of elastosil RT601 A (Wacker, #124690) and B (Wacker, #124691) was prepared at a ratio of 9:1. The mixture was applied to fill the interior and lateral fenestrations. Subsequently, the impeller was placed at 37 °C to solidify. Later, the spinner flask was sent to the autoclave and was ready to use.

2.2.2.2. Spheroid formation assay

Adherent A172 cells were washed with DPBS (-/-) and detached using 0.05% (v/v) trypsin-EDTA (Gibco, #25200056)**.** Subsequently, trypsin was inactivated with a complete A172 culture medium with 10% (v/v) of FBS, counted with trypan blue solution 0.1% (v/v) (Gibco, #15250-061) in a fuchs-rosenthal counting chamber (Karl Hetch #4049712). Afterward, cells were centrifuged at 300 × *g* for 5 min using a 5810R centrifuge equipped with an A-4-81 rotor (Eppendorf) and the supernatant was discarded. The cell pellet was suspended in fresh A172 medium, supplemented with serum. Subsequently, the cell suspension was filtered through a 70 µm cell strainer (Falcon, #352350) to ensure a single-cell suspension.

Then, A172 cells were inoculated into 125 mL glass spinner vessels with 70 mm flat center cap, two 32 mm angled side arms, and three side baffles (Corning, #4500-125) at a concentration of $2x10^5$ cell/mL. A172 cells were cultured up to four days at 37 °C and 5% CO_2 under different stirring rates (60 rpm, 80 rpm, and 100 rpm), set by a bioMIXdrive 1 single point stirring drive (2mag AG) with bioMIX control 4MS external control unit (2mag AG) set.

Cell viability was assessed by fluorescein diacetate (FDA)/TO-PRO™-3 staining as described below using the DMI6000B fluorescence microscope (Leica) with the Las X Life Science Software, every day during the culture. On day 4, cell morphology parameters (area, max feret diameter, and roundness) were determined using the icy bioimaging analysis software [253].

2.3. Neurosphere/Spheroid differentiation assay

Neurospheres and spheroids suspension cultures were plated under a plastic surface. After 24 h, 3D structures adhered to a plastic surface, and the medium was replaced with A172 medium supplemented with 10% (v/v) FBS. Cells were incubated for 2-3 days at 37 °C and 5% CO_2 until cells reached full 2D adherence. Subsequently, cells were subjected to RNA extraction and RT-qPCR analysis, as described below. Gene expression levels of *POU5F1*, *NANOG*, *SOX2*, *NES, IL10, CCL2, CSF1,* and *TGFB1* in the 3D cell cultures (before plating in 2D) and after adherence in 2D cultures were analyzed by RT-qPCR analysis, comparing the gene expression levels with the ones detected in the original 2D cell culture, used to establish neurospheres and spheroid cultures. Results are shown as fold change in gene expression compared to the original 2D cell culture, which was set to 1.

2.4. Microglia and macrophage differentiation

2.4.1. Microglia differentiation from monocytes

Induction of MLC-Mo was performed according to the protocol described by S. Etemad *et al.* [118]. In brief, peripheral blood mononuclear cells (PBMCs) were plated in primaria™ 6-well plates (Corning #353846), at a seeding density of $9x10^6$ cell/ well, in RPMI 1640 medium (Gibco, #11875093), in serum-free conditions, and kept in a humified incubator at 37 °C and 5% CO_2. The following day, non-adherent cells (mostly T and NK cells) were removed through three washes with DPBS (-/-). The adherent monocytes were cultured in RPMI supplemented with 10 ng/mL of M-CSF, 10 ng/mL GM-CSF, 100 ng/mL CCL2, 10 ng/mL of human β-nerve growth factor (β -NGF) and 1% (v/v) of penicillin-streptomycin (PenStrep), as described in table 2. Half of the culture supernatant was exchanged by fresh medium every 3 to 4 days, up to 14 days, providing fresh medium and factors (Figure 2.2).

Table 2 - Culture media composition for differentiation of microglia like cells derived from monocytes (MLC-Mo).

Medium components	Concentration	Brand	Catalogue number
Roswell Park Memorial Institute 1640 (RPMI 1640)	[1X]	Gibco™	#11875085
Macrophage Colony Stimulating Factor (M-CSF)	10 ng/mL	PeproTech	#300-25
Granulocyte Macrophage Colony Stimulating Factor (GM-CSF)	10 ng/mL	PeproTech	#300-03
C-C Motif Chemokine 2 (CCL2)	100 ng/mL	PeproTech	#300-4
Human β-Nerve Growth Factor (β-NGF)	10 ng/mL	PeproTech	#450-01
Penicillin-Streptomycin (PenStrep)	1% (v/v)	PeproTech	#15140-11

2.4.2. Macrophage differentiation from monocytes

PBMCs were thawed and plated in primaria™ 6-well cell plate (Corning #353846) at a seeding density of $9x10^6$ cell/well, in RPMI supplemented with 10% (v/v) FBS, and 50 ng/mL M-CSF (Peprotech). Cells were kept in a humified incubator at 37 °C and 5% CO_2 for seven days. At day seven, cells were washed three times with DPBS (-/-) to remove non-adherent cells and fresh medium was added to maintain macrophages (Mφ) in culture with a M0 phenotype (Figure 2.2).

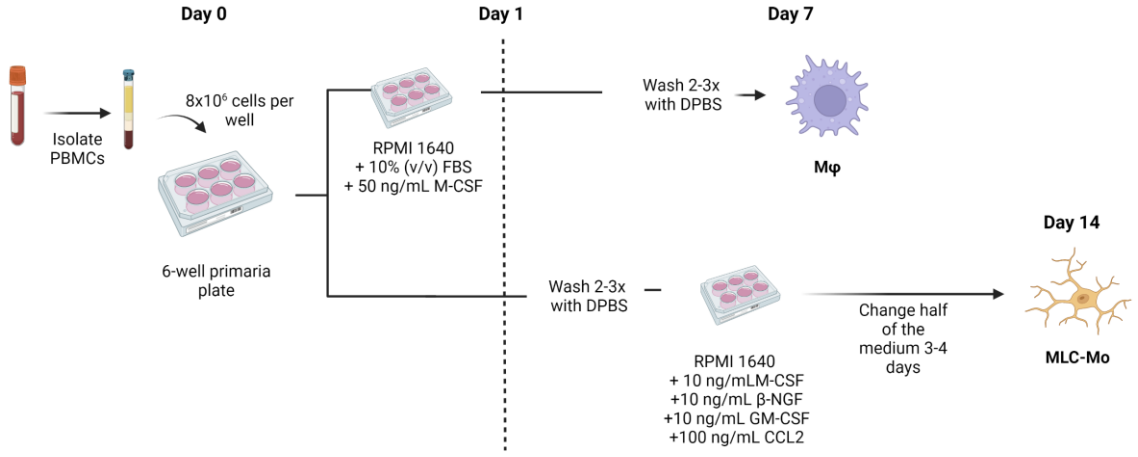

Figure 2.2- Microglia like cells and macrophages (Mφ) differentiation protocol derived from peripherical blood mononuclear cells (PBMCs).

2.5. Co-cultures of microglial and GBM cells

For co-culture assays, PBMCs were thawed and differentiated into MLC-Mo, for 14 days (Figure 2.3). For the GBM component, A172 neurosphere formation was initiated on the 7th day of microglia differentiation. After seven days of neurosphere formation, cells were dissociated with TrypLE™ express enzyme (without phenol red, GibcoTM, #126050010), and resuspended in DPBS (-/-) to determine the cell concentration.

For detachment of MLC-Mo, cells were incubated in 10 mM EDTA, pH 8.0 (diluted from a 0.5 M stock, Invitrogen, #15575020), at 37 °C, for 10 min. MLC-Mo was then labeled with CellTrace™ Yellow (Invitrogen, #34567), to distinguish the cell population in the co-cultures and to track single cell infiltration within the neurospheres. MLC-Mo collected in DPBS (-/-) were centrifuged at 400 x *g* for 10 min and suspended in 2.5 µM of CellTrace™ Yellow (diluted in DPBS (-/-) with 2% (v/v) FBS), and incubated under agitation, for 20 min, at 37 ºC. Then, cells were incubated with RPMI 1640 medium supplemented with 1% (v/v) FBS, for 5 min, at 37 ºC, to remove unbound dye.

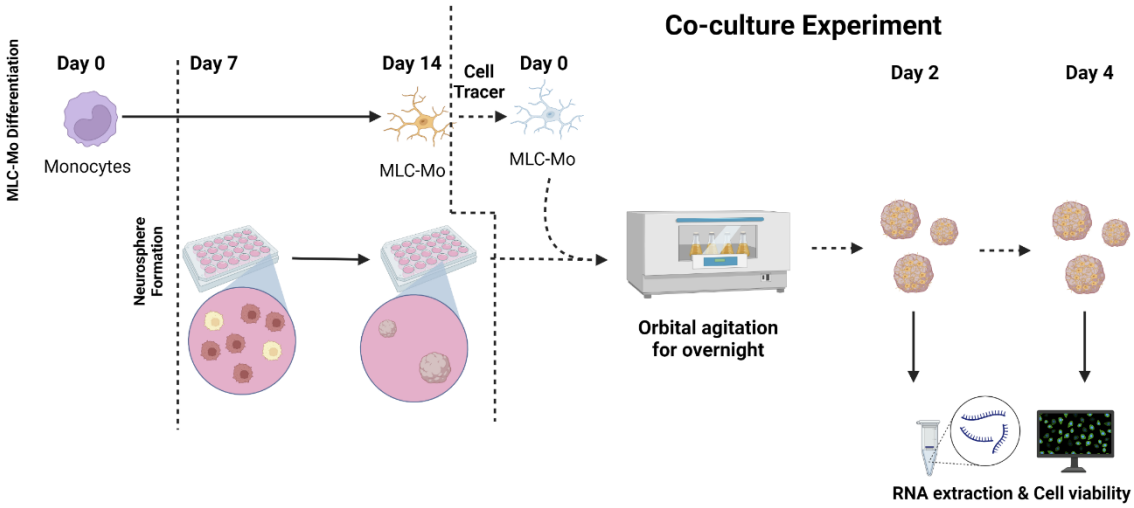

Figure 2.3 - Schematic representation of the co-culture experiment haboring glioblastoma (GBM) neurospheres and microglia-like cells derived from monocytes (MLC-Mo).

Cells were then centrifuged 400 x *g* for 10 min and resuspended in RPMI 1640 medium supplemented with the growth factors used in microglia differentiation and in neurosphere formation, as described above (Section 2.4.1 and 2.2.1 respectively). MLC-Mos labelled with CellTrace™ Yellow were added to 7th-day A172 neurosphere cultures, in 24 ULA culture flasks (Corning, #CLS3473), to obtain co-cultures of MLC-Mo: GBM cells at a 1:1, co-cultures were cultured under agitation (80 rpm), overnight, to promote MLC-Mo adherence to the neurospheres. After this period, the co-cultures were kept in static conditions for four days, at 37 °C. On days two and four, cell viability and MLC-Mo adherence to neurospheres were assessed by fluorescence microscopy. Cells were collected for RNA extraction, to characterize expression of M1 and M2 marker genes. MLC-Mo challenged with prototypical pro- and anti-inflammatory stimuli were used as positive controls and A172 neurospheres as the negative control. The analytical procedures are described below (Section 2.8).

2.6. Challenge of microglial cells

In order to polarize Mφ/microglial cells to an inflammatory (M1) state, cells were incubated with 10 ng/mL lipopolysaccharide (LPS, #L4391, Sigma-Aldrich) and 50 ng/mL interferon-γ (IFN-γ, #300-02-100, PeproTech EC Ltd.); to polarize cell to an anti-inflammatory (M2) state, 20 ng/mL interleukin-4 (IL-4) and 20 ng/mL interleukin-13 (IL-13, #AF-200-04 and #AF-200-10, respectively, from PeproTech EC Ltd) were used.

To assess the effect of GBM neurosphere-derived factors on the phenotype of MLC-Mo, cells were exposed to CM from A172 neurosphere cultures, diluted 1:1 in fresh microglia medium. As control, cells were incubated with fresh neurosphere medium (NF) diluted 1:1 in microglia medium or fresh microglia medium only.

During the 48 h of challenge, cells were kept in a humified incubator with 5% CO_2 at 37 °C. Afterwards, cells were either fixed for immunofluorescence (IF) analysis or subjected to RNA extraction for gene expression analysis (Section 2.8.3-5).

2.7. Cell assays

2.7.1. Cell viability assay

For viability assessment, cells were incubated with 10 µg/mL FDA, (Sigma-Aldrich, #F7378), a cell permeating substrate of cytoplasmic esterases, which is transformed into a fluorescent product. For labeling of dead cells, 1 µM TO-PRO™-3 iodine (Invitrogen, #T3605), a cell-impermeant DNA probe, was used. Both reagents were diluted in DPBS (-/-). After exposing cells to FDA/TO-PRO™-3, cells were observed under a fluorescence inverted microscope (DMI6000B Leica Microsystems), and analyzed with FIJI software [254].

2.7.2. Cell morphology

For the characterization of spheroid and neurospheres, area, max ferret diameter and roundness was determined using icy bioimaging software [253].

2.8. Analytical methods

2.8.1. Protein extraction

2D cell cultures were washed once with cold DPBS (-/-) and lysed with RIPA buffer (diluted from a 10X stock, #20-188, Millipore) containing protease inhibitor (PI, Roche, #4906837001) [1X] and phosphatase inhibitor Phosphostop (Roche, #4693132001) [1X]. In the case of neurospheres, cells were centrifuged at 400 x *g* for 5 min to discard the medium before being washed with DPBS (-/-). Subsequently, a second centrifugation was performed. RIPA buffer supplemented with protease and phosphatase inhibitors was then added to the 3D cell culture.

Lysates were incubated for 20 min on ice before the centrifugation at 13 000 rpm at 4 °C for 10 min. The supernatant was retrieved into new eppendorf tubes and stored at -80 °C until further use.

Protein concentration was quantified with the BCA protein assay kit (Thermo Scientific™ Pierce™ # 23227), according to the manufacturer instructions.

2.8.2. Western blot

2.8.2.1. Sample Preparation

To prepare the protein samples for gel loading, they were mixed with NUPAGE™ LDS sample buffer [6X] (ThermoFisher Scientific™, #NP0007) and NUPAGE™ reducing agent [10X] (ThermoFisher Scientific™, #NP0004), until reaching the final concentration [1X]. Protein samples were incubated at 70 °C for 10 min and then sonicated for 2 min in Branson 5800 ultrasonic cleaner before the gel loading.

2.8.2.2. Sodium dodecyl-sulfate polyacrylamide gel electrophoresis (SDS-PAGE)

Xcell surelock mini-cell electrophoresis system (Thermo Fisher) was assembled using a NuPAGE™ 4-12% (w/v) bis-tris gel (Invitrogen, #NP0321), and chambers were filled with a NuPAGE MES SDS running buffer [20X] (Invitrogen, #NP0002) in ddH_2O. 500 µL of NuPage™ antioxidant (Invitrogen, #NP0005) was added to the inner chamber. For SDS-PAGE, 11-30 µg protein, depending on the samples, was loaded in each lane and Seeblue™ plus 2 pre-strained protein standards (Invitrogen, #LC5925) were used as a ladder.

The gel supply power was set at 150 V using the Powerpac universal power supply (Bio-Rad) for 30-60 min depending on the size of the protein of interest.

2.8.2.3. Membrane transfer

For western blot, proteins separated with SDS-PAGE gel were electrically transferred to the PVDF membrane (GE Healthcare, RPN1416F). PVDF membranes were previously activated in methanol for 1 min and washed in ddH_2O until no water droplets were visible on the membrane surface. Gel-membrane protein transfer procedure was performed by using the mini blot wet transfer modules (Invitrogen), at 20 V for 1 h, using the Powerpac universal power supply (Bio-Rad). After protein transfer, SDS-PAGE was stained for 30 min with Instablue™ coomassie based

staining solution (Expedeon #ISB1L) to verify the efficiency of protein transfer into the PVDF membrane.

2.8.2.4. Immunoblot

PVDF membranes were blocked with 5% (w/v) low-fat milk (panReac AppliChem, #AO383) diluted with tris buffered saline tween (TBST) buffer for 1 h to prevent unspecific antibody binding. To prepare TBST for this procedure, 0.1% (v/v) tween 20 and prepacked tris buffered saline, pH 8.0 were dissolved in 0.5 L of ddH_2O. Subsequently, membranes were washed with TBST followed by the incubation of the primary antibody (table 3) in the blocking solution plus 0.1% (v/v) sodium azide. After the primary antibody incubation, membranes were washed with TBST and incubated with the secondary antibody (Table 4) diluted with a blocking solution at a ratio of 1:5000, 1 h at room temperature (RT).

To reveal the western blot, membranes were washed with TBST after antibody incubation, followed by exposure to Amersham ECL select western blotting detection buffer for 1 min inside a plastic cover. Afterwards, excess liquid was removed and revealed in an iBright™ FL1500 Imaging System (Invitrogen #A44241). For analysis purposes, image J software was used [254].

Table 3 - Primary Antibodies used for western blot

Primary Antibody	Brand	Reference	Host	Dilution	Incubation Conditions
Anti-Glial Fibrillary Acidic Protein (GFAP)	Sigma-Aldrich	#C9205	Mouse-IgG (Monoclonal)	1:1000	Overnight at 4 ºC
Anti-Ionized-calcium binding adapter molecule (IBA1)	Cell Signalling Technology	#17198	Rabbit-IgG (Monoclonal)	1:1000	Overnight at 4 ºC
Anti-β-actin	Sigma-Aldrich	#A5441	Mouse-IgG (Monoclonal)	1:5000	1 h at RT
Anti-CD68	Cell Signalling Technology	#D4B9C	Rabbit-IgG (Monoclonal)	1:1000	Overnight at 4 ºC
Anti-Triggering receptor on myeloid cells 2 (TREM2)	R&D Systems	#AF1828	Goat-IgG (Polyclonal)	1:500	Overnight at 4 ºC
Anti-CD44	Cell Signalling Technology	#8E2	Mouse-IgG (Monoclonal)	1:1000	Overnight at 4 ºC
Anti-Nestin	Merck Millipore	#MAB353	Mouse-IgG (Monoclonal)	1:1000	Overnight at 4 ºC

Table 4 - Secondary antibodies used for western blot

Secondary Antibody	Brand	Reference	Host	Dilution	Incubation Conditions
ECL Anti-Mouse HRP-Link	GE Healthcare	#NA931	Sheep-IgG (Monoclonal)	1:5000	1 h at RT
ECL Anti-Rabbit HRP-Link	GE Healthcare	#NA934	Sheep-IgG (Monoclonal)	1:5000	1 h at RT
Anti-Goat HRP-Link	Invitrogen	#81-1620	Rabbit-IgG (Polyclonal)	1:5000	1 h at RT

2.8.3. RNA extraction

For RNA extraction, the high pure RNA isolation kit (Roche #11828665001) was used, following the supplier protocol. Prior to cell lysis, 2D cell cultures were washed with DPBS (-/-), while 3D cell cultures were centrifuged at 400 *x g* for 5 min to remove the culture medium. The procedure was then repeated with DPBS (-/-). After the extraction, RNA samples were stored at -80 °C immediately. When direct RNA extraction could not be performed due to the lack of time, samples were stored in RNA later solution -80 °C (Invitrogen, AM7021) until use.

2.8.4. Reverse transcription

The reverse transcription reactions were performed using the Sensiscript® reverse transcription kit (Qiagen #205213) following the supplier's protocol. The reaction was carried over 2 h incubation at 37 °C in a SimpliAMP™ thermal cycler (Applied Biosystems). Resulting cDNA from the reactions were either stored at -20 °C or used immediately. Resulting cDNAs were diluted at least 3 times with DNAse/RNAse free water prior use in RT-qPCR procedures.

2.8.5. Reverse transcription quantitative polymerase chain reaction (RT-qPCR)

PCR reactions were performed in PCR 384 well plates (Thermo Fisher #AB1384) using the LightCycler 480 SYBR green I master (Roche, #04887352001), supplemented with 2.5 µl of Ultra-Pure DNase/Rna-Free, 1 µL of forward and reverse primer (final concentration: 500 nM each), and 4.5 µL of SYBR Green solution (Roche, [1X] final concentration). PCR reactions were performed in triplicates for each condition and to ensure the lack of contamination in the PCR mixes, a non-template control (NTC) with only PCR mix was added as a negative control for each gene mix preparation. PCR reactions were carried out in a LightCycler 480 II (Roche). The sequence primers used in this project are listed in Table 5. The specificity of each sequence was assessed by PRIMER blast (https://www.ncbi.nlm.nih.gov/tools/primer-blast/) analysis. Prior to usage, each primer couple was analyzed to assess primer efficiency and ensure the absence of dimers.

Cycle threshold (Ct) and melting curves were determined by LightCycler 480 software version 1.5 (Roche). All data analyses were based on the relative gene expression, using the $2^{-\Delta\Delta Ct}$ method [255]. First, the geometric mean of housekeeping genes (*RPL22* and *36B4*) is determined. Then, the mean of the Ct sample gene is subtracted by the housekeeping genes of the same condition (ΔCt). Fold change of Ct was assessed relative to the control group (ΔΔCt) and normalized to the

control set as 1 ($2^{-\Delta\Delta Ct}$). The determination of relative transcript abundance was calculated with ΔCt by the power of two ($2^{-\Delta Ct}$). The representation of error propagation of the standard deviation was calculated with formula 1. The representation of error propagation of the standard deviation in relative transcript abundance analysis was calculated with formula 2.

(1) $$SD = relative\ gene\ expression * ln2 * \sqrt{\sqrt{SD_{condition}{}^2 + SD_{housekeeping\ genes}{}^2}^2 + \sqrt{SD_{control\ condition}{}^2 + SD_{control\ housekeeping\ genes}{}^2}^2}$$

(2) $$SD = relative\ transcript\ abundance * ln2 * \sqrt{SD_{condition}{}^2 + SD_{housekeeping\ genes}{}^2}$$

2.8.6. Agarose gel

RT-qPCR amplification products generated by co-cultures between A172 GBM neurospheres and MLC-Mo, were separated by electrophoresis. First, 2% (w/v) agarose was prepared by mixing in Tris-acetate-EDTA (TAE) buffer [1X] (Thermo Scientific™, B49) with agarose (Nzytech, #MB027). This mixture was homogenized through heating and agitation. Then, RedSafe nucleic acid staining solution (Intron Biotechnology, #21141) was added to visualize the amplicons after the electrophoresis. Afterwards, agarose was poured into the support and let polymerize. After polymerization, the support was embedded in ddH2O with a TAE buffer [1X]. Relative to sample preparation, RT-qPCR amplicons were loaded into the agarose after mixing with a DNA gel-loading dye (BioLabs, #B7024A).

Subsequently, samples and 100bp DNA ladder (BioLabs, #N0467S) were added to the agarose gel, and run for 60 min at 150 V using a Biometra P25T electrophoresis power supply. Electrophoresis results were visualized in Gel Doc XR imaging system (Biorad).

Table 5 - List of primers used in RT-qPCR. Description of gene name, the protein encoded, and primer sequence. The primer sequence column displays the 5`-3`nucleotide sequence of the forward primer (top) and reverses primer (bottom).

Gene	Protein Encoded	Primer Sequence 5'-3'	
ITGAM	Integrin Subunit Alpha M (CD11B)	TTG TGG TTC CTC AGT GGT GC GGT CAT TGC GTT TTC AGT GTCC	FW 5'-3' RW 5'-3'
P2RY12	Purinergic Receptor P2Y12	ACTCTCTCTTCCAGCCCAGGT CCAGGACCAGTTCCTTGGCGTA	FW 5'-3' RW 5'-3'
P2RY13	Purinergic Receptor P2Y13	GCCGACTTGATAATGACACTCATG CCTAACAGCACGATGCCCACAT	FW 5'-3' RW 5'-3'
AIF1	Ionized Calcium-Binding Adapter Molecule 1 (IBA1)	TCATGTCCCTGAAACGAATG CCAGCATCATCCTGAGAAAG	FW 5'-3' RW 5'-3'
GPR34	G Protein-Coupled Receptor 34	CTGGTTGGGAACATAATCGCCC GGCAGAAGATGAGTAGGAGGTC	FW 5'-3' RW 5'-3'
CD68	CD68 Molecule	CTTCTCTCATTCCCCTATGGACA GAAGGACACATTGTACTCCACC	FW 5'-3' RW 5'-3'
TMEM119	Transmembrane Protein 119	TCCAGGGTCAGATTACAAGAGCAC ACTGTTGATTCTGGAGGGTTTGA	FW 5'-3' RW 5'-3'
CX3CR1	C-X3-C Motif Chemokine Receptor 1	GTGGTGCTGACAAAGCTTGGAA TCACTGGGTGCCATCGTAAGAA	FW 5'-3' RW 5'-3'
PTPRC	Protein Tyrosine Phosphatase Receptor Type C (CD45)	ACCACAAGTTTACTAACGCAAGT TTTGAGGGGGATTCCAGGTAAT	FW 5'-3' RW 5'-3'
CD80	CD80 Molecule	CTCAGAAGTGGAGTCTTACCC AGA GAT TGG AGG GTG TTC CTG	FW 5'-3' RW 5'-3'
CD86	CD86 Molecule	TGGAGAGGGAAGAGAGTGAACA AAAACACGCTGGGCTTCATC	FW 5'-3' RW 5'-3'
CD163	CD163 Molecule	TTTGTCAACTTGAGTCCCTTCAC TCCCGCTACACTTGTTTTCAC	FW 5'-3' RW 5'-3'
MRC1	Mannose Receptor C-Type 1 (CD206)	GGGTTGCTATCACTCTCTATGC TTTCTTGTCTGTTGCCGTAGTT	FW 5'-3' RW 5'-3'
IL6	Interleukin 6	GCAGAAAAAGGCAAAGAATC CTACATTTGCCGAAGAGC	FW 5'-3' RW 5'-3'
IL1B	Interleukin 1β	CTC AAG TGT CTG AAG CAG CC AGT GGT GGT CGG AGA TTC GT	FW 5'-3' RW 5'-3'
TGFB1	Transforming Growth Factor Beta 1	CATGGGGGCTGTATTTAAGG GAGGGAGAGAGAGGGAGTGG	FW 5'-3' RW 5'-3'
SOX2	SRY-Box Transcription Factor 2	GCGGAAAACCAAGACGCT ATGTGCGCGTAACTGTCCAT	FW 5'-3' RW 5'-3'
POU5F1	POU Class 5 Homeobox 1	GACAACAATGAAAATCTTCAGGAG CTGGCGCCGGTTACAGAACCA	FW 5'-3' RW 5'-3'
NANOG	Nanog Homeobox 1	CAGCTGTGTGTACTCAATGATAGA TTT ACACCATTGCTATTCTTCGGCCAG TTG	FW 5'-3' RW 5'-3'
NES	Nestin	TAAGGTGAAAAGGGGTGTGG GCAAGAGATTCCCTTTGCAG	FW 5'-3' RW 5'-3'
IL10	Interleukin 10	GCC TAA CAT GCT TCG AGA TC TGA TGT CTG GGT CTT GGT TC	FW 5'-3' RW 5'-3'
CCL2	C-C Motif Chemokine Ligand 2	CCAAGCAGAAGTGGGTTCAG TAAAACAGGGTGTCTGGGGA	FW 5'-3' RW 5'-3'
CSF1	Colony Stimulating Factor 1	AGCAGGAGTATCACCGAGGA TTGGCACGAGGTCTCCATCT	FW 5'-3' RW 5'-3'
RPL22	Ribosomal Protein L22	CACGAAGGAGGAGTGACTGG TGTGGCACACCACTGACATT	FW 5'-3' RW 5'-3'
36B4	60S Ribosomal Phosphoprotein P0	GTGTTCGACAATGGCAGCAT GACACCCTCCAGGAAGCGA	FW 5'-3' RW 5'-3'

2.8.7. Immunofluorescence

For immunofluorescence, cell lines HMC-3 C20 and A172 were plated in 13 mm cover slips (VWR, #631-1578) in a 24-well culture plate (Falcon, #353047) and kept in a humified environment at 37 ºC and 5% CO_2 for 2 days before being fixed. MLC-Mo was cultured in a 8-well chamber (IBIDI, #80841) coated with poly-D-lysine (Gibco # A3890401) after the differentiation step.

2.8.7.1. Fixation

The first step of the fixation procedure was to remove the cell culture medium, wash with DPBS (+/+), and fixed with a solution of 4% (v/v) paraformaldehyde (PFA, Fluka, #762470) + 4% (v/v) sucrose (Sigma-Aldrich, #S9378) in DPBS (+/+), for 10 min, at RT. Fixed cells were washed twice with PBS(+/+) and stored at 4 ºC in DPBS (+/+), in 24-well plates or IBIDI chambers sealed with parafilm.

2.8.7.2. Permeabilization and blocking

Fixed cells were permeabilized and blocked with 0.1% TX-100 (Sigma-Aldrich, #T-8787) + 0.2% (v/v) fish skin gelatin (FSG) (Sigma-Aldrich, #S4521) for 10 min, at RT.

2.8.7.3. Antibody incubation

Antibody incubations were performed in a dark moisture chamber to prevent drying of the coverslips, or 8-well IBIDI chamber in the case of MLC-Mo. Primary antibodies were diluted in 0.2% (v/v) FSG + 0.1% TX-100 (table 6), and incubated for 2 h, at RT. For 3D cultures, primary antibodies were incubated overnight at 4 °C. After incubation, coverslips were washed with DPBS (+/+) twice and incubated with the fluorescent-conjugated secondary antibody diluted at 1:500, in 0.2% (v/v) FSG + 0.1% TX-100 (table 7), for 1 h at RT. After two washes with DPBS (+/+), 4′,6-diamidino-2-phenylindole (DAPI, Invitrogen, #D1306) was diluted into 1:1000 with DPBS (-/-) from a 5 mg/mL stock solution.

Table 6 - Primary antibodies used for immunofluorescence.

Primary Antibody	Brand	Reference	Host	Dilution
Anti-GFAP	Merk Millipore	AB5894	Rabbit IgG (Polyclonal)	1:700
Anti-Nestin	Merk Millipore	AB5922	Rabbit IgG (Polyclonal)	1:200
Anti-CD133	Cell Signalling	D4W4N	Rabbit IgG (Polyclonal)	1:200
Anti-Sox2	Merk Millipore	AB5603	Rabbit IgG (Polyclonal)	1:200
Anti-Trem2	R&D Systems	Cat#AF1828	Goat IgG (Monoclonal)	1:200
Anti-P2Y12	Sigma	HPA014518	Rabbit IgG (Polyclonal)	1:200
Anti-IBA1	Cell Signalling	E4O4W	Rabbit IgG (Monoclonal)	1:200
Anti-CD45	BioLegend	368512	Mouse IgG (Monoclonal)	1:200
Anti-CD68	Cell Signaling Technology	D4B9C	Rabbit IgG (Monoclonal)	1:600
Anti-TMEM119	Abcam	ab185333	Rabbit IgG (Polyclonal)	1:200
Anti-CD163	Invitrogen	MA5-17716	Rabbit IgG (Monoclonal)	1:500
Anti-CD206	Invitrogen	MA5-32498	Mouse IgG (Monoclonal)	1:300

Table 7 – Secondary antibodies for immunofluorescence.

Secondary Antibody	Brand	Reference	Host
Anti-Rabbit Alexa Fluor 488	Invitrogen	#A11008	Goat-IgG (Polyclonal)
Anti-Goat Alexa Fluor 488	Invitrogen	#A21447	Donkey-IgG (Polyclonal)
Anti-Mouse Alexa Fluor 647	Invitrogen	#A31571	Donkey-IgG (Polyclonal)
Anti-Mouse Alexa Fluor 488	Invitrogen	#AB150105	Donkey-IgG (Polyclonal)

2.8.8. Flow Cytometry

For flow cytometry (FC), Mφ and MLC-Mo were recovered with 10 mM of UltraPure™ 0.5 M EDTA, pH 8.0 (Thermo ScientificTM, #15575020). A172 and MDA-MB-231 2D cell culture recovery, as well as dissociation of 3D cell culture spheroids and neurospheres, were performed by incubating TrypLE™ Express Enzyme (1X) (Thermo Scientific™, # 12604013). Afterward, cells were centrifuged at 400 x *g* for 10 min and resuspended in DPBS (-/-) supplemented with 2% (v/v) FBS (referred to as FC buffer). Subsequently, cells were incubated with the antibodies listed in Table 8 for 45 min on ice. After the antibody incubation, cells were washed twice in FC buffer to remove unbound antibodies. Cells were stained with DAPI diluted 1:1000 with DPBS (-/-) from a 5 mg/mL stock solution to exclude dead cells from the analysis. Samples were analyzed in a flow cytometer (BD Celesta), and result analysis was performed in the FlowJo software.

Table 8 - Conjugted antibodies used for flow cytometry.

Protein	Conjugate	Brand	Reference	Host	Final Dilution
CD11B	PE	Miltenyi Biotec	#130-110-611	Mouse	1:20
CD45	APC	BD Biosciences	#368512	Mouse	1:20
TREM2	Alexa Fluor® 488	R&D Systems	#FAB17291G-100UG	Mouse	1:100
CD44	PE	Invitrogen	#12-0441-82	Rat	1:100

2.9. Statistical Analysis

Data from independent biological sample experiments or technical replicates are expressed as the mean ± standard deviation.

The nonparametric Kruskal-Wallis test was applied to analyze the potential significance of the statistical hypothesis of experiments harboring a minimum of three biological replicates (except spheroid morphology characterization experiments). The parametric ANOVA was applied to analyze the potential significance of the statistical hypothesis of experiments that characterized spheroid morphology. Significances are depicted as: ns – non-significant, *$p < 0.05$, **$p < 0.01$, ***$p < 0.001$, ****$p < 0.0001$. Levene test was used to assess the equality of variances between spheroid populations. Significances are depicted as: $^{\#}p < 0.05$.

Chapter 3. Results & Discussion

3.1. Selection of a microglia source

3.1.1. Phenotypical analysis of different human microglia sources

In the first task we aimed to characterize the phenotype of different human microglial cell sources, namely immortalized microglia cell lines (HMC3 and C20), microglia-like cells derived from monocytes (MLC-Mo) and hiPSC (MLC-hiPSC). MLC-Mo and microglia cell lines were derived and cultured as described in the Materials & Methods section (Section 2.1.2 and 2.4). Representative images are shown in (Figure 3.1). MLC-hiPSC were generated within the scope of another project ongoing in the host laboratory, as described in supplementary information, and included here for comparison (Figure S.1).

Immortalized microglia cell lines presented morphological characteristics typically observed in microglia, like small cell bodies and single or multiple elongated ramifications under healthy conditions [256,257]. These ramified structures allow microglia to surveil the CNS, and screen for pathogens and cell damage. In addition, morphological heterogeneity was observed, with varying lengths and number of ramifications among the population, as also described for *bona fide* microglia [258].

The M0 MLC-Mo, and monocyte-derived M0 macrophages (Mφ), that we generated for comparison from the same donors, presented amoeboid morphology with one to two ramifications on opposing sides of the cells. This morphology has also been described in human/murine microglia and macrophages cell culture and freshly isolated murine microglia [259–262]. Moreover, a fraction of the MLC-Mos were rounded, especially in the cells derived from PBMCs of donor #1. Mφ presented population heterogeneity and morphologies similar to MLC-Mo with rounded cells and 1 or 2 ramifications.

In summary, all microglial cell sources displayed a microglia-like morphology, but each differed in the number, length of ramifications, and heterogeneity among the population (Figure 3.1). The immortalized microglia cell lines C20 and HMC3 showed a more homogeneous population with a higher number of ramifications than MLC-Mo, which was in accordance with a previous report [221]. Mφ and microglia-like cells (MLC-Mo and MLC-hiPSC) had a similar morphology with MLC-hiPSC presenting a higher heterogeneity than any of the other cell sources, with more elongated ramifications (Figure S.1).

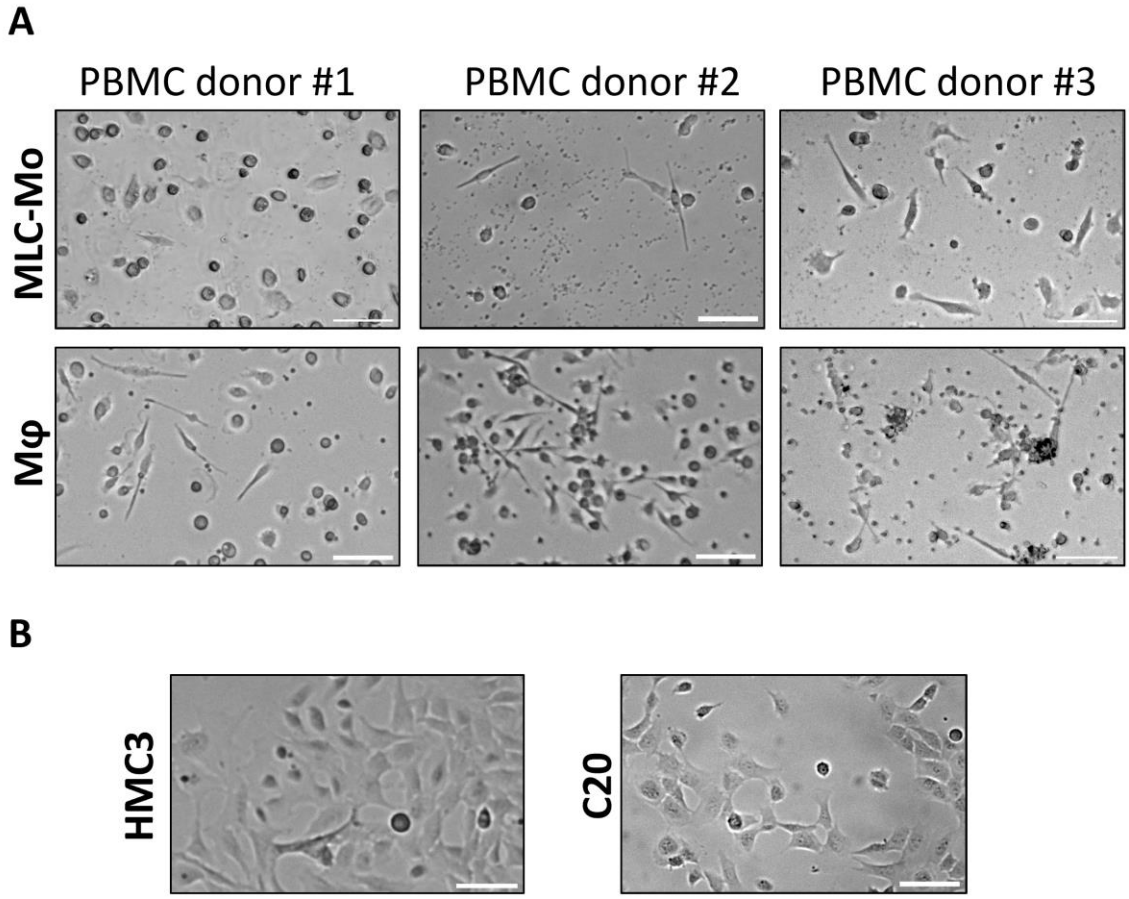

Figure 3.1 - Phase contrast images of different microglial cell sources. Monocyte-derived M0 microglia-like cells (MLC-Mo) and monocyte-derived M0 macrophages (Mφ) were derived from cells of three different PBMC donors, Immortalized microglia cell lines (HMC3 and C20) were cultured according to published protocols (See Materials and Methods, 2.1.2 and 2.4). Representative images from an N=3 experiment. Scale bar: 50 µm.

To better characterize the microglial cell sources, gene expression analysis of human microglia markers was performed. The genes that we selected were chosen according to recent literature reports [76,121], as described in the introduction (Section 1.5.2.1.1). These genes included: *ITGAM* (codes for CD11B), *P2RY12/3*, *AIF1* (codes for IBA1), *GPR34*, *CD68, CX3CR1* and *PTPRC* (codes for CD45).

Figure 3.2A presents the gene expression analysis, represented as fold change relative to MLC-hiPSC. Immortalized cell lines showed the lowest level of expression of all the genes assessed. For the genes coding for *CX3CR1* and *PTPRC*, no gene expression was detected. Furthermore, when comparing the relative transcript abundance (Figure 3.2B), normalized by the housekeeping genes *RPL22* and *36B4,* it was within the range of 10^{-2} to 10^{-6}, further indicating that the HMC3 and C20 cell lines poorly express all microglia genes tested. The low detection of microglia markers in HMC3 and C20 cell lines, compared to MLC-hiPSC and MLC-Mo, has already been reported relative in the literature through protein-based assays such as flow cytometry (FC) and immunofluorescence (IF) [221].

For MLC-Mo (Figure 3.2A), cells generated from monocytes of two PBMC donors were evaluated (PBMC donor #1 and #2). MLC-Mo presented a 4.7-, 8.3-, and 1.6-fold increase in the expression of *ITGAM*, *CD68*, and *PTPRC*, respectively, when compared with MLC-hiPSC.

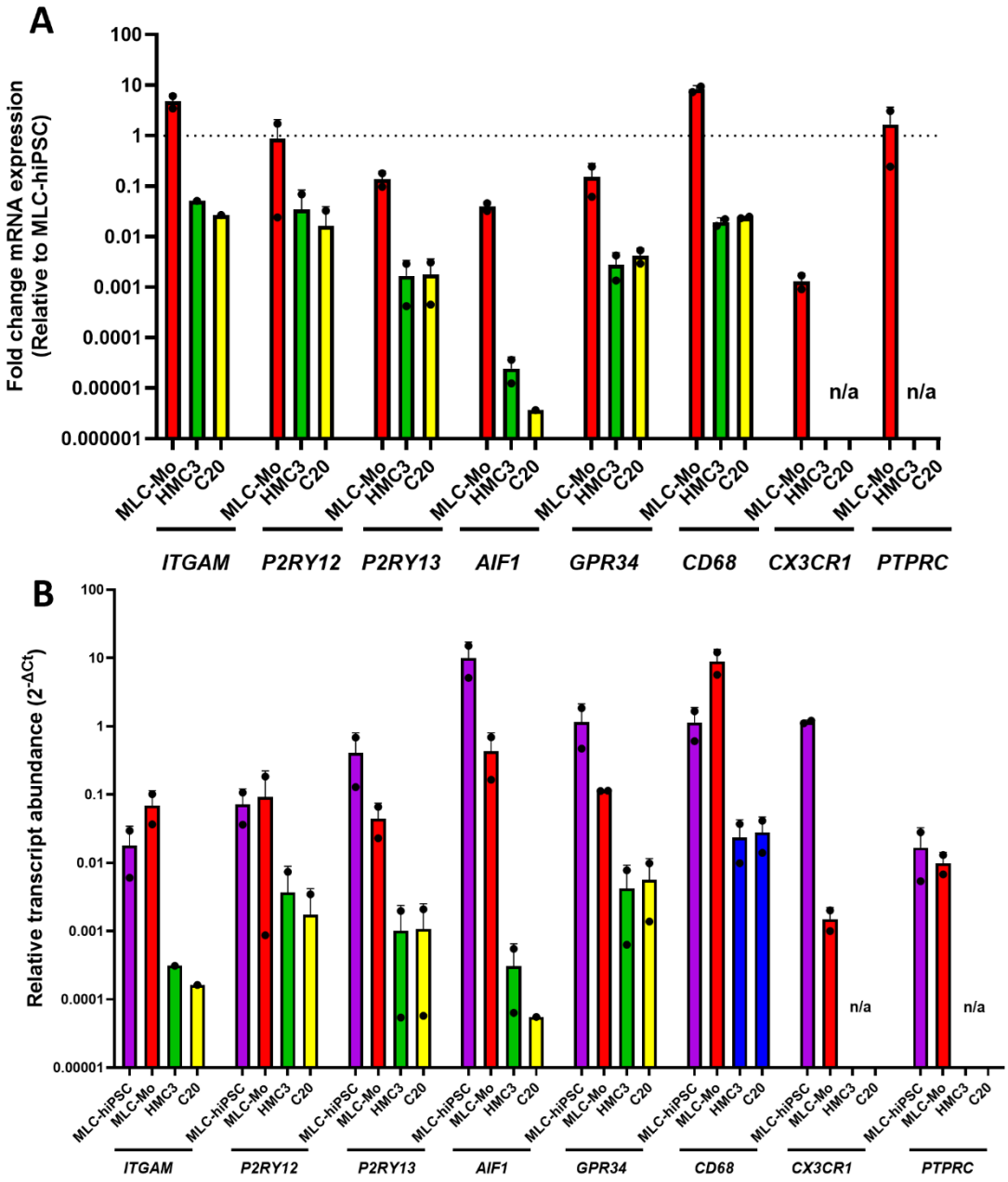

Figure 3.2 - Microglia marker gene expression in different microglial cell sources assessed by RT-qPCR. A – Fold change of gene expression in microglia-like cells derived from monocytes (MLC-Mo), with monocytes isolated from PBMCs of donors #1 and #2; HMC3 and C20 cell lines determined by the $2^{-\Delta\Delta Ct}$ method. Values were normalized to the expression of the housekeeping genes *36B4* and *RPL22*. Data are represented as fold change relative to microglia-like cells derived from human induced pluripotent stem cells (MLC-hiPSC). Error bars represent the SD of the 2 independent experiments. **B –** Relative transcript abundance ($2^{-\Delta Ct}$) in MLC-hiPSC, MLC-Mo, HMC3, and C20 cell lines relative to plot A. Error bars represent the mean of SD of the 2 biological triplicates. **A-B** -Representative plot of N=2 independent experiments. n/a indicates no gene expression (cycle threshold values above 35). Microglia genes: *ITGAM* (CD11B) – Integrin Subunit Alpha M; *P2RY12/13* – Purinergic Receptor 12/13; *AIF* (IBA1) – Allograft Inflammatory Factor 1; *GPR34* - G-protein coupled receptor 34; *CD68* – Cluster Differentiation 68; *CX3CR1* - CX3C chemokine receptor 1; *PTPRC* (CD45) **-** Protein Tyrosine Phosphatase Receptor Type C**.** Housekeeping genes: *36B4* – 60S Ribosomal Phosphoprotein P0 and *RPL22* – Ribosomal protein L22.

Additionally, the *P2RY12* expression in MLC-Mo was similar to MLC-hiPSC, although with a high standard deviation (SD). Moreover, the expression of *AIF1* and *CX3CR1* in MLC-Mo was lower than in MLC-hiPSC, in accordance with a previous report, where the transcriptional profile among microglia sources were evaluated [221]. The genes observed to be upregulated in MLC-hiPSC compared to MLC-Mo (*AIF1, GPR34, and CX3CR1*) are associated with inflammatory response [129,132–134]. *AIF1* and *GPR34* are reported to be associated with phagocytosis [129,132], whereas *CX3CR1* activation regulates genes associated with inflammatory response [133,134]. Additionally, *AIF1* up regulation is associated with an inflammatory macrophage (Mφ) phenotype (M1) [263].

Still, the overall gene expression of microglia markers was higher in MLC-Mo compared to the C20 and HMC3 cell lines. These data are concordant with a previous report on the characterization of the different microglia sources [221]. In this study, Rai *et al.* reported that MLC-hiPSC and MLC-Mo were transcriptionally similar to adult microglia, while established cell lines were completely divergent in terms of gene expression, casting doubt on the usage of immortalized cell lines as *bona fide* microglia cell sources [221]. Nevertheless, microglia immortalized cell lines have been widely used as an *in vitro* microglia human cell model to assess HIV infection [216]. In addition, these cells retain the ability to respond to inflammatory stimuli. In fact, it has been shown that C20 cells responded to exposure to the pro-inflammatory cytokine IL-1B, by activating Nf-kB signalling, secreting CXCL10, IL-6 and CCL2 [264]. Similarly, HMC3 cells have been shown to respond to LPS and IFN-γ, releasing IL-6 and CXCL10 [232]. This can be explained by the fact that, even if the transcriptional profile of immortalized microglia cell lines is not similar to the adult microglia, they may still retain the ability to respond to inflammation, which is one of the main functions of the microglia in the CNS [265].

Microglia and bone marrow derived Mφ express a series of common markers that reflect their myeloid origin, such as CD11B (*ITGAM*), IBA1 *(AIF1*), CD68, and CD45 (*PTPRC*). Some other markers are more specific for microglia, namely P2RY12, P2RY13 and GPR34 [266]. Therefore, we assessed the differences in gene expression of MLC-Mo and Mφ derived from the same donor. After differentiation, RNA was extracted from MLC-Mo and Mφ and the gene expression was analyzed by RT-qPCR, using the Mφ from each donor as control. Relative gene expression levels, using *RPL22* and *36B4* as housekeeping controls, were calculated (Figure 3.3).

In a first stage, data from each donor was analyzed independently, as variability among immune cells from different donors is expected [267–269]. A high variability among donors was indeed observed for the genes *ITGAM, P2YR12, P2YR13, GPR34,* and *CX3CR1* (Figure 3.3). For *AIF1*, *CD68*, and *PTPRC* genes, downregulation in MLC-Mo relative to Mφ was observed for all donors. Regarding *P2YR12, P2YR13*, and *GPR34* were reported to be more highly expressed in microglia than Mφ [270–273], but in Figure 3.3, it is observed that upregulation was donor-dependent. These results indicated a high inconsistency in expression of specific microglia markers in MLC-Mo. Nevertheless, the requirement of additional replicates is mandatory since

this variation could be technical and not biological. Regarding CD45 *(PTPRC)*, a higher detection in Mφ than in MLC-Mo was consistent among donors and has been previously reported by FC [274]. As for *AIF1* and *CD68,* they have both been indicated as being expressed in microglia and Mφ [121]. Since mRNA expression does not always represent the cell phenotype [275], the protein levels were assessed by FC, IF and western blot (WB).

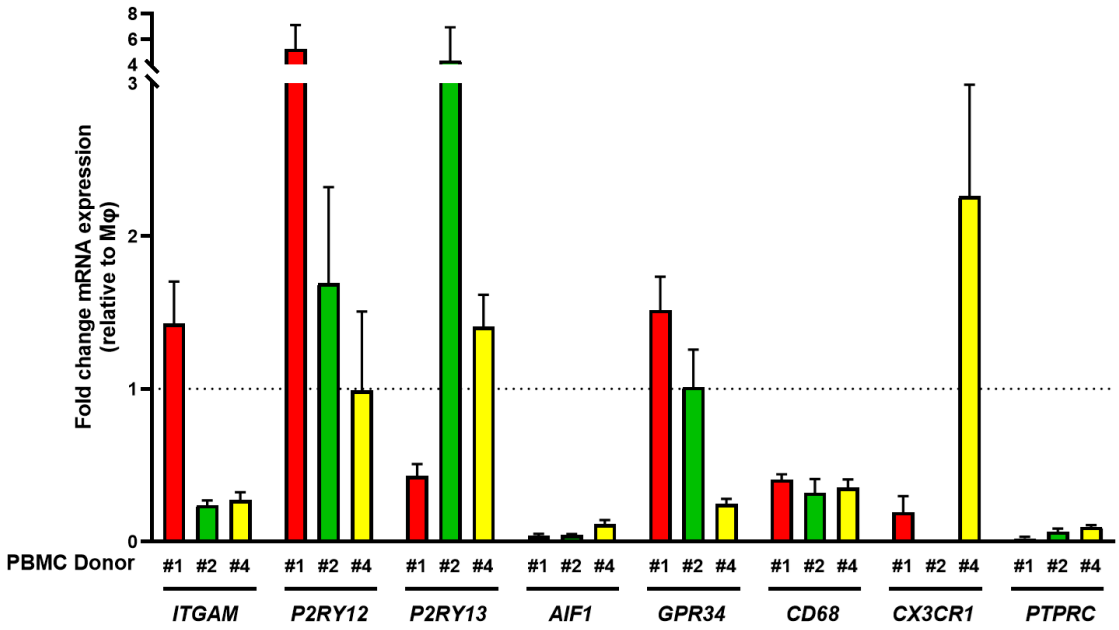

Figure 3.3 - Microglia marker gene expression in microglia-like cells derived from monocytes (MLC-mo) of different peripheral blood mononuclear cells (PBMC) donors assessed by RT-qPCR. A – Fold change in gene expression, in MLC-Mo established from monocytes isolated from PBMC donors #1, #2, and #4, determined by the $2^{-\Delta\Delta Ct}$ method. Target gene expression was normalized to the expression of housekeeping genes *36B4* and *RPL22*. Data are represented as fold change relative to Mφ derived from circulating monocytes gene expression, set as 1 (dashed line). Error bars are shown as a mean of SD of technical triplicates. *Microglia genes: ITGAM (*CD11B*)* – Integrin Subunit Alpha M; *P2RY12/13* – Purinergic Receptor 12/13; *AIF (*IBA1*)* – Allograft Inflammatory Factor 1*; GPR34* - G-protein coupled receptor 34*; CD68* – Cluster Differentiation 68*; CX3CR1* - CX3C chemokine receptor 1; *PTPRC (*CD45*)* Protein Tyrosine Phosphatase Receptor Type C**.** Housekeeping genes: *36B4* – 60S Ribosomal Phosphoprotein P0 and *RPL22* – Ribosomal protein L22*.*

MLC-Mo and Mφ, both obtained from monocytes derived from three different donors, as well as established microglia cell lines HMC3 and C20 were analysed by FC, to assess CD45, CD11B and TREM2 levels. HMC3 and C20 cell lines showed a negligible $CD45^+/CD11B^+$ population, lower than 0.04% as shown in figure 3.4A. Moreover, within each donor, both CD45 and CD11B MFI and ratio of $CD45^+/CD11B^+$ were higher in Mφ than in MLC-Mo (Donor #6: 80% vs 54.5%; Donor #8: 32% vs 17%; Donor #9: 14.5 vs 10%; Mφ vs MLC-Mo, respectively, Figure 3.4A-C). Additionally, there is an increase in CD45 and CD11B detection levels in Mφ compared to MLC-Mo (Figure 3.4D). The reduced CD45 detection in MLC-Mo agrees with the reduced *PTPRC* (codes CD45) gene expression, reported in figure 3.3.

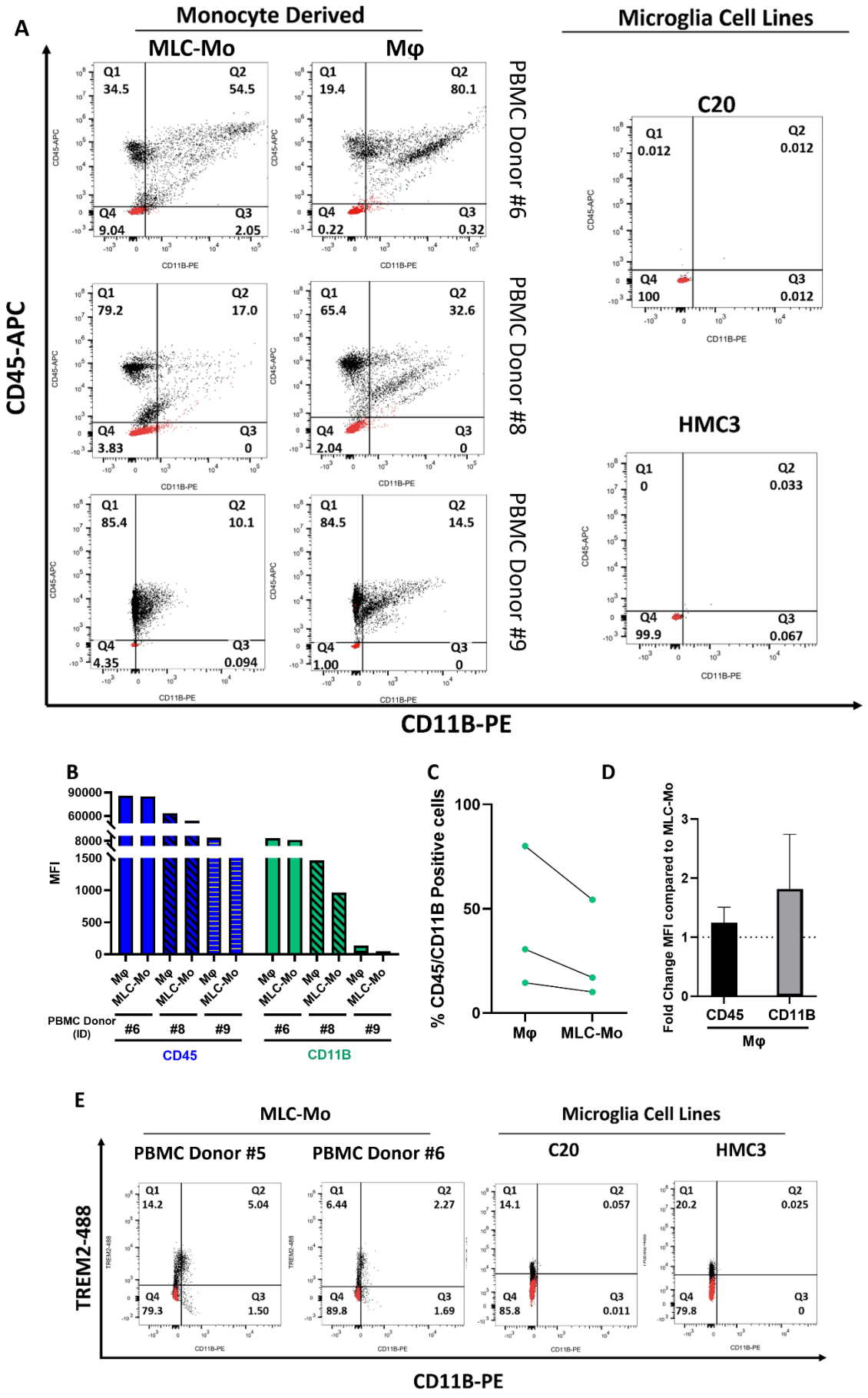
A
Monocyte Derived
Microglia Cell Lines
MLC-Mo
Mφ
C20
HMC3
PBMC Donor #6
PBMC Donor #8
PBMC Donor #9
CD45-APC
CD11B-PE
Q1 34.5
Q2 54.5
Q4 9.04
Q3 2.05
Q1 19.4
Q2 80.1
Q4 0.22
Q3 0.32
Q1 0.012
Q2 0.012
Q4 100
Q3 0.012
Q1 79.2
Q2 17.0
Q4 3.83
Q3 0
Q1 65.4
Q2 32.6
Q4 2.04
Q3 0
Q1 0
Q2 0.033
Q4 99.9
Q3 0.067
Q1 85.4
Q2 10.1
Q4 4.35
Q3 0.094
Q1 84.5
Q2 14.5
Q4 1.00
Q3 0
B
MFI
90000
60000
8000
1500
1000
500
0
Mφ
MLC-Mo
PBMC Donor (ID)
#6
#8
#9
CD45
CD11B
C
% CD45/CD11B Positive cells
100
50
0
Mφ
MLC-Mo
D
Fold Change MFI compared to MLC-Mo
3
2
1
0
CD45
CD11B
Mφ
E
MLC-Mo
Microglia Cell Lines
PBMC Donor #5
PBMC Donor #6
C20
HMC3
TREM2-488
CD11B-PE
Q1 14.2
Q2 5.04
Q4 79.3
Q3 1.50
Q1 6.44
Q2 2.27
Q4 89.8
Q3 1.69
Q1 14.1
Q2 0.057
Q4 85.8
Q3 0.011
Q1 20.2
Q2 0.025
Q4 79.8
Q3 0

Figure 3.4 - CD45 and CD11B flow cytometry analysis of monocytes derived microglia-like cells (MLC-Mo) and macrophages (Mφ) from peripheral blood mononuclear cells (PBMCs). A – Double dot plot, indicating $CD45^{+}/CD11B^{+}$ population in MLC-Mo, Mφ derived from monocytes of three PBMC donors (#6, #8, #9), and HMC and C20 cell lines (represented in black). The X-axis represents CD45(APC), and Y-axis the CD11B (PE). Unstained cells are represented in red**. B** – CD45 and CD11B mean fluorescence index (MFI) plot of MLC-Mo and Mφ of different PBMC donors (#6, #8, #9). **C –** Fold change of MFI of Mφ relative to MLC-Mo. Representative plot of N=3 independent experiments. **D** – Plot representing percentage of $CD45^{High}/CD11B^{High}$ cells in MLC-Mo and Mφ of three PBMC donors (#6, #8, #9. Representative plot of N=3 independent experiments. **E** – Double dot plot indicating $TREM2^{+}/CD11B^{+}$ positive population of MLC-Mo two PBMC donors (#5, #6) and HMC and C20 cell lines. The X-axis represents TREM2-488, and Y-axis the CD11B-PE. Red cells indicated unstained sample.

However, the results were not statistically significant, and additional biological replicates are required, since PBMC donors and primary macrophages present a high variability in response to pro- and anti-inflammatory stimuli [267–269]. The identification of $CD45^{+}/CD11B^{+}$ as Mφ and $CD45^{low}/CD11B^{+}$ as microglia has been reported from studies performed in mouse models [276,277]. In addition, a study performed in human brain-derived post-mortem microglia showed that it is possible to distinguish choroid plexus Mφ from white matter microglia according to the differential detection of CD11B and CD45 expression (higher CD45/CD11B MFI in Mφ than in microglia) [229]. In general, the usage of differential levels of CD45 to distinguish microglia from macrophages has, nevertheless, being debated, since CD45 increases in microglia upon inflammation [136,137].

Interestingly, MLC-Mo and microglia cell lines showed a cell subpopulation positive for TREM2, although with low detection levels (Figure 3.4E). It is observed that $TREM2^{+}$ population differs between the two donors analyzed, therefore it is necessary to have more biological replicates to assess whether this variability is donor dependent or technical. Nevertheless, TREM2 was additionally assessed by WB and IF along with other microglia markers.

By WB analysis, CD68 and IBA1 were detected in MLC-Mo and Mφ from all donors (Figure 3.5A-B). For CD68, the relative intensity compared to β-actin (using a low exposure detection) was higher in MLC-Mo than in Mφ from donors #3 and #5 (Figure 3.5B). For cells of donor #4, a higher CD68 relative intensity was detected in Mφ, also in accordance with the RT-qPCR results (Figure 3.3).

Interestingly, we observed a different band pattern for CD68 in MLC-Mo and Mφ. Specifically, the migration rate of CD68 from Mφ was accelerated compared to MLC-Mo in the three donors analysed (Figure 3.5A). This suggests an alteration in the glycosylation pattern of CD68 between MLC-Mo and Mφ-Mo. In fact, CD68 is a heavily glycosylated protein [128]. Differential CD68 electrophoretic patterns have already been reported in mice derived Mφ. A study showed altered CD68 WB band migration, caused by exposure to receptor activator of NF-kB ligand (RANKL) in bone marrow-derived and RAW264.7 macrophages [278]. The authors suggested that the altered CD68 band migration pattern was explainable due to a differential CD68 glycosylation status. Interestingly, differential CD68 glycosylation has been reported in response to phagocytosis in Mφ [279]. Further studies and specific techniques such as mass spectrometry

are required to confirm the potential differential CD68 glycosylation pattern between MLC-Mo and Mφ [280].

Semi-quantitative analysis of the myeloid marker detection intensity relative to β-actin showed enrichment of IBA1 in Mφ compared to MLC-Mo (Figure 3.5B) for two of the three donors. CD68 and IBA1 are markers that are commonly detected in cells of myeloid origin, as mentioned before (e.g., macrophages, microglia, kupffer cells), so our WB data agree with such observations [121]. CD68 and IBA1 have been detected also in the human brain, indicating that they are relevant microglia markers in vivo [281].

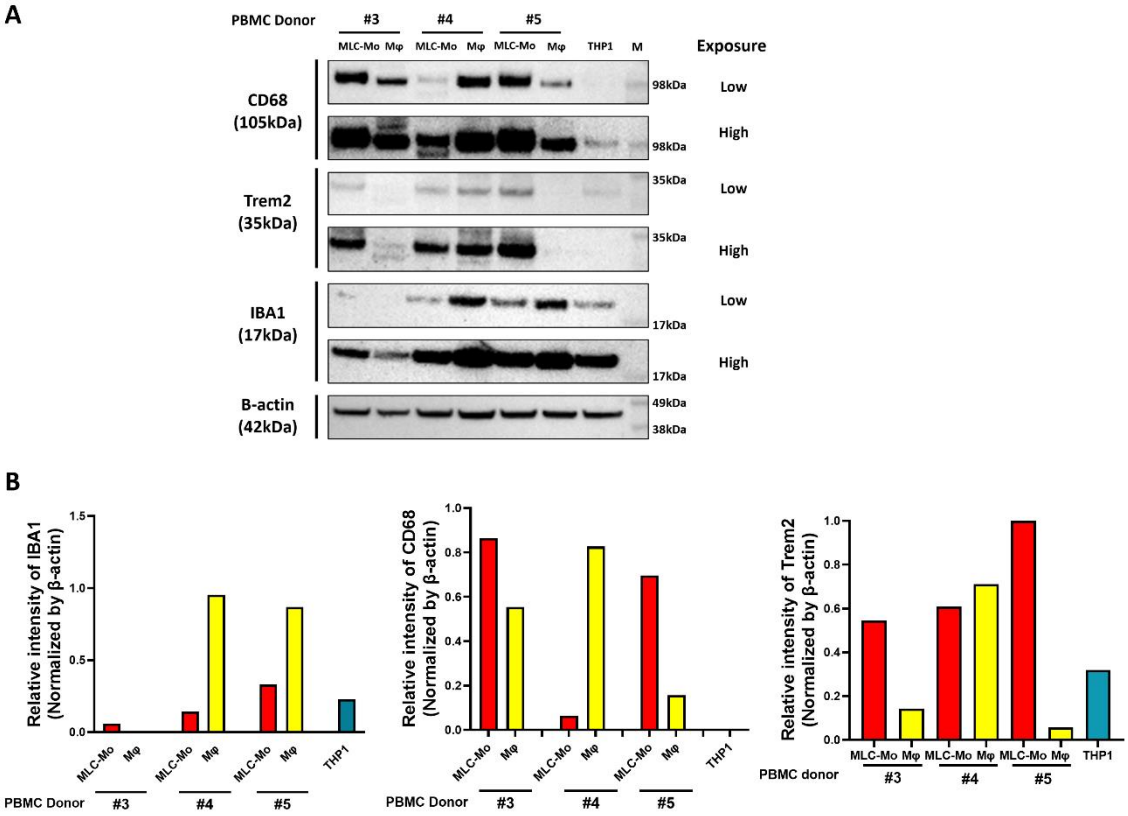

Figure 3.5 - Western blot (WB) analysis of microglia markers in microglia like cells (MLC-Mo) and macrophages (Mφ) derived from monocytes. A–MLC-Mo and Mφ from three peripheral blood mononuclear cells (PBMC) donors (#3, #4 and #5). The THP1 cell line was used as positive control. CD68, TREM2 and IBA1 were detected by western blot, employing different exposures times. β-actin was used as a loading control. M represents the molecular weight ladder. **B** – Semi-quantitative analysis of microglia markers normalized by β-actin, performed using ImageJ software [256] using the low exposure WB**. A-B –** Scans and plots from N=3 independent experiments. Microglia markers: CD68 – Cluster Differentiation 68**;** TREM2 – Triggering Receptor Expressed on Myeloid cells; AIF (IBA1) – Allograft Inflammatory Factor 1**.** Uncropped scans of western blots are shown annex (Figure S.2-5).

TREM2 relative intensity was higher in MLC-Mo from #3 and #5 than in their Mφ counterparts, and similar between cell types (MLC-Mo and Mϕ) for the #4 donor. TREM2 has been detected in human microglia and its implication in microglia normal brain physiology and in Alzheimer's disease have been reported [282]. We observed a relatively low TREM2 expression in Mφ, compared to MLC-Mo as mentioned before, in two out of three samples. Even though TREM2 is reported to be expressed in Mφ [283], its levels increase substantially in tumor-associated macrophages (TAM), where TREM2^{+}TAM exert a immunosuppressive and pro-tumorigenic

function in the TME [284]. In general, both cell types presented microglia markers, and relative abundance values seemed to be donor-dependent, both at gene and protein level.

In addition, CD45, IBA1, TMEM119 and P2RY12 were detected by IF in MLC-Mo from three PBMC donors (#1, #2 and #9). TREM2-positive cells were observed in MLC-Mo from the two donors evaluated. The detection of CD45, IBA1, TMEM119, and P2RY12 was observed in MLC-Mo but not in microglia cell lines by IF (Figure 3.6), in agreement with the RT-qPCR data (Figure 3.2). In supplementary Figure S.6, MLC-hiPSC showed positive staining for IBA1 and TREM2 which confirmed previous RT-qPCR data and reports from the literature although employing a different microglia differentiation strategy (via embryonic bodies) [285,286].

In summary, HMC3 and C20 cell lines did not show gene expression and protein detection of all microglia markers tested, except for TREM2 that was detected by FC in a reduced percentage of the cell population (20.2% and 14.2% respectively). In a study from Rai and colleagues [221], it has been shown by FC analysis that CD45 and CD11B were not detected in HMC3 or C20, as well as TMEM119 analysed by IF, confirming our analysis (Figure 3.6 and 3.4E). Nevertheless, they showed that HMC3 and C20 both expressed IBA1. IBA1 detection in HMC3 cells was also reported by other studies, by Dello Russo [215], and Etemad et al [118]. In contrast, our RT-qPCR and IF analysis showed that IBA1 was barely detected in both immortalized cell lines.

Furthermore, in the case of HMC3, it has been reported that since its establishment in 1995, this cell line has circulated in various laboratories. This may explain, in part, such phenotypic diversity. Nevertheless, lab-to-lab cell line variability is a general drawback associated to the use of cell lines [222]. In fact, clonal expansion (for example due to incomplete trypsinization), differential medium composition among labs, high number of passages (which is associated to genetic drift), different cell sources altogether contribute to this phenomenon. Additionally, cell phenotype may be altered due to the presence of mycoplasma, and/or differential seeding density. Still, for the development of immortalized cell lines, the transduction of genes to bypass senescence in the cell lines potentially alters the original cell phenotype [287]. In addition, cell immortalization by SV40 antigen has been associated with the acquisition of oncogenic properties, which is an issue to be considered during immortalization procedures and cell line characterization [288].

In conclusion, since all data pointed to the lack of expression of the majority of the microglia markers evaluated in HMC3 and C20, no further experiments were carried out with the microglia cell lines. On the other hand, MLC-Mo and MLC-hiPSC express a large panel of microglia markers, with MLC-hiPSC expressing higher levels of microglia genes in general than MLC-Mo, in concordance with a previous report [221]. Since MLC-Mo and MLC-hiPSC expressed microglia markers, we further characterized these microglia cell sources in their ability to respond to pro- and anti-inflammatory stimuli, as will be shown in the following section.

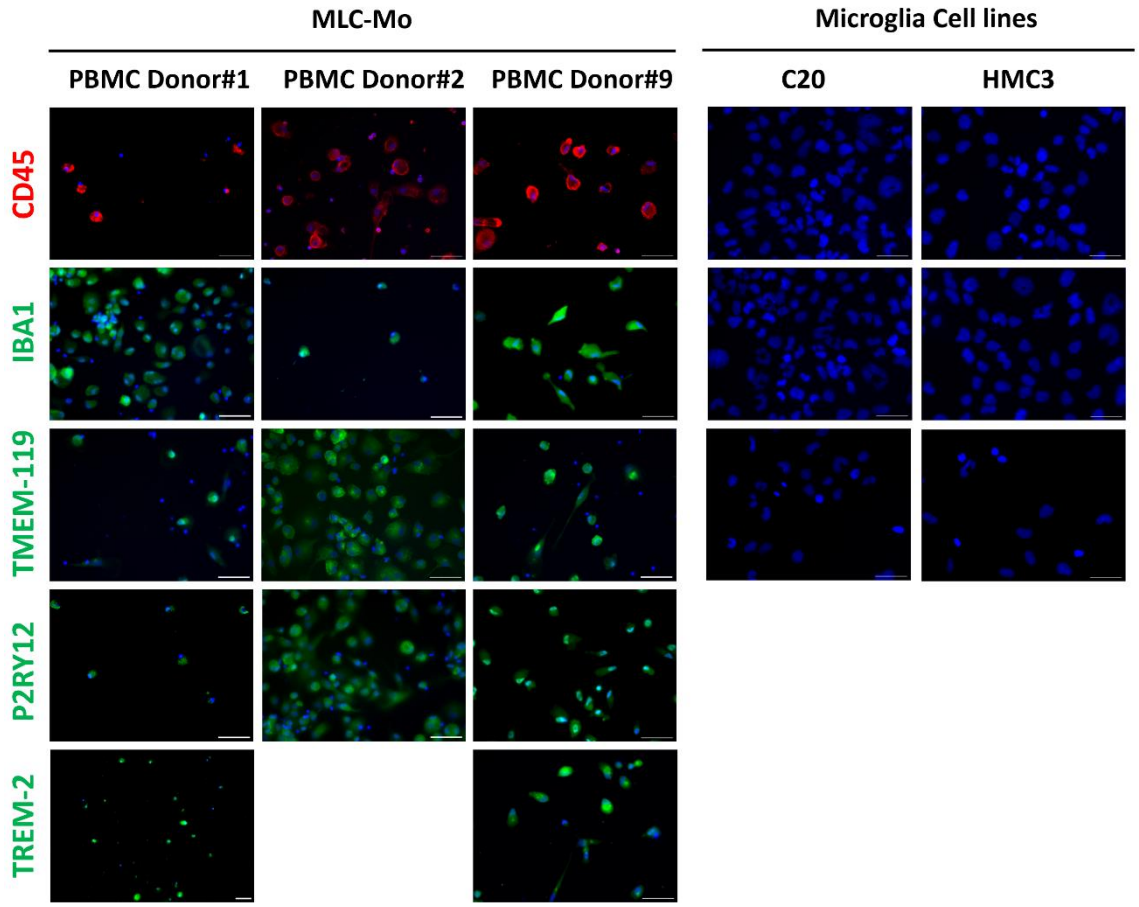

Figure 3.6 - **Microglia protein analysis by immunofluorescence microscopy in different *in vitro* microglia models. A -** CD45 labelled in green (APC) in microglia like cells derived from monocytes (MLC-Mo) of three peripheral blood mononuclear cells (PBMC) donors, HMC3 and C20 cell lines. IBA1, TMEM-119, TREM2, and P2RY12 labelled in green (AlexaFluor® 488) in MLC-Mo, and immortalized microglia cell lines HMC3 and C20. Cells were counterstained with 4',6-diamidino-2- phenylindole (DAPI, blue) for nuclei identification. Representative image from N=3 of independent experiments except for TREM (n=2). Scale bar: 50 µm. Microglia markers: TREM2 – Triggering Receptor Expressed on Myeloid Cells 2; IBA1 (*AIF1*) – Allograft inflammatory factor 1; TMEM119 – Transmembrane Protein 119, P2RY12/3 – Purinergic Receptor 12/3 – Purinergic Receptor 12; CD45 (*PTPRC*) – Protein Tyrosine Phosphatase Receptor Type C**.**

3.1.2. Ability to respond to inflammatory and anti-inflammatory stimuli

To evaluate the MLC-Mo and MLC-hiPSC functionality, cells were challenged with prototypical pro- and anti-inflammatory stimuli. As pro-inflammatory challenge, cells were cultured in their respective medium (described in Material and Methods section 2.6) containing 10 ng/ml of LPS and 50 ng/ml of IFN-γ for 48 h, according to the standard protocol described in the literature to replicate an inflammatory response to pathogens [289]. LPS is an endotoxin released by many gram-negative bacteria during cell lysis, which binds to TLR-4, activating NF-kB and leading to the expression of genes responsible for inflammation [290]. IFN-γ is a cytokine that binds to the IFN-γ receptor that, in turn, activates STAT1, crucial for the expression of interferon-stimulated genes, as observed during antiviral response, immune modulation, and cytotoxicity [181].

As for the anti-inflammatory condition, cells were incubated with 20 ng/mL of IL-4 and IL-13 for 48 h and the gene modulation of anti-inflammatory genes typically associated with M2 phenotypes was assessed. IL-4 and IL-13 are anti-inflammatory cytokines that bind to the IL-4 receptor, leading to the activation and translocation of STAT6 into the nucleus, crucial for the expression of M2-related genes [150].

The response of MLC-hiPSC and MLC-Mo from three PBMC donors was evaluated by expression analysis (RT-qPCR) of *AIF1, CD86, IL6 and IL1B* or *MRC1, CD163 and TGFB1,* genes described to be upregulated upon pro- and anti-inflammatory signals [121]. Figure 3.7A shows RT-qPCR analysis of genes associated with pro-inflammatory Mφ phenotype (M1) and anti-inflammatory Mφ phenotype (M2), in MLC-Mo and MLC-hiPSC relative to the respective untreated controls, designed as M0 microglia. Both microglia sources showed an upregulation in *IL6* expression compared to the unchallenged control, with a 5- and 23- fold increase in MLC-hiPSC and MLC-M0, respectively. Moreover, there was a clear upregulation of *IL1B* in MLC-Mo, from the three donors analyzed, which is not observed in MLG-hiPSC. For *CD86* and *AIF1,* very small or no differences in expression were detected upon the challenge of both cell types, except for *CD86* upregulation for MLC-Mo, which was statistically significant. The relative transcript abundance analysis (using the housekeeping gene *RPL22* for normalization), showed that relative transcript abundance of *AIF1, CD86* and *IL1B* were already high in the untreated controls of the MLC-hiPSC, indicating that the M0 state already had a high expression of these genes, which may explain the poor response to the inflammatory stimulus (Figure 3.7B). Further biological replicates of MLC-hiPSC are required to confirm this hypothesis. Comparing these results with the literature, it has been reported that MLC-hiPSC treated with LPS showed a 1.5-fold increase in *IL1B* which is in agreement with the obtained results [291]. Another report from MLC-hiPSC reported an increase in cytokine secretion of IL-1β and IL-6 in response to LPS stimuli. However, other cytokines/chemokines in microglia-like cells derived from embryonic cells showed already had high secretion levels of inflammatory markers without LPS treatment (IL-8, MIP1β, and Fractalkine). This suggests that a certain level of activation is already present in microglia-like cells derived from embryonic/pluripotent stem cells, but which can be still further stimulated by strong inflammatory stimuli such as LPS [292]. The results obtained along with these reports could indicate that MLC-Mo may be a relevant *in vitro* model that responds to inflammatory stimuli. Additional replicates are required to confirm this hypothesis, as well as to expand the panel of inflammatory markers tested (e.g., *IL8*, *CD40*), and use other techniques such as FC or ELISA to analyse protein detection and cytokine secretion respectively. Cells were also challenged with an anti-inflammatory stimulus, resulting in no modulation or a tendency to downregulation of the proinflammatory markers evaluated (Figure 3.7A-B).

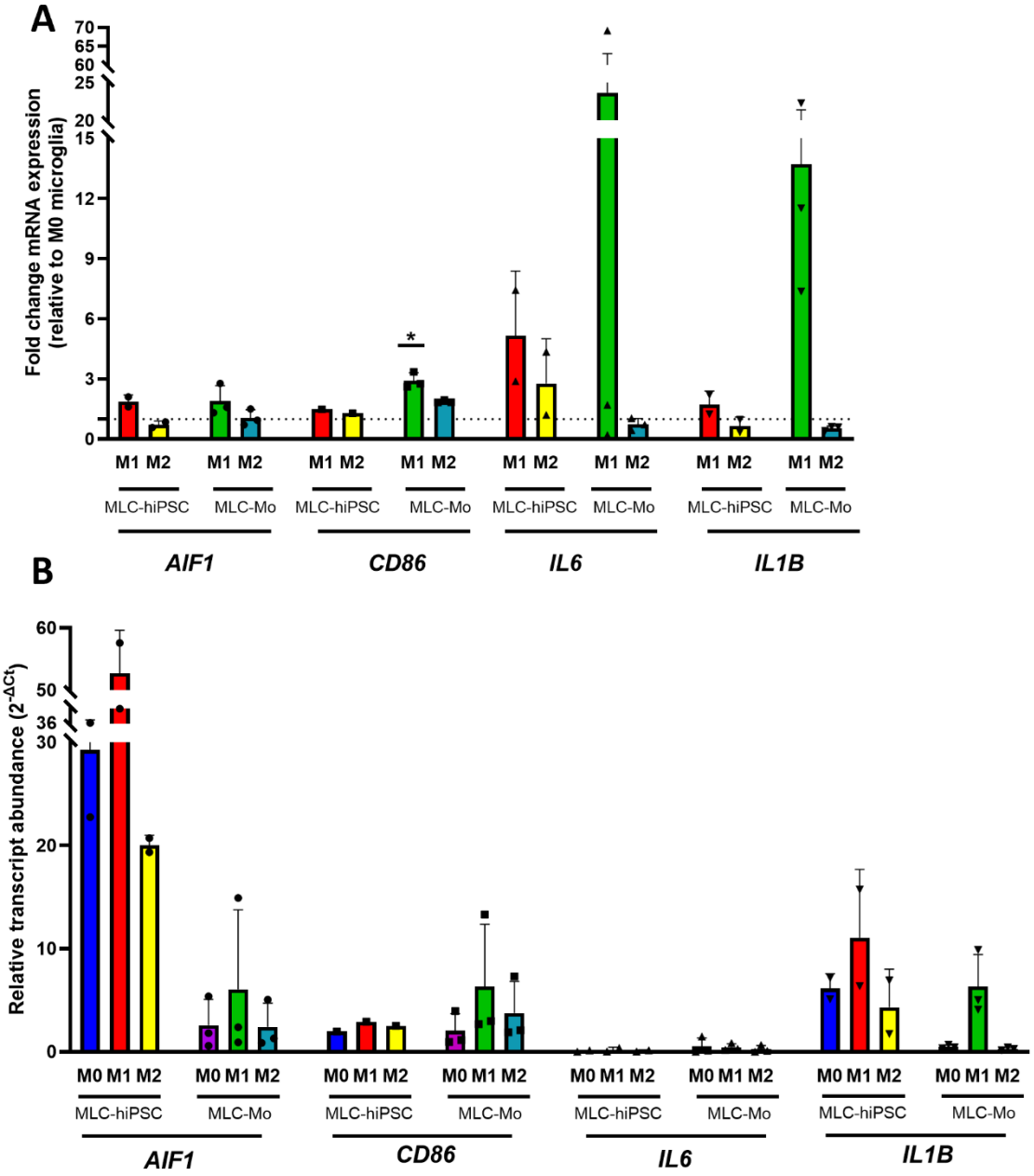

Figure 3.7 - **Pro-inflammatory marker expression in microglia-like cells derived from hiPSC (MLC-hiPSC) and monocytes (MLC-Mo) exposed to LPS + IFN-γ (M1 condition) and IL-4 + IL-13 (M2 condition) assessed by RT-qPCR. A** - Fold change *AIF1*, *CD86*, *IL6* and *IL1B* gene expression in MLC-hiPSC and MLC-Mo established from three peripheral blood PBMC donors (#2 #4, and #6) exposed to M1 and M2 stimuli and determined by the $2^{-\Delta\Delta Ct}$ method. Values were normalized to the expression of the housekeeping gene *RPL22* and are represented as fold change relative to the unchallenged condition (M0 microglia), set to 1 (dashed line). Error bars are shown as a mean of SD of biological triplicates. Nonparametric Kruskal-Wallis Test was performed. Significances are depicted as: *p < 0.05, **p < 0.01, ***p < 0.001, ****p < 0.0001. **B –** Relative transcript abundance ($2^{-\Delta Ct}$) in MLC-hiPSC and MLC-Mo established from monocytes isolated from PBMC donors (#2, #4, and #5) relative to Plot A. Error bars represent the mean of SD of biological triplicates. Reference gene targets used were *RPL22.* **A-B** - MLC-Mo fold change represents N=3 independent experiments. MLC-hiPSC fold change of *AIF1, IL6*, and *IL1B* represents N=2 independent experiments while *CD86* fold change represents N=1 independent experiment. Microglia Markers: *AIF1*(IBA1) **–** Allograft inflammatory factor 1; *CD86* – T-Lymphocyte Activation Antigen CD86**;** *IL6* – Interleukin 6; *IL1B* – Interleukin 1 beta. Housekeeping genes:*RPL22* – Ribosomal protein L22.

To better visualize inter-donor variability in MLC-Mos differentiated from PBMC-derived monocytes, data are shown for each donor (Figure 3.8A). Inter-donor variability in response to the inflammatory M1 stimuli was observed. *IL6* up-regulation was observed for only donor #6, with a fold increase of 74.2 compared to the unchallenged condition (Figure 3.8A). As mentioned before, *IL1B* upregulation was observed in MLC-Mos from all donors, although values varied greatly among donors (9.49-, 18.07-, and 7.74-fold increase in donor #2, #4 and #6 respectively). IL-6 and IL-1B secretion in the medium of LPS-challenged MLC-Mo have also been reported by another study, in agreement with our results [223]. In the case of *CD86*, up-regulation compared to the untreated control was observed in two out of three donors (2.61-, 3.36-, and 2.71-fold increase in donor #2, #4 and #6 respectively). In addition, data shown indicated that, as expected, the anti-inflammatory M2 challenge does not increase the expression of the inflammatory genes analyzed. In summary, while *IL1B* and *CD86* were found upregulated despite each donor, *IL6* expression was highly variable among donors.

For this task, Mφ differentiated from monocytes of the same PBMC donors were also treated with M1 or M2 stimuli, as a positive control. In Figure 3.8B shows the expression levels of pro-inflammatory markers in response to stimuli (M1 and M2). In pro-inflammatory Mφ (described as M1 in Figure 3.8B), it is only observed a 6.42-fold increase in CD86 expression in donor #4, with a slight increase in the other two (1.34- and 1.55-fold increase in donor #2 and #6 respectively). This observation may indicate that Mφ did not respond to the inflammatory stimuli. Nevertheless, other inflammatory markers will be required to validate this scenario, such as IL-8 and TNF-α, as reported in the literature [293]. These markers should then be analyzed not only at the gene expression level, but also at the protein level, using for example a cytokine array and ELISA methodologies, as were applied in the past in the host lab [251,294].

In addition, flow cytometry detection of inflammatory cell surface markers such as CD80, CD86, CCR7 and CD40 would certainly be necessary to complement and expand these observations [295,296]. Another crucial factor to consider when discussing these results is the exposure time applied. Our analysis was performed 48 h post-challenge with LPS and IFN-γ, both for Mφ and MLC-Mo. A study performed in human Mφ showed a time-dependent response on the magnitude of induction of inflammatory genes upon LPS and IFN-γ challenge. This study showed that, in general, the maximal induction in gene expression of a series of inflammatory markers (such as *IL1B, CXCL9, CXCL10* and *TNF-α*) was maximal for shorter time-points post-exposure (4-12 h) and tended to decrease at later time points (24-72 h) post-exposure [297]. This may potentially explain the reduced up-regulation of pro-inflammatory genes that we observed (at 48 h post-exposure to M1 stimuli). Shorter exposure times and/or time-dependent stimulation are then necessary to better define the inflammatory response kinetics in Mφ, in comparison with MLC-Mo established in parallel from the same donor. When comparing these results to MLC-Mo and MLC-hiPSC (Figure 3.8A and 3.7A, respectively), it is clear that MLC-Mo and Mφ responded differently to the inflammation, at least in the experimental conditions that have been applied. In addition and as expected, Mφ treated with the M2 condition (IL-4 +IL-13) did not upregulate inflammatory markers (Figure 3.8B) just like MLC-Mo and MLC-hiPSC (Figure 3.7A and 3.8A).

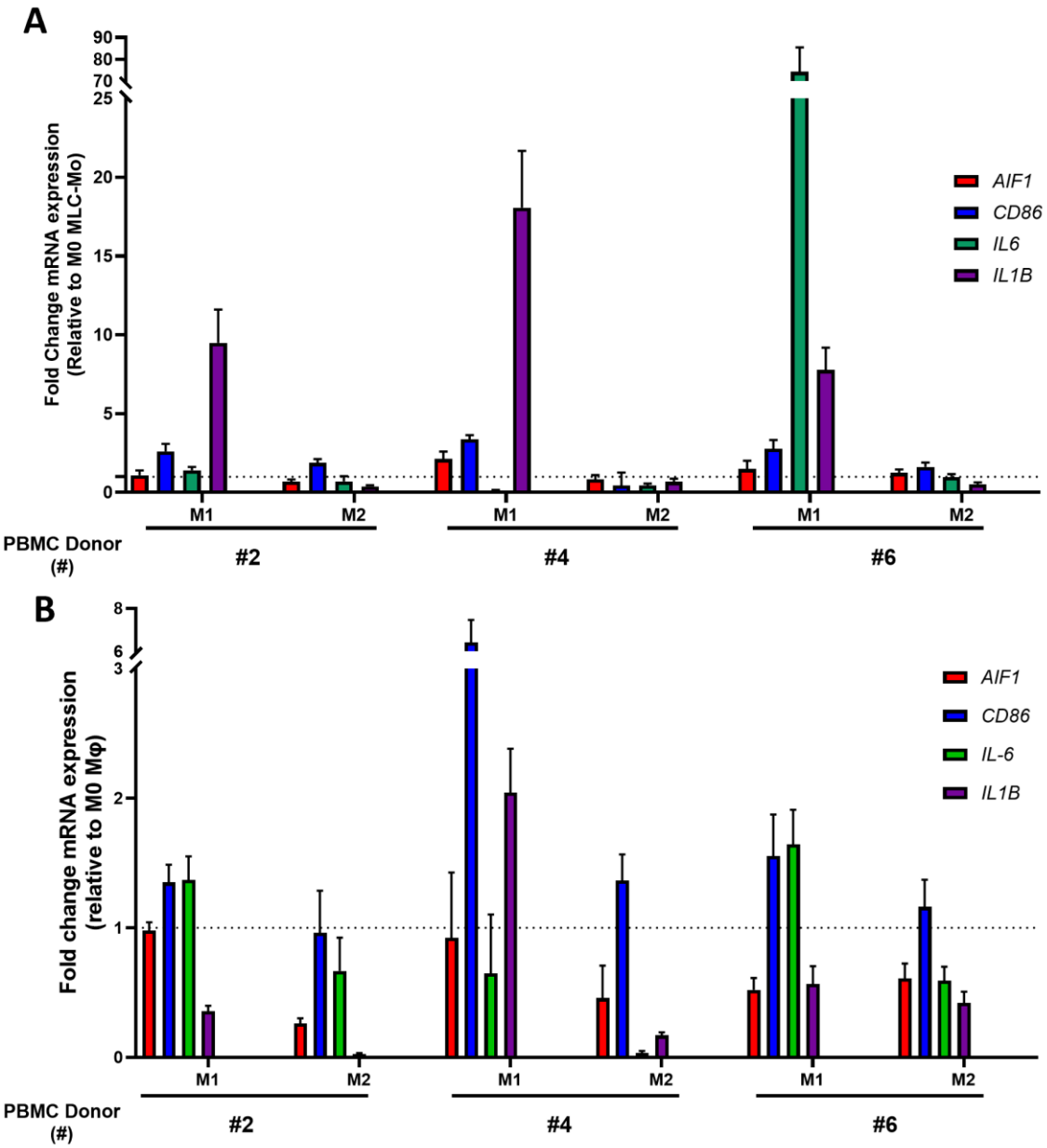

Figure 3.8 - Pro-inflammatory marker expression in monocytes derived microglia-like cells (MLC-Mo) and macrophages (Mφ), established form three peripheral blood mononuclear cell (PBMC) donors (#2 #4, and #6) exposed to LPS + IFN-γ (M1 condition) and IL-4 + IL-13 (M2 condition) assessed by RT-qPCR. **A** - Fold change *AIF1*, *CD86*, *IL6* and *IL1B* gene expression in MLC-Mo. Values were normalized to the expression of the housekeeping genes *RPL22* and 36B4, represented as fold change relative to unchallenged condition (M0 microglia), set as 1 (dashed line). **B –** Fold change *AIF1*, *CD86*, *IL6* and *IL1B* gene expression in Mφ. Values were normalized to the expression of the housekeeping genes *RPL22* and 36B4 represented as fold change relative to unchallenged condition (M0 macrophage), set as 1 (dashed line). **A-B** - Fold change values determined by the $2^{-\Delta\Delta Ct}$ method. Error bars are shown as a mean of SD of technical triplicates**.** Microglia markers: *AIF1*(IBA1) **–** Allograft inflammatory factor 1; *CD86* – T-Lymphocyte Activation Antigen CD86**;** *IL6* – Interleukin 6; *IL1B* – Interleukin 1 beta. Housekeeping genes: *36B4* – 60S Ribosomal Phosphoprotein P0 and *RPL22* – Ribosomal protein L22.

The results obtained for the anti-inflammatory response genes are shown in figure 3.9A. *MRC1* was upregulated upon anti-inflammatory challenge relative to the untreated control (designated as M0 microglia), both in MLC-Mos and MLC-hiPSC. *MRC1* up-regulation in MLC-Mo upon IL-4 exposure (2.41 ± 0.90 fold increase) has been also reported in a previous study [298], confirming the relevance of *MRC1* as marker of anti-inflammatory response in MLC-Mo.

In addition, MLC-Mo showed a statistically significant 3.13 ± 1 fold increase in *TGFB1* gene expression upon IL-4 + IL-13 challenge (M2 stimuli). In the relative transcript abundance analysis (Figure 3.9B), it was observed that MLC-Mo and MLC-hiPSC expressed significant levels of *TGFB1* in basal conditions (M0). Interestingly, it has been shown that TGF-β signaling is important for maturation and functionality of microglia [299]. Furthermore, in transforming growth factor beta receptor 2 (TGFBR2) knockout in mice are characterized by altered microglia homeostasis and activation [144]. These results may explain the relatively high abundance on TGFB1 transcript in both microglia sources.

In MLC-hiPSC, *CD163* expression was upregulated upon anti-inflammatory challenge (10.92-fold increase), but also upon pro-inflammatory stimulus (3.71-fold increase). This result is unexpected, since CD163 is a marker of the M2 phenotype, intensively described in the literature [121]. Moreover, unpublished data from the host lab showed upregulation of CD163 upon incubation of cells with anti-inflammatory stimuli, but not pro-inflammatory. Therefore, this was probably the result of a technical issue.

Due to the high variability among primary cells, MLC-Mo gene expression is displayed for each donor independently (Figure 3.10A). *MRC1 and TGFB1* were upregulated in MLC-Mo from all donors upon the anti-inflammatory challenge, with 1.7-to 7.9-and 2.5- to 4.5-fold increases in expression (for *MRC1 and TGFB1*, respectively).

In addition, no changes in the gene expression of the M2 marker genes were observed when MLC-Mo from the different donors were treated with M1 stimuli, as expected. To conclude, *MRC1* expression was increased in MLC-hiPSC and MLC-Mo, and *TGFB1* expression was upregulated in all MLC-Mo donors.

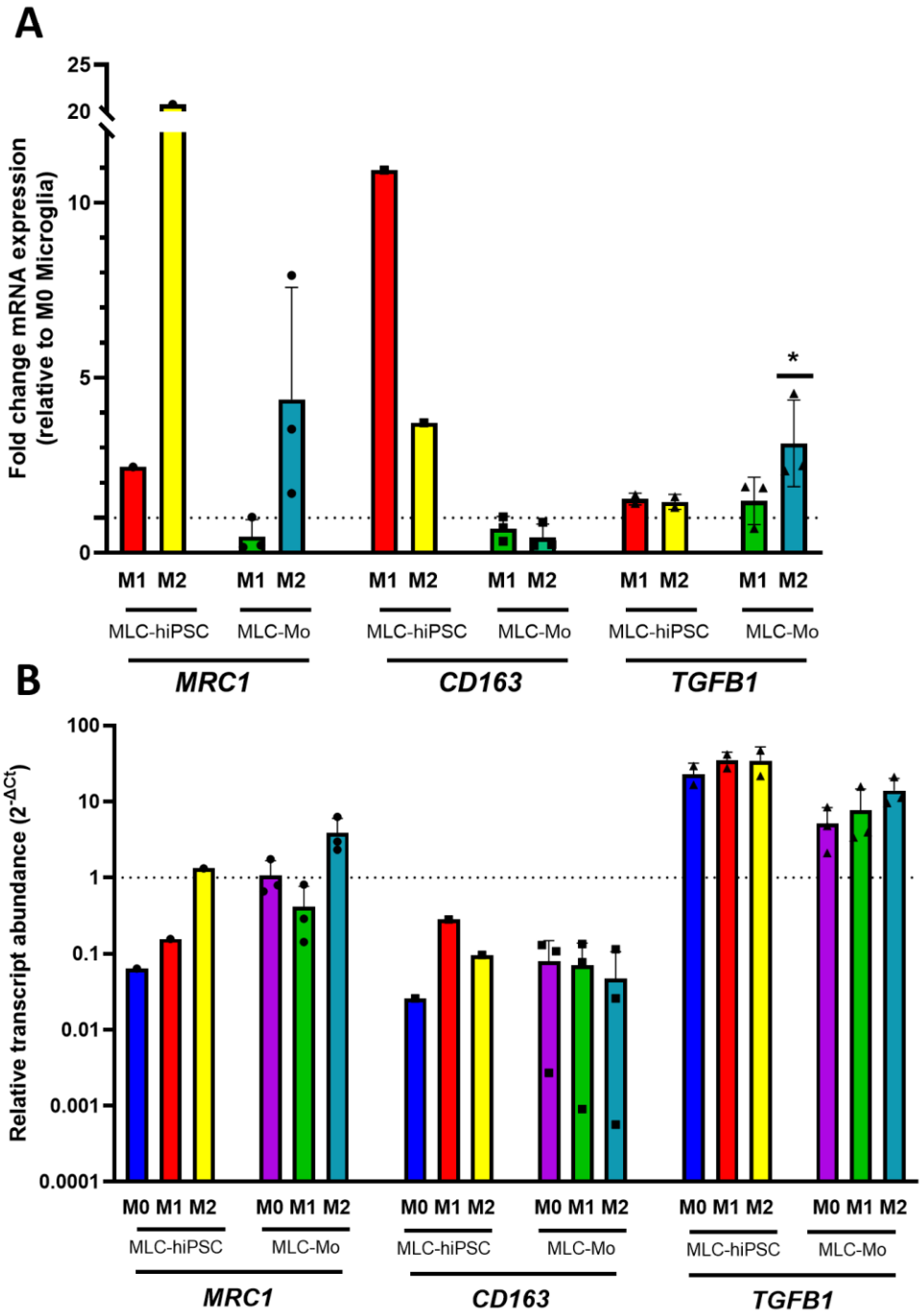

Figure 3.9 - **Anti-inflammatory marker expression in microglia-like cells derived from hiPSC (MLC-hiPSC) and monocytes (MLC-Mo) exposed to LPS + IFN-γ (M1 condition) and IL-4 + IL-13 (M2 condition) assessed by RT-qPCR. A** - Fold change for *MRC1*, *CD163*, *TGFB* gene expression in MLC-hiPSC and MLC-Mo, established form three peripheral blood PBMC donors (#2 #4, and #6) exposed to M1 and M2 stimuli, determined by the $2^{-\Delta\Delta Ct}$ method. Values were normalized to the expression of the housekeeping gene *RPL22* and are represented as fold change relative to the unchallenged condition (M0 microglia), set as 1 (dashed line). Error bars are shown as a mean of SD of biological triplicates. The Nonparametric Kruskal-Wallis Test was performed. Significances are depicted as: *p < 0.05, **p < 0.01, ***p < 0.001, ****p < 0.0001. **B –** Relative transcript abundance ($2^{-\Delta Ct}$) in MLC-hiPSC and MLC-Mo established from monocytes isolated from PBMC donors (#2 #4, and #6) relative to Plot A. Error bars represent the mean of SD of biological triplicates. Reference gene targets used were *RPL22.* **A-B** - MLC-Mo fold change represents N=3 independent experiments. MLC-hiPSC fold change of *TGFB1* represents N=2 independent experiments while *MRC1 and CD163* fold change represents N=1 experiment. Microglia Markers: *MRC1* (CD206**)** – Macrophage mannose receptor 1; *CD163* – Haemoglobin Scavenger Receptor**;** *TGFB1* – Transforming growth factor beta 1. Housekeeping genes: *RPL22* – Ribosomal protein L22.

Expression of anti-inflammatory markers was also evaluated in Mφ (Figure 3.10B) for each donor independently. In M1-treated Mφ, upregulation of anti-inflammatory markers was not observed, as expected. In addition, an upregulation of *CD163* and an increase of *TGFB1* expression in donor #2 was observed compared to untreated Mφ. Comparing these results to MLC-Mo, a trend in upregulation of anti-inflammatory markers in Mφ upon M2 stimuli challenge is observed, but it was in general not consistent with the relative Mφ counterpart derived from the same donor (Figure 3.10A and B)

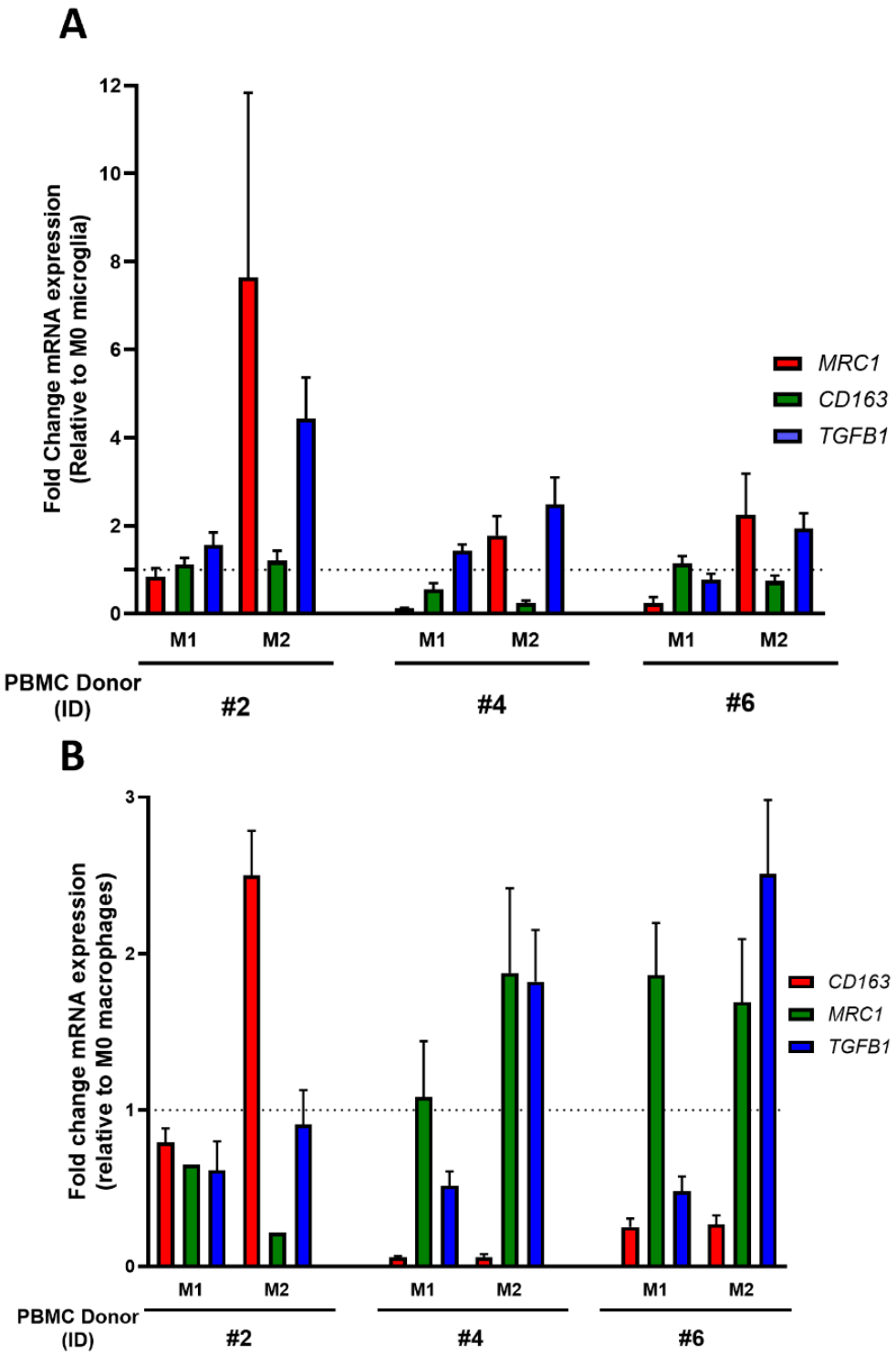

Figure 3.10 - Anti-inflammatory marker expression in monocytes derived microglia-like cells (MLC-Mo) and macrophages (Mφ), established form three peripheral blood mononuclear cell (PBMC) donors (#2 #4, and #6) exposed to LPS + IFN-γ (M1 condition) and IL4 + IL13 (M2 condition) assessed by RT-qPCR. **A** - Fold change for *CD163*, *MRC1*, and *TGFB1* gene expression in MLC-Mo. Values were normalized to the expression of the housekeeping genes *RPL22* and 36B4 and represented as fold change relative to the unchallenged condition (M0 microglia), set as 1 (dashed line). **B –** Fold change for *AIF1*, *CD163*, *MRC1*, and *TGFB1* gene expression in Mφ. Values were normalized to the expression of the housekeeping genes *RPL22* and 36B4 and represented as fold change relative to the unchallenged condition (M0 macrophage), set as 1 (dashed line). **A-B** - Fold change values determined by the $2^{-\Delta\Delta Ct}$ method. Error bars are shown as a mean of SD of technical triplicates**.** Microglia markers: *MRC1* (CD206**)** – Macrophage mannose receptor 1; *CD163* **–** Haemoglobin Scavenger Receptor; *TGFB1* – Transforming growth factor beta. Housekeeping genes: *36B4* – 60S Ribosomal Phosphoprotein P0 and *RPL22* – Ribosomal protein L22.

M2 stimuli effect was further characterized in MLC-Mo in four different donors (#2, #6, #7 and #8) by IF, exposing MLC-Mo to IL-4 and IL-13 under the same condition used for the gene expression analysis (Figure 3.11). The IF showed that, under this condition, neither CD163 nor CD206 protein expression was upregulated, which in the case of CD163 corroborates the RT-qPCR results (Figure 3.9).

Moreover, CD206 presented high detection levels in MLC-Mo without treatment. Recently, single-cell mass cytometry data suggested that CD206 is detectable also in human microglia [300]. Marzolo et al. also reported that CD206 is expressed by primary rat microglia [301], indicating that it is already present in basal level in these cells without anti-inflammatory challenge. In addition, the upregulation observed in *MRC1* by RTq-PCR after M2 challenge (Figures 3.8 and 3.9A) is not confirmed by IF.

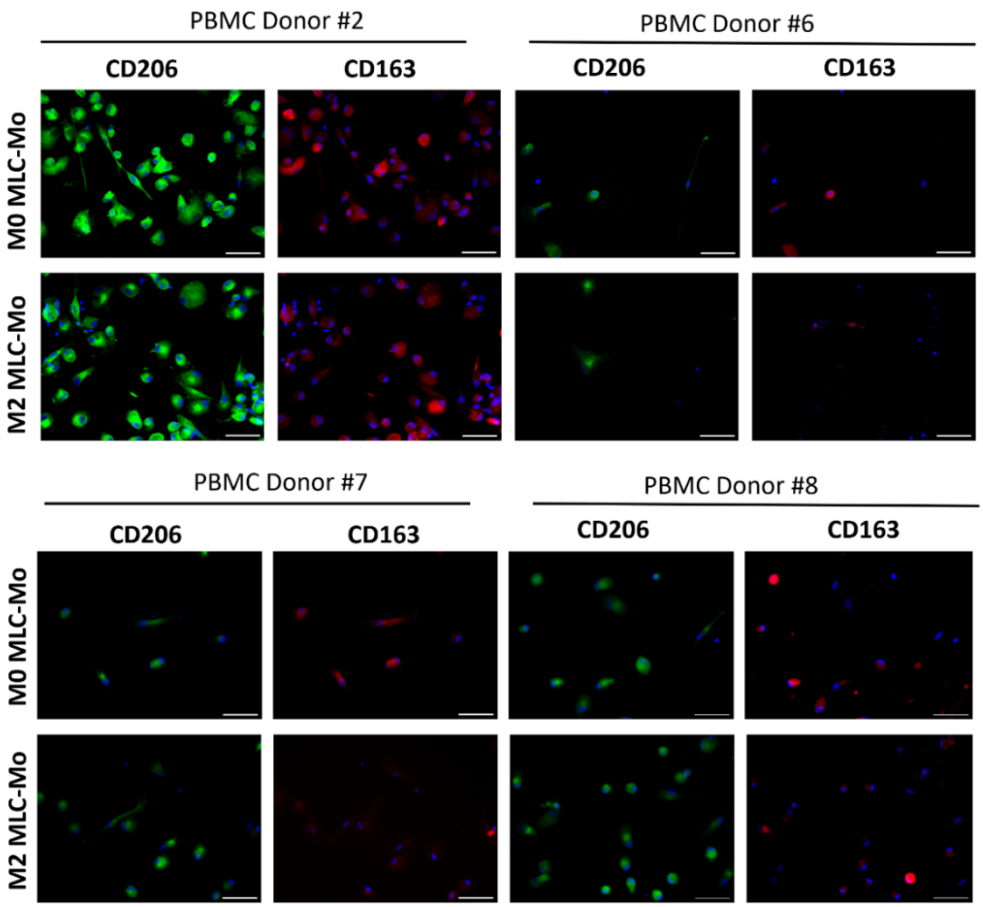

Figure 3.11 - **CD206 and CD163 analysis by immunofluorescence in monocyte derived microglia-like cells (MLC-Mo).** MLC-Mo was established form 4 different donors (#2, #6, #7, and #8), exposed to anti-inflammatory stimuli (IL4 and IL13) (M2 MLC-Mo) and compared to unchallenged condition (M0 MLC-Mo). CD206 was labelled in green (AlexaFluor® 488) and CD163 was labelled in red (AlexaFluor® 594). Cells were counterstained with 4',6-diamidino-2-phenylindole (DAPI, blue) for nuclei identification. Scale bar: 50µm Microglia markers: Scavenger Receptor Cysteine-Rich Type 1 Protein M130; CD206: Macrophage Mannose Receptor 1-Like Protein 1.

However, this could be explained by the fact that the RNA and protein expression may not correlate [275], and that longer exposure time is potentially required to observe a clear increase in CD206 protein level.

In addition, only one technique (IF) was used to detect these M2 markers, so further analysis by FC may help to further confirm or challenge these results. Still, it is difficult to define a "M2 status" using only a few markers, and extending the protein panel analysis of typical structural M2/Immunosuppressive markers such as CSF1R, DC-SIGN, CD204 or secreted (IL-10, CCL22, CCL24) will be much more informative and contribute to shed light on the ability of these cells to respond to anti-inflammatory stimuli such as IL-4 and IL-13 [251,297]. Response to prototypical inflammatory stimuli (LPS + IFN-γ) appeared to be much more consistent and in the future could be confirmed by ELISA analysis of secretion of pro-inflammatory cytokines (e.g., IL-6, IL-8, TNF-α). In addition, considering the high variability among donors, already observed in the literature [269], it is required to analyze additional replicates to confirm such data [302]. Moreover, other functional assays, such as microglia/macrophage phagocytic activity, would be critical to complement the data presented here. In fact, the ability to phagocytose dead cells [302], debris and pathogens is one of the main function of microglia in the CNS [76].

3.2. Establishment and characterization of 3D Cell GBM culture

3.2.1. Implementation/establishment of two 3D cell culture strategies

In order to perform co-cultures of glioma cells with microglia, as an *in vitro* model to study glioblastoma (GBM) immunosuppression, it was decided to employ a 3D glioma cell culture approach, due to its ability to provide more realistically biochemical and biomechanical microenvironments than 2D monolayer cell culture formats [303]. As such, two distinct methods for generation of cell spheroids were implemented, the neurosphere formation assay and the spheroid formation in stirred-tank culture systems.

The neurosphere formation is based on culturing cells at low densities, on ultra-low attach (ULA) surfaces. This condition can activate anoikis, a form of programmed cell death activated when cell adhesion to an extracellular matrix (ECM)/scaffold is absent [188]. As differentiated epithelial cells are highly sensitive to anoikis and, on the other hand, cancer stem cells (CSC) are typically resistant to this type of cell death, the culture conditions favor CSC enrichment from the start. Additionally, the medium is supplemented with stem cell growth factors, to promote CSC proliferation. Therefore, the neurosphere assay leads to the formation of GBM spheroids largely enriched in CSCs-like cells [185]. The cells that compose the neurospheres proliferate and

differentiate within the spheroids in suspension [194]. This methodology has gained enormous importance in GBM and DMG research, since it has been instrumental to show the relevance of CSCs in GBM tumor progression, chemoresistance and immunosuppression [304].

In this work, for the neurosphere formation assay, cells were plated at a low density (20 000 cell/mL, in ultra-low attachment T25 flasks, in serum-free medium containing the stem cell growth factors, epidermal growth factor (EGF) and basic fibroblast growth factor (BFGF), the neurotrophic supplements B27 and N2 and heparin, for up to 14 days. (Materials and Methods section 2.2.1) [243].

In the second method, GBM cells were cultured in a spinner flask, under stirring conditions. This approach has been established in the host lab and optimized for a wide range of cancer cell lines [250]. This culture system requires a high cell density ($2x10^5$ cell/mL), compared to neurospheres, to increase the chance of collision, which in turn promotes cell aggregation, as described in the Introduction (section 1.6.4.1). The main differences from the neurosphere assay are the dynamic culture conditions and the use of a serum-supplemented medium, which favors cell adhesion after an initial collision. Serum has been described to favor differentiation and, therefore, may affect the GSC population [305–307].

For aggregation of A172 cells in spinner vessels, we followed an empirical approach previously established by the host lab to select the most favorable stirring conditions for individual cancer cell lines [250]. This consists in testing aggregation in parallel at three different stirring rates (60, 80, and 100 rpm).

3.2.2. Cell viability and morphological analysis of A172 cells in neurospheres and spheroids

For neurospheres, we observed a population heterogenous in size (phase contrast microscopy, Figure 3.12A). Viability assays were performed at the 7^{th} and 14^{th} days of culture. Cell viability was always high, and no considerable or regionalized cell death could be detected within the 3D structures. Neurospheres morphological analysis included determination of area, maximal Feret diameter, and roundness of neurospheres, at days 7 and 14 of culture. All parameters showed a high variance at both timepoints, which increased from day 7 to day 14 for the area and the maximal Feret diameter. Roundness was constant throughout the culture time. The mean of the maximal Feret diameter value obtained in the neurospheres (114 ± 50.6 and 128 ± 91.01 µm at day 7 and day 14 respectively) is relatively lower than for a primary CSC culture protocol reported in the literature. This protocol states that around day 7 or 10 of culture, the neurosphere size could reach 150 to 200 µm [308]. However, in this article the authors plated 50 000 GBM cell/mL, which is higher than the seeding density we used for the neurosphere assay (20 000 cell/mL). This increased cell density may provide an improved initial adherence between cells in suspension. This effect potentially ensures cell survival in higher than in lower cell density, which may then result in an increased final neurosphere diameter. Nevertheless, it is important to refer that the initial neurosphere seeding density that is possible to find across the literature for

A172 GBM cells is quite variable among reports, even if the same serum-free culture medium was employed [243,248], which in the end may impact the final neurosphere diameter.

Regarding the spheroid aggregation under different stirring rates, cell viability remained very high in all conditions (Figure 3.12A). On day 1, there was a high number of single cells in suspension in all rates (Figure S.7), which decreased through the time of the experience, being incorporated in spheroids. Spheroids formed under stirring rates of 80 rpm and 100 rpm showed high compaction and were homogeneous in size, compared to the ones formed at 60 rpm, as confirmed by morphological analysis (roundness, area, and diameter) (Figure 3.12B). Spheroids obtained at stirring rates of 80 rpm and 100 rpm showed lower variation in all morphological parameters within the same biological replicate compared to spheroids prepared at 60 rpm. Relative to the spheroids at stirring rates of 80 rpm from different replicates, no statistically significant differences were found between biological replicates, except for roundness in one of the replicates (Figure 3.12B).

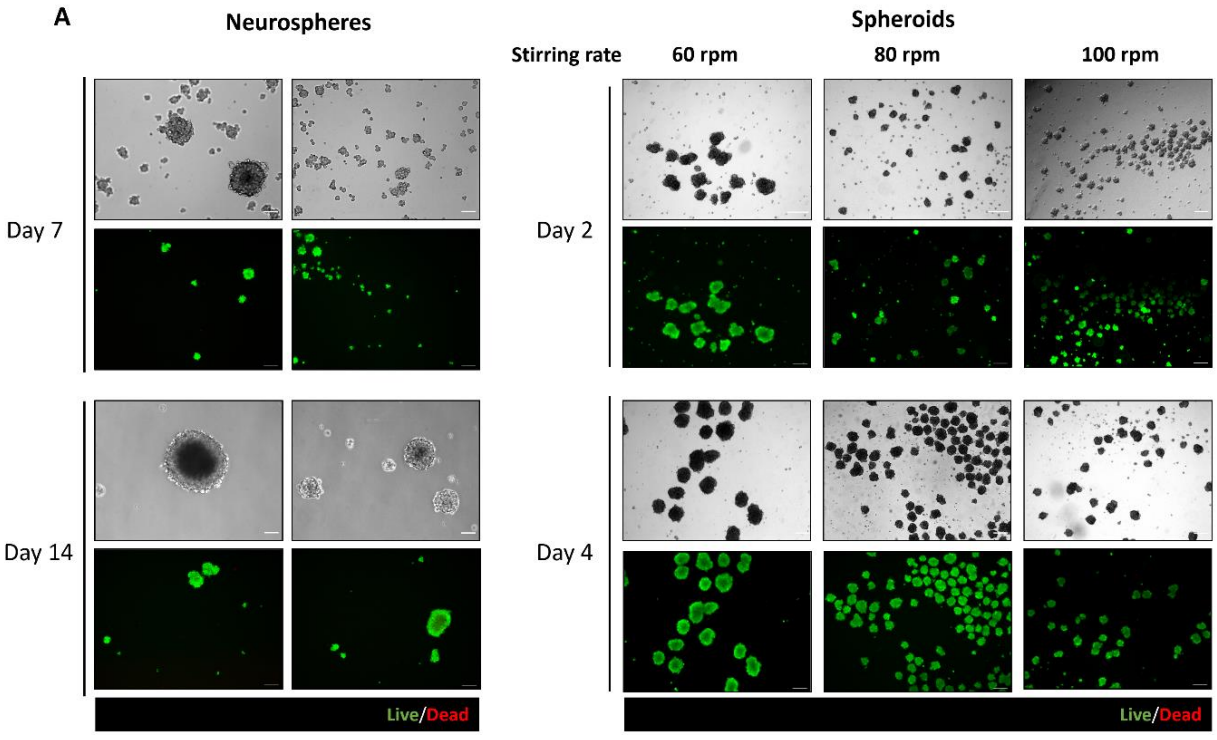

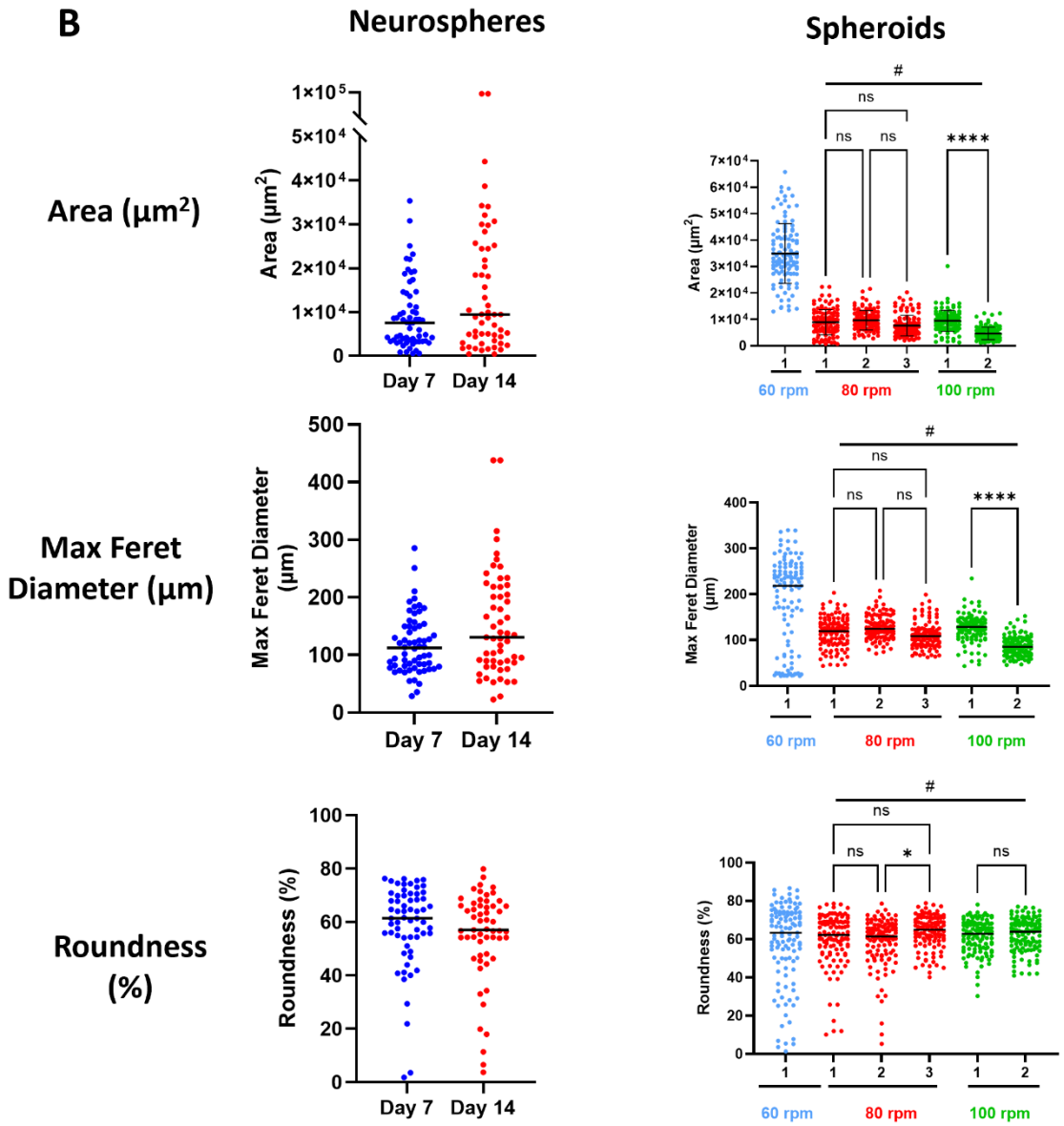

Figure 3.12 - **Morphological characterization of two different A172 glioblastoma (GBM) cell line 3D cell culture strategies. A –** Cell viability of neurospheres and spheroids analysed during and at the end of the culture, assessed by fluorescence microscopy (FDA, shown in green) shows live cells, while ToPro™-3 (red) shows dead cells. Representative images are shown N=3 for neurospheres and spheroids under a stirring rate of 80 rotations per minute (rpm); N=2 spheroids under a stirring rate of 80 rpm, and N=1 spheroids under a stirring rate of 60 rpm Scale bar: 50µm. **B–** Morphological characterization of neurospheres at day 7 and day 14 and at spheroids at the end of culture. For spheroids, the biological replicates (designed as 1,2 and/or 3) are represented independently. Both 3D culture strategies were characterized by Area (µm), max Feret diameter (µm^2) and roundness (%). For each morphological parameter, 55 neurospheres and 114 spheroids were analysed. Bars represent the mean of all spheroids/neurospheres within each parameter. Analysis was performed using the ICY Software [255]. Parametric the one-way ANOVA was performed. Significances are depicted as: ns – non-significant, *p < 0.05, **p < 0.01, ***p < 0.001, ****p < 0.0001. Levene`s test for comparison of spheroid diameter dispersion ($^{\#}$p < 0.05) in different replicates and agitation rates.

In the case of spheroids at stirring rates of 100 rpm, we found a statistically significant difference in the area and maximal Feret diameter from both biological replicates. In addition, by applying the Levene´s test, we confirmed variance homogeneity (represented as # in figure 3.12B) between spheroids under a stirring rate of 80 and 100 rpm. Spheroids at a stirring rate of 60 rpm showed the highest variance among all spheroids within the same replicate as previously mentioned. This goes in concordance with previous work from the lab when implementing

spheroids from cancer cell lines using a stirring rate of 60 rpm [250]. Due to this high heterogeneity of spheroids among the same biological replicate, no further experiments were performed using a stirring rate of 60 rpm.

Moreover, in GBM spheroids generated at stirring rates of 80 and 100 rpm (Figure 3.12B), we observed a similar diameter compared to other cancer cell line spheroids produced under the same stirring rate (A172 - 80 rpm: 118± 30; 100rpm 106±32.44; MCF7 - 80 rpm: 144±29; BT474 - 80 rpm: 107±29; H157 - 80/100 rpm141±21) [250]. Moreover, spheroids obtained at stirring rates of 80 rpm and 100 rpm showed (Figures 3.15A and B) spherical characteristics (no surface edges), which were observed in breast, lung, and colorectal cancer cell lines under a stirring rate of 40-100 rpm [250].

Additionally, the spheroid concentration was determined on day 4 (Figure 3.13). Spheroids prepared with a stirring rate of 80 and 100 rpm showed a similar spheroid concentration of 739 spheroid/mL ± 110.3 and 830 spheroid/mL ± 174.7. Spheroids formed with a stirring rate of 60 rpm showed the lowest concentration registered from all spinners with a value of 177 ± 30 spheroid/mL. This, together with the morphological analysis, suggests that cells did not die at this agitation rate, just formed larger spheroids, with more cells per spheroid.

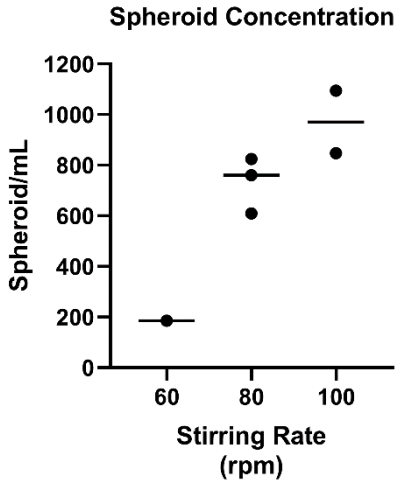

Figure 3.13- Spheroid concentration under different stirring rates. Represented in dots is the spheroid concentration in spheroid per mL in each biological replicate of spheroids formed at different stirring rates (60, 80 and 100 rotations per minute (rpm)). Bars represent the mean spheroid concentration from the biological replicates performed. Spheroids obtained at 60 rotations per minute (rpm) N=1 independent experiment. Spheroids prepared at 80 rpm, N=3 independent experiments. Spheroids formed at 100 rpm, N=2 independent experiments.

Gathering all these results, 80 rpm and 100 rpm appeared to be the stirring rates generating A172 spheroids with higher reproducibility than 60 rpm, with very similar results between biological replicates. Therefore, spheroids formed at stirring rates of 80 and 100 rpm were further characterized alongside 3D structures formed in the neurosphere formation assay, by detection of CSC markers and immunosuppressive/chemoattractant cytokines.

Finally, comparing neurospheres with spheroids, we observed that the first were more heterogeneous than spheroids, which appeared more spherical and compact. This can be explained by the continuous stirring into spinner-vessels of the initial cell suspension. This

guarantees a homogeneous cell suspension, in which cells progressively cluster to form the final spheroids [309]. In addition, another important factor that can explain the better compaction of spheroids compared to neurospheres could be the use of by fetal bovine serum (FBS). It has been reported that serum supplementation (absent in neurosphere cultures) to generate spheroids improves cell-to-cell adherence and compaction [310].

3.2.3. Analysis of cancer stem cells markers expression in A172 2D cultures, neurospheres and spheroids

With the successful implementation of two distinct 3D culture methods for A172 GBM cells, we proceeded with an in-depth cellular characterization. As mentioned previously, one of the main characteristics of neurosphere culture is the enrichment in CSCs [185–187]. In addition, by analysis of expression data in GBM deposited in the GEPIA database (Figure 3.14), we observed most of the CSC genes analyzed (*SOX2*, *NESTIN, PROM1 (*which codes for CD133), and *CD44*), were more expressed in GBM tumor tissues compared to normal brain tissue (*POU5F1*, which codes for OCT4, and *NANOG* were the exceptions*)* [311]. These factors have been reported to be important in GBM tumorigenesis, progression and poor outcome [312–315].

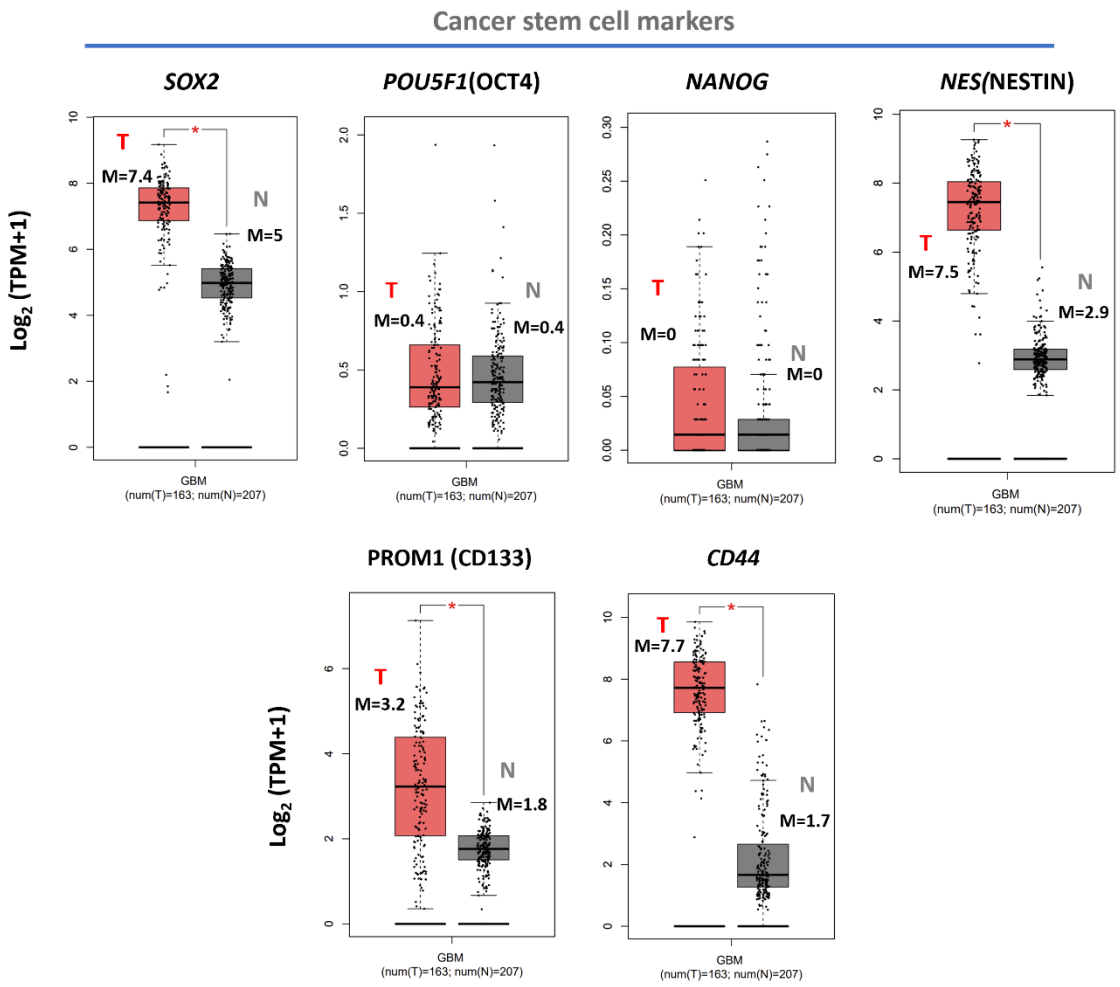

Figure 3.14 - *In silico* data on cancer stem cancer cell (CSC) markers in glioblastoma (GBM). RNA bulk results from 163 healthy brain tissues (N) and 207 GBM tissues (T) of the expression of different CSC markers. Data from GEPIA database (http://gepia.cancer-pku.cn/), based on the cancer genome atlas (TCGA) tumors vs TCGA normal + Genotype-Tissue Expression (GTEx) normal datasets, accessed in July 2022 [313]. Results are displayed as log_2 of transcripts per million (TPM) +1. CSC markers: *SOX2* - SRY-Box Transcription Factor 2; *POU5F1*(OCT4) – POU Class 5 Homeobox 1; *NANOG* – Nanog Homeobox; *NES* – Nestin; *PROM1* (CD133) – Prominin 1; *CD44* – CD44 molecule

In addition, these stemness markers have been already reported in other cancer types, such as colorectal, gastric and ovarian [316–319].

Additionally, as described in the introduction section, high expression of *PROM1* in GBM patients correlates with a worse outcome [320]. Furthermore, CSCs have been proposed to have a role in immunosuppression, by secreting multiple immunosuppression mediators, such as cytokines (e.g., IL-10, TGF-β), ECM proteins (e.g., periostin) and exosomes [94,98,321].

SOX2, *POU5F1*, *NES*, and *NANOG* expression in A172 cells cultured in 3D was then assessed by RT-qPCR, by comparison with 2D culture conditions (Figure 3.15). We observed that A172 neurospheres showed a trend for the higher fold increase in *SOX2*, *POU5F1*, and *NES* compared to spheroids formed under stirring and a significant fold increase than 2D cultures.

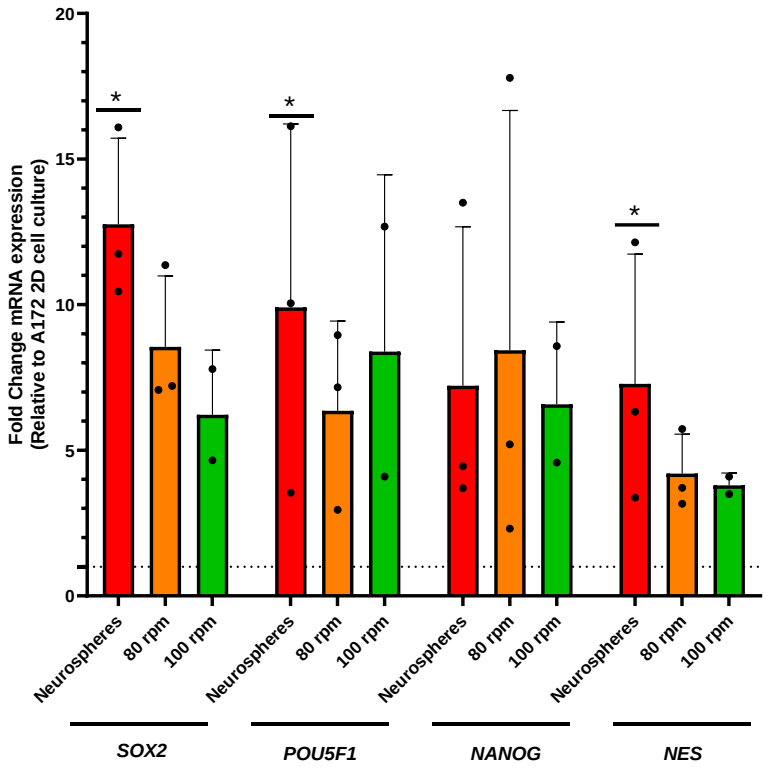

Figure 3.15- Cancer stem cell (CSC) marker identification in different 3D culture strategies. A – Fold change gene expression in GSC markers in neurospheres and spheroids under stirring rate of 80 and 100 rotations per minute compared to A172 2D cell cultures, determined by the $2^{-\Delta\Delta Ct}$ method. Values were normalized to the expression of housekeeping genes *36B4* and *RPL22*. Data are represented as fold change relative to A172 2D culture, set as 1 (dashed line). Data show mean ±SD of N= 3 independent biological replicates. Nonparametric Kruskal-Wallis Test was performed. Significances are depicted as: *p < 0.05, **p < 0.01, ***p < 0.001, ****p < 0.0001. CSC markers: *SOX2* - SRY-Box Transcription Factor 2; *POU5F1* - POU Class 5 Homeobox 1, *NANOG* – Nanog Homeobox; *NES* - Nestin

In addition, an increased expression of *NANOG* was observed as well in neurospheres compared to 2D cultures, even though it was not significant. *NANOG* was similarly expressed in all the 3D cell cultures tested, compared to 2D cells (Figure 3.15). *SOX2* fold increase in detection compared to 2D cultures has also been observed in the U87-MG GBM cell line spheres by FC [322]. Moreover, in GBM primary neurosphere generated by $CD133^+$ fluorescent activated cell sorting (FACS), *SOX2* and *POU5F1* had a higher expression compared to $CD133^-$ neurospheres [323]. This indicates that various stemness genes tend to be co-expressed in GBM CSCs [324]. Interestingly, it has been reported that the stem and reprograming factors SOX2, NANOG and POU5F1 [325] form an interconnected regulatory circuit, in which each factor activates its own promoter and those of each other [326]. This ultimately leads to the reinforcement and maintenance of the stemness state in pluripotent stem cells. Interestingly, the transgenic co-expression of POUF51 and SOX2 in A172 GBM cells has been reported to induce CSC phenotype through the increase of CD133, OLIG-2 and *NANOG,* indicating that such positive regulation between the stem and reprogramming factors may exist even in GBM [323]. Finally, such positive autoregulatory loop has been shown also in the MCF-7 breast cancer cell line, where the overexpression of *NANOG*, *POU5F1* and *SOX2* increased the expression of each of the others [327]. These observations indicate that such regulatory loop exists in cancer cells and not only in embryonic or pluripotent stem cells.

Additionally, we assessed the CSC markers CD133, SOX2 and NESTIN by IF (Figure 3.16A). Neurospheres compared to spheroids formed under stirring showed higher staining for CD133, widespread along the 3D structures; in A172 cells in 2D cultures, CD133 was not detected. The detection of CD133 in neurospheres has already been shown in other GBM cell lines (U87-MG and U251-MG) and neurospheres established from patient-derived GBM cells [193,328].

SOX2 showed a higher detection in neurospheres than in other culture formats. These results confirm the RT-qPCR data previously observed (Figure 3.15). Interestingly, we observed cytosolic SOX2 (Figure 3.16B), which is generally expected to be localized in the cell nucleus, being a nuclear transcription factor [329]. Nevertheless, it has been reported that transcription factors (TF) such as SOX2, SOX9 and OCT4 may have also cytoplasmatic localization even though its biological relevance in cancer is not yet clear [330,331]. Interestingly, SOX9, another TF involved in GBM tumorigenesis and stemness [332], has been reported to be in a cytosolic state in pancreatic cancer, where it was associated with worse outcome in patients [331]. Additionally, cytosolic SOX2 has been observed in colon rectal cancer, tongue squamous cell carcinoma, GBM [330,333] and primary pediatric brain tumor cultured as neurospheres [334]. It is well established that nuclear or cytosolic SOX2 localization is governed by post-translational modifications - SOX2 phosphorylation at Thr118 triggered by AKT protein kinase inducing nuclear accumulation, while acetylation at Lys75 induces SOX2 nuclear export [335]. Nonetheless, there

are no indications, to our knowledge, of the cytoplasmic SOX2 role in cancer. Interestingly, it has been shown that cytosolic SOX2 exerts a functional role in human neutrophils, where it serves as bacterial DNA sensor. Here, upon SOX2 high-mobility group binding to bacterial DNA, SOX2 dimerizes and create a complex with the Tat associated kinase 1/TGF-β activated kinase 1 binding protein 1 (TAK1/TAB2) to ultimately activate Nf-kB and induce inflammation [336].

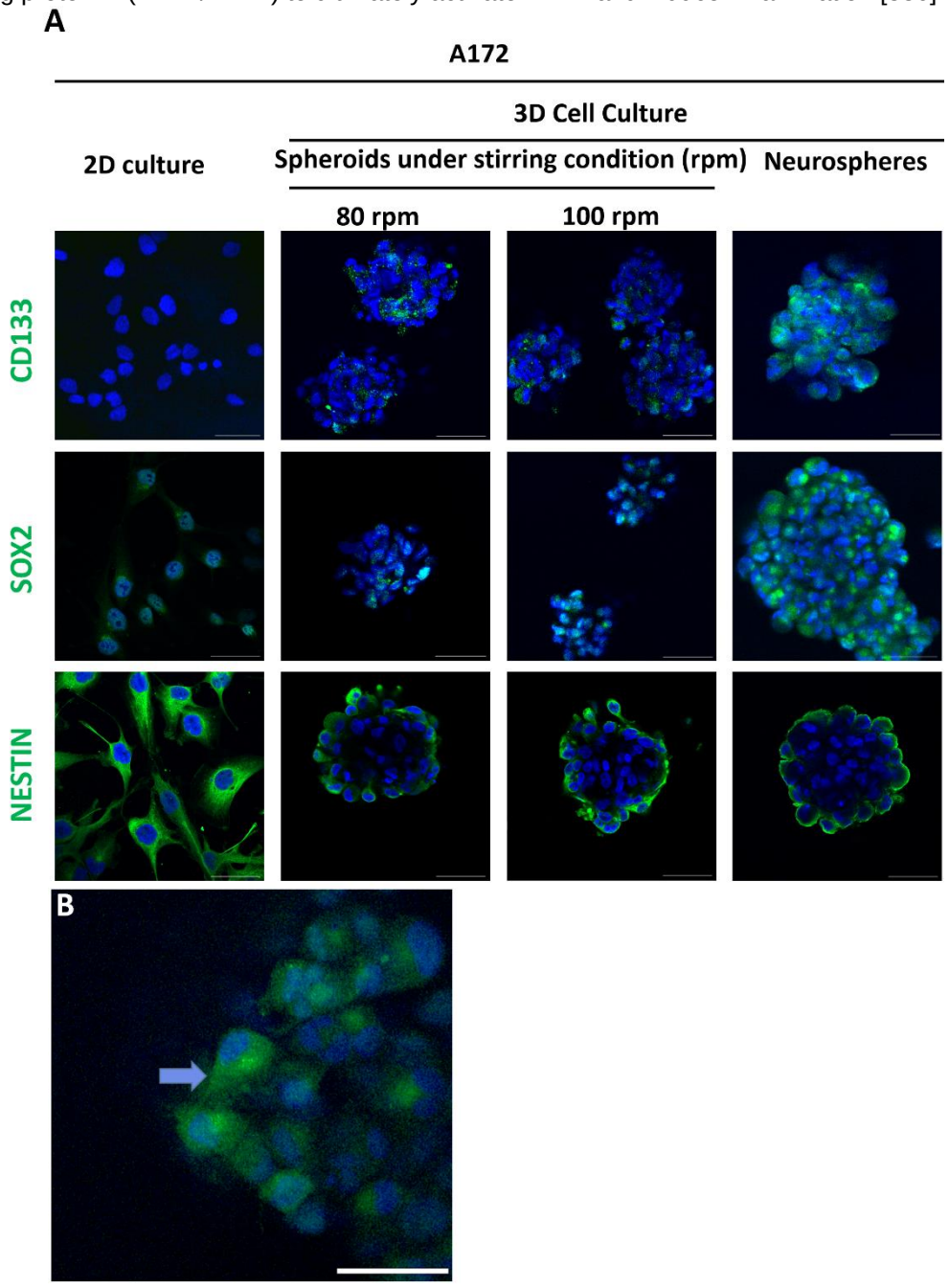

Figure 3.16 - Cancer stem cell (CSC) marker identification in different 3D culture strategies. A – Immunofluorescence of CSC markers CD133, SOX2, NESTIN, labelled in green (AlexaFluor® 488). Cells were counterstained with 4',6-diamidino-2-phenylindole (DAPI, blue) for nuclei identification. Images composed from a Z-Stack projection of 10 slices with 1 µm thickness. Representative images of 2 independent experiments (CD133, SOX2 and GFAP). **B** - Detection of cytosolic SOX2 indicated in arrows. Image composed from a Z-Stack projection of 10 slices with 1 µm thickness. Representative images of 2 independent experiments. Scale bar: 50 µm. CSC markers: *SOX2* - SRY-Box Transcription Factor 2; *NES* – Nestin; *PROM1* (CD133) – Prominin 1.

We further characterized A172 neurosphere cultures by FC, analysing the surface expression of CD44. CD44 is a cell surface adhesion receptor expressed in multiple cancer types. It plays a role in cell-cell interactions, cell adhesion and migration, promoting cancer cell invasion and metastasis [337]. Furthermore, high CD44 expression has been reported to be positively associated with poor prognosis and immunosuppression in gliomas [338]. We observed that A172 cells, both in neurospheres and in 2D cultures were characterized by high CD44 expression (Figure 3.17A). As a positive control, we used the triple negative breast cancer cell line MDA-MB-231, that displayed high CD44 level, as expected [339]. CD44 detection was also confirmed by WB (Figure 3.17B), corroborating the FC data and previous reports in A172 cultures [178,340]. Furthermore, CD44 is a glycosylated protein, and differences in CD44 glycosylation between 2D and neurosphere cultures may be present. In fact, we observed a differential CD44 WB migration rate, as previously described for CD68 [341]. Finally, high CD44 expression has been associated with an increased in glioma grade and it is especially elevated in the mesenchymal glioma subtype, to which A172 belong [338].

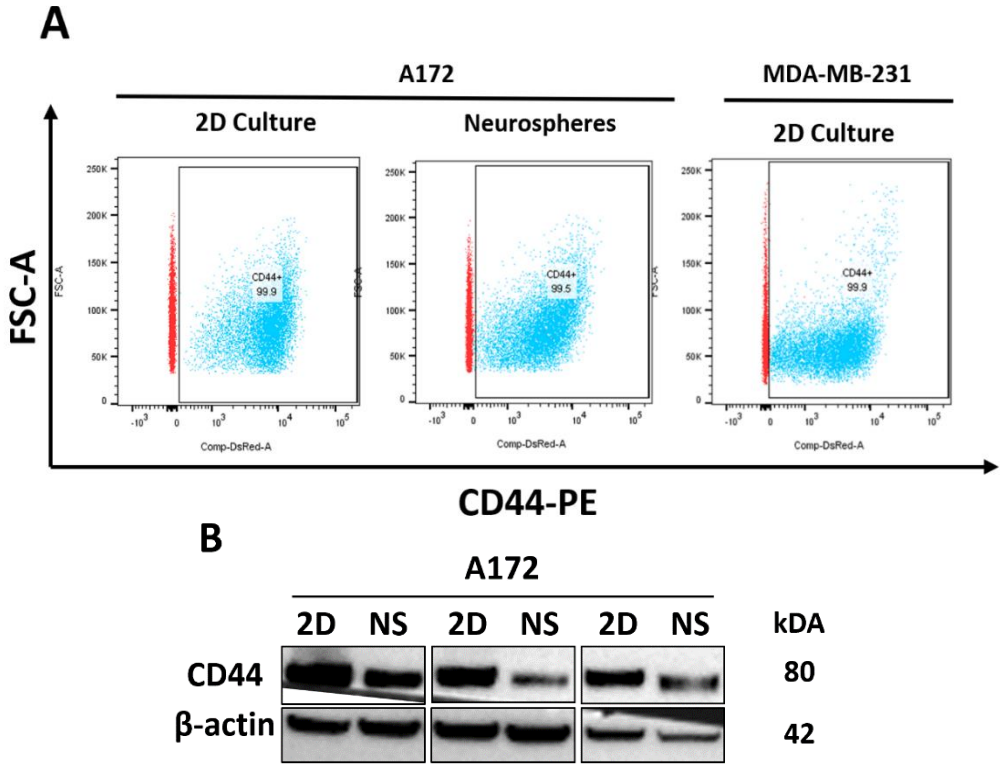

Figure 3.17 - CD44 marker detection in different in neurospheres. A - Double dot plot, indicating CD44 population (labelled in blue) of A172 in 2D culture and neurospheres. The X-axis represents CD44-PE, and Y-axis the forward scatter area (FSC-A). MDA-MB-231 breast cancer cell line was used as positive control. Plots represent n=1 independent experiments. Unlabelled samples represented in red. **B -** Western Blot of the CD44, in A172 cells cultured in 2D and as neurospheres (NS). β-actin was used as a loading control. Western blot represents N=3 independent experiments. Uncropped scans of western blots are shown in the Supplementary Information (Figure S.8-9).

Overall, from the characterization of CSC markers in the different cell culture systems, neurospheres displayed the highest content of several stem cell markers, as suggested by RT-qPCR and protein detection. Neurospheres are cultured in serum free medium and in the presence of stem growth factors, that promote an increase in CSC content [187,304–307]. This is a typical approach followed to generate *in vitro* floating colonies enriched in cancer stem cells

even for other cancer types, such as breast (mammospheres) [342] and prostate (prostaspheres) [343].

Still, by RT-qPCR spheroids generated in spinners showed a trend for an increase in expression of the CSC markers tested compared to 2D cultures, and a slight increase in CD133 by IF. However, there is a need to repeat the experiments with more biological replicates and increase the panel of tested CSC markers to confirm these results. We were not expecting these findings, since spheroids are generated in the presence of FBS, which is shown to differentiate stem cells in culture [344,345]. Nevertheless, it has been reported that non-small-cell lung cancer-derived cell lines cultured in bioreactors showed a slight increase in aldehyde-dehydrogenase-positive CSC ($ALDH^+$) [346], compared to 2D cultures [347]. ALDH is a detoxifying enzyme responsible for the oxidation of intracellular aldehydes, reported to be associated with CSC in breast cancer [348] and GBM [349]. In addition, it has been shown that HT29 colorectal cell line cultured in 3D showed an increase in $ALDH^+$ cells compared to 2D cultures [350]. Additionally, a study from S. Kalkanis and colleagues showed that neurospheres generated with GBM cell lines (LN229, T98G, U251n, and U87) expressed CSCs markers equally, regardless of serum presence [194].

With those findings, it was hypothesized that the 3D structure itself promotes an increase in the stem cell population, more pronounced in neurospheres than in spinner-derived spheroids. Therefore, to further confirm that the increase in gene expression of CSC markers was due to the 3D growth regardless of the culture medium composition, spinner-derived spheroids and neurospheres were re-cultured in petri dishes until a monolayer was formed, in presence of serum (differentiation assay, Material and Methods section 2.3). Subsequently, CSC-related gene expression was analyzed (Figure 3.18). The results showed a decrease in all CSC markers, both from neurospheres and spinner-vessel derived cultures, showing that A172 3D cell culture by itself promoted an increase in CSCs-related gene expression. This experimental strategy has been already reported in the literature to induce differentiation of patient-derived neurosphere cultures. Here, in agreement with our results, serum-induced differentiation induced a drastic reduction in *SOX2*, *NANOG* and *POU5F1* expression compared with the original 3D neurosphere cultures [351]. Nonetheless, the preliminary results presented here were obtained from one biological replicate; further biological replicates are then required to confirm such observations and to be performed in other GBM cell lines. Altogether, these results showed that two different 3D cell culture strategies were successfully implemented, with an indication of CSC enrichment confirmed by gene expression and protein detection of CSC-related markers.

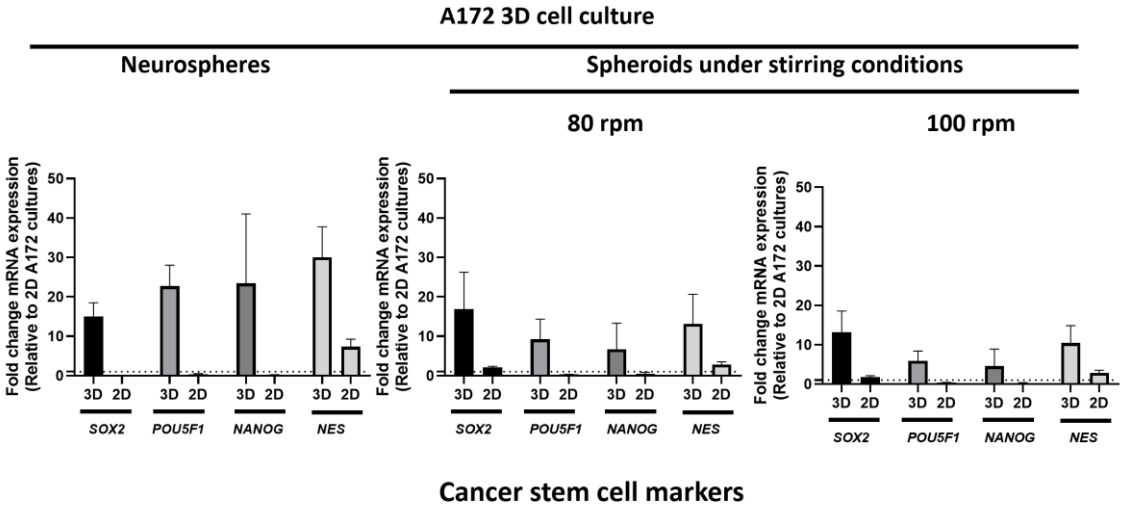

Figure 3.18 - Cancer stem cell (CSC) gene expression of 3D cell culture generated from A172 glioblastoma cell line when replated into a 2D cell culture in serum-containing medium. Fold change gene expression, of spheroids (80 and 100 rotations per minute (rpm)) and neurospheres replated in 2D culture determined by the $2^{-\Delta\Delta Ct}$ method. Values were normalized to the expression of housekeeping genes *36B4* and *RPL22* and represented as fold change relative to the starting A172 2D culture, set as 1 (dash line). Data are represented as fold change relative to A172 2D culture, set as 1 (dashed line). Plots representing N=1 independent experiment. Error bars are shown as a mean of SD of technical triplicates GSC markers: *SOX2* - SRY-Box Transcription Factor 2; *POU5F1* - POU Class 5 Homeobox 1, *NANOG* – Nanog Homeobox; *NES* – Nestin.

3.2.4. Analysis of Immunosuppressive and chemoattractant markers expression in A172 2D cultures, neurospheres and spheroids

After confirming the expression of CSC markers in the implemented 3D cell cultures, especially in neurospheres, we proceeded with the assessment of the potential differential expression of genes associated with GBM immunosuppression, such as *IL10*, *CSF-1/M-CSF* and *TGFB1* [113]. In addition, we evaluated *CCL2* gene expression, a known macrophages and microglia chemotactic factor [76].

We used again the GEPIA database (Figure 3.19) [311], to analyse the expression of these markers in normal CNS tissues versus GBM samples. The analysis showed that these cytokines are significantly more expressed in GBM than in normal brain samples

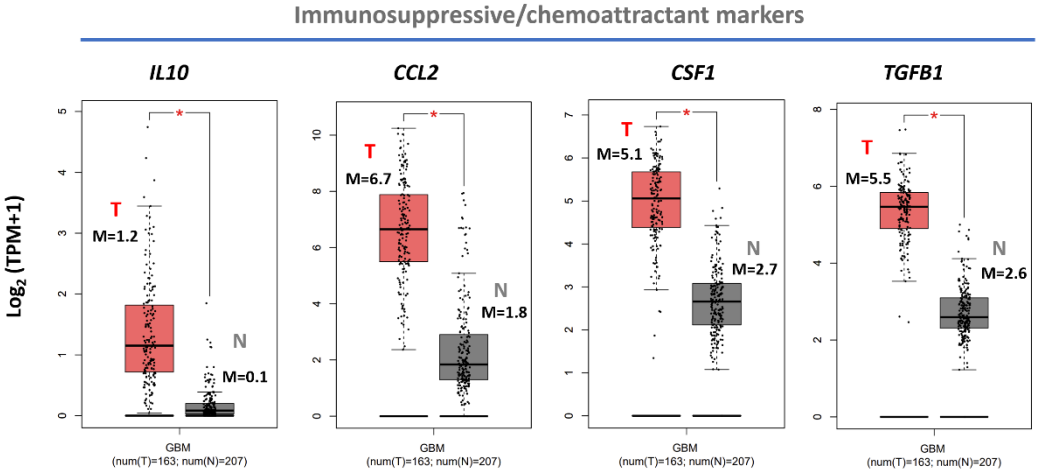

Figure 3.19 - *In silico* data on immunosuppressive/chemoattractant markers in glioblastoma (GBM). RNA bulk results from 163 healthy brain tissues (N) and 207 GBM tissues (T) of the expression of different cancer stem cell markers. Data from GEPIA database (http://gepia.cancer-pku.cn/), based on the cancer genome atlas (TCGA) tumors vs TCGA normal + Genotype-Tissue Expression (GTEx) normal datasets, accessed in July 2022 [313]. Results are displayed as log_2 of transcripts per million (TPM) +1. Immunosuppressive/chemoattractant cytokines: *IL10* – Interleukin-10; *CCL2* - C-C Motif Chemokine Ligand 2; *CSF1* – Colony Stimulating Factor 1; *TGFB1* – Transforming Growth Factor Beta 1.

We analyzed by RT-qPCR the expression of *IL10*, *CSF1*(M-CSF), *CCL2*, and *TGFB1* in 2D and 3D cell cultures (both neurospheres and spinner-vessel derived spheroids) (Figure 3.20).

In general, we observed variability among biological replicates for all the genes assessed. Nevertheless, neurosphere cultures showed a significant fold increase in gene expression over 2D cell cultures, especially regarding *CCL2* and *TGFB1* (16.40 ± 18.10 and 35.76 ± 38.5 fold increase respectively).

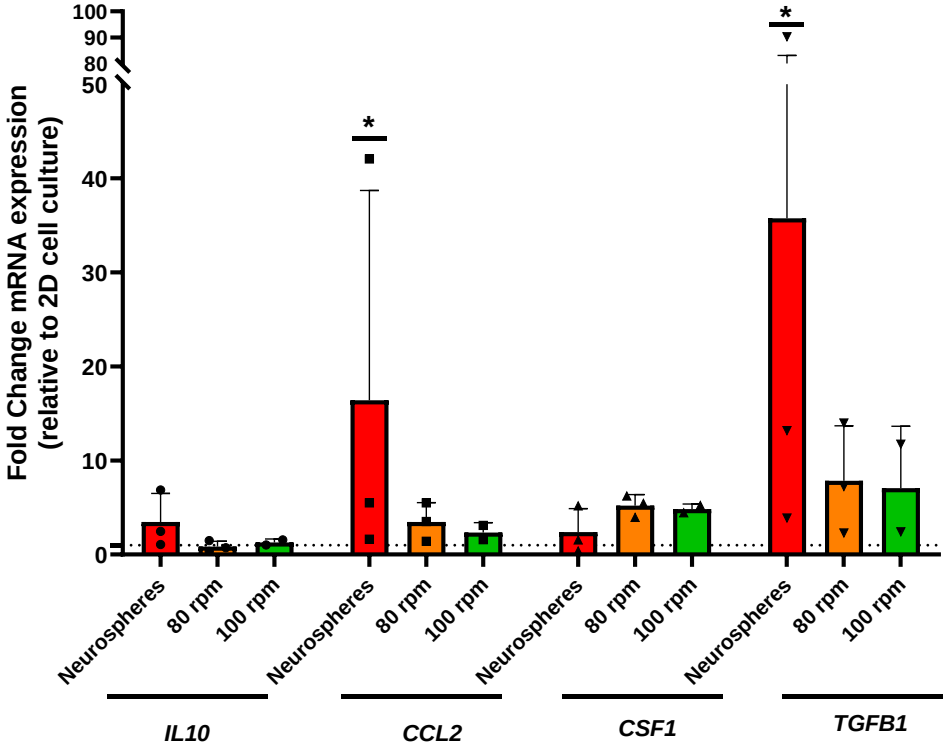

Figure 3.20 – Immunosuppressive/chemoattractant cytokine expression in glioblastoma (GBM) 3D cell culture strategies assessed by RT-qPCR. Fold change gene expression og immunosuppressive/chemoattractant markers in neurospheres and spheroids under a stirring rate of 80 and 100 rotations per minute (rpm) compared to A172 2D cell cultures determined by the $2^{-\Delta\Delta CT}$ method. Values were normalized to the expression of housekeeping genes *36B4* and *RPL22*. Data are represented as fold change relative to A172 2D culture, set as 1 (dashed line). Error bars are shown as a mean of SD of biological triplicates. Graph representing N= 3 independent biological replicates of neurospheres and spheroids obtained under 80 rpm and N=2 of spheroids produced under 100 rpm. Immunosuppressive/chemoattractant cytokines: *IL10* – Interleukin-10; *CCL2* - C-C Motif Chemokine Ligand 2; *CSF1* – Colony Stimulating Factor 1; *TGFB1* – Transforming Growth Factor Beta 1.

Spheroids showed a fold increase in gene expression in both *CSF1* (5.20 ± 0.94 and 4.82 ± 0.39 fold) and *TGFB1* (7.83 ± 4.78 and 7.06 ± 4.65 fold), under 80 and 100 rpm stirring rate, respectively, compared to 2D cultures.

GBM cells secrete TGF-β, as previously shown in patient-derived GBM cell cultures [352] and GBM cell lines such as U87 [353,354]. Furthermore, $CD133^+$ patient-derived neurospheres

secrete TGF- β as well as CSF-1 [94], suggesting that CSCs are contributing to the secretion of these immunosuppressive cytokines within the GBM TME. Activation of TGF-β signalling in A172 neurospheres should be further characterized in the future, for example by assessing SMAD2/3 phosphorylation, which occur after exposure to TGF-β [355]. TGF-β signalling in other GBM cell lines cultured in 2D has already been demonstrated. Interestingly, U87 and LN229 GBM cell lines displayed a clear SMAD2/3 activation, while A172 2D cultures showed negligible levels of SMAD2/3 phosphorylation, suggesting that the basal level of TGF-β secretion varies among different GBM cell lines, being lower in A172 compared to U87 and LN229 [356,357].

In the case of CCL2, it has been shown to be fundamental for Tregs and macrophages with M2-like phenotype recruitment within the GBM TME [358]. Lastly, it has been shown that glioma cell lines such as U-105 MG and U-251 MG can actively secrete CCL2 [235].

Regarding *IL10* and *CSF1*, we did not observe significant changes in gene expression among the conditions analyzed. Interestingly, neurospheres established from CSC isolated from GBM patient-derived cells did not secreted IL-10, which suggests that IL-10 is not potentially secreted by CSCs [94].

Altogether, these results indicate that A172 neurospheres express higher levels of *CCL2* and *TGFB1* compared to 2D cultures, since they are enriched in CSCs. TGF-β is highly present in the GBM TME to induce immunosuppression, as mentioned in the introduction, (section 1.5.1 and figure 1.8). This will be important also for future and more representative complex 3D GBM culture approaches, based on bioreactors and integrating CNS neurospheroids to recapitulate immunosuppressive TME features.

Subsequently, we followed the same approach used before (neurosphere/spheroid differentiation assay, figure 3.18), to assess whether the differentiation of A172 GBM 3D cell cultures may have had an impact on the expression of *IL10*, *CCL2*, *CSF1* and *TGB1*. As observed previously for CSC markers expression, immunosuppressive/chemoattractant mRNA decreased in 3D cell cultures re-plated in 2D, except for *TGFB1* (Figure 3.21), suggesting that the 3D cell culture by itself promotes a higher expression of immunosuppressive/chemoattractant cytokines.

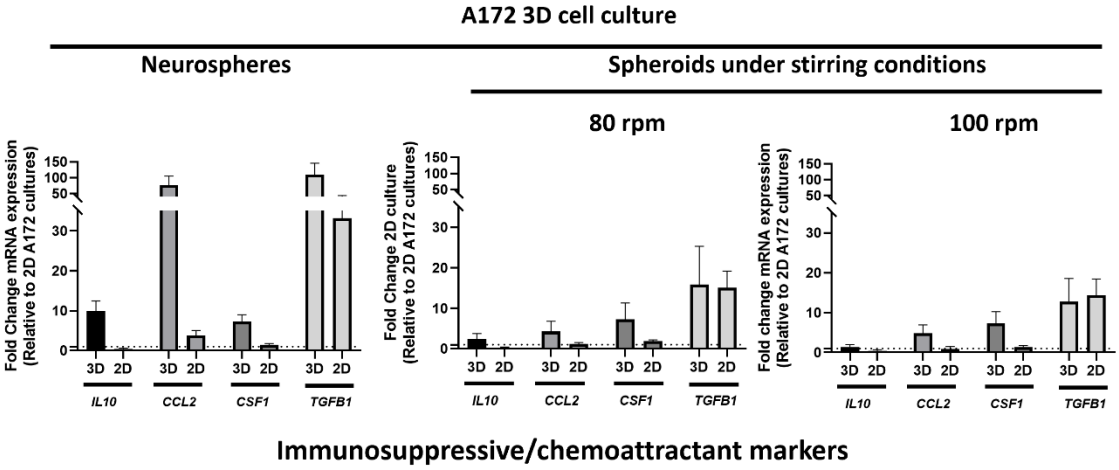

Figure 3.21 – Immunosuppressive/chemoattractant gene expression of A172 glioblastoma (GBM) cell line when replated 3D culture strategies into a 2D culture in serum-containing medium experiment. Fold change gene expression, of spheroids (80 and 100 rotations per minute (rpm)) and neurospheres replated in 2D culture determined by the $2^{-\Delta\Delta Ct}$ method. Values were normalized to the expression of housekeeping genes *36B4* and *RPL22* and represented as fold change relative to the starting A172 2D culture. Data are represented as fold change relative to A172 2D culture, set as 1 (dashed line). Plots representing N=1 independent experiment. Error bars are shown as a mean of SD of technical triplicates. Immunosuppressive/chemoattractant Cytokines: *IL10* – Interleukin-10; *CCL2* - C-C Motif Chemokine Ligand 2; *CSF1* – Colony Stimulating Factor 1; TGFB1 – Transforming Growth Factor Beta 1.

However, these results need to be confirmed with additional replicates, and even by analyzing a larger panel of immunosuppressive molecules (e.g., IL4, IL13) [359]. In addition, in the future, pro-inflammatory markers should be analysed in parallel (e.g., *TNF-α*, *IL1B*, *IL8*, *CXCL10*) [360], both at gene expression and protein level (e.g., ELISA), to further characterize the secretory milieu of such 3D A172 GBM cell cultures, to further confirm the immunosuppressive nature of these cultures.

Altogether, the neurosphere methodology was the 3D culture system that showed the highest content of CSC markers and expression of immunosuppressive cytokines and *CCL2* compared to other culture formats. Since we aim to recapitulate immunosuppressive events in a 3D GBM cell culture model, we chose neurospheres for the first assessment of co-culture with microglia in objective 3.

3.3. Proof of concept: Initial co-culture assessment

3.3.1. Characterization of microglia-like cells derived from monocytes exposed to neurosphere conditioned medium

High-grade gliomas are generally characterized by a complex secretory milieu that altogether supports the building of an immunosuppressive TME, which in turn promotes tumor proliferation and growth [76]. Considering this, it was hypothesized that the conditioned medium (CM) derived from neurosphere cultures, (in which we detected high expression of *TGFB1* and detectable levels of *IL10*, Figure 3.20) would be able to affect the microglia gene expression and phenotype, polarizing them mostly towards an M2-like state (e.g., $CD163^{+}/CD206^{+}$) [121]. To test this hypothesis, MLC-Mo derived from two different donors (#4 and #5) were cultured for 48 h in a medium mixture composed of 50% neurosphere CM and 50% MLC-Mo medium. As basal

condition, MLC-Mo was cultured in a ratio of 50:50 fresh neurosphere medium (NF): MLC-Mo medium.

We observed by gene expression analysis both M1 (*AIF1*, *CD86*, *IL6*, and *IL1B)* and M2 (*CD163*, *MRC1,* and *TGFB1*) markers already tested before (Objective 1). In addition, IF analysis of CD163 and CD206 was performed.

For the gene expression analysis, we displayed the results for the two donors independently. For positive control, MLC-Mos were treated with pro-inflammatory (M1) or anti-inflammatory (M2) stimuli, and gene expression results were compared to untreated MLC-Mo (designed as M0 MLC-Mo).

In both donors analysed, no relevant changes in gene expression of the M1 markers analysed (Figure 3.22), were observed, neither in MLC-Mo exposed to CM nor after exposure to NF. The M1 stimuli (LPS+IFN-γ) upregulated *IL1B* in both donors and *IL6* in donor 6. Although CM does not seem to promote MLC-Mo M1 polarization, these results were performed with only 2 donors, and more donors will be required to draw a definitive conclusion. In addition, gene expression analysis should be completed by FC analysis of inflammatory surface markers (e.g., CCR7, CD80, CD86, CD40) [295,296].

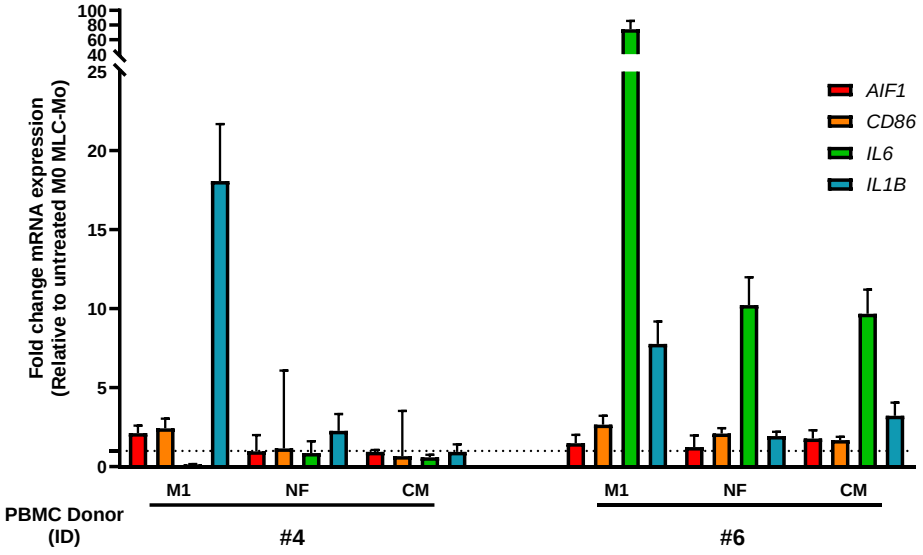

Figure 3.22 – Pro-inflammatory markers expression in microglia-like cells derived from monocytes (MLC-Mo) exposed to neurosphere medium (NF) and conditioned medium (CM), assessed by RT-qPCR. Fold change of in gene expression of MLC-Mo from 2 different peripheral blood mononuclear cell (PBMC) donors (#4 and #5) exposed to NF and CM, determined by the $2^{-\Delta\Delta Ct}$ method. Values were normalized to the expression of the housekeeping genes *RPL22* and *36B4* represented as fold change relative to control M0 MLC-Mo mRNA expression, set as 1 (dashed line). Error bars are shown as a mean of SD of technical triplicates. Representative plot of N=2 independent experiments. Pro-inflammatory markers: *AIF1*(IBA1) **–**Allograft inflammatory factor 1; *CD86* **–** T-Lymphocyte Activation Antigen CD86**;** *IL6* – Interleukin 6; *IL1B* – Interleukin 1 beta.

In the case of M2 polarization, we analysed *CD163*, *MRC1,* and *TGFB1* markers to observe any potential increase in MLC-Mo exposed to CM. Unfortunately, due to high technical variability, it was not possible to draw any preliminary conclusion (Supplementary information, Figure S.10). Also in this case, it is necessary to have more biological replicates to draw a clear conclusion.

To complement the results of gene expression, CD163 and CD206 immunofluorescence was performed on MLC-Mo established from four donors (#2, #6, #7, and #8) (Figure 3.23), and exposed to NF and CM derived from A172. We observed that, in the unchallenged condition, it was possible to detect both CD206 and CD163 in M0 MLC-Mo as previously observed (section 3.1.2) and reported [301]. Comparing the cells exposed to CM to the MLC-Mo untreated and cultured with NF, it was observed a slightly higher detection of CD206 in #6 and #7 while no changes were observed in #2 and #8. Regarding CD163, its levels in MLC-Mo cultured with CM showed no changes compared to the untreated and NF in all the MLC-Mo analysed. More replicates are necessary to confirm such observations, even employing FC. FC is certainly one of the most powerful and used techniques to assess macrophage phenotypes [251], as shown in a study where 3D U87-Mφ co-cultures were established [361]. In the future, we aim to analyse by FC the expression of various Mφ/Microglia surface markers (e.g., CD80, CD86, CD40, CD204, DC-SIGN) in MLC-Mo exposed to GBM neurospheres CM [121,295,296,362]. This will be pivotal to analyse not only the general marker expression, but also to assess the presence of discrete microglia cell populations with differential expression levels of marker combinations.

We were expecting to observe a clear increase of both CD206 and CD163 M2 markers in microglia exposed to A172 neurosphere CM. Nevertheless, apart from the expected donor variability in response to the CM, there are some potential explanations to justify these results. First of all, the CM exposure time may not be optimal to detect phenotypical changes in M2 MLC-Mo; under this view, different CM exposure time points should be included in further studies. Additionally, neurospheres are generated at a very low cell density. For this, even if we observed an increase in gene expression of immunosuppressive factors, their concentration in the CM is potentially extremely low to be able to skew MLC-Mo toward a M2-like phenotype. For future work, it will be advisable to decrease the volume used to establish the neurosphere cultures (without creating cell physiological stress), aiming to increase the concentration of neurosphere-secreted factors. In this case, before proceeding to the MLC-Mo exposure to neurosphere CM, it will also be important to assess the concentration of such immunosuppressive factors, to ensure that they fall into the concentration range in which they are considered able to exert any biological effect. For example, TGF-β has been reported to induce *in vitro* the differentiation of Mφ towards an immunosuppressive M2-like state, at the concentration of 5 or 20 ng/mL [363,364].

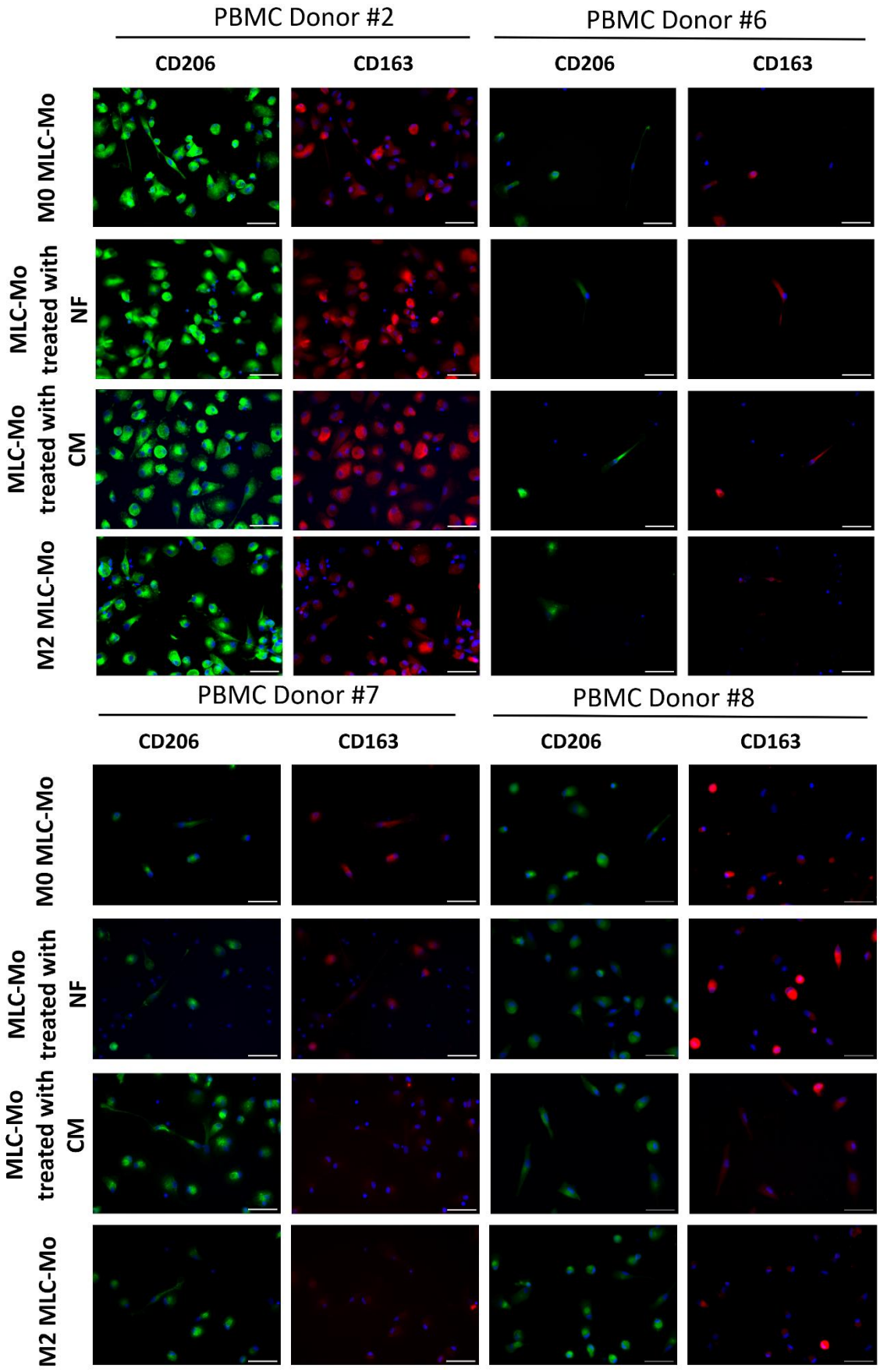
PBMC Donor #2
PBMC Donor #6
CD206
CD163
CD206
CD163
M0 MLC-Mo
MLC-Mo treated with NF
MLC-Mo treated with CM
M2 MLC-Mo
PBMC Donor #7
PBMC Donor #8
CD206
CD163
CD206
CD163
M0 MLC-Mo
MLC-Mo treated with NF
MLC-Mo treated with CM
M2 MLC-Mo

Figure 3.23 - CD206 and CD163 analysis in microglia-like cells derived from monocytes (MLC-Mo) exposed to neurosphere medium (NF), conditioned medium (CM) and anti-inflammatory stimuli (M2, IL4 + IL13) assessed by immunofluorescence. MLC-Mo were differentiated from four different peripheral blood mononuclear cells (PBMC) donors (#2, #6, #7, #8). CD206 was labelled in green (AlexaFluor® 488) and CD163 labelled in red (AlexaFluor® 594). Cells were counterstained with 4',6-diamidino-2-phenylindole (DAPI, blue) for nuclei identification. Representative images of N=4 independent experiments. Scale bar: 50 µm. Anti-inflammatory markers: CD163: Scavenger Receptor Cysteine-Rich Type 1 Protein M130; CD206: Macrophage Mannose Receptor 1-Like Protein 1.

3.3.2. Implementation of glioma/microglia co-cultures and characterization of microglia-like cells gene expression

To set up a preliminary co-culture strategy between microglia and GBM cells, as first step towards the development of a more complex 3D GBM TME model, we selected MLC-Mo, that express microglia markers (e.g., IBA1, TMEM119), and A172 neurospheres, that presented CSC enrichment (e.g., CD133, SOX2) and expression of immunosuppressive/chemoattractant genes (*TGFB1*, *CCL2*).

For the co-cultures, the neurospheres were generated in 24-well ULA plates for seven days, after which we added MLC-Mo. MLC-Mo established from the donor #9 was stained with a cell tracker to observe potential infiltration in the neurosphere, which was analysed on days two and four post-co-culture. At the beginning of the co-culture, neurospheres and MLC-Mo were kept under agitation overnight to promote adherence between cell types and then remained in a static condition at 37 ºC afterward for up to four days. On days two and four post co-culture, high cell viability was observed both in A172 neurospheres as well as in MLC-Mo. In addition, it was possible to observe MLC-Mo adherence to the neurospheres (Figure 3.24). High cell viability of both cell types has also been observed in a 3D cell model in which biopsy-derived UP-007 GBM cell line and HMC3 cells were co-cultured in a hyaluronic acid hydrogel [232].

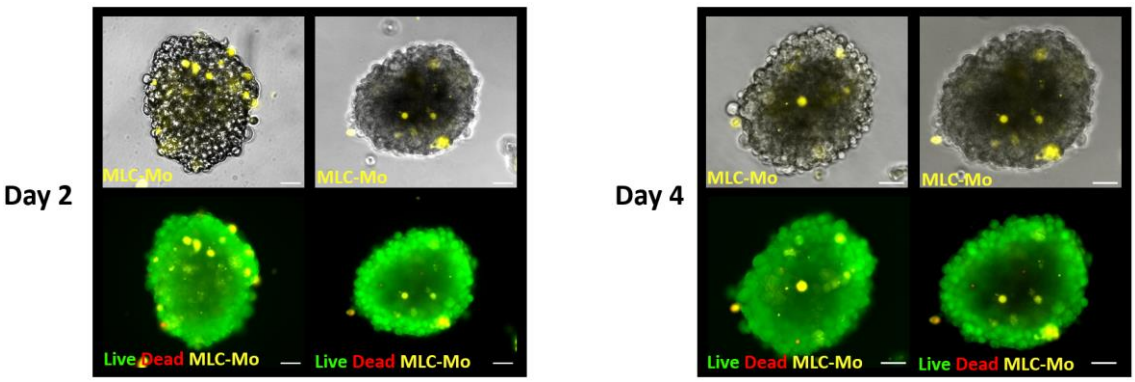

Figure 3.24 - Characterization of a 3D heterotypic co-culture between microglia-like cells derived from monocytes (MLC-Mo) and A172 neurospheres at days two and four, assessed by immunofluorescence. Cell viability of MLC-Mo and neurospheres analysed at the end of the culture, assessed by fluorescence microscopy. Fluorescein diacetate (FDA, green) shows live cells, while ToPro™-3 (red) shows dead cells and cell trace (Yellow) mark MLC-Mo. Representative images of N=2 experiments. Scale bar: 10 µm.

We further characterized this co-culture by gene expression analysis of microglia markers. Agarose gel analysis of RT-qPCR products derived from neurospheres co-cultures (Figure 3.25A) confirmed the presence of MLC-Mo. We detected *CD68* and *P2RY12* at both 2 and 4-days post co-culture, being absent, in the A172 neurosphere monoculture as expected.

After having assessed that MLC-Mo were maintained in co-culture, we performed a preliminary assessment of the phenotype of these cells by gene expression analysis. Figure 3.25B showed the relative transcript abundance plot from co-cultures at days two and four of two inflammatory markers (*AIF1* and *CD86*) and two anti-inflammatory markers (*MRC1* and *CD163*). MLC-Mo (2D culture) of the same donor is shown for comparison. The anti-inflammatory marker *CD163* showed no gene expression changes during the experiment, and it was barely expressed.

At day two of co-cultures, we observed higher transcript abundance of *AIF1* and *CD86* and a decrease in *MRC1* expression in co-cultures compared to MLC-Mo.

After four days of co-culture, both M1 markers *AIF1* and *CD86* expression decreased compared to day two, while *MRC1* expression increased compared to MLC-Mo.

Nevertheless, inflammatory markers still showed higher transcript abundance in co-culture compared to MLC-Mo. These observations could be explained by the fact that MLC-Mo in an initial stage of the co-culture were activated (increased IBA-1 expression) [365], but after an initial adaptation stage they may tend to skew toward an M2-like phenotype ($MRC1^+$) [361]. At this point, this is merely speculative and requires further biological replicates to support this hypothesis.

Interestingly, in a previous report, $CD11B^+$ microglia were isolated from glioma biopsies and $CD11B^+$ monocytes were isolated from the blood of the same patients and differentiated to MLC-Mo by culture with IL-34 and GM-CSF [366]. RT-qPCR analysis revealed a high expression of *MRC1* in both microglia cell sources, and immunohistochemistry showed a remarkable infiltration of $CD206^+$ cells in GBM tissues. These findings support our preliminary results, indicating the presence of $MRC1^+$ in gliomas, including GBM, and the use of MLC-Mo as a microglia source in GBM-microglia co-cultures.

In addition, these preliminary results are in agreement with previous works that showed that it is not possible to define a complete M2-like GAMs phenotype in gliomas such as GBM and DMG. They are rather represented by a continuum of expression of M1/M2 markers, as shown by the *in silico* analysis performed using the GEPIA database (figure 3.25C), and reported in [78,112,311].

Nevertheless, further studies with more PBMC donors will be required to confirm our observations. In addition, it is necessary to employ a larger panel of GBM cell lines as well as DMG cells, to extend these observations to other rare gliomas. Moreover, protein-based assays like FC will be pivotal to observe potential discrete microglia sub-cell populations which arise during co-culture.

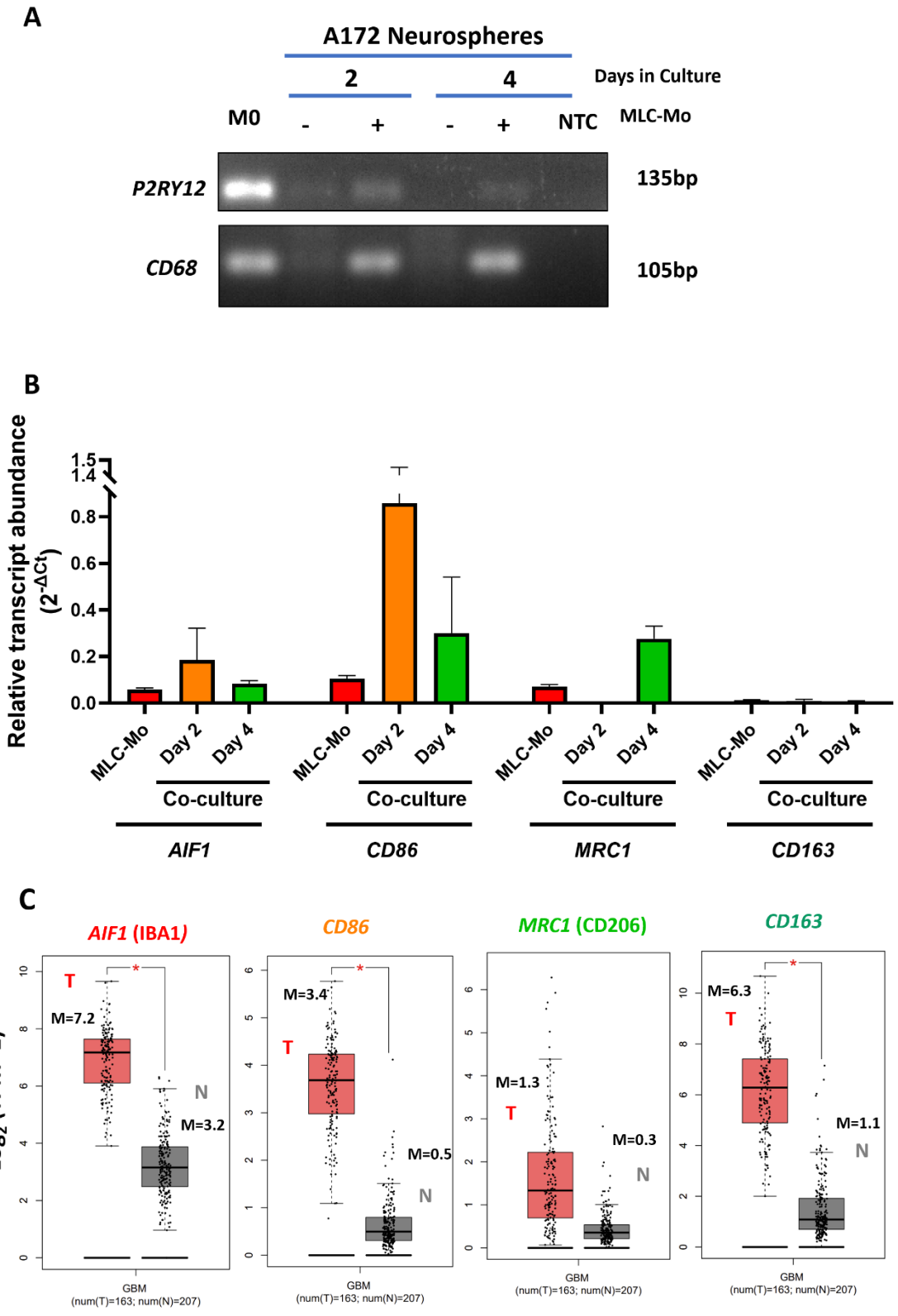
A
A172 Neurospheres
2
4
Days in Culture
M0
-
+
-
+
NTC
MLC-Mo
P2RY12
135bp
CD68
105bp
B
Relative transcript abundance
(2^-ΔCt)
1.5
1.4
0.8
0.6
0.4
0.2
0.0
MLC-Mo
Day 2
Day 4
Co-culture
AIF1
CD86
MRC1
CD163
C
AIF1 (IBA1)
CD86
MRC1 (CD206)
CD163
Log2 (TPM+1)
T
N
M=7.2
M=3.2
M=3.4
M=0.5
M=1.3
M=0.3
M=6.3
M=1.1
GBM
(num(T)=163; num(N)=207)

Figure 3.25 - Characterization of MLC-Mo co-cultured with neurospheres. A – Agarose gel on the identification of microglia markers (*P2RY12* and *CD68*) in the co-cultures. For positive control MLC-Mo in 2D cultures was used, and for negative control A172 neurospheres were used. No template control (NTC) represents the PCR without cDNA. Agarose gel represents a N=1 independent experiment. **B** – Relative transcript abundance in MLC-Mo exposed to anti and pro-inflammatory stimuli and co-culture at day 2 and day 4 determined by the $2^{-\Delta Ct}$. Error bars represent the mean of SD of technical triplicates. Reference gene target used was *CD68*. Plot representing a N=1 independent experiment. **C –** *In silico* data on cancer stem cancer cells markers in glioblastoma (GBM). RNA bulk results from 163 healthy brain tissue (N) and 207 GBM tissue (T) of the expression of different cancer stem cell markers. Data from GEPIA database (http://gepia.cancer-pku.cn/), based on the cancer genome atlas (TCGA) tumors vs TCGA normal + Genotype-Tissue Expression (GTEx) normal datasets, assessed in July 2022 [313]. Pro- and anti-inflammatory markers: *AIF1* (IBA1) – Allograft inflammatory factor 1; *CD86* **-** T-Lymphocyte Activation Antigen CD86; *CD163:* Scavenger Receptor Cysteine-Rich Type 1 Protein M130; *MRC1* (CD206): Macrophage Mannose Receptor 1-Like Protein 1.

One of the main issues present in this preliminary experiment was the low amount of biological material obtained. Future assays should consider the generation of a higher amount of starting material (MLC-Mo and neurospheres) to perform other analytical assays, such as IF and FC, to characterize the immunosuppressive status and phenotype of GBM-co-cultured MLC-Mo. This will be important to confirm this preliminary gene expression analysis at protein level. It is important to point out that other research groups have already established methodologies to study in vitro brain cancer cells/microglia crosstalk. A relevant one, which employs human cells, has been established by Chen and colleagues. Here, patient-derived GBM cells and HMC3 microglia cell lines were cultured in separated hydrogel disks, allowing soluble signalling without physical contact [233]. The authors reported HMC3 activation, showed by increased CD68 detection level by WB and ameboid phenotype (both associated with microglia activation [367,368]. Interestingly, the authors showed, through transcriptomic analysis that GBM cells co-cultured with microglia, even if physically separated, downregulated the expression of pathways associated with inflammation such as tumor necrosis factor (TNF) signaling,and nuclear factor kappa-beta (NF-κB) signaling, indicating that the soluble mediators were implicated in the establishment of such phenotype. Taking this into account, further characterization of these microglia-neurosphere co-cultures will involve the analysis of the downregulation of these inflammatory pathways in GBM neurosphere/microglia co-culture versus neurospheres monocultures.

Although preliminary, these results suggest that it is possible to co-culture microglia-like cells with GBM neurospheres enriched in CSC. We foresee the use of neurospheres from A172 and other GBM cell lines (e.g., U87, that has been already proven to be an immunosuppressive GBM cell line [159,356], secreting TGF-β and promoting M2-like differentiation in Mφ) and DMG cells. In the future, we aim to establish a more complex 3D glioma TME model, based on bioreactor cultures of GBM/DMG neurospheres, neurospheroids (enriched in neurons, astrocytes and oligodendrocytes, developed according to the methodology established by the host Lab [240]) and microglia. This will have as final aim to establish a relevant cell model that better recapitulates the cellular crosstalk of the brain tumor TME and its immunosuppressive events.

Chapter 4. Conclusion

GBM and DMG are known to have extremely low patient survival, and no current therapeutic modality has been found to significantly improve patient overall survival and life quality. Immunotherapies are one of the current therapeutic options that are being investigated in depth and have shown promise for future cancer therapies. Their main aim is to boost the patient's immune system to react against tumor cells. Cancers that are characterized by a “cold” TME, such as brain cancer, are described as having a high infiltration of immune cells (mostly microglia and blood-derived macrophages in brain tumors) that do not react against cancer cells, promote its immune escape and enhance proliferation. It was hypothesized that reversing microglia and macrophages' immunosuppressive phenotype would improve current patient survival.

These immunotherapies, on the other hand, are tested in vivo and in 2D in vitro models. These models may not recapitulate brain tumor complexity and an immunosuppressive phenotype. The absence of these features slows down the successful development rate of novel therapeutical modalities. 3D models are potent tools to recapitulate TME characteristics and can be used as a preclinical model as well as a research platform for the discovery of new biological targets.

This master thesis compiles a series of experimental approaches to seed the basis for a more complex and ambitious project. Under this perspective, we aim to recapitulate in a more complete manner the brain tumor TME, by co-culture of CNS neurospheroids-derived hiPSC, (enriched in CNS resident cells), microglia and glioma neurospheres. Microglia cell models were characterized, demonstrating that MLC-hiPSC and MLC-Mo express microglia markers and tended to respond to pro-and anti-inflammatory stimuli, both being potentially useful in GBM/DMG co-culture studies (although more biological replicates are required to confirm these results). Subsquently, two A172 GBM cell line-derived 3D culture strategies were implemented and compared (neurospheres and agitation-based spheroids). The results presented in the thesis showed that the neurosphere model is enriched in CSCs and immunosuppressive markers TME (e.g., *SOX2, POU5F1, NES, TGFB1*) compared to 2D cell cultures and agitation-based spheroids. This indicates that neurosphere cultures are a suitable brain cancer cell 3D culture model that maximizes the expression of typical CSCs markers expressed within the GBM TME.

Finally, a preliminary co-culture assay was performed with MLC-Mo and A172-derived neurospheres. In this preliminary assay, results show both pro- and anti-inflammatory gene expression markers, while cell viability was maintained in both MLC-Mo and neurospheres during co-cultures. Moreover, the implementation of 3D GBM cell cultures and characterization of microglia models were successful and are important components for the development of a more complex model.

Future work in this project will be to continue to characterize MLC-Mo and MLC-hiPSC for future co-culture experiments, such as phagocytic assay and FC analysis of M1 and M2 markers upon prototypical stimuli. Future experiments on the development of complex GBM/DMG co-culture models will be required. Those will rely on preliminary shake-flask based agitation co-

culture of CNS neurospheroids, microglia and brain cancer neurospheres, to fine-tune some technical aspects such as cell ratio and culture medium composition to be employed in bioreactor cultures in a later stage. This bioreactor-based complex model will serve as a potent platform for the discovery of novel immunosuppressive brain cancer axes as well as a platform to assess the potential of innovative immunotherapeutic modalities against brain tumors.

5. References

[1] I.T. Gavrilovic, J.B. Posner, Brain metastases: Epidemiology and pathophysiology, J. Neurooncol. 75 (2005) 5–14. https://doi.org/10.1007/s11060-004-8093-6.

[2] M. Weller, W. Wick, K. Aldape, M. Brada, M. Berger, S.M. Pfister, R. Nishikawa, M. Rosenthal, P.Y. Wen, R. Stupp, G. Reifenberger, Glioma, Nat. Rev. Dis. Prim. 1 (2015). https://doi.org/10.1038/nrdp.2015.17.

[3] S.M. Pfister, D. Capper, D.T.W. Jones, Modern principles of CNS tumor classification, Brain Tumors Child. (2018) 117–129. https://doi.org/10.1007/978-3-319-43205-2_6.

[4] M.J. Amsbaugh, C.S. Kim, Cancer, Brain Metastasis, StatPearls Publishing, 2019. https://www.ncbi.nlm.nih.gov/books/NBK470246/ (accessed November 13, 2022).

[5] S.R. Chandana, S. Movva, M. Arora, T. Singh, Primary brain tumors in adults, Am. Fam. Physician. 77 (2008) 1423–1430. https://doi.org/10.1017/cbo9781316134993.088.

[6] F.M. Mezzacappa, W. Thorell, Neuronal Brain Tumors, StatPearls Publishing, 2022. https://www.ncbi.nlm.nih.gov/books/NBK576406/ (accessed January 4, 2023).

[7] A. Shergalis, A. Bankhead, U. Luesakul, N. Muangsin, N. Neamati, Current challenges and opportunities in treating glioblastomas, Pharmacol. Rev. 70 (2018) 412–445. https://doi.org/10.1124/pr.117.014944.

[8] D.N. Louis, A. Perry, P. Wesseling, D.J. Brat, I.A. Cree, D. Figarella-Branger, C. Hawkins, H.K. Ng, S.M. Pfister, G. Reifenberger, R. Soffietti, A. Von Deimling, D.W. Ellison, The 2021 WHO classification of tumors of the central nervous system: A summary, Neuro. Oncol. 23 (2021) 1231–1251. https://doi.org/10.1093/neuonc/noab106.

[9] A.M. Molinaro, J.W. Taylor, J.K. Wiencke, M.R. Wrensch, Genetic and molecular epidemiology of adult diffuse glioma, Nat. Rev. Neurol. 15 (2019) 405–417. https://doi.org/10.1038/s41582-019-0220-2.

[10] Q.T. Ostrom, H. Gittleman, G. Truitt, A. Boscia, C. Kruchko, J.S. Barnholtz-Sloan, CBTRUS statistical report: Primary brain and other central nervous system tumors diagnosed in the United States in 2011-2015, Neuro. Oncol. 20 (2018) iv1–iv86. https://doi.org/10.1093/neuonc/noy131.

[11] F. Yamasaki, K. Kurisu, K. Satoh, K. Arita, K. Sugiyama, M. Ohtaki, J. Takaba, A. Tominaga, R. Hanaya, H. Yoshioka, S. Hama, Y. Ito, Y. Kajiwara, K. Yahara, T. Saito, M.T. Arifin, Apparent diffusion coefficient of human brain tumors at MR imaging, Radiology. 235 (2005) 985–991. https://doi.org/10.1148/radiol.2353031338.

[12] S.K. Carlsson, S.P. Brothers, C. Wahlestedt, Emerging treatment strategies for glioblastoma multiforme, EMBO Mol. Med. 6 (2014) 1359–1370. https://doi.org/10.15252/emmm.201302627.

[13] E. Cocucci, G. Racchetti, J. Meldolesi, Shedding microvesicles: artefacts no more, Trends Cell Biol. 19 (2009) 43–51. https://doi.org/10.1016/j.tcb.2008.11.003.

[14] M. Hassn Mesrati, A.B. Behrooz, A. Y Abuhamad, A. Syahir, Understanding Glioblastoma Biomarkers: Knocking a Mountain with a Hammer, Cells. 9 (2020). https://doi.org/10.3390/cells9051236.

[15] M. Abedalthagafi, D. Barakeh, K.M. Foshay, Immunogenetics of glioblastoma: the future of personalized patient management, Npj Precis. Oncol. 2018 21. 2 (2018) 1–8. https://doi.org/10.1038/s41698-018-0070-1.

[16] R. Richterová, B. Kolarovszki, R. Richterová, B. Kolarovszki, Genetic Alterations of Glioblastoma, Neurooncology - Newer Dev. (2016). https://doi.org/10.5772/63127.

[17] R.G.W. Verhaak, K.A. Hoadley, E. Purdom, V. Wang, Y. Qi, M.D. Wilkerson, C.R. Miller, L. Ding, T. Golub, J.P. Mesirov, G. Alexe, M. Lawrence, M. O'Kelly, P. Tamayo, B.A. Weir, S. Gabriel, W. Winckler, S. Gupta, L. Jakkula, H.S. Feiler, J.G. Hodgson, C.D. James, J.N.

Sarkaria, C. Brennan, A. Kahn, P.T. Spellman, R.K. Wilson, T.P. Speed, J.W. Gray, M. Meyerson, G. Getz, C.M. Perou, D.N. Hayes, Integrated genomic analysis identifies clinically relevant subtypes of glioblastoma characterized by abnormalities in PDGFRA, IDH1, EGFR, and NF1, Cancer Cell. 17 (2010) 98–110. https://doi.org/10.1016/J.CCR.2009.12.020.

[18] Z. Turkalp, J. Karamchandani, S. Das, IDH mutation in glioma: new insights and promises for the future, JAMA Neurol. 71 (2014) 1319–1325. https://doi.org/10.1001/JAMANEUROL.2014.1205.

[19] H. Xu, H. Zong, C. Ma, X. Ming, M. Shang, K. Li, X. He, H. Du, L. Cao, Epidermal growth factor receptor in glioblastoma (Review), Oncol. Lett. 14 (2017) 512–516. https://doi.org/10.3892/ol.2017.6221.

[20] S. Bedoui, M.J. Herold, A. Strasser, Emerging connectivity of programmed cell death pathways and its physiological implications, Nat. Rev. Mol. Cell Biol. 2020 2111. 21 (2020) 678–695. https://doi.org/10.1038/s41580-020-0270-8.

[21] H.M. Linden, K.A. Krohn, R.B. Livingston, D.A. Mankoff, Monitoring targeted therapy: Is fluorodeoxylucose uptake a marker of early response?, Clin. Cancer Res. 12 (2006) 5608–5610. https://doi.org/10.1158/1078-0432.CCR-06-1152.

[22] J. Liang, J. Zubovitz, T. Petrocelli, R. Kotchetkov, M.K. Connor, K. Han, J. hwa Lee, S. Ciarallo, C. Catzavelos, R. Beniston, E. Franssen, J.M. Slingerland, PKB/Akt phosphorylates p27, impairs nuclear import of p27 and opposes p27-mediated G1 arrest, Nat. Med. 2002 810. 8 (2002) 1153–1160. https://doi.org/10.1038/nm761.

[23] M. Abbastabar, M. Kheyrollah, K. Azizian, N. Bagherlou, S.S. Tehrani, M. Maniati, A. Karimian, Multiple functions of p27 in cell cycle, apoptosis, epigenetic modification and transcriptional regulation for the control of cell growth: A double-edged sword protein, DNA Repair (Amst). 69 (2018) 63–72. https://doi.org/10.1016/J.DNAREP.2018.07.008.

[24] J. Zou, T. Lei, P. Guo, J. Yu, Q. Xu, Y. Luo, R. Ke, D. Huang, Mechanisms shaping the role of ERK1/2 in cellular senescence (Review), Mol. Med. Rep. 19 (2019) 759–770. https://doi.org/10.3892/MMR.2018.9712.

[25] Y. Mebratu, Y. Tesfaigzi, How ERK1/2 activation controls cell proliferation and cell death is subcellular localization the answer?, Cell Cycle. 8 (2009) 1168–1175. https://doi.org/10.4161/cc.8.8.8147.

[26] J. Bartek, J. Lukas, Cyclin D1 multitasks, Nat. 2011 4747350. 474 (2011) 171–172. https://doi.org/10.1038/474171a.

[27] K.J. Hatanpaa, S. Burma, D. Zhao, A.A. Habib, Epidermal growth factor receptor in glioma: signal transduction, neuropathology, imaging, and radioresistance, Neoplasia. 12 (2010) 675–684. https://doi.org/10.1593/NEO.10688.

[28] N. Shinojima, K. Tada, S. Shiraishi, T. Kamiryo, M. Kochi, H. Nakamura, K. Makino, H. Saya, H. Hirano, J.I. Kuratsu, K. Oka, Y. Ishimaru, Y. Ushio, Prognostic Value of Epidermal Growth Factor Receptor in Patients with Glioblastoma Multiforme, Cancer Res. 63 (2003) 6962–6970. http://aacrjournals.org/cancerres/article-pdf/63/20/6962/2509276/ch2003006962.pdf (accessed January 3, 2023).

[29] H. Yamazaki, Y. Ohba, N. Tamaoki, M. Shibuya, A deletion mutation within the ligand binding domain is responsible for activation of epidermal growth factor receptor gene in human brain tumors, Jpn. J. Cancer Res. 81 (1990) 773–779. https://doi.org/10.1111/J.1349-7006.1990.TB02644.X.

[30] S.Y. Shieh, M. Ikeda, Y. Taya, C. Prives, DNA damage-induced phosphorylation of p53 alleviates inhibition by MDM2, Cell. 91 (1997) 325–334. https://doi.org/10.1016/S0092-8674(00)80416-X.

[31] K.T. Bieging, S.S. Mello, L.D. Attardi, Unravelling mechanisms of p53-mediated tumour suppression, Nat Rev Cancer. 14 (2014) 359–370. https://doi.org/10.1038/nrc3711.

[32] Y. Zhang, C. Dube, M. Gibert, N. Cruickshanks, B. Wang, M. Coughlan, Y. Yang, I. Setiady, C. Deveau, K. Saoud, C. Grello, M. Oxford, F. Yuan, R. Abounader, The p53 Pathway in Glioblastoma, Cancers (Basel). 10 (2018). https://doi.org/10.3390/CANCERS10090297.

[33] J. O'Campo, J. Uyehara-Lock, K.D. Aldape, E.C. Burton, K.R. Lamborn, M. Prados, M. Berger, P. Forsyth, J. Scott, S. Passe, R.B. Jenkins, J. Uhm, B.P. O'Neill, Aberrant p53, mdm2, and proliferation differ in glioblastomas from long-term compared with typical survivors, Clin. Cancer Res. 8 (2002) 180–187. https://mdanderson.elsevierpure.com/en/publications/aberrant-p53-mdm2-and-proliferation-differ-in-glioblastomas-from- (accessed June 16, 2022).

[34] R. Endersby, S.J. Baker, PTEN signaling in brain: neuropathology and tumorigenesis, Oncogene 2008 2741. 27 (2008) 5416–5430. https://doi.org/10.1038/onc.2008.239.

[35] N. Chapuis, J. Tamburini, A.S. Green, L. Willems, V. Bardet, S. Park, C. Lacombe, P. Mayeux, D. Bouscary, Perspectives on inhibiting mTOR as a future treatment strategy for hematological malignancies, Leuk. 2010 2410. 24 (2010) 1686–1699. https://doi.org/10.1038/leu.2010.170.

[36] H. Harada, J.S. Andersen, M. Mann, N. Terada, S.J. Korsmeyer, p70S6 kinase signals cell survival as well as growth, inactivating the pro-apoptotic molecule BAD, Proc. Natl. Acad. Sci. U. S. A. 98 (2001) 9666–9670. https://doi.org/10.1073/pnas.171301998.

[37] X. Qin, B. Jiang, Y. Zhang, 4E-BP1, a multifactor regulated multifunctional protein, Cell Cycle. 15 (2016) 781. https://doi.org/10.1080/15384101.2016.1151581.

[38] M.R. Srividya, B. Thota, B.C. Shailaja, A. Arivazhagan, K. Thennarasu, B.A. Chandramouli, A.S. Hegde, V. Santosh, Homozygous 10q23/PTEN deletion and its impact on outcome in glioblastoma: a prospective translational study on a uniformly treated cohort of adult patients, Neuropathology. 31 (2011) 376–383. https://doi.org/10.1111/J.1440-1789.2010.01178.X.

[39] F. Han, R. Hu, H. Yang, J. Liu, J. Sui, X. Xiang, F. Wang, L. Chu, S. Song, PTEN gene mutations correlate to poor prognosis in glioma patients: a meta-analysis, Onco. Targets. Ther. 9 (2016) 3485. https://doi.org/10.2147/OTT.S99942.

[40] K.G. Abdullah, C. Adamson, S. Brem, The Molecular Pathogenesis of Glioblastoma, Glioblastoma. (2016) 21–31. https://doi.org/10.1016/B978-0-323-47660-7.00003-3.

[41] G. Jin, Z.J. Reitman, C.G. Duncan, I. Spasojevic, D.M. Gooden, B.A. Rasheed, R. Yang, G.Y. Lopez, Y. He, R.E. McLendon, D.D. Bigner, H. Yan, Disruption of wild type IDH1 suppresses D-2-hydroxyglutarate production in IDH1-mutated gliomas, Cancer Res. 73 (2013) 496. https://doi.org/10.1158/0008-5472.CAN-12-2852.

[42] L.L. Chen, Y. Xiong, Tumour metabolites hinder DNA repair, Nature. 582 (2020) 492–494. https://doi.org/10.1038/d41586-020-01569-1.

[43] N.K. Kloosterhof, L.B.C. Bralten, H.J. Dubbink, P.J. French, M.J. van den Bent, Isocitrate dehydrogenase-1 mutations: a fundamentally new understanding of diffuse glioma?, Lancet. Oncol. 12 (2011) 83–91. https://doi.org/10.1016/S1470-2045(10)70053-X.

[44] L. Qiu, X. Hu, Q. Jing, X. Zeng, K.M. Chan, J. Han, Mechanism of cancer: Oncohistones in action, J. Genet. Genomics. 45 (2018) 227–236. https://doi.org/10.1016/j.jgg.2018.04.004.

[45] T.M. Cooney, E. Lubanszky, R. Prasad, C. Hawkins, S. Mueller, Diffuse midline glioma: review of epigenetics, J. Neurooncol. 150 (2020) 27–34. https://doi.org/10.1007/s11060-020-03553-1.

[46] D. Sturm, H. Witt, V. Hovestadt, D.A. Khuong-Quang, D.T.W. Jones, C. Konermann, E. Pfaff, M. Tönjes, M. Sill, S. Bender, M. Kool, M. Zapatka, N. Becker, M. Zucknick, T. Hielscher, X.Y. Liu, A.M. Fontebasso, M. Ryzhova, S. Albrecht, K. Jacob, M. Wolter, M. Ebinger, M.U. Schuhmann, T. van Meter, M.C. Frühwald, H. Hauch, A. Pekrun, B. Radlwimmer, T. Niehues, G. Von Komorowski, M. Dürken, A.E. Kulozik, J. Madden, A.

Donson, N.K. Foreman, R. Drissi, M. Fouladi, W. Scheurlen, A. von Deimling, C. Monoranu, W. Roggendorf, C. Herold-Mende, A. Unterberg, C.M. Kramm, J. Felsberg, C. Hartmann, B. Wiestler, W. Wick, T. Milde, O. Witt, A.M. Lindroth, J. Schwartzentruber, D. Faury, A. Fleming, M. Zakrzewska, P.P. Liberski, K. Zakrzewski, P. Hauser, M. Garami, A. Klekner, L. Bognar, S. Morrissy, F. Cavalli, M.D. Taylor, P. van Sluis, J. Koster, R. Versteeg, R. Volckmann, T. Mikkelsen, K. Aldape, G. Reifenberger, V.P. Collins, J. Majewski, A. Korshunov, P. Lichter, C. Plass, N. Jabado, S.M. Pfister, Hotspot Mutations in H3F3A and IDH1 Define Distinct Epigenetic and Biological Subgroups of Glioblastoma, Cancer Cell. 22 (2012) 425–437. https://doi.org/10.1016/j.ccr.2012.08.024.

[47] J. Schwartzentruber, A. Korshunov, X.Y. Liu, D.T.W. Jones, E. Pfaff, K. Jacob, D. Sturm, A.M. Fontebasso, D.A.K. Quang, M. Tönjes, V. Hovestadt, S. Albrecht, M. Kool, A. Nantel, C. Konermann, A. Lindroth, N. Jäger, T. Rausch, M. Ryzhova, J.O. Korbel, T. Hielscher, P. Hauser, M. Garami, A. Klekner, L. Bognar, M. Ebinger, M.U. Schuhmann, W. Scheurlen, A. Pekrun, M.C. Frühwald, W. Roggendorf, C. Kramm, M. Dürken, J. Atkinson, P. Lepage, A. Montpetit, M. Zakrzewska, K. Zakrzewski, P.P. Liberski, Z. Dong, P. Siegel, A.E. Kulozik, M. Zapatka, A. Guha, D. Malkin, J. Felsberg, G. Reifenberger, A. Von Deimling, K. Ichimura, V.P. Collins, H. Witt, T. Milde, O. Witt, C. Zhang, P. Castelo-Branco, P. Lichter, D. Faury, U. Tabori, C. Plass, J. Majewski, S.M. Pfister, N. Jabado, Driver mutations in histone H3.3 and chromatin remodelling genes in paediatric glioblastoma, Nature. 482 (2012) 226–231. https://doi.org/10.1038/nature10833.

[48] P.D.. Soonjo Hwang, M.D.1,*, Zachary T. Nolan, B.A.2, Stuart F. White, Ph.D.3, W. Craig Williams, B.A.4, Stephen Sinclair, Ph.D.5, and R. J. R. Blair, N.P.S. Daniel E Shumer, Natalie J Nokoff, L.M.S. Das C Hansen KC and Tyler JK, | Jarred M. Kaiser, PhD*,†, Michael F. Vignos, MS†, Richard Kijowski, MD‡, Geoffrey Baer, MD, PhD§, and Darryl G. Thelen, PhD†,§, Somatic Histone H3 Alterations in Paediatric Diffuse Intrinsic Pontine Gliomas and Non-Brainstem Glioblastomas, Physiol. Behav. 176 (2017) 139–148. https://doi.org/10.1038/ng.1102.Somatic.

[49] L. Gan, Y. Yang, Q. Li, Y. Feng, T. Liu, W. Guo, Epigenetic regulation of cancer progression by EZH2: From biological insights to therapeutic potential, Biomark. Res. 6 (2018) 1–10. https://doi.org/10.1186/s40364-018-0122-2.

[50] S. Bender, Y. Tang, A.M. Lindroth, V. Hovestadt, D.T.W. Jones, M. Kool, M. Zapatka, P.A. Northcott, D. Sturm, W. Wang, B. Radlwimmer, J.W. Højfeldt, N. Truffaux, D. Castel, S. Schubert, M. Ryzhova, H. Şeker-Cin, J. Gronych, P.D. Johann, S. Stark, J. Meyer, T. Milde, M. Schuhmann, M. Ebinger, C.M. Monoranu, A. Ponnuswami, S. Chen, C. Jones, O. Witt, V.P. Collins, A. VonDeimling, N. Jabado, S. Puget, J. Grill, K. Helin, A. Korshunov, P. Lichter, M. Monje, C. Plass, Y.J. Cho, S.M. Pfister, Reduced H3K27me3 and DNA Hypomethylation Are Major Drivers of Gene Expression in K27M Mutant Pediatric High-Grade Gliomas, Cancer Cell. 24 (2013) 660–672. https://doi.org/10.1016/j.ccr.2013.10.006.

[51] S. Mehta, E. Huillard, S. Kesari, C.L. Maire, D. Golebiowski, E.P. Harrington, J.A. Alberta, M.F. Kane, M. Theisen, K.L. Ligon, D.H. Rowitch, C.D. Stiles, The Central Nervous System-Restricted Transcription Factor Olig2 Opposes p53 Responses to Genotoxic Damage in Neural Progenitors and Malignant Glioma, Cancer Cell. 19 (2011) 359–371. https://doi.org/10.1016/J.CCR.2011.01.035.

[52] K.E. Warren, Diffuse intrinsic pontine glioma: poised for progress, Front. Oncol. 2 (2012) 1–9. https://doi.org/10.3389/fonc.2012.00205.

[53] R. Stupp, W.P. Mason, M.J. van den Bent, M. Weller, B. Fisher, M.J.B. Taphoorn, K. Belanger, A.A. Brandes, C. Marosi, U. Bogdahn, J. Curschmann, R.C. Janzer, S.K. Ludwin, T. Gorlia, A. Allgeier, D. Lacombe, J.G. Cairncross, E. Eisenhauer, R.O. Mirimanoff, Radiotherapy plus concomitant and adjuvant temozolomide for glioblastoma, N. Engl. J. Med. 352 (2005) 987–996. https://doi.org/10.1056/NEJMOA043330.

[54] E.S. Newlands, M.F.G. Stevens, S.R. Wedge, R.T. Wheelhouse, C. Brock, Temozolomide: a review of its discovery, chemical properties, pre-clinical development and clinical trials, Cancer Treat. Rev. 23 (1997) 35–61. https://doi.org/10.1016/S0305-7372(97)90019-0.

[55] R. Watanabe, Y. Nakasu, H. Tashiro, K. Mitsuya, I. Ito, S. Nakasu, T. Nakajima, O 6-Methylguanine DNA methyltransferase expression in tumor cells predicts outcome of radiotherapy plus concomitant and adjuvant temozolomide therapy in patients with primary glioblastoma, (2011). https://doi.org/10.1007/s10014-011-0022-8.

[56] S. Annavarapu, A. Gogate, T. Pham, K. Davies, P. Singh, N. Robert, Treatment patterns and outcomes for patients with newly diagnosed glioblastoma multiforme: A retrospective cohort study, CNS Oncol. 10 (2021). https://doi.org/10.2217/cns-2021-0007.

[57] M. Butler, L. Pongor, Y.T. Su, L. Xi, M. Raffeld, M. Quezado, J. Trepel, K. Aldape, Y. Pommier, J. Wu, MGMT Status as a Clinical Biomarker in Glioblastoma, Trends in Cancer. 6 (2020) 380–391. https://doi.org/10.1016/j.trecan.2020.02.010.

[58] R. Hashizume, Epigenetic targeted therapy for diffuse intrinsic pontine glioma, Neurol. Med. Chir. (Tokyo). 57 (2017) 331–342. https://doi.org/10.2176/NMC.RA.2017-0018.

[59] L.M. Weiner, R. Surana, S. Wang, Monoclonal antibodies: versatile platforms for cancer immunotherapy, Nat. Rev. Immunol. 2010 105. 10 (2010) 317–327. https://doi.org/10.1038/nri2744.

[60] N. Ferrara, K.J. Hillan, W. Novotny, Bevacizumab (Avastin), a humanized anti-VEGF monoclonal antibody for cancer therapy, Biochem. Biophys. Res. Commun. 333 (2005) 328–335. https://doi.org/10.1016/J.BBRC.2005.05.132.

[61] M.R. Gilbert, J.J. Dignam, T.S. Armstrong, J.S. Wefel, D.T. Blumenthal, M.A. Vogelbaum, H. Colman, A. Chakravarti, S. Pugh, M. Won, R. Jeraj, P.D. Brown, K.A. Jaeckle, D. Schiff, V.W. Stieber, D.G. Brachman, M. Werner-Wasik, I.W. Tremont-Lukats, E.P. Sulman, K.D. Aldape, W.J. Curran, M.P. Mehta, A randomized trial of bevacizumab for newly diagnosed glioblastoma, N. Engl. J. Med. 370 (2014) 699–708. https://doi.org/10.1056/NEJMOA1308573.

[62] K.J. Hamblett, C.J. Kozlosky, S. Siu, W.S. Chang, H. Liu, I.N. Foltz, E.S. Trueblood, D. Meininger, T. Arora, B. Twomey, S.L. Vonderfecht, Q. Chen, J.S. Hill, W.C. Fanslow, AMG 595, an anti-EGFRvIII antibody-drug conjugate, induces potent antitumor activity against EGFRvIII-expressing glioblastoma, Mol. Cancer Ther. 14 (2015) 1614–1624. https://doi.org/10.1158/1535-7163.MCT-14-1078.

[63] L.A. Lampson, Monoclonal antibodies in neuro-oncology: Getting past the blood-brain barrier, MAbs. 3 (2011) 153–160. https://doi.org/10.4161/MABS.3.2.14239.

[64] L. Wang, L.S. Chard Dunmall, Z. Cheng, Y. Wang, Remodeling the tumor microenvironment by oncolytic viruses: beyond oncolysis of tumor cells for cancer treatment, J. Immunother. Cancer. 10 (2022) e004167. https://doi.org/10.1136/JITC-2021-004167.

[65] C. Groeneveldt, T. van Hall, S.H. van der Burg, P. ten Dijke, N. van Montfoort, Immunotherapeutic Potential of TGF-β Inhibition and Oncolytic Viruses, Trends Immunol. 41 (2020) 406–420. https://doi.org/10.1016/J.IT.2020.03.003.

[66] F. Benencia, M.C. Courrèges, J.R. Conejo-García, A. Mohamed-Hadley, L. Zhang, R.J. Buckanovich, R. Carroll, N. Fraser, G. Coukos, HSV oncolytic therapy upregulates interferon-inducible chemokines and recruits immune effector cells in ovarian cancer, Mol. Ther. 12 (2005) 789–802. https://doi.org/10.1016/J.YMTHE.2005.03.026.

[67] M.J. Atherton, K.B. Stephenson, F. Tzelepis, D. Bakhshinyan, J.K. Nikota, H.H. Son, A. Jirovec, C. Lefebvre, A. Dvorkin-Gheva, A.A. Ashkar, Y. Wan, D.F. Stojdl, E.C. Belanger, R.H. Breau, J.C. Bell, F. Saad, S.K. Singh, J.S. Diallo, B.D. Lichty, Transforming the prostatic tumor microenvironment with oncolytic virotherapy, Oncoimmunology. 7 (2018). https://doi.org/10.1080/2162402X.2018.1445459.

[68] K. Twumasi-Boateng, J.L. Pettigrew, Y.Y.E. Kwok, J.C. Bell, B.H. Nelson, Oncolytic viruses as engineering platforms for combination immunotherapy, Nat. Rev. Cancer 2018 187. 18 (2018) 419–432. https://doi.org/10.1038/s41568-018-0009-4.

[69] F.F. Lang, C. Conrad, C. Gomez-Manzano, W.K. Alfred Yung, R. Sawaya, J.S. Weinberg,

S.S. Prabhu, G. Rao, G.N. Fuller, K.D. Aldape, J. Gumin, L.M. Vence, I. Wistuba, J. Rodriguez-Canales, P.A. Villalobos, C.M.F. Dirven, S. Tejada, R.D. Valle, M.M. Alonso, B. Ewald, J.J. Peterkin, F. Tufaro, J. Fueyo, Phase I study of DNX-2401 (delta-24-RGD) oncolytic adenovirus: replication and immunotherapeutic effects in recurrent malignant glioma, J. Clin. Oncol. 36 (2018) 1419–1427. https://doi.org/10.1200/JCO.2017.75.8219.

[70] J. Gállego Pérez-Larraya, M. Garcia-Moure, S. Labiano, A. Patiño-García, J. Dobbs, M. Gonzalez-Huarriz, M. Zalacain, L. Marrodan, N. Martinez-Velez, M. Puigdelloses, V. Laspidea, I. Astigarraga, B. Lopez-Ibor, O. Cruz, M. Oscoz Lizarbe, S. Hervas-Stubbs, G. Alkorta-Aranburu, I. Tamayo, B. Tavira, R. Hernandez-Alcoceba, C. Jones, G. Dharmadhikari, C. Ruiz-Moreno, H. Stunnenberg, E. Hulleman, J. van der Lugt, M.Á. Idoate, R. Diez-Valle, I. Esparragosa Vázquez, M. Villalba, C. de Andrea, J.M. Núñez-Córdoba, B. Ewald, J. Robbins, J. Fueyo, C. Gomez-Manzano, F.F. Lang, S. Tejada, M.M. Alonso, Oncolytic DNX-2401 Virus for Pediatric Diffuse Intrinsic Pontine Glioma, N. Engl. J. Med. 386 (2022) 2471–2481. https://doi.org/10.1056/nejmoa2202028.

[71] J. Banchereau, A.K. Palucka, Dendritic cells as therapeutic vaccines against cancer, Nat. Rev. Immunol. 2005 54. 5 (2005) 296–306. https://doi.org/10.1038/nri1592.

[72] C.M. Le Gall, J. Weiden, L.J. Eggermont, C.G. Figdor, Dendritic cells in cancer immunotherapy, Nat. Mater. 2018 176. 17 (2018) 474–475. https://doi.org/10.1038/s41563-018-0093-6.

[73] C.A. Crane, S.J. Han, B. Ahn, J. Oehlke, V. Kivett, A. Fedoroff, N. Butowski, S.M. Chang, J. Clarke, M.S. Berger, M.W. McDermott, M.D. Prados, A.T. Parsa, Individual patient-specific immunity against high-grade glioma after vaccination with autologous tumor derived peptides bound to the 96 KD chaperone protein, Clin. Cancer Res. 19 (2013) 205–214. https://doi.org/10.1158/1078-0432.CCR-11-3358.

[74] S. Polyzoidis, K. Ashkan, DCVax®-L - Developed by Northwest Biotherapeutics, Hum. Vaccines Immunother. 10 (2014) 3139–3145. https://doi.org/10.4161/hv.29276.

[75] D. Benitez-Ribas, R. Cabezón, G. Flórez-Grau, M.C. Molero, P. Puerta, A. Guillen, S. Paco, A.M. Carcaboso, V.S.M. Lopez, O. Cruz, C. de Torres, N. Salvador, M. Juan, J. Mora, A.M. La Madrid, Immune Response Generated With the Administration of Autologous Dendritic Cells Pulsed With an Allogenic Tumoral Cell-Lines Lysate in Patients With Newly Diagnosed Diffuse Intrinsic Pontine Glioma, Front. Oncol. 8 (2018) 127. https://doi.org/10.3389/FONC.2018.00127.

[76] S. Roesch, C. Rapp, S. Dettling, C. Herold-Mende, When immune cells turn bad—tumor-associated microglia/macrophages in glioma, Int. J. Mol. Sci. 19 (2018). https://doi.org/10.3390/ijms19020436.

[77] S.M. Razavi, K.E. Lee, B.E. Jin, P.S. Aujla, S. Gholamin, G. Li, Immune Evasion Strategies of Glioblastoma, Front. Surg. 3 (2016) 1–9. https://doi.org/10.3389/fsurg.2016.00011.

[78] G.L. Lin, S. Nagaraja, M.G. Filbin, M.L. Suvà, H. Vogel, M. Monje, Non-inflammatory tumor microenvironment of diffuse intrinsic pontine glioma, Acta Neuropathol. Commun. 6 (2018) 51. https://doi.org/10.1186/S40478-018-0553-X.

[79] L. Annovazzi, M. Mellai, E. Bovio, S. Mazzetti, B. Pollo, D. Schiffer, Microglia immunophenotyping in gliomas, Oncol. Lett. 15 (2018) 998–1006. https://doi.org/10.3892/ol.2017.7386.

[80] Q. Li, B.A. Barres, Microglia and macrophages in brain homeostasis and disease, Nat. Rev. Immunol. 18 (2018) 225–242. https://doi.org/10.1038/nri.2017.125.

[81] A. Buonfiglioli, D. Hambardzumyan, Macrophages and microglia: the cerberus of glioblastoma, Acta Neuropathol. Commun. 9 (2021). https://doi.org/10.1186/S40478-021-01156-Z.

[82] D.F. Quail, J.A. Joyce, The Microenvironmental Landscape of Brain Tumors, Cancer Cell. 31 (2017) 326–341. https://doi.org/10.1016/j.ccell.2017.02.009.

[83] K. Piper, L. DePledge, M. Karsy, C. Cobbs, Glioma Stem Cells as Immunotherapeutic

Targets: Advancements and Challenges, Front. Oncol. 11 (2021) 92. https://doi.org/10.3389/fonc.2021.615704.

[84] G. Choe, J.K. Park, L. Jouben-Steele, T.J. Kremen, L.M. Liau, H. V. Vinters, T.F. Cloughesy, P.S. Mischel, Active matrix metalloproteinase 9 expression is associated with primary glioblastoma subtype, Clin. Cancer Res. 8 (2002) 2894–2901.

[85] K.J. Wolf, J. Chen, J.D. Coombes, M.K. Aghi, S. Kumar, Dissecting and rebuilding the glioblastoma microenvironment with engineered materials, Nat. Rev. Mater. 4 (2019) 651–668. https://doi.org/10.1038/s41578-019-0135-y.

[86] A. Belousov, S. Titov, N. Shved, M. Garbuz, G. Malykin, V. Gulaia, A. Kagansky, V. Kumeiko, The Extracellular Matrix and Biocompatible Materials in Glioblastoma Treatment, Front. Bioeng. Biotechnol. 7 (2019) 341. https://doi.org/10.3389/fbioe.2019.00341.

[87] D.A. Senthebane, A. Rowe, N.E. Thomford, H. Shipanga, D. Munro, M.A.M. Al Mazeedi, H.A.M. Almazyadi, K. Kallmeyer, C. Dandara, M.S. Pepper, M.I. Parker, K. Dzobo, The Role of Tumor Microenvironment in Chemoresistance: To Survive, Keep Your Enemies Closer, Int. J. Mol. Sci. 18 (2017). https://doi.org/10.3390/IJMS18071586.

[88] J. Feng, N.M. Byrne, W. Al Jamal, J.A. Coulter, Exploiting current understanding of hypoxia mediated tumour progression for nanotherapeutic development, Cancers (Basel). 11 (2019) 1–25. https://doi.org/10.3390/cancers11121989.

[89] E. Gonzalez-Gugel, M. Saxena, N. Bhardwaj, Modulation of innate immunity in the tumor microenvironment, Cancer Immunol. Immunother. 65 (2016) 1261–1268. https://doi.org/10.1007/S00262-016-1859-9/FIGURES/3.

[90] M. Hasmim, Y. Messai, L. Ziani, J. Thiery, J.H. Bouhris, M.Z. Noman, S. Chouaib, Critical role of tumor microenvironment in shaping NK cell functions: Implication of hypoxic stress, Front. Immunol. 6 (2015) 482. https://doi.org/10.3389/fimmu.2015.00482.

[91] M. Davoodzadeh Gholami, G.A. Kardar, Y. Saeedi, S. Heydari, J. Garssen, R. Falak, Exhaustion of T lymphocytes in the tumor microenvironment: Significance and effective mechanisms, Cell. Immunol. 322 (2017) 1–14. https://doi.org/10.1016/j.cellimm.2017.10.002.

[92] B.D. Liebelt, T. Shingu, X. Zhou, J. Ren, S.A. Shin, J. Hu, Glioma Stem Cells: Signaling, Microenvironment, and Therapy, Stem Cells Int. 2016 (2016). https://doi.org/10.1155/2016/7849890.

[93] S. Liu, C. Zhang, B. Wang, H. Zhang, G. Qin, C. Li, L. Cao, Q. Gao, Y. Ping, K. Zhang, J. Lian, Q. Zhao, D. Wang, Z. Zhang, X. Zhao, L. Yang, L. Huang, B. Yang, Y. Zhang, Regulatory T cells promote glioma cell stemness through TGF-β–NF-κB–IL6–STAT3 signaling, Cancer Immunol. Immunother. 70 (2021) 2601–2616. https://doi.org/10.1007/s00262-021-02872-0.

[94] A. Wu, J. Wei, L.Y. Kong, Y. Wang, W. Priebe, W. Qiao, R. Sawaya, A.B. Heimberger, Glioma cancer stem cells induce immunosuppressive macrophages/microglia, Neuro. Oncol. 12 (2010) 1113–1125. https://doi.org/10.1093/neuonc/noq082.

[95] W. Zhou, S.Q. Ke, Z. Huang, W. Flavahan, X. Fang, L. Wu, A.E. Sloan, R.E. Mclendon, X. Li, J.N. Rich, Periostin Secreted by Glioblastoma Stem Cells Recruits M2 Tumor-associated Macrophages and Promotes Malignat Growth, Nat. Cell Biol. 17 (2015) 170–182. https://doi.org/10.1038/ncb3090.

[96] K. Gabrusiewicz, X. Li, J. Wei, Y. Hashimoto, A.L. Marisetty, M. Ott, F. Wang, D. Hawke, J. Yu, L.M. Healy, A. Hossain, J.C. Akers, S.N. Maiti, S. Yamashita, Y. Shimizu, K. Dunner, M.A. Zal, J.K. Burks, J. Gumin, F. Nwajei, A. Rezavanian, S. Zhou, G. Rao, R. Sawaya, G.N. Fuller, J.T. Huse, J.P. Antel, S. Li, L. Cooper, E.P. Sulman, C. Chen, C. Geula, R. Kalluri, T. Zal, A.B. Heimberger, Glioblastoma stem cell-derived exosomes induce M2 macrophages and PD-L1 expression on human monocytes, Oncoimmunology. 7 (2018). https://doi.org/10.1080/2162402X.2017.1412909.

[97] M. Bausart, V. Préat, A. Malfanti, Immunotherapy for glioblastoma: the promise of combination strategies, J. Exp. Clin. Cancer Res. 41 (2022) 1–22. https://doi.org/10.1186/s13046-022-02251-2.

[98] K. Gabrusiewicz, X. Li, J. Wei, Y. Hashimoto, A.L. Marisetty, M. Ott, F. Wang, D. Hawke, J. Yu, L.M. Healy, A. Hossain, J.C. Akers, S.N. Maiti, S. Yamashita, Y. Shimizu, K. Dunner, M.A. Zal, J.K. Burks, J. Gumin, F. Nwajei, A. Rezavanian, S. Zhou, G. Rao, R. Sawaya, G.N. Fuller, J.T. Huse, J.P. Antel, S. Li, L. Cooper, E.P. Sulman, C. Chen, C. Geula, R. Kalluri, T. Zal, A.B. Heimberger, Glioblastoma stem cell-derived exosomes induce M2 macrophages and PD-L1 expression on human monocytes, Oncoimmunology. 7 (2018). https://doi.org/10.1080/2162402X.2017.1412909.

[99] Nicola J. Allen, Ben A. Barres, Glia-more than just brain glue, Nature. 457 (2009) 675–677.

[100] S.A. Liddelow, B.A. Barres, Reactive Astrocytes: Production, Function, and Therapeutic Potential, Immunity. 46 (2017) 957–967. https://doi.org/10.1016/J.IMMUNI.2017.06.006.

[101] J.K. Reid, H.F. Kuipers, She Doesn't Even Go Here: The Role of Inflammatory Astrocytes in CNS Disorders, Front. Cell. Neurosci. 15 (2021) 332. https://doi.org/10.3389/FNCEL.2021.704884.

[102] Z. Bin Ding, L.J. Song, Q. Wang, G. Kumar, Y.Q. Yan, C.G. Ma, Astrocytes: a double-edged sword in neurodegenerative diseases, Neural Regen. Res. 16 (2021) 1702. https://doi.org/10.4103/1673-5374.306064.

[103] D. Henrik Heiland, V.M. Ravi, S.P. Behringer, J.H. Frenking, J. Wurm, K. Joseph, N.W.C. Garrelfs, J. Strähle, S. Heynckes, J. Grauvogel, P. Franco, I. Mader, M. Schneider, A.L. Potthoff, D. Delev, U.G. Hofmann, C. Fung, J. Beck, R. Sankowski, M. Prinz, O. Schnell, Tumor-associated reactive astrocytes aid the evolution of immunosuppressive environment in glioblastoma, Nat. Commun. 2019 101. 10 (2019) 1–12. https://doi.org/10.1038/s41467-019-10493-6.

[104] D. Matias, J. Balça-Silva, G.C. da Graça, C.M. Wanjiru, L.W. Macharia, C.P. Nascimento, N.R. Roque, J.M. Coelho-Aguiar, C.M. Pereira, M.F. Dos Santos, L.S. Pessoa, F.R.S. Lima, A. Schanaider, V.P. Ferrer, T.C.L. de S. e Spohr, V. Moura-Neto, Microglia/astrocytes–glioblastoma crosstalk: Crucial molecular mechanisms and microenvironmental factors, Front. Cell. Neurosci. 12 (2018) 235. https://doi.org/10.3389/fncel.2018.00235.

[105] T. Yu, X.F. Wang, T. Zhi, J. Zhang, Y. Wang, E. Nie, F. Zhou, Y. You, N. Liu, Delivery of MGMT mRNA to glioma cells by reactive astrocyte-derived exosomes confers a temozolomide resistance phenotype, Cancer Lett. 433 (2018) 210–220. https://doi.org/10.1016/J.CANLET.2018.06.041.

[106] C.E. Holt, K.C. Martin, E.M. Schuman, Local translation in neurons: visualization and function, Nat. Struct. Mol. Biol. 2019 267. 26 (2019) 557–566. https://doi.org/10.1038/s41594-019-0263-5.

[107] H.S. Venkatesh, T.B. Johung, V. Caretti, A. Noll, Y. Tang, S. Nagaraja, E.M. Gibson, C.W. Mount, J. Polepalli, S.S. Mitra, P.J. Woo, R.C. Malenka, H. Vogel, M. Bredel, P. Mallick, M. Monje, Neuronal activity promotes glioma growth through neuroligin-3 secretion, Cell. 161 (2015) 803–816. https://doi.org/10.1016/j.cell.2015.04.012.

[108] G. Huberfeld, C.J. Vecht, Seizures and gliomas — towards a single therapeutic approach, Nat. Rev. Neurol. 2016 124. 12 (2016) 204–216. https://doi.org/10.1038/nrneurol.2016.26.

[109] M. Asslaber, S. Schauer, M. Gogg-Kamerer, E. Bernhart, F. Quehenberger, J. Haybaeck, Native Oligodendrocytes in Astrocytomas Might Inhibit Tumor Proliferation by WIF1 Expression, J. Neuropathol. Exp. Neurol. 76 (2017) 16–26. https://doi.org/10.1093/JNEN/NLW098.

[110] Y. Huang, C. Hoffman, P. Rajappa, J.H. Kim, W. Hu, J. Huse, Z. Tang, X. Li, B. Weksler, J. Bromberg, D.C. Lyden, J.P. Greenfield, Oligodendrocyte progenitor cells promote

neovascularization in glioma by disrupting the blood-brain barrier, Cancer Res. 74 (2014) 1011–1121. https://doi.org/10.1158/0008-5472.CAN-13-1072.

[111] M. Prinz, J. Priller, Microglia and brain macrophages in the molecular age: from origin to neuropsychiatric disease, Nat. Rev. Neurosci. 2014 155. 15 (2014) 300–312. https://doi.org/10.1038/nrn3722.

[112] K. Gabrusiewicz, B. Rodriguez, J. Wei, Y. Hashimoto, L.M. Healy, S.N. Maiti, G. Thomas, S. Zhou, Q. Wang, A. Elakkad, B.D. Liebelt, N.K. Yaghi, R. Ezhilarasan, N. Huang, J.S. Weinberg, S.S. Prabhu, G. Rao, R. Sawaya, L.A. Langford, J.M. Bruner, G.N. Fuller, A. Bar-Or, W. Li, R.R. Colen, M.A. Curran, K.P. Bhat, J.P. Antel, L.J. Cooper, E.P. Sulman, A.B. Heimberger, Glioblastoma-infiltrated innate immune cells resemble M0 macrophage phenotype, JCI Insight. 1 (2016). https://doi.org/10.1172/JCI.INSIGHT.85841.

[113] M.M. Grabowski, E.W. Sankey, K.J. Ryan, P. Chongsathidkiet, S.J. Lorrey, · Daniel, S. Wilkinson, · Peter, E. Fecci, Immune suppression in gliomas, J. Neurooncol. 151 (2021) 3–12. https://doi.org/10.1007/s11060-020-03483-y.

[114] K. Kondělková, D. Vokurková, J. Krejsek, L. Borská, Z. Fiala, A. Ctirad, Regulatory T cells (TREG) and their roles in immune system with respect to immunopathological disorders, Acta Medica (Hradec Kral. 53 (2010) 73–77. https://doi.org/10.14712/18059694.2016.63.

[115] S.R. Anderson, M.L. Vetter, Developmental roles of microglia: a window into mechanisms of disease, Dev. Dyn. 248 (2019) 98. https://doi.org/10.1002/DVDY.1.

[116] K. Kierdorf, D. Erny, T. Goldmann, V. Sander, C. Schulz, E.G. Perdiguero, P. Wieghofer, A. Heinrich, P. Riemke, C. Hölscher, D.N. Müller, B. Luckow, T. Brocker, K. Debowski, G. Fritz, G. Opdenakker, A. Diefenbach, K. Biber, M. Heikenwalder, F. Geissmann, F. Rosenbauer, M. Prinz, Microglia emerge from erythromyeloid precursors via Pu.1- and Irf8-dependent pathways, Nat. Neurosci. 16 (2013) 273–280. https://doi.org/10.1038/NN.3318.

[117] O. Matcovitch-Natan, D.R. Winter, A. Giladi, S.V. Aguilar, A. Spinrad, S. Sarrazin, H. Ben-Yehuda, E. David, F.Z. González, P. Perrin, H. Keren-Shaul, M. Gury, D. Lara-Astaiso, C.A. Thaiss, M. Cohen, K.B. Halpern, K. Baruch, A. Deczkowska, E. Lorenzo-Vivas, S. Itzkovitz, E. Elinav, M.H. Sieweke, M. Schwartz, I. Amit, Microglia development follows a stepwise program to regulate brain homeostasis, Science (80-.). 353 (2016). https://doi.org/10.1126/science.aad8670.

[118] S. Etemad, R.M. Zamin, M.J. Ruitenberg, L. Filgueira, A novel in vitro human microglia model: Characterization of human monocyte-derived microglia, J. Neurosci. Methods. 209 (2012) 79–89. https://doi.org/10.1016/j.jneumeth.2012.05.025.

[119] T.L. Tay, J.C. Savage, C.W. Hui, K. Bisht, M.È. Tremblay, Microglia across the lifespan: from origin to function in brain development, plasticity and cognition, J. Physiol. 595 (2017) 1929–1945. https://doi.org/10.1113/JP272134.

[120] A.M. Casano, F. Peri, Microglia: multitasking specialists of the brain, Dev. Cell. 32 (2015) 469–477. https://doi.org/10.1016/J.DEVCEL.2015.01.018.

[121] A.M. Jurga, M. Paleczna, K.Z. Kuter, Overview of General and Discriminating Markers of Differential Microglia Phenotypes, Front. Cell. Neurosci. 14 (2020) 1–18. https://doi.org/10.3389/fncel.2020.00198.

[122] I. Yang, S.J. Han, G. Kaur, C. Crane, A.T. Parsa, The Role of Microglia in Central Nervous System Immunity and Glioma Immunology, J. Clin. Neurosci. 17 (2010) 6. https://doi.org/10.1016/J.JOCN.2009.05.006.

[123] A. Etzerodt, S.K. Moestrup, CD163 and inflammation: biological, diagnostic, and therapeutic aspects, Antioxid. Redox Signal. 18 (2013) 2352–2363. https://doi.org/10.1089/ARS.2012.4834.

[124] S.M. Pyonteck, L. Akkari, A.J. Schuhmacher, R.L. Bowman, L. Sevenich, D.F. Quail, O.C. Olson, M.L. Quick, J.T. Huse, V. Teijeiro, M. Setty, C.S. Leslie, Y. Oei, A. Pedraza, J. Zhang, C.W. Brennan, J.C. Sutton, E.C. Holland, D. Daniel, J.A. Joyce, CSF-1R inhibition

alters macrophage polarization and blocks glioma progression HHS Public Access Author manuscript, Nat Med. 19 (2013) 1264–1272. https://doi.org/10.1038/nm.3337.CSF-1R.

[125] K.E. Hopperton, D. Mohammad, M.O. Trépanier, V. Giuliano, R.P. Bazinet, Markers of microglia in post-mortem brain samples from patients with Alzheimer's disease: a systematic review, Mol. Psychiatry. 23 (2018) 177–198. https://doi.org/10.1038/MP.2017.246.

[126] A.H. Courtney, A.A. Shvets, W. Lu, G. Griffante, M. Mollenauer, V. Horkova, W.L. Lo, S. Yu, O. Stepanek, A.K. Chakraborty, A. Weiss, CD45 functions as a signaling gatekeeper in T cells, Sci. Signal. 12 (2019). https://doi.org/10.1126/scisignal.aaw8151.

[127] S.Q. Khan, I. Khan, V. Gupta, CD11b activity modulates pathogenesis of lupus nephritis, Front. Med. 5 (2018) 52. https://doi.org/10.3389/fmed.2018.00052.

[128] D.A. Chistiakov, M.C. Killingsworth, V.A. Myasoedova, A.N. Orekhov, Y. V. Bobryshev, CD68/macrosialin: not just a histochemical marker, Lab. Invest. 97 (2017) 4–13. https://doi.org/10.1038/LABINVEST.2016.116.

[129] Y. Sasaki, K. Ohsawa, H. Kanazawa, S. Kohsaka, Y. Imai, Iba1 is an actin-cross-linking protein in macrophages/microglia, Biochem. Biophys. Res. Commun. 286 (2001) 292–297. https://doi.org/10.1006/BBRC.2001.5388.

[130] T.R. Jay, V.E. Von Saucken, G.E. Landreth, TREM2 in Neurodegenerative Diseases, Mol. Neurodegener. 12 (2017). https://doi.org/10.1186/S13024-017-0197-5.

[131] P. Jiang, F. Xing, B. Guo, J. Yang, Z. Li, W. Wei, F. Hu, I. Lee, X. Zhang, L. Pan, J. Xu, Nucleotide transmitters ATP and ADP mediate intercellular calcium wave communication via P2Y12/13 receptors among BV-2 microglia, PLoS One. 12 (2017) e0183114. https://doi.org/10.1371/JOURNAL.PONE.0183114.

[132] J. Preissler, A. Grosche, V. Lede, D. Le Duc, K. Krügel, V. Matyash, F. Szulzewsky, S. Kallendrusch, K. Immig, H. Kettenmann, I. Bechmann, T. Schöneberg, A. Schulz, Altered microglial phagocytosis in GPR34-deficient mice, Glia. 63 (2015) 206–215. https://doi.org/10.1002/GLIA.22744.

[133] M. Lee, Y. Lee, J. Song, J. Lee, S.Y. Chang, Tissue-specific Role of CX3CR1 Expressing Immune Cells and Their Relationships with Human Disease, Immune Netw. 18 (2018). https://doi.org/10.4110/IN.2018.18.E5.

[134] G.K. Sheridan, K.J. Murphy, Neuron-glia crosstalk in health and disease: fractalkine and CX3CR1 take centre stage, Open Biol. 3 (2013). https://doi.org/10.1098/RSOB.130181.

[135] A.D. Bachstetter, J.M. Morganti, J. Jernberg, A. Schlunk, S.H. Mitchell, K.W. Brewster, C.E. Hudson, M.J. Cole, J.K. Harrison, P.C. Bickford, C. Gemma, Fractalkine and CX 3 CR1 regulate hippocampal neurogenesis in adult and aged rats, Neurobiol. Aging. 32 (2011) 2030–2044. https://doi.org/10.1016/J.NEUROBIOLAGING.2009.11.022.

[136] S. V. Kushchayev, T. Sankar, L.L. Eggink, Y.S. Kushchayeva, P.C. Wiener, J. Kenneth Hoober, J. Eschbacher, R. Liu, F.D. Shi, M.G. Abdelwahab, A.C. Scheck, M.C. Preul, Monocyte galactose/N-acetylgalactosamine-specific C-type lectin receptor stimulant immunotherapy of an experimental glioma. Part 1: stimulatory effects on blood monocytes and monocyte-derived cells of the brain, Cancer Manag. Res. 4 (2012) 309. https://doi.org/10.2147/CMAR.S33248.

[137] A. Müller, S. Brandenburg, K. Turkowski, S. Müller, P. Vajkoczy, Resident microglia, and not peripheral macrophages, are the main source of brain tumor mononuclear cells, Int. J. Cancer. 137 (2015) 278–288. https://doi.org/10.1002/IJC.29379.

[138] D.H.G.& H.K. Dolores Hambardzumyan, The role of microglia and macrophages in glioma maintenance and progression, Nat. Neurosci. 19 (2017) 20–27. https://doi.org/10.1038/nn.4185.

[139] Y. Komohara, K. Ohnishi, J. Kuratsu, M. Takeya, Possible involvement of the M2 anti-inflammatory macrophage phenotype in growth of human gliomas, J. Pathol. 216 (2008)

15–24. https://doi.org/10.1002/PATH.2370.

[140] M. Maxwell, T. Galanopoulos, J. Neville-Golden, H.N. Antoniades, Effect of the expression of transforming growth factor-β2 in primary human glioblastomas on immunosuppression and loss of immune surveillance, J. Neurosurg. 76 (1992) 799–804. https://doi.org/10.3171/JNS.1992.76.5.0799.

[141] J. Han, C.A. Alvarez-Breckenridge, Q.E. Wang, J. Yu, TGF-β signaling and its targeting for glioma treatment, Am. J. Cancer Res. 5 (2015) 945. /pmc/articles/PMC4449428/ (accessed July 5, 2022).

[142] D.A. Thomas, J. Massagué, TGF-beta directly targets cytotoxic T cell functions during tumor evasion of immune surveillance, Cancer Cell. 8 (2005) 369–380. https://doi.org/10.1016/J.CCR.2005.10.012.

[143] C. Stolfi, E. Troncone, I. Marafini, G. Monteleone, Role of tgf-beta and smad7 in gut inflammation, fibrosis and cancer, Biomolecules. 11 (2021) 1–15. https://doi.org/10.3390/BIOM11010017.

[144] T. Zöller, A. Schneider, C. Kleimeyer, T. Masuda, P.S. Potru, D. Pfeifer, T. Blank, M. Prinz, B. Spittau, Silencing of TGFβ signalling in microglia results in impaired homeostasis, Nat. Commun. 2018 91. 9 (2018) 1–13. https://doi.org/10.1038/s41467-018-06224-y.

[145] H. Xu, H. Zong, C. Ma, X. Ming, M. Shang, K. Li, X. He, H. Du, L. Cao, Epidermal growth factor receptor in glioblastoma, Oncol. Lett. 14 (2017) 512. https://doi.org/10.3892/OL.2017.6221.

[146] Z. Chen, D. Hambardzumyan, Immune microenvironment in glioblastoma subtypes, Front. Immunol. 9 (2018) 1–8. https://doi.org/10.3389/fimmu.2018.01004.

[147] S. Guo, H. Wang, Y. Yin, Microglia Polarization From M1 to M2 in Neurodegenerative Diseases, Front. Aging Neurosci. 14 (2022) 75. https://doi.org/10.3389/fnagi.2022.815347.

[148] M. Saraiva, P. Vieira, A. O'Garra, Biology and therapeutic potential of interleukin-10, J. Exp. Med. 217 (2020). https://doi.org/10.1084/JEM.20190418.

[149] T. Sato, M. Terai, Y. Tamura, V. Alexeev, M.J. Mastrangelo, S.R. Selvan, Interleukin 10 in the tumor microenvironment: A target for anticancer immunotherapy, Immunol. Res. 51 (2011) 170–182. https://doi.org/10.1007/S12026-011-8262-6/FIGURES/4.

[150] A. Bhattacharjee, M. Shukla, V.P. Yakubenko, A. Mulya, S. Kundu, M.K. Cathcart, IL-4 and IL-13 employ discrete signaling pathways for target gene expression in alternatively activated monocytes/macrophages, Free Radic. Biol. Med. 54 (2013) 1–16. https://doi.org/10.1016/J.FREERADBIOMED.2012.10.553.

[151] J. Li, Z. Yin, B. Huang, K. Xu, J. Su, Stat3 Signaling Pathway: A Future Therapeutic Target for Bone-Related Diseases, Front. Pharmacol. 13 (2022) 1416. https://doi.org/10.3389/fphar.2022.897539.

[152] H. Islam, T.C. Chamberlain, A.L. Mui, J.P. Little, Elevated Interleukin-10 Levels in COVID-19: Potentiation of Pro-Inflammatory Responses or Impaired Anti-Inflammatory Action?, Front. Immunol. 12 (2021) 2485. https://doi.org/10.3389/fimmu.2021.677008.

[153] R.K. Ramachandran, M.D. Sørensen, C. Aaberg-Jessen, S.K. Hermansen, B.W. Kristensen, Expression and prognostic impact of matrix metalloproteinase-2 (MMP-2) in astrocytomas, PLoS One. 12 (2017). https://doi.org/10.1371/JOURNAL.PONE.0172234.

[154] A. Suzumura, M. Sawada, H. Yamamoto, T. Marunouchi, Transforming growth factor-beta suppresses activation and proliferation of microglia in vitro., J. Immunol. 151 (1993).

[155] K. Frei, H. Lins, C. Schwerdel, A. Fontana, Antigen presentation in the central nervous system. The inhibitory effect of IL-10 on MHC class II expression and production of cytokines depends on the inducing signals and the type of cell analyzed., J. Immunol. 152 (1994).

[156] K.A. Fitzgerald, L.A.J. O'Neill, A.J.H. Gearing, R.E. Callard, FasL, in: Cytokine Factsb. Webfacts, 2nd ed., Academic Press, 2001: pp. 225–229. https://doi.org/10.1016/b978-012155142-1/50049-x.

[157] A.S. Plant, S. Koyama, C. Sinai, I.H. Solomon, G.K. Griffin, K.L. Ligon, P. Bandopadhayay, R. Betensky, R. Emerson, G. Dranoff, M.W. Kieran, J. Ritz, Immunophenotyping of pediatric brain tumors: correlating immune infiltrate with histology, mutational load, and survival and assessing clonal T cell response, J. Neurooncol. 137 (2018) 269–278. https://doi.org/10.1007/S11060-017-2737-9.

[158] A.M. Griesinger, D.K. Birks, A.M. Donson, V. Amani, L.M. Hoffman, A. Waziri, M. Wang, M.H. Handler, N.K. Foreman, Characterization of distinct immunophenotypes across pediatric brain tumor types, J. Immunol. 191 (2013) 4880–4888. https://doi.org/10.4049/JIMMUNOL.1301966.

[159] N.A.P. Lieberman, K. Degolier, H.M. Kovar, A. Davis, V. Hoglund, J. Stevens, C. Winter, G. Deutsch, S.N. Furlan, N.A. Vitanza, S.E.S. Leary, C.A. Crane, Characterization of the immune microenvironment of diffuse intrinsic pontine glioma: implications for development of immunotherapy, Neuro. Oncol. 21 (2019) 83–94. https://doi.org/10.1093/NEUONC/NOY145.

[160] C.J. Pachocki, E.M. Hol, Current perspectives on diffuse midline glioma and a different role for the immune microenvironment compared to glioblastoma, J. Neuroinflammation 2022 191. 19 (2022) 1–16. https://doi.org/10.1186/S12974-022-02630-8.

[161] T. Kuntzel, D. Bagnard, Manipulating Macrophage/Microglia Polarization to Treat Glioblastoma or Multiple Sclerosis, Pharmaceutics. 14 (2022). https://doi.org/10.3390/PHARMACEUTICS14020344.

[162] A Study of BLZ945 Single Agent or BLZ945 in Combination With PDR001 in Advanced Solid Tumors - Full Text View - ClinicalTrials.gov, (n.d.). https://clinicaltrials.gov/ct2/show/NCT02829723 (accessed January 5, 2023).

[163] L. Zhang, D. Alizadeh, M. van Handel, M. Kortylewski, H. Yu, B. Badie, Stat3 inhibition activates tumor macrophages and abrogates glioma growth in mice, Glia. 57 (2009) 1458–1467. https://doi.org/10.1002/GLIA.20863.

[164] J. Dong, X.D. Cheng, W.D. Zhang, J.J. Qin, Recent Update on Development of Small-Molecule STAT3 Inhibitors for Cancer Therapy: From Phosphorylation Inhibition to Protein Degradation, J. Med. Chem. 64 (2021) 8884–8915. https://doi.org/10.1021/acs.jmedchem.1c00629.

[165] A. Mantovani, E. Dejana, Endothelium, in: Encycl. Immunol., Elsevier, 1998: pp. 802–806. https://doi.org/10.1006/rwei.1999.0212.

[166] S. Ferber, G. Tiram, A. Sousa-Herves, A. Eldar-Boock, A. Krivitsky, A. Scomparin, E. Yeini, P. Ofek, D. Ben-Shushan, L.I. Vossen, K. Licha, R. Grossman, Z. Ram, J. Henkin, E. Ruppin, N. Auslander, R. Haag, M. Calderón, R. Satchi-Fainaro, Co-targeting the tumor endothelium and P-selectin-expressing glioblastoma cells leads to a remarkable therapeutic outcome, Elife. 6 (2017). https://doi.org/10.7554/ELIFE.25281.

[167] E. Yeini, P. Ofek, S. Pozzi, N. Albeck, D. Ben-Shushan, G. Tiram, S. Golan, R. Kleiner, R. Sheinin, S. Israeli Dangoor, S. Reich-Zeliger, R. Grossman, Z. Ram, H. Brem, T.M. Hyde, P. Magod, D. Friedmann-Morvinski, A. Madi, R. Satchi-Fainaro, P-selectin axis plays a key role in microglia immunophenotype and glioblastoma progression, Nat. Commun. 2021 121. 12 (2021) 1–22. https://doi.org/10.1038/s41467-021-22186-0.

[168] D.A. Reardon, A.A. Brandes, A. Omuro, P. Mulholland, M. Lim, A. Wick, J. Baehring, M.S. Ahluwalia, P. Roth, O. Bähr, S. Phuphanich, J.M. Sepulveda, P. De Souza, S. Sahebjam, M. Carleton, K. Tatsuoka, C. Taitt, R. Zwirtes, J. Sampson, M. Weller, Effect of Nivolumab vs Bevacizumab in Patients With Recurrent Glioblastoma: The CheckMate 143 Phase 3 Randomized Clinical Trial, JAMA Oncol. 6 (2020) 1003–1010. https://doi.org/10.1001/JAMAONCOL.2020.1024.

[169] L. Chen, Y. Zhang, J. Yang, J.P. Hagan, M. Li, Vertebrate animal models of glioma: understanding the mechanisms and developing new therapies, Biochim. Biophys. Acta. 1836 (2013) 158–165. https://doi.org/10.1016/J.BBCAN.2013.04.003.

[170] F. Andreatta, G. Beccaceci, N. Fortuna, M. Celotti, D. De Felice, M. Lorenzoni, V. Foletto, S. Genovesi, J. Rubert, A. Alaimo, The organoid era permits the development of new applications to study glioblastoma, Cancers (Basel). 12 (2020) 1–16. https://doi.org/10.3390/cancers12113303.

[171] E. Izumchenko, J. Meir, A. Bedi, P.T. Wysocki, M.O. Hoque, D. Sidransky, Patient-derived xenografts as tools in pharmaceutical development, Clin. Pharmacol. Ther. 99 (2016) 612–621. https://doi.org/10.1002/CPT.354.

[172] C.R. Ireson, M.S. Alavijeh, A.M. Palmer, E.R. Fowler, H.J. Jones, The role of mouse tumour models in the discovery and development of anticancer drugs, Br. J. Cancer 2019 1212. 121 (2019) 101–108. https://doi.org/10.1038/s41416-019-0495-5.

[173] A. Richmond, S. Yingjun, Mouse xenograft models vs GEM models for human cancer therapeutics, DMM Dis. Model. Mech. 1 (2008) 78–82. https://doi.org/10.1242/dmm.000976.

[174] T.M. Allen, M.A. Brehm, S. Bridges, S. Ferguson, P. Kumar, O. Mirochnitchenko, K. Palucka, R. Pelanda, B. Sanders-Beer, L.D. Shultz, L. Su, M. PrabhuDas, Humanized immune system mouse models: progress, challenges and opportunities, Nat. Immunol. 20 (2019) 770–774. https://doi.org/10.1038/S41590-019-0416-Z.

[175] G. Dranoff, Experimental mouse tumour models: what can be learnt about human cancer immunology?, Nat. Rev. Immunol. 2011 121. 12 (2011) 61–66. https://doi.org/10.1038/nri3129.

[176] V. Brinks, D. Weinbuch, M. Baker, Y. Dean, P. Stas, S. Kostense, B. Rup, W. Jiskoot, Preclinical models used for immunogenicity prediction of therapeutic proteins, Pharm. Res. 30 (2013) 1719–1728. https://doi.org/10.1007/s11095-013-1062-z.

[177] P. De La Rochere, S. Guil-Luna, D. Decaudin, G. Azar, S.S. Sidhu, E. Piaggio, Humanized Mice for the Study of Immuno-Oncology, Trends Immunol. 39 (2018) 748–763. https://doi.org/10.1016/j.it.2018.07.001.

[178] L.N. Kiseleva, A. V. Kartashev, N.L. Vartanyan, A.A. Pinevich, M.P. Samoilovich, A172 and T98G cell lines characteristics, Cell Tissue Biol. 10 (2016) 341–348. https://doi.org/10.1134/S1990519X16050072.

[179] Y. Xie, T. Bergström, Y. Jiang, P. Johansson, V.D. Marinescu, N. Lindberg, A. Segerman, G. Wicher, M. Niklasson, S. Baskaran, S. Sreedharan, I. Everlien, M. Kastemar, A. Hermansson, L. Elfineh, S. Libard, E.C. Holland, G. Hesselager, I. Alafuzoff, B. Westermark, S. Nelander, K. Forsberg-Nilsson, L. Uhrbom, The Human Glioblastoma Cell Culture Resource: Validated Cell Models Representing All Molecular Subtypes, EBioMedicine. 2 (2015) 1351–1363. https://doi.org/10.1016/j.ebiom.2015.08.026.

[180] A. Li, J. Walling, Y. Kotliarov, A. Center, M.E. Steed, S.J. Ahn, M. Rosenblum, T. Mikkelsen, J.C. Zenklusen, H.A. Fine, Genomic changes and gene expression profiles reveal that established glioma cell lines are poorly representative of primary human gliomas, Mol. Cancer Res. 6 (2008) 21–30. https://doi.org/10.1158/1541-7786.MCR-07-0280.

[181] T.R. Jones, S.H. Bigner, S.C. Schold, L.F. Eng, Anaplastic human gliomas grown in athymic mice. Morphology and glial fibrillary acidic protein expression, Am. J. Pathol. 105 (1981) 316–327.

[182] S. Breslin, L. O'Driscoll, Three-dimensional cell culture: the missing link in drug discovery, Drug Discov. Today. 18 (2013) 240–249. https://doi.org/10.1016/J.DRUDIS.2012.10.003.

[183] S.A. Langhans, Three-dimensional in vitro cell culture models in drug discovery and drug repositioning, Front. Pharmacol. 9 (2018) 6. https://doi.org/10.3389/fphar.2018.00006.

[184] C.Y. Cho, T.H. Chiang, L.H. Hsieh, W.Y. Yang, H.H. Hsu, C.K. Yeh, C.C. Huang, J.H. Huang, Development of a Novel Hanging Drop Platform for Engineering Controllable 3D Microenvironments, Front. Cell Dev. Biol. 8 (2020) 327. https://doi.org/10.3389/fcell.2020.00327.

[185] H.F. Bahmad, K. Cheaito, R.M. Chalhoub, O. Hadadeh, A. Monzer, F. Ballout, A. El-Hajj, D. Mukherji, Y.N. Liu, G. Daoud, W. Abou-Kheir, Sphere-Formation Assay: Three-dimensional in vitro culturing of prostate cancer stem/Progenitor sphere-forming cells, Front. Oncol. 8 (2018) 1–14. https://doi.org/10.3389/fonc.2018.00347.

[186] Y.C. Chen, P.N. Ingram, S. Fouladdel, S.P. Mcdermott, E. Azizi, M.S. Wicha, E. Yoon, High-throughput single-cell derived sphere formation for cancer stem-like cell identification and analysis, Sci. Rep. 6 (2016) 1–12. https://doi.org/10.1038/srep27301.

[187] E. Pastrana, V. Silva-Vargas, F. Doetsch, Eyes Wide Open: A Critical Review of Sphere-Formation as an Assay For Stem Cells, Cell Stem Cell. 8 (2011) 486. https://doi.org/10.1016/J.STEM.2011.04.007.

[188] P. Paoli, E. Giannoni, P. Chiarugi, Anoikis molecular pathways and its role in cancer progression, Biochim. Biophys. Acta - Mol. Cell Res. 1833 (2013) 3481–3498. https://doi.org/10.1016/J.BBAMCR.2013.06.026.

[189] L.F. Pavon, L.C. Marti, T.T. Sibov, S.M.F. Malheiros, R.A. Brandt, S. Cavalheiro, L.F. Gamarra, In vitro analysis of neurospheres derived from glioblastoma primary culture: A novel methodology paradigm, Front. Neurol. 4 JAN (2014) 1–9. https://doi.org/10.3389/fneur.2013.00214.

[190] C.H. Chang, W.T. Liu, H.C. Hung, C.Y. Gean, H.M. Tsai, C.L. Su, P.W. Gean, Synergistic inhibition of tumor growth by combination treatment with drugs against different subpopulations of glioblastoma cells, BMC Cancer. 17 (2017). https://doi.org/10.1186/S12885-017-3924-Y.

[191] C.E. Griguer, C.R. Oliva, E. Gobin, P. Marcorelles, D.J. Benos, J.R. Lancaster, G.Y. Gillespie, CD133 is a marker of bioenergetic stress in human glioma, PLoS One. 3 (2008). https://doi.org/10.1371/JOURNAL.PONE.0003655.

[192] M. Ognibene, A. Pezzolo, Roniciclib down-regulates stemness and inhibits cell growth by inducing nucleolar stress in neuroblastoma, Sci. Rep. 10 (2020). https://doi.org/10.1038/S41598-020-69499-6.

[193] C. Zhang, L. Hai, M. Zhu, S. Yu, T. Li, Y. Lin, B. Liu, X. Zhou, L. Chen, P. Zhao, H. Zhou, Y. Huang, K. Zhang, B. Ren, X. Yang, Actin cytoskeleton regulator Arp2/3 complex is required for DLL1 activating Notch1 signaling to maintain the stem cell phenotype of glioma initiating cells, Oncotarget. 8 (2017) 33353–33364. https://doi.org/10.18632/ONCOTARGET.16495.

[194] X. Hong, K. Chedid, S.N. Kalkanis, Glioblastoma cell line-derived spheres in serum-containing medium versus serum-free medium: A comparison of cancer stem cell properties, Int. J. Oncol. 41 (2012) 1693–1700. https://doi.org/10.3892/ijo.2012.1592.

[195] M. Paolillo, S. Comincini, S. Schinelli, In vitro glioblastoma models: A journey into the third dimension, Cancers (Basel). 13 (2021) 1–25. https://doi.org/10.3390/cancers13102449.

[196] H.K. Kleinman, G.R. Martin, Matrigel: basement membrane matrix with biological activity, Semin. Cancer Biol. 15 (2005) 378–386. https://doi.org/10.1016/J.SEMCANCER.2005.05.004.

[197] A. Shakouri-Motlagh, A.J. O'Connor, S.P. Brennecke, B. Kalionis, D.E. Heath, Native and solubilized decellularized extracellular matrix: A critical assessment of their potential for improving the expansion of mesenchymal stem cells, Acta Biomater. 55 (2017) 1–12. https://doi.org/10.1016/J.ACTBIO.2017.04.014.

[198] E.A. Aisenbrey, W.L. Murphy, Synthetic alternatives to Matrigel, Nat. Rev. Mater. 2020 57. 5 (2020) 539–551. https://doi.org/10.1038/s41578-020-0199-8.

[199] Y.S. Zhang, A. Khademhosseini, Advances in engineering hydrogels, Science. 356 (2017). https://doi.org/10.1126/SCIENCE.AAF3627.

[200] G.P. Raeber, M.P. Lutolf, J.A. Hubbell, Molecularly engineered PEG hydrogels: a novel model system for proteolytically mediated cell migration, Biophys. J. 89 (2005) 1374–1388. https://doi.org/10.1529/BIOPHYSJ.104.050682.

[201] E.L.S. Fong, S.E. Lamhamedi-Cherradi, E. Burdett, V. Ramamoorthy, A.J. Lazar, F.K. Kasper, M.C. Farach-Carson, D. Vishwamitra, E.G. Demicco, B.A. Menegaz, H.M. Amin, A.G. Mikos, J.A. Ludwig, Modeling Ewing sarcoma tumors in vitro with 3D scaffolds, Proc. Natl. Acad. Sci. U. S. A. 110 (2013) 6500–6505. https://doi.org/10.1073/pnas.1221403110.

[202] L.M. Weber, K.N. Hayda, K. Haskins, K.S. Anseth, The effects of cell-matrix interactions on encapsulated beta-cell function within hydrogels functionalized with matrix-derived adhesive peptides, Biomaterials. 28 (2007) 3004–3011. https://doi.org/10.1016/J.BIOMATERIALS.2007.03.005.

[203] X.Y. Tang, S. Wu, D. Wang, C. Chu, Y. Hong, M. Tao, H. Hu, M. Xu, X. Guo, Y. Liu, Human organoids in basic research and clinical applications, Signal Transduct. Target. Ther. 2022 71. 7 (2022) 1–17. https://doi.org/10.1038/s41392-022-01024-9.

[204] F. Jacob, R.D. Salinas, D.Y. Zhang, P.T.T. Nguyen, J.G. Schnoll, S.Z.H. Wong, R. Thokala, S. Sheikh, D. Saxena, S. Prokop, D. ao Liu, X. Qian, D. Petrov, T. Lucas, H.I. Chen, J.F. Dorsey, K.M. Christian, Z.A. Binder, M. Nasrallah, S. Brem, D.M. O'Rourke, G. li Ming, H. Song, A Patient-Derived Glioblastoma Organoid Model and Biobank Recapitulates Inter- and Intra-tumoral Heterogeneity, Cell. 180 (2020) 188-204.e22. https://doi.org/10.1016/J.CELL.2019.11.036.

[205] S. Bian, M. Repic, Z. Guo, A. Kavirayani, T. Burkard, J.A. Bagley, C. Krauditsch, J.A. Knoblich, Genetically engineered cerebral organoids model brain tumor formation, Nat. Methods 2018 158. 15 (2018) 631–639. https://doi.org/10.1038/s41592-018-0070-7.

[206] A. Linkous, D. Balamatsias, M. Snuderl, L. Edwards, K. Miyaguchi, T. Milner, B. Reich, L. Cohen-Gould, A. Storaska, Y. Nakayama, E. Schenkein, R. Singhania, S. Cirigliano, T. Magdeldin, Y. Lin, G. Nanjangud, K. Chadalavada, D. Pisapia, C. Liston, H.A. Fine, Modeling Patient-Derived Glioblastoma with Cerebral Organoids, Cell Rep. 26 (2019) 3203-3211.e5. https://doi.org/10.1016/J.CELREP.2019.02.063.

[207] B. da Silva, R.K. Mathew, E.S. Polson, J. Williams, H. Wurdak, Spontaneous Glioblastoma Spheroid Infiltration of Early-Stage Cerebral Organoids Models Brain Tumor Invasion, SLAS Discov. Adv. Life Sci. R D. 23 (2018) 862–868. https://doi.org/10.1177/2472555218764623.

[208] R. Sivakumar, M. Chan, J.S. Shin, N. Nishida-Aoki, H.L. Kenerson, O. Elemento, H. Beltran, R. Yeung, T.S. Gujral, Organotypic tumor slice cultures provide a versatile platform for immuno-oncology and drug discovery, Oncoimmunology. 8 (2019). https://doi.org/10.1080/2162402X.2019.1670019.

[209] Y. Liu, F. Lang, X. Xie, S. Prabhu, J. Xu, D. Sampath, K. Aldape, G. Fuller, V.K. Puduvalli, Efficacy of adenovirally expressed soluble TRAIL in human glioma organotypic slice culture and glioma xenografts, Cell Death Dis. 2011 22. 2 (2011) e121–e121. https://doi.org/10.1038/cddis.2010.95.

[210] J. V. van Asperen, E.J. van Bodegraven, P.A.J.T. Robe, E.M. Hol, Determining glioma cell invasion and proliferation in ex vivo organotypic mouse brain slices using whole-mount immunostaining and tissue clearing, STAR Protoc. 3 (2022). https://doi.org/10.1016/J.XPRO.2022.101703.

[211] M. Sliwa, D. Markovic, K. Gabrusiewicz, M. Synowitz, R. Glass, M. Zawadzka, A. Wesolowska, H. Kettenmann, B. Kaminska, The invasion promoting effect of microglia on glioblastoma cells is inhibited by cyclosporin A, Brain. 130 (2007) 476–489. https://doi.org/10.1093/BRAIN/AWL263.

[212] E.R. Shamir, A.J. Ewald, Three-dimensional organotypic culture: experimental models of mammalian biology and disease, Nat. Rev. Mol. Cell Biol. 2014 1510. 15 (2014) 647–664. https://doi.org/10.1038/nrm3873.

[213] R. Timmerman, S.M. Burm, J.J. Bajramovic, An overview of in vitro methods to study microglia, Front. Cell. Neurosci. 12 (2018) 242. https://doi.org/10.3389/fncel.2018.00242.

[214] N. Janabi, S. Peudenier, B. Héron, K.H. Ng, M. Tardieu, Establishment of human microglial cell lines after transfection of primary cultures of embryonic microglial cells with the SV40 large T antigen, Neurosci. Lett. 195 (1995) 105–108. https://doi.org/10.1016/0304-3940(94)11792-H.

[215] C. Dello Russo, N. Cappoli, I. Coletta, D. Mezzogori, F. Paciello, G. Pozzoli, P. Navarra, A. Battaglia, The human microglial HMC3 cell line: where do we stand? A systematic literature review, J. Neuroinflammation 2018 151. 15 (2018) 1–24. https://doi.org/10.1186/S12974-018-1288-0.

[216] Y. Garcia-Mesa, T.R. Jay, M.A. Checkley, B. Luttge, C. Dobrowolski, S. Valadkhan, G.E. Landreth, J. Karn, D. Alvarez-Carbonell, Immortalization of primary microglia: a new platform to study HIV regulation in the central nervous system, J. Neurovirol. 23 (2017) 47–66. https://doi.org/10.1007/S13365-016-0499-3.

[217] P.S. Crooke Iii, J.T. Tossberg, R.M. Heinrich, K.P. Porter, T.M. Aune, Reduced RNA adenosine-to-inosine editing in hippocampus vasculature associated with Alzheimer's disease, Brain Commun. 4 (2022). https://doi.org/10.1093/BRAINCOMMS/FCAC238.

[218] J. Linder, S.E. Koplik, A. Kundaje, G. Seelig, Deciphering the impact of genetic variation on human polyadenylation using APARENT2, Genome Biol. 23 (2022) 1–33. https://doi.org/10.1186/s13059-022-02799-4.

[219] L. Germelli, E. Da Pozzo, C. Giacomelli, C. Tremolanti, L. Marchetti, C.H. Wetzel, E. Barresi, S. Taliani, F. Da Settimo, C. Martini, B. Costa, De novo Neurosteroidogenesis in Human Microglia: Involvement of the 18 kDa Translocator Protein, Int. J. Mol. Sci. 2021, Vol. 22, Page 3115. 22 (2021) 3115. https://doi.org/10.3390/IJMS22063115.

[220] R.L. Davis, D.J. Buck, K. McCracken, G.W. Cox, S. Das, Interleukin-1β-induced inflammatory signaling in C20 human microglial cells, Neuroimmunol. Neuroinflammation. 2018 (2018) 50–61. https://doi.org/10.20517/2347-8659.2018.60.

[221] M.A. Rai, J. Hammonds, M. Pujato, C. Mayhew, K. Roskin, P. Spearman, Comparative analysis of human microglial models for studies of HIV replication and pathogenesis, Retrovirology. 17 (2020) 1–21. https://doi.org/10.1186/s12977-020-00544-y.

[222] A. Frattini, M. Fabbri, R. Valli, E. De Paoli, G. Montalbano, L. Gribaldo, F. Pasquali, E. Maserati, High variability of genomic instability and gene expression profiling in different HeLa clones, Sci. Reports 2015 51. 5 (2015) 1–9. https://doi.org/10.1038/srep15377.

[223] M. Ohgidani, T.A. Kato, D. Setoyama, N. Sagata, R. Hashimoto, K. Shigenobu, T. Yoshida, K. Hayakawa, N. Shimokawa, D. Miura, H. Utsumi, S. Kanba, Direct induction of ramified microglia-like cells from human monocytes: Dynamic microglial dysfunction in Nasu-Hakola disease, Sci. Reports 2014 41. 4 (2014) 1–7. https://doi.org/10.1038/srep04957.

[224] P.R. Ormel, C. Böttcher, F.A.J. Gigase, R.D. Missall, W. van Zuiden, M.C. Fernández Zapata, D. Ilhan, M. de Goeij, E. Udine, I.E.C. Sommer, J. Priller, T. Raj, R.S. Kahn, E.M. Hol, L.D. de Witte, A characterization of the molecular phenotype and inflammatory response of schizophrenia patient-derived microglia-like cells, Brain. Behav. Immun. 90 (2020) 196–207. https://doi.org/10.1016/J.BBI.2020.08.012.

[225] Y. Liang, D.Y.W. Lee, S. Zhen, H. Sun, B. Zhu, J. Liu, D. Lei, C.C.J. Lin, S. Zhang, N.A. Jacques, L. Quinti, C. Ran, C. Wang, A. Griciuc, S.H. Choi, R.H. Dai, T. Efferth, R.E. Tanzi, C. Zhang, Natural medicine HLXL targets multiple pathways of amyloid-mediated neuroinflammation and immune response in treating alzheimer's disease, Phytomedicine. 104 (2022) 154158. https://doi.org/10.1016/J.PHYMED.2022.154158.

[226] S.W. Chen, Y.S. Hung, J.L. Fuh, N.J. Chen, Y.S. Chu, S.C. Chen, M.J. Fann, Y.H. Wong, Efficient conversion of human induced pluripotent stem cells into microglia by defined transcription factors, Stem Cell Reports. 16 (2021) 1363–1380. https://doi.org/10.1016/j.stemcr.2021.03.010.

[227] A.M. Smith, M. Dragunow, The human side of microglia, Trends Neurosci. 37 (2014) 125–135. https://doi.org/10.1016/J.TINS.2013.12.001.

[228] L.R. Watkins, M.R. Hutchinson, A concern on comparing “apples” and “oranges” when differences between microglia used in human and rodent studies go far, far beyond simply species: Comment on Smith and Dragunow, Trends Neurosci. 37 (2014) 189–190. https://doi.org/10.1016/j.tins.2014.02.004.

[229] M.R. Mizee, S.S. M Miedema, M. van der Poel, K.G. Schuurman, M.E. van Strien, J. Melief, J. Smolders, D.A. Hendrickx, K.M. Heutinck, J. Hamann, I. Huitinga, Isolation of primary microglia from the human post-mortem brain: effects of ante-and post-mortem variables, (n.d.). https://doi.org/10.1186/s40478-017-0418-8.

[230] M. Tang, Q. Xie, R.C. Gimple, Z. Zhong, T. Tam, J. Tian, R.L. Kidwell, Q. Wu, B.C. Prager, Z. Qiu, A. Yu, Z. Zhu, P. Mesci, H. Jing, J. Schimelman, P. Wang, D. Lee, M.H. Lorenzini, D. Dixit, L. Zhao, S. Bhargava, T.E. Miller, X. Wan, J. Tang, B. Sun, B.F. Cravatt, A.R. Muotri, S. Chen, J.N. Rich, Three-dimensional bioprinted glioblastoma microenvironments model cellular dependencies and immune interactions, Cell Res. 30 (2020) 833–853. https://doi.org/10.1038/s41422-020-0338-1.

[231] M. Kvisten, V.E. Mikkelsen, A.L. Stensjøen, O. Solheim, J. Van Der Want, S.H. Torp, Microglia and macrophages in human glioblastomas: A morphological and immunohistochemical study, Mol. Clin. Oncol. 11 (2019) 31–36. https://doi.org/10.3892/MCO.2019.1856.

[232] D.M. Leite, B. Zvar Baskovic, P. Civita, C. Neto, M. Gumbleton, G.J. Pilkington, A human co-culture cell model incorporating microglia supports glioblastoma growth and migration, and confers resistance to cytotoxics, FASEB J. 34 (2020) 1710–1727. https://doi.org/10.1096/fj.201901858RR.

[233] J.W.E. Chen, J. Lumibao, S. Leary, J.N. Sarkaria, A.J. Steelman, H.R. Gaskins, B.A.C. Harley, Crosstalk between microglia and patient-derived glioblastoma cells inhibit invasion in a three-dimensional gelatin hydrogel model, J. Neuroinflammation. 17 (2020) 1–15. https://doi.org/10.1186/s12974-020-02026-6.

[234] E. Yeini, P. Ofek, S. Pozzi, N. Albeck, D. Ben-Shushan, G. Tiram, S. Golan, R. Kleiner, R. Sheinin, S. Israeli Dangoor, S. Reich-Zeliger, R. Grossman, Z. Ram, H. Brem, T.M. Hyde, P. Magod, D. Friedmann-Morvinski, A. Madi, R. Satchi-Fainaro, P-selectin axis plays a key role in microglia immunophenotype and glioblastoma progression, Nat. Commun. 12 (2021) 1–22. https://doi.org/10.1038/s41467-021-22186-0.

[235] J. ichi Kuratsu, E.J. Leonard, T. Yoshimura, Production and characterization of human glioma cell-derived monocyte chemotactic factor, J. Natl. Cancer Inst. 81 (1989) 347–351. https://doi.org/10.1093/JNCI/81.5.347.

[236] L. Neufeld, E. Yeini, N. Reisman, Y. Shtilerman, D. Ben-Shushan, S. Pozzi, A. Madi, G. Tiram, A. Eldar-Boock, S. Ferber, R. Grossman, Z. Ram, R. Satchi-Fainaro, Microengineered perfusable 3D-bioprinted glioblastoma model for in vivo mimicry of tumor microenvironment, Sci. Adv. 7 (2021) 9119–9137. https://doi.org/10.1126/SCIADV.ABI9119.

[237] H.G. Yi, Y.H. Jeong, Y. Kim, Y.J. Choi, H.E. Moon, S.H. Park, K.S. Kang, M. Bae, J. Jang, H. Youn, S.H. Paek, D.W. Cho, A bioprinted human-glioblastoma-on-a-chip for the identification of patient-specific responses to chemoradiotherapy, Nat. Biomed. Eng. 3 (2019) 509–519. https://doi.org/10.1038/s41551-019-0363-x.

[238] D.M. Leite, B. Zvar Baskovic, P. Civita, C. Neto, M. Gumbleton, G.J. Pilkington, A human co-culture cell model incorporating microglia supports glioblastoma growth and migration, and confers resistance to cytotoxics, FASEB J. 34 (2020) 1710–1727.

https://doi.org/10.1096/FJ.201901858RR.

[239] D. Hanahan, R.A. Weinberg, Hallmarks of cancer: The next generation, Cell. 144 (2011) 646–674. https://doi.org/10.1016/j.cell.2011.02.013.

[240] D. Simão, M.M. Silva, A.P. Terrasso, F. Arez, M.F.Q. Sousa, N.Z. Mehrjardi, T. Šarić, P. Gomes-Alves, N. Raimundo, P.M. Alves, C. Brito, Recapitulation of Human Neural Microenvironment Signatures in iPSC-Derived NPC 3D Differentiation, Stem Cell Reports. 11 (2018) 552. https://doi.org/10.1016/J.STEMCR.2018.06.020.

[241] J.A. Hickman, R. Graeser, R. de Hoogt, S. Vidic, C. Brito, M. Gutekunst, H. van der Kuip, Imi Predect consortium, Three-dimensional models of cancer for pharmacology and cancer cell biology: Capturing tumor complexity in vitro/ex vivo, Biotechnol. J. 9 (2014) 1115–1128. https://doi.org/10.1002/biot.201300492.

[242] H.S. Phillips, S. Kharbanda, R. Chen, W.F. Forrest, R.H. Soriano, T.D. Wu, A. Misra, J.M. Nigro, H. Colman, L. Soroceanu, P.M. Williams, Z. Modrusan, B.G. Feuerstein, K. Aldape, Molecular subclasses of high-grade glioma predict prognosis, delineate a pattern of disease progression, and resemble stages in neurogenesis, Cancer Cell. 9 (2006) 157–173. https://doi.org/10.1016/J.CCR.2006.02.019.

[243] X. Lv, J. Sun, L. Hu, Y. Qian, C. Fan, N. Tian, Curcumol inhibits malignant biological behaviors and TMZ-resistance in glioma cells by inhibiting long noncoding RNA FOXD2-As1-promoted EZH2 activation, Aging (Albany. NY). 13 (2021) 24101–24116. https://doi.org/10.18632/aging.203662.

[244] C. Ke, K. Tran, Y. Chen, A.T. di Donato, L. Yu, Y. Hu, M.E. Linskey, P.H. Wang, C.L. Limoli, Y.H. Zhou, Linking differential radiation responses to glioma heterogeneity, Oncotarget. 5 (2014) 1657. https://doi.org/10.18632/ONCOTARGET.1823.

[245] F. Pinto, Â.M. Costa, R.P. Andrade, R.M. Reis, Brachyury Is Associated with Glioma Differentiation and Response to Temozolomide, Neurotherapeutics. 17 (2020) 2015. https://doi.org/10.1007/S13311-020-00911-9.

[246] K. Rolón-Reyes, Y. V. Kucheryavykh, L.A. Cubano, M. Inyushin, S.N. Skatchkov, M.J. Eaton, J.K. Harrison, L.Y. Kucheryavykh, Microglia Activate Migration of Glioma Cells through a Pyk2 Intracellular Pathway, PLoS One. 10 (2015). https://doi.org/10.1371/JOURNAL.PONE.0131059.

[247] J. Li, Y. Sun, X. Sun, X. Zhao, Y. Ma, Y. Wang, X. Zhang, AEG-1 silencing attenuates M2-polarization of glioma-associated microglia/macrophages and sensitizes glioma cells to temozolomide, Sci. Reports 2021 111. 11 (2021) 1–12. https://doi.org/10.1038/s41598-021-96647-3.

[248] H. Gal, A. Makovitzki, N. Amariglio, G. Rechavi, Z. Ram, D. Givol, A rapid assay for drug sensitivity of glioblastoma stem cells, Biochem. Biophys. Res. Commun. 358 (2007) 908–913. https://doi.org/10.1016/J.BBRC.2007.05.020.

[249] Y. Manome, S. Mizuno, N. Akiyama, K. Fujioka, H. Saito, Y. Hataba, T. Kobayashi, M. Watanabe, Three-dimensional cell culture of glioma and morphological comparison of four different human cell lines, Anticancer Res. 30 (2010) 383–389.

[250] V.E. Santo, M.F. Estrada, S.P. Rebelo, S. Abreu, I. Silva, C. Pinto, S.C. Veloso, A.T. Serra, E. Boghaert, P.M. Alves, C. Brito, Adaptable stirred-tank culture strategies for large scale production of multicellular spheroid-based tumor cell models, J. Biotechnol. 221 (2016) 118–129. https://doi.org/10.1016/j.jbiotec.2016.01.031.

[251] S.P. Rebelo, C. Pinto, T.R. Martins, N. Harrer, M.F. Estrada, P. Loza-Alvarez, J. Cabeçadas, P.M. Alves, E.J. Gualda, W. Sommergruber, C. Brito, 3D-3-culture: A tool to unveil macrophage plasticity in the tumour microenvironment, Biomaterials. 163 (2018) 185–197. https://doi.org/10.1016/j.biomaterials.2018.02.030.

[252] X. Lv, J. Sun, L. Hu, Y. Qian, C. Fan, N. Tian, Curcumol inhibits malignant biological behaviors and TMZ-resistance in glioma cells by inhibiting long noncoding RNA FOXD2-As1-promoted EZH2 activation, Aging (Albany NY). 13 (2021) 24101.

https://doi.org/10.18632/AGING.203662.

[253] F. De Chaumont, S. Dallongeville, N. Chenouard, N. Hervé, S. Pop, T. Provoost, V. Meas-Yedid, P. Pankajakshan, T. Lecomte, Y. Le Montagner, T. Lagache, A. Dufour, J.C. Olivo-Marin, Icy: An open bioimage informatics platform for extended reproducible research, Nat. Methods. 9 (2012) 690–696. https://doi.org/10.1038/NMETH.2075.

[254] J. Schindelin, I. Arganda-Carreras, E. Frise, V. Kaynig, M. Longair, T. Pietzsch, S. Preibisch, C. Rueden, S. Saalfeld, B. Schmid, J.Y. Tinevez, D.J. White, V. Hartenstein, K. Eliceiri, P. Tomancak, A. Cardona, Fiji: an open-source platform for biological-image analysis, Nat. Methods 2012 97. 9 (2012) 676–682. https://doi.org/10.1038/nmeth.2019.

[255] K.J. Livak, T.D. Schmittgen, Analysis of relative gene expression data using real-time quantitative PCR and the 2(-Delta Delta C(T)) Method, Methods. 25 (2001) 402–408. https://doi.org/10.1006/METH.2001.1262.

[256] J. Leyh, S. Paeschke, B. Mages, D. Michalski, M. Nowicki, I. Bechmann, K. Winter, Classification of Microglial Morphological Phenotypes Using Machine Learning, Front. Cell. Neurosci. 15 (2021). https://doi.org/10.3389/fncel.2021.701673.

[257] C.J.A. De Groot, L. Montagne, I. Janssen, R. Ravid, P. Van Der Valk, R. Veerhuis, Isolation and characterization of adult microglial cells and oligodendrocytes derived from postmortem human brain tissue, Brain Res. Protoc. 5 (2000) 85–94. https://doi.org/10.1016/S1385-299X(99)00059-8.

[258] M. del M. Fernández-Arjona, J.M. Grondona, P. Granados-Durán, P. Fernández-Llebrez, M.D. López-Ávalos, Microglia morphological categorization in a rat model of neuroinflammation by hierarchical cluster and principal components analysis, Front. Cell. Neurosci. 11 (2017) 235. https://doi.org/10.3389/FNCEL.2017.00235/BIBTEX.

[259] Y. Yao, K.Y. Fu, Serum-deprivation leads to activation-like changes in primary microglia and BV-2 cells but not astrocytes, Biomed. Reports. 13 (2020) 1–8. https://doi.org/10.3892/br.2020.1358.

[260] H.S. Lee, S.J. Stachelek, N. Tomczyk, M.J. Finley, R.J. Composto, D.M. Eckmann, Correlating macrophage morphology and cytokine production resulting from biomaterial contact, J. Biomed. Mater. Res. A. 101 (2013) 203. https://doi.org/10.1002/JBM.A.34309.

[261] M. Bouvet, A. Turkieh, A.E. Acosta-Martin, M. Chwastyniak, O. Beseme, P. Amouyel, F. Pinet, Proteomic profiling of macrophages by 2D electrophoresis, J. Vis. Exp. 93 (2014) 1–7. https://doi.org/10.3791/52219.

[262] K. Weigelt, W. Ernst, Y. Walczak, S. Ebert, T. Loenhardt, M. Klug, M. Rehli, B.H.F. Weber, T. Langmann, Dap12 expression in activated microglia from retinoschisin-deficient retina and its PU.1-dependent promoter regulation, J. Leukoc. Biol. 82 (2007) 1564–1574. https://doi.org/10.1189/JLB.0707447.

[263] Y. Sasaki, K. Ohsawa, H. Kanazawa, S. Kohsaka, Y. Imai, Iba1 Is an Actin-Cross-Linking Protein in Macrophages/Microglia, Biochem. Biophys. Res. Commun. 286 (2001) 292–297. https://doi.org/10.1006/BBRC.2001.5388.

[264] R.L. Davis, D.J. Buck, K. McCracken, G.W. Cox, S. Das, Interleukin-1β-induced inflammatory signaling in C20 human microglial cells, Neuroimmunol. Neuroinflammation. 2018 (2018) 50–61. https://doi.org/10.20517/2347-8659.2018.60.

[265] M.B. Graeber, W. Li, M.L. Rodriguez, Role of microglia in CNS inflammation, FEBS Lett. 585 (2011) 3798–3805. https://doi.org/10.1016/J.FEBSLET.2011.08.033.

[266] S. David, A. Kroner, A.D. Greenhalgh, J.G. Zarruk, R. López-Vales, Myeloid cell responses after spinal cord injury, J. Neuroimmunol. 321 (2018) 97–108. https://doi.org/10.1016/J.JNEUROIM.2018.06.003.

[267] L. Wieczorek, B.K. Brown, C. DelSarto Macedo, M. Wesberry-Schmierer, V. Ngauy, A. Rosa Borges, N.L. Michael, M.A. Marovich, D.C. Montefiori, V.R. Polonis, Mitigation of variation observed in a peripheral blood mononuclear cell (PBMC) based HIV-1

neutralization assay by donor cell pooling, Virology. 447 (2013) 240–248. https://doi.org/10.1016/J.VIROL.2013.09.014.

[268] N. Ketterl, G. Brachtl, C. Schuh, K. Bieback, K. Schallmoser, A. Reinisch, D. Strunk, A robust potency assay highlights significant donor variation of human mesenchymal stem/progenitor cell immune modulatory capacity and extended radio-resistance, Stem Cell Res. Ther. 6 (2015) 1–11. https://doi.org/10.1186/s13287-015-0233-8.

[269] M.C. Nielsen, M.N. Andersen, H.J. Møller, Monocyte isolation techniques significantly impact the phenotype of both isolated monocytes and derived macrophages in vitro, Immunology. 159 (2020) 63–74. https://doi.org/10.1111/imm.13125.

[270] M.L. Bennett, F.C. Bennett, S.A. Liddelow, B. Ajami, J.L. Zamanian, N.B. Fernhoff, S.B. Mulinyawe, C.J. Bohlen, A. Adil, A. Tucker, I.L. Weissman, E.F. Chang, G. Li, G.A. Grant, M.G. Hayden Gephart, B.A. Barres, New tools for studying microglia in the mouse and human CNS, Proc. Natl. Acad. Sci. U. S. A. 113 (2016) E1738–E1746. https://doi.org/10.1073/pnas.1525528113.

[271] O. Butovsky, M.P. Jedrychowski, C.S. Moore, R. Cialic, A.J. Lanser, G. Gabriely, T. Koeglsperger, B. Dake, P.M. Wu, C.E. Doykan, Z. Fanek, L. Liu, Z. Chen, J.D. Rothstein, R.M. Ransohoff, S.P. Gygi, J.P. Antel, H.L. Weiner, Identification of a unique TGF-β–dependent molecular and functional signature in microglia, Nat. Neurosci. 2013 171. 17 (2013) 131–143. https://doi.org/10.1038/nn.3599.

[272] L.M. Healy, G. Perron, S.Y. Won, V.T.S. Rao, M.C. Guiot, C. Moore, A. Bar-Or, J.P. Antel, Differential transcriptional response profiles in human myeloid cell populations, Clin. Immunol. 189 (2018) 63–74. https://doi.org/10.1016/J.CLIM.2016.04.006.

[273] S.E. Hickman, N.D. Kingery, T.K. Ohsumi, M.L. Borowsky, L.C. Wang, T.K. Means, J. El Khoury, The microglial sensome revealed by direct RNA sequencing, Nat. Neurosci. 2013 1612. 16 (2013) 1896–1905. https://doi.org/10.1038/nn.3554.

[274] S. Brandenburg, A. Blank, A.D. Bungert, P. Vajkoczy, Distinction of microglia and macrophages in glioblastoma: Close relatives, different tasks?, Int. J. Mol. Sci. 22 (2021) 1–17. https://doi.org/10.3390/IJMS22010194.

[275] Y. Guo, P. Xiao, S. Lei, F. Deng, G.G. Xiao, Y. Liu, X. Chen, L. Li, S. Wu, Y. Chen, H. Jiang, L. Tan, J. Xie, X. Zhu, S. Liang, H. Deng, How is mRNA expression predictive for protein expression? A correlation study on human circulating monocytes, Acta Biochim. Biophys. Sin. (Shanghai). 40 (2008) 426–436. https://doi.org/10.1111/J.1745-7270.2008.00418.X.

[276] S. V. Kushchayev, T. Sankar, L.L. Eggink, Y.S. Kushchayeva, P.C. Wiener, J. Kenneth Hoober, J. Eschbacher, R. Liu, F.D. Shi, M.G. Abdelwahab, A.C. Scheck, M.C. Preul, Monocyte galactose/N-acetylgalactosamine-specific C-type lectin receptor stimulant immunotherapy of an experimental glioma. Part 1: Stimulatory effects on blood monocytes and monocyte-derived cells of the brain, Cancer Manag. Res. 4 (2012) 309–323. https://doi.org/10.2147/CMAR.S33248.

[277] T. Veremeyko, S.C. Starossom, H.L. Weiner, E.D. Ponomarev, Detection of microRNAs in microglia by real-time PCR in normal CNS and during neuroinflammation., J. Vis. Exp. 65 (2012) 1–22. https://doi.org/10.3791/4097.

[278] J.W. Ashley, Z. Shi, H. Zhao, X. Li, R.A. Kesterson, X. Feng, Genetic Ablation of CD68 Results in Mice with Increased Bone and Dysfunctional Osteoclasts, PLoS One. 6 (2011) e25838. https://doi.org/10.1371/JOURNAL.PONE.0025838.

[279] R.P. Da Silva, S. Gordon, Phagocytosis stimulates alternative glycosylation of macrosialin (mouse CD68), a macrophage-specific endosomal protein, Biochem. J. 338 (1999) 687–694. https://doi.org/10.1042/0264-6021:3380687.

[280] H.J. An, J.W. Froehlich, C.B. Lebrilla, Determination of Glycosylation Sites and Site-specific Heterogeneity in Glycoproteins, Curr. Opin. Chem. Biol. 13 (2009) 421. https://doi.org/10.1016/J.CBPA.2009.07.022.

[281] D.G. Walker, L.F. Lue, Immune phenotypes of microglia in human neurodegenerative disease: Challenges to detecting microglial polarization in human brains, Alzheimer's Res. Ther. 7 (2015) 1–9. https://doi.org/10.1186/s13195-015-0139-9.

[282] J. Hou, Y. Chen, G. Grajales-Reyes, M. Colonna, TREM2 dependent and independent functions of microglia in Alzheimer's disease, Mol. Neurodegener. 2022 171. 17 (2022) 1–19. https://doi.org/10.1186/S13024-022-00588-Y.

[283] T.H. Do, F. Ma, P.R. Andrade, R. Teles, B.J. de Andrade Silva, C. Hu, A. Espinoza, J.E. Hsu, C.S. Cho, M. Kim, J. Xi, X. Xing, O. Plazyo, L.C. Tsoi, C. Cheng, J. Kim, B.D. Bryson, A.M. O'Neill, M. Colonna, J.E. Gudjonsson, E. Klechevsky, J.H. Lee, R.L. Gallo, B.R. Bloom, M. Pellegrini, R.L. Modlin, TREM2 macrophages induced by human lipids drive inflammation in acne lesions, Sci. Immunol. 7 (2022) eabo2787. https://doi.org/10.1126/sciimmunol.abo2787.

[284] M. Binnewies, J.L. Pollack, J. Rudolph, S. Dash, M. Abushawish, T. Lee, N.S. Jahchan, P. Canaday, E. Lu, M. Norng, S. Mankikar, V.M. Liu, X. Du, A. Chen, R. Mehta, R. Palmer, V. Juric, L. Liang, K.P. Baker, L. Reyno, M.F. Krummel, M. Streuli, V. Sriram, Targeting TREM2 on tumor-associated macrophages enhances immunotherapy, Cell Rep. 37 (2021) 109844. https://doi.org/10.1016/j.celrep.2021.109844.

[285] P.W. Brownjohn, J. Smith, R. Solanki, E. Lohmann, H. Houlden, J. Hardy, S. Dietmann, F.J. Livesey, Functional Studies of Missense TREM2 Mutations in Human Stem Cell-Derived Microglia, Stem Cell Reports. 10 (2018) 1294–1307. https://doi.org/10.1016/J.STEMCR.2018.03.003.

[286] M. Reich, I. Paris, M. Ebeling, N. Dahm, C. Schweitzer, D. Reinhardt, R. Schmucki, M. Prasad, F. Köchl, M. Leist, S.A. Cowley, J.D. Zhang, C. Patsch, S. Gutbier, M. Britschgi, Alzheimer's Risk Gene TREM2 Determines Functional Properties of New Type of Human iPSC-Derived Microglia, Front. Immunol. 11 (2021) 3918. https://doi.org/10.3389/fimmu.2020.617860.

[287] M.R. Stampfer, A. Bodnar, J. Garbe, M. Wong, A. Pan, B. Villeponteau, P. Yaswen, Gradual Phenotypic Conversion Associated with Immortalization of Cultured Human Mammary Epithelial Cells, Mol. Biol. Cell. 8 (1997) 2391. https://doi.org/10.1091/MBC.8.12.2391.

[288] D. Ahuja, M.T. Sáenz-Robles, J.M. Pipas, SV40 large T antigen targets multiple cellular pathways to elicit cellular transformation, Oncogene. 24 (2005) 7729–7745. https://doi.org/10.1038/SJ.ONC.1209046.

[289] Y. Yao, X.H. Xu, L. Jin, Macrophage polarization in physiological and pathological pregnancy, Front. Immunol. 10 (2019) 792. https://doi.org/10.3389/fimmu.2019.00792.

[290] Y.C. Lu, W.C. Yeh, P.S. Ohashi, LPS/TLR4 signal transduction pathway, Cytokine. 42 (2008) 145–151. https://doi.org/10.1016/J.CYTO.2008.01.006.

[291] K. Badanjak, P. Mulica, S. Smajic, S. Delcambre, L.C. Tranchevent, N. Diederich, T. Rauen, J.C. Schwamborn, E. Glaab, S.A. Cowley, P.M.A. Antony, S.L. Pereira, C. Venegas, A. Grünewald, iPSC-Derived Microglia as a Model to Study Inflammation in Idiopathic Parkinson's Disease, Front. Cell Dev. Biol. 9 (2021) 3037. https://doi.org/10.3389/fcell.2021.740758.

[292] A. Grubman, T.H. Vandekolk, J. Schröder, G. Sun, J. Hatwell-Humble, J. Chan, M. Oksanen, S. Lehtonen, C. Hunt, J.E. Koistinaho, S.K. Nilsson, J.M. Haynes, C.W. Pouton, J.M. Polo, A CX3CR1 Reporter hESC Line Facilitates Integrative Analysis of In-Vitro-Derived Microglia and Improved Microglia Identity upon Neuron-Glia Co-culture, Stem Cell Reports. 14 (2020) 1018–1032. https://doi.org/10.1016/J.STEMCR.2020.04.007.

[293] V. Bezold, P. Rosenstock, J. Scheffler, H. Geyer, R. Horstkorte, K. Bork, Glycation of macrophages induces expression of pro-inflammatory cytokines and reduces phagocytic efficiency, Aging (Albany. NY). 11 (2019) 5258–5275. https://doi.org/10.18632/AGING.102123.

[294] M.F. Estrada, S.P. Rebelo, E.J. Davies, M.T. Pinto, H. Pereira, V.E. Santo, M.J. Smalley, S.T. Barry, E.J. Gualda, P.M. Alves, E. Anderson, C. Brito, Modelling the tumour microenvironment in long-term microencapsulated 3D co-cultures recapitulates phenotypic features of disease progression, Biomaterials. 78 (2016) 50–61. https://doi.org/10.1016/J.BIOMATERIALS.2015.11.030.

[295] S.D. Jayasingam, M. Citartan, T.H. Thang, A.A. Mat Zin, K.C. Ang, E.S. Ch'ng, Evaluating the Polarization of Tumor-Associated Macrophages Into M1 and M2 Phenotypes in Human Cancer Tissue: Technicalities and Challenges in Routine Clinical Practice, Front. Oncol. 9 (2020) 1512. https://doi.org/10.3389/fonc.2019.01512.

[296] J. Oh, A.E. Riek, S. Weng, M. Petty, D. Kim, M. Colonna, M. Cella, C. Bernal-Mizrachi, Endoplasmic reticulum stress controls M2 macrophage differentiation and foam cell formation, J. Biol. Chem. 287 (2012) 11629–11641. https://doi.org/10.1074/JBC.M111.338673.

[297] D.U. Purcu, A. Korkmaz, S. Gunalp, D.G. Helvaci, Y. Erdal, Y. Dogan, A. Suner, G. Wingender, D. Sag, Effect of stimulation time on the expression of human macrophage polarization markers, PLoS One. 17 (2022) e0265196. https://doi.org/10.1371/JOURNAL.PONE.0265196.

[298] A. Banerjee, Y. Lu, K. Do, T. Mize, X. Wu, X. Chen, J. Chen, Validation of Induced Microglia-Like Cells (iMG Cells) for Future Studies of Brain Diseases, Front. Cell. Neurosci. 15 (2021) 85. https://doi.org/10.3389/FNCEL.2021.629279/BIBTEX.

[299] B. Spittau, N. Dokalis, M. Prinz, The Role of TGFβ Signaling in Microglia Maturation and Activation, Trends Immunol. 41 (2020) 836–848. https://doi.org/10.1016/J.IT.2020.07.003.

[300] C. Böttcher, S. Schlickeiser, M.A.M. Sneeboer, D. Kunkel, A. Knop, E. Paza, P. Fidzinski, L. Kraus, G.J.L. Snijders, R.S. Kahn, A.R. Schulz, H.E. Mei, E.M. Hol, B. Siegmund, R. Glauben, E.J. Spruth, L.D. de Witte, J. Priller, Human microglia regional heterogeneity and phenotypes determined by multiplexed single-cell mass cytometry, Nat. Neurosci. 2018 221. 22 (2018) 78–90. https://doi.org/10.1038/s41593-018-0290-2.

[301] M.P. Marzolo, R. Von Bernhardi, N.C. Inestrosa, Mannose receptor is present in a functional state in rat microglial cells, J. Neurosci. Res. 58 (1999) 387–395. https://doi.org/10.1002/(SICI)1097-4547(19991101)58:3<387::AID-JNR4>3.0.CO;2-L.

[302] V. Hübschmann, M. Korkut-Demirbaş, S. Siegert, Assessing human iPSC-derived microglia identity and function by immunostaining, phagocytosis, calcium activity, and inflammation assay, STAR Protoc. 3 (2022). https://doi.org/10.1016/J.XPRO.2022.101866.

[303] K. Duval, H. Grover, L.H. Han, Y. Mou, A.F. Pegoraro, J. Fredberg, Z. Chen, Modeling Physiological Events in 2D vs. 3D Cell Culture, Physiology (Bethesda). 32 (2017) 266–277. https://doi.org/10.1152/PHYSIOL.00036.2016.

[304] P. C. Jayakrishnan, E. H. Venkat, G. M. Ramachandran, K. K. Kesavapisharady, S. N. Nair, B. Bharathan, N. Radhakrishnan, S. Gopala, In vitro neurosphere formation correlates with poor survival in glioma, IUBMB Life. 71 (2019) 244–253. https://doi.org/10.1002/IUB.1964.

[305] A. Pisciotta, M. Riccio, G. Carnevale, F. Beretti, L. Gibellini, T. Maraldi, G.M. Cavallini, A. Ferrari, G. Bruzzesi, A. de Pol, Human Serum Promotes Osteogenic Differentiation of Human Dental Pulp Stem Cells In Vitro and In Vivo, PLoS One. 7 (2012) 10–17. https://doi.org/10.1371/JOURNAL.PONE.0050542.

[306] S. Fedoroff, C. Hall, Effect of horse serum on neural cell differentiation in tissue culture, In Vitro. 15 (1979) 641–648. https://doi.org/10.1007/BF02623400.

[307] Y. Duo, L. Na, Effect of serum concentrations on differentiation of adipose-derived stem cells into adipocytes, Chinese J. Tissue Eng. Res. 22 (2018) 2669–2673. https://doi.org/10.3969/J.ISSN.2095-4344.0518.

[308] S.S. Kim, K.F. Pirollo, E.H. Chang, Isolation and Culturing of Glioma Cancer Stem Cells,

Curr. Protoc. Cell Biol. 67 (2015) 23.10.1. https://doi.org/10.1002/0471143030.CB2310S67.

[309] M.A. Kinney, C.Y. Sargent, T.C. McDevitt, The multiparametric effects of hydrodynamic environments on stem cell culture, Tissue Eng. Part B. Rev. 17 (2011) 249–262. https://doi.org/10.1089/TEN.TEB.2011.0040.

[310] J.I. Heger, K. Froehlich, J. Pastuschek, A. Schmidt, C. Baer, R. Mrowka, C. Backsch, E. Schleußner, U.R. Markert, A. Schmidt, Human serum alters cell culture behavior and improves spheroid formation in comparison to fetal bovine serum, Exp. Cell Res. 365 (2018) 57–65. https://doi.org/10.1016/J.YEXCR.2018.02.017.

[311] Z. Tang, C. Li, B. Kang, G. Gao, C. Li, Z. Zhang, GEPIA: a web server for cancer and normal gene expression profiling and interactive analyses, Nucleic Acids Res. 45 (2017) W98–W102. https://doi.org/10.1093/NAR/GKX247.

[312] H. Lopez-Bertoni, A. Johnson, Y. Rui, B. Lal, S. Sall, M. Malloy, J.B. Coulter, M. Lugo-Fagundo, S. Shudir, H. Khela, C. Caputo, J.J. Green, J. Laterra, Sox2 induces glioblastoma cell stemness and tumor propagation by repressing TET2 and deregulating 5hmC and 5mC DNA modifications, Signal Transduct. Target. Ther. 2022 71. 7 (2022) 1–12. https://doi.org/10.1038/s41392-021-00857-0.

[313] W. Zhang, H. Chen, S. Lv, H. Yang, High CD133 Expression Is Associated with Worse Prognosis in Patients with Glioblastoma, Mol. Neurobiol. 53 (2016) 2354–2360. https://doi.org/10.1007/S12035-015-9187-1.

[314] Q. Wang, H. Wu, J. Hu, H. Fu, Y. Qu, Y. Yang, Q. Cai, A. Efimov, M. Wu, T. Yen, Y. Wang, Z.J. Yang, Nestin Is Required for Spindle Assembly and Cell-Cycle Progression in Glioblastoma Cells, Mol. Cancer Res. 19 (2021). https://doi.org/10.1158/1541-7786.MCR-20-0994.

[315] B. Polat, G. Wohlleben, R. Kosmala, D. Lisowski, F. Mantel, V. Lewitzki, M. Löhr, R. Blum, P. Herud, M. Flentje, C.M. Monoranu, Differences in stem cell marker and osteopontin expression in primary and recurrent glioblastoma, Cancer Cell Int. 22 (2022) 1–11. https://doi.org/10.1186/s12935-022-02510-4.

[316] S.H. Sahlberg, D. Spiegelberg, B. Glimelius, B. Stenerlöw, M. Nestor, Evaluation of Cancer Stem Cell Markers CD133, CD44, CD24: Association with AKT Isoforms and Radiation Resistance in Colon Cancer Cells, PLoS One. 9 (2014) e94621. https://doi.org/10.1371/JOURNAL.PONE.0094621.

[317] K. Dzobo, D. Senthebane, C. Ganz, N. Thomford, The Significance of Cancer Stem Cell Markers' Gene Expression and Relevance for Survival Outcomes, (2020). https://doi.org/10.20944/PREPRINTS202005.0047.V1.

[318] X. Shu, H. Liu, Y. Pan, L. Sun, L. Yu, L. Sun, Z. Yang, Y. Ran, Distinct biological characterization of the CD44 and CD90 phenotypes of cancer stem cells in gastric cancer cell lines, Mol. Cell. Biochem. 459 (2019) 35–47. https://doi.org/10.1007/S11010-019-03548-1.

[319] S. Karmakar, P. Seshacharyulu, I. Lakshmanan, A.P. Vaz, S. Chugh, Y.M. Sheinin, S. Mahapatra, S.K. Batra, M.P. Ponnusamy, hPaf1/PD2 interacts with OCT3/4 to promote self-renewal of ovarian cancer stem cells, Oncotarget. 8 (2017) 14806–14820. https://doi.org/10.18632/ONCOTARGET.14775.

[320] M. Kase, A. Minajeva, K. Niinepuu, S. Kase, M. Vardja, T. Asser, J. Jaal, Impact of CD133 positive stem cell proportion on survival in patients with glioblastoma multiforme, Radiol. Oncol. 47 (2013) 405–410. https://doi.org/10.2478/RAON-2013-0055.

[321] W. Zhou, S.Q. Ke, Z. Huang, W. Flavahan, X. Fang, J. Paul, L. Wu, A.E. Sloan, R.E. McLendon, X. Li, J.N. Rich, S. Bao, Periostin secreted by glioblastoma stem cells recruits M2 tumour-associated macrophages and promotes malignant growth, Nat. Cell Biol. 17 (2015) 170–182. https://doi.org/10.1038/ncb3090.

[322] V. Lamour, A. Henry, J. Kroonen, M.J. Nokin, Z. Von Marschall, L.W. Fisher, T.L. Chau,

A. Chariot, M. Sanson, J.Y. Delattre, A. Turtoi, O. Peulen, B. Rogister, V. Castronovo, A. Bellahcène, Targeting osteopontin suppresses glioblastoma stem-like cell character and tumorigenicity in vivo, Int. J. Cancer. 137 (2015) 1047–1057. https://doi.org/10.1002/IJC.29454.

[323] H. Lopez-Bertoni, B. Lal, A. Li, M. Caplan, H. Guerrero-Cázares, C.G. Eberhart, A. Quiñones-Hinojosa, M. Glas, B. Scheffler, J. Laterra, Y. Li, DNMT-dependent suppression of microRNA regulates the induction of GBM tumor-propagating phenotype by Oct4 and Sox2, Oncogene. 34 (2015) 3994. https://doi.org/10.1038/ONC.2014.334.

[324] W. Scheper, S. Copray, The Molecular Mechanism of Induced Pluripotency: A Two-Stage Switch, Stem Cell Rev. Reports 2009 53. 5 (2009) 204–223. https://doi.org/10.1007/S12015-009-9077-X.

[325] K. Takahashi, S. Yamanaka, Induction of Pluripotent Stem Cells from Mouse Embryonic and Adult Fibroblast Cultures by Defined Factors, Cell. 126 (2006) 663–676. https://doi.org/10.1016/j.cell.2006.07.024.

[326] L.A. Boyer, I.L. Tong, M.F. Cole, S.E. Johnstone, S.S. Levine, J.P. Zucker, M.G. Guenther, R.M. Kumar, H.L. Murray, R.G. Jenner, D.K. Gifford, D.A. Melton, R. Jaenisch, R.A. Young, Core transcriptional regulatory circuitry in human embryonic stem cells, Cell. 122 (2005) 947–956. https://doi.org/10.1016/J.CELL.2005.08.020.

[327] B.M. Simões, M. Piva, O. Iriondo, V. Comaills, J.A. López-Ruiz, I. Zabalza, J.A. Mieza, O. Acinas, M.D.M. Vivanco, Effects of estrogen on the proportion of stem cells in the breast, Breast Cancer Res. Treat. 129 (2011) 23–35. https://doi.org/10.1007/S10549-010-1169-4.

[328] M. Nakada, E. Nambu, N. Furuyama, Y. Yoshida, T. Takino, Y. Hayashi, H. Sato, Y. Sai, T. Tsuji, K.I. Miyamoto, A. Hirao, J.I. Hamada, Integrin α3 is overexpressed in glioma stem-like cells and promotes invasion, Br. J. Cancer 2013 10812. 108 (2013) 2516–2524. https://doi.org/10.1038/bjc.2013.218.

[329] S. Zhang, W. Cui, Sox2, a key factor in the regulation of pluripotency and neural differentiation, World J. Stem Cells. 6 (2014) 305. https://doi.org/10.4252/WJSC.V6.I3.305.

[330] B. Van Schaijik, P.F. Davis, A.C. Wickremesekera, S.T. Tan, T. Itinteang, Subcellular localisation of the stem cell markers OCT4, SOX2, NANOG, KLF4 and c-MYC in cancer: a review, J. Clin. Pathol. 71 (2018) 88–91. https://doi.org/10.1136/JCLINPATH-2017-204815.

[331] L. Huang, A. Holtzinger, I. Jagan, M. Begora, I. Lohse, N. Ngai, C. Nostro, R. Wang, L.B. Muthuswamy, H.C. Crawford, C. Arrowsmith, S.E. Kalloger, D.J. Renouf, A.A. Connor, S. Cleary, D.F. Schaeffer, M. Roehrl, M.S. Tsao, S. Gallinger, G. Keller, S.K. Muthuswamy, Ductal pancreatic cancer modeling and drug screening using human pluripotent stem cell–and patient-derived tumor organoids, Nat. Med. 2015 2111. 21 (2015) 1364–1371. https://doi.org/10.1038/nm.3973.

[332] P. Aldaz, N. Martín-martín, A. Saenz-antoñanzas, E. Carrasco-garcia, M. Álvarez-satta, A. Elúa-pinin, S.M. Pollard, C.H. Lawrie, M. Moreno-valladares, N. Samprón, J. Hench, R. Lovell-badge, A. Carracedo, A. Matheu, High SOX9 Maintains Glioma Stem Cell Activity through a Regulatory Loop Involving STAT3 and PML, Int. J. Mol. Sci. 23 (2022). https://doi.org/10.3390/IJMS23094511.

[333] S. Saigusa, K. Tanaka, Y. Toiyama, T. Yokoe, Y. Okugawa, Y. Ioue, C. Miki, M. Kusunoki, Correlation of CD133, OCT4, and SOX2 in rectal cancer and their association with distant recurrence after chemoradiotherapy, Ann. Surg. Oncol. 16 (2009) 3488–3498. https://doi.org/10.1245/S10434-009-0617-Z.

[334] D. Hussein, W. Punjaruk, L.C.D. Storer, L. Shaw, R. Ottoman, A. Peet, S. Miller, G. Bandopadhyay, R. Heath, R. Kumari, K.J. Bowman, P. Braker, R. Rahman, G.D.D. Jones, S. Watson, J. Lowe, I.D. Kerr, R.G. Grundy, B. Coyle, Pediatric brain tumor cancer stem cells: Cell cycle dynamics, DNA repair, and etoposide extrusion, Neuro. Oncol. 13 (2011)

70–83. https://doi.org/10.1093/NEUONC/NOQ144.

[335] G.A. Baltus, M.P. Kowalski, H. Zhai, A. V. Tutter, D. Quinn, D. Wall, S. Kadam, Acetylation of sox2 induces its nuclear export in embryonic stem cells, Stem Cells. 27 (2009) 2175–2184. https://doi.org/10.1002/STEM.168.

[336] P. Xia, S. Wang, B. Ye, Y. Du, G. Huang, P. Zhu, Z. Fan, Sox2 functions as a sequence-specific DNA sensor in neutrophils to initiate innate immunity against microbial infection, Nat. Immunol. 2015 164. 16 (2015) 366–375. https://doi.org/10.1038/ni.3117.

[337] L.T. Senbanjo, M.A. Chellaiah, CD44: A multifunctional cell surface adhesion receptor is a regulator of progression and metastasis of cancer cells, Front. Cell Dev. Biol. 5 (2017) 18. https://doi.org/10.3389/fcell.2017.00018.

[338] Y. Xiao, K. Yang, Z. Wang, M. Zhao, Y. Deng, W. Ji, Y. Zou, C. Qian, Y. Liu, H. Xiao, H. Liu, CD44-Mediated Poor Prognosis in Glioma Is Associated With M2-Polarization of Tumor-Associated Macrophages and Immunosuppression, Front. Surg. 8 (2022) 785. https://doi.org/10.3389/fsurg.2021.775194.

[339] G. Tzircotis, R.F. Thorne, C.M. Isacke, Chemotaxis towards hyaluronan is dependent on CD44 expression and modulated by cell type variation in CD44-hyaluronan binding, J. Cell Sci. 118 (2005) 5119–5128. https://doi.org/10.1242/JCS.02629.

[340] A. Vaidyanath, H.B. Mahmud, A.C. Khayrani, A. KoKo Oo, A. Seno, M. Asakura, T. Kasai, M. Seno, Hyaluronic Acid Mediated Enrichment of CD44 Expressing Glioblastoma Stem Cells in U251MG Xenograft Mouse Model, J. Stem Cell Res. Ther. 07 (2017). https://doi.org/10.4172/2157-7633.1000384.

[341] C. Liao, Q. Wang, J. An, J. Chen, X. Li, Q. Long, L. Xiao, X. Guan, J. Liu, CD44 Glycosylation as a Therapeutic Target in Oncology, Front. Oncol. 12 (2022). https://doi.org/10.3389/FONC.2022.883831.

[342] G. Domenici, I. Aurrekoetxea-Rodríguez, B.M. Simões, M. Rábano, S.Y. Lee, J.S. Millán, V. Comaills, E. Oliemuller, J.A. López-Ruiz, I. Zabalza, B.A. Howard, R.M. Kypta, M. d. M. Vivanco, A Sox2-Sox9 signalling axis maintains human breast luminal progenitor and breast cancer stem cells, Oncogene. 38 (2019) 3151–3169. https://doi.org/10.1038/S41388-018-0656-7.

[343] Z. Al Shareef, H. Kardooni, V. Murillo-Garzón, G. Domenici, E. Stylianakis, J.H. Steel, M. Rabano, I. Gorroño-Etxebarria, I. Zabalza, M.M. Vivanco, J. Waxman, R.M. Kypta, Protective effect of stromal Dickkopf-3 in prostate cancer: opposing roles for TGFBI and ECM-1, Oncogene. 37 (2018) 5305. https://doi.org/10.1038/S41388-018-0294-0.

[344] L. Huang, S. Xu, D. Hu, W. Lu, X. Xie, X. Cheng, IQGAP1 is involved in enhanced aggressive behavior of epithelial ovarian cancer stem cell-like cells during differentiation, Int. J. Gynecol. Cancer. 25 (2015) 559–565. https://doi.org/10.1097/IGC.0000000000000394.

[345] E.J. Kim, X. Jin, O.R. Kim, S.W. Ham, S.H. Park, H. Kim, Glioma stem cells and their non-stem differentiated glioma cells exhibit differences in mitochondrial structure and function, Oncol. Rep. 39 (2018) 411–416. https://doi.org/10.3892/or.2017.6075.

[346] D.W. Clark, K. Palle, Aldehyde dehydrogenases in cancer stem cells: potential as therapeutic targets, Ann. Transl. Med. 4 (2016). https://doi.org/10.21037/ATM.2016.11.82.

[347] A.T. Serra, M. Serra, A.C. Silva, T. Brckalo, A. Seshire, C. Brito, M. Wolf, P.M. Alves, Scalable culture strategies for the expansion of patient-derived cancer stem cell lines, Stem Cells Int. 2019 (2019). https://doi.org/10.1155/2019/8347595.

[348] C. Ginestier, M.H. Hur, E. Charafe-Jauffret, F. Monville, J. Dutcher, M. Brown, J. Jacquemier, P. Viens, C.G. Kleer, S. Liu, A. Schott, D. Hayes, D. Birnbaum, M.S. Wicha, G. Dontu, ALDH1 is a marker of normal and malignant human mammary stem cells and a predictor of poor clinical outcome, Cell Stem Cell. 1 (2007) 555. https://doi.org/10.1016/J.STEM.2007.08.014.

[349] E. Soehngen, A. Schaefer, J. Koeritzer, V. Huelsmeyer, C. Zimmer, F. Ringel, J. Gempt, J. Schlegel, Hypoxia upregulates aldehyde dehydrogenase isoform 1 (ALDH1) expression and induces functional stem cell characteristics in human glioblastoma cells, Brain Tumor Pathol. 31 (2014) 247–256. https://doi.org/10.1007/s10014-013-0170-0.

[350] I. Silva, M.F. Estrada, C. V. Pereira, A.B. da Silva, M.R. Bronze, P.M. Alves, C.M.M. Duarte, C. Brito, A.T. Serra, Polymethoxylated Flavones from Orange Peels Inhibit Cell Proliferation in a 3D Cell Model of Human Colorectal Cancer, Nutr. Cancer. 70 (2018) 257–266. https://doi.org/10.1080/01635581.2018.1412473.

[351] J. V. Joseph, I.A.M. Van Roosmalen, E. Busschers, T. Tomar, S. Conroy, E. Eggens-Meijer, N.P. Fajardo, M.M. Pore, V. Balasubramanyian, M. Wagemakers, S. Copray, W.F.A. Den Dunnen, F.A.E. Kruyt, Serum-Induced Differentiation of Glioblastoma Neurospheres Leads to Enhanced Migration/Invasion Capacity That Is Associated with Increased MMP9, PLoS One. 10 (2015). https://doi.org/10.1371/JOURNAL.PONE.0145393.

[352] G.L. Lin, S. Nagaraja, M.G. Filbin, M.L. Suvà, H. Vogel, M. Monje, Non-inflammatory tumor microenvironment of diffuse intrinsic pontine glioma, Acta Neuropathol. Commun. 6 (2018) 51. https://doi.org/10.1186/S40478-018-0553-X.

[353] K.H. Ho, P.H. Chen, C.M. Shih, Y.T. Lee, C.H. Cheng, A.J. Liu, C.C. Lee, K.C. Chen, miR-4286 is Involved in Connections Between IGF-1 and TGF-β Signaling for the Mesenchymal Transition and Invasion by Glioblastomas, Cell. Mol. Neurobiol. 42 (2022) 791–806. https://doi.org/10.1007/s10571-020-00977-1.

[354] C.C. Liu, C.L. Wu, M.X. Lin, C.I. Sze, P.W. Gean, Disulfiram sensitizes a therapeutic-resistant glioblastoma to the TGF-β receptor inhibitor, Int. J. Mol. Sci. 22 (2021) 10496. https://doi.org/10.3390/ijms221910496.

[355] B. Schmierer, C.S. Hill, TGFβ–SMAD signal transduction: molecular specificity and functional flexibility, Nat. Rev. Mol. Cell Biol. 2007 812. 8 (2007) 970–982. https://doi.org/10.1038/nrm2297.

[356] F. Ahmad, S. Ghosh, S. Sinha, S.D. Joshi, V.S. Mehta, E. Sen, TGF-β-induced hCG-β regulates redox homeostasis in glioma cells, Mol. Cell. Biochem. 399 (2015) 105–112. https://doi.org/10.1007/s11010-014-2237-6.

[357] T. Yan, Y. Tan, G. Deng, Z. Sun, B. Liu, Y. Wang, F. Yuan, Q. Sun, P. Hu, L. Gao, D. Tian, Q. Chen, TGF-β induces GBM mesenchymal transition through upregulation of CLDN4 and nuclear translocation to activate TNF-α/NF-κB signal pathway, Cell Death Dis. 13 (2022). https://doi.org/10.1038/S41419-022-04788-8.

[358] A.L. Chang, J. Miska, D.A. Wainwright, M. Dey, C. V Rivetta, D. Yu, D. Kanojia, K.C. Pituch, J. Qiao, P. Pytel, Y. Han, M. Wu, L. Zhang, C.M. Horbinski, A.U. Ahmed, M.S. Lesniak, CCL2 produced by the glioma microenvironment is essential for the recruitment of regulatory T cells and myeloid-derived suppressor cells HHS Public Access, Cancer Res. 76 (2016) 5671–5682. https://doi.org/10.1158/0008-5472.CAN-16-0144.

[359] D. Briukhovetska, J. Dörr, S. Endres, P. Libby, C.A. Dinarello, S. Kobold, Interleukins in cancer: from biology to therapy, Nat. Rev. Cancer. 21 (2021) 481–499. https://doi.org/10.1038/s41568-021-00363-z.

[360] A.S. Basheer, F. Abas, I. Othman, R. Naidu, Role of Inflammatory Mediators, Macrophages, and Neutrophils in Glioma Maintenance and Progression: Mechanistic Understanding and Potential Therapeutic Applications, Cancers 2021, Vol. 13, Page 4226. 13 (2021) 4226. https://doi.org/10.3390/CANCERS13164226.

[361] M.J. Gattas, I.G. Estecho, M.A. Lago Huvelle, A.E. Errasti, E.A. Carrera Silva, M. Simian, A heterotypic tridimensional model to study the interaction of macrophages and glioblastoma in vitro, Int. J. Mol. Sci. 22 (2021) 5105. https://doi.org/10.3390/IJMS22105105/S1.

[362] G. Lugo-Villarino, A. Troegeler, L. Balboa, C. Lastrucci, C. Duval, I. Mercier, A. Bénard, F.

Capilla, T. Al Saati, R. Poincloux, I. Kondova, F.A.W. Verreck, C. Cougoule, I. Maridonneau-Parini, M. del C. Sasiain, O. Neyrolles, The C-type lectin receptor DC-SIGN has an anti-inflammatory role in Human M(IL-4) macrophages in response to Mycobacterium tuberculosis, Front. Immunol. 9 (2018) 1123. https://doi.org/10.3389/fimmu.2018.01123.

[363] F. Zhang, H. Wang, X. Wang, G. Jiang, H. Liu, G. Zhang, H. Wang, R. Fang, X. Bu, S. Cai, J. Du, TGF-β induces M2-like macrophage polarization via SNAIL-mediated suppression of a pro-inflammatory phenotype, Oncotarget. 7 (2016) 52294. https://doi.org/10.18632/ONCOTARGET.10561.

[364] D. Gong, W. Shi, S. ju Yi, H. Chen, J. Groffen, N. Heisterkamp, TGFβ signaling plays a critical role in promoting alternative macrophage activation, BMC Immunol. 13 (2012) 1–10. https://doi.org/10.1186/1471-2172-13-31.

[365] I.B. Hovens, C. Nyakas, R.G. Schoemaker, A novel method for evaluating microglial activation using ionized calcium-binding adaptor protein-1 staining: cell body to cell size ratio, Neuroimmunol. Neuroinflammation. 1 (2014) 82–88. https://doi.org/10.4103/2347-8659.139719.

[366] S. Tanaka, M. Ohgidani, N. Hata, S. Inamine, N. Sagata, N. Shirouzu, N. Mukae, S.O. Suzuki, H. Hamasaki, R. Hatae, Y. Sangatsuda, Y. Fujioka, K. Takigawa, Y. Funakoshi, T. Iwaki, M. Hosoi, K. Iihara, M. Mizoguchi, T.A. Kato, CD206 Expression in Induced Microglia-Like Cells From Peripheral Blood as a Surrogate Biomarker for the Specific Immune Microenvironment of Neurosurgical Diseases Including Glioma, Front. Immunol. 12 (2021) 24–35. https://doi.org/10.3389/fimmu.2021.670131.

[367] I.E. Papageorgiou, A. Lewen, L. V. Galow, T. Cesetti, J. Scheffel, T. Regen, U.K. Hanisch, O. Kann, TLR4-activated microglia require IFN-γ to induce severe neuronal dysfunction and death in situ, Proc. Natl. Acad. Sci. U. S. A. 113 (2016) 212–217. https://doi.org/10.1073/pnas.1513853113.

[368] D. Giulian, Ameboid microglia as effectors of inflammation in the central nervous system, J. Neurosci. Res. 18 (1987) 155–171. https://doi.org/10.1002/JNR.490180123.

Supplementary information

Microglia differentiation from hiPSC

Hematopoietic differentiation

Microglia differentiation from hiPSC was performed by Catarina Gomes, PhD student from the Lab. The resulting biological material (cells, RNA) was then used as part of this thesis mostly for microglia sources comparison purposes. For microglia differentiation, hiPSC IMR90-4 cells were first differentiated into hematopoietic progenitor cells (HPCs) using STEMdiff™ hematopoietic kit (Stem Cell Technologies, #05310). The differentiation started by coating a 12-well plate with 0.08 mg/mL of Corning® Matrigel® (Corning®, #CLS356238) diluted in cold DMEM-F12 (Gibco, #11320033), filtered through a 40 µm cell strainer (Falcon, #352340), and incubated at 37°C for 1 h. Afterwards, cells were detached with versene solution (Gibco, #15040066) resulting in small aggregates. These aggregates were suspended with DMEM-F12 in a 1:9 ratio and in triplicates. Subsequently, 60-152 colonies were plated in the 12-well plates, coated with Matrigel®, 1 mL of mTeSR™1 (Stem Cell Technologies, #85851), incubated at 37°C and 5% CO_2 for 24 h. The following day, conditioned medium was removed, and medium A provided by the Kit was added. Differentiation into hematopoietic progenitor last 12 days in total. Differentiation into HPC was assessed by CD43 analysis and by flow cytometry.

Microglia differentiation

After achieving HPC differentiation, STEMdiff™ microglia differentiation kit (Stem Cell Technologies, #100-0019) and STEMdiff™ microglia maturation kit (Stem Cell Technologies, #100-0020) was used and the entire process took additional 28 days to yield mature microglia-like cells. First, cells in suspension were washed with DPBS (-/-), and 0.5 mL ACCUTASE™ (Stem Cell Technologies, #07920) was added to each well for 20 min at 37°C, to detach adherent cells. Afterwards, single-cell suspension was collected, and cells were centrifuged at 300 *x g* for 5 min at RT using a 5810R Centrifuge equipped with an A-4-81 rotor (Eppendorf). Later, cells were suspended with STEMdiff™ microglia differentiation medium (Stem Cell Technologies, #100-0020).

Then, cells were counted with trypan blue solution 0,1% (v/v) (Gibco, #15250-061) in a Fuchs-Rosenthal counting chamber (Karl Hetch #4049712) and inoculated in Matrigel®-coated 6-well plate with a cell density of 1.1 x 10^4 - 2.2 x 10^4 cell/cm^2 and incubated at 37°C. Subsequent steps followed the supplier protocol.

Microglia maturation

On day 24, microglia maturation preceded using the STEMdiff™ microglia maturation kit. Cells were centrifuged at 300 *x g* for 5 min, resuspended at a lower volume, and counted with trypan blue solution 0,1% (v/v) in a Fuchs-Rosenthal counting chamber. Cells were seeded at 1 x 10^6 cells per coated 6-well plate containing 1 mL fresh STEMdiff™ microglia maturation medium. Every other day, half of the starting volume of STEMdiff™ microglia maturation medium was added to the culture until day 40.

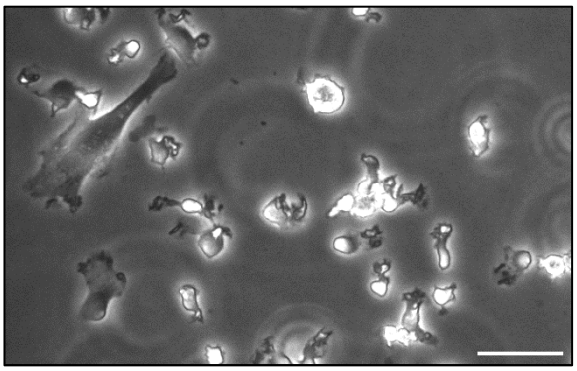

Figure S.1 - Phase contrast images of different microglia-like cells derived from human induced pluripotent stem cells. Representative image of N=3 independent experiments. Scale bar: 50 µm

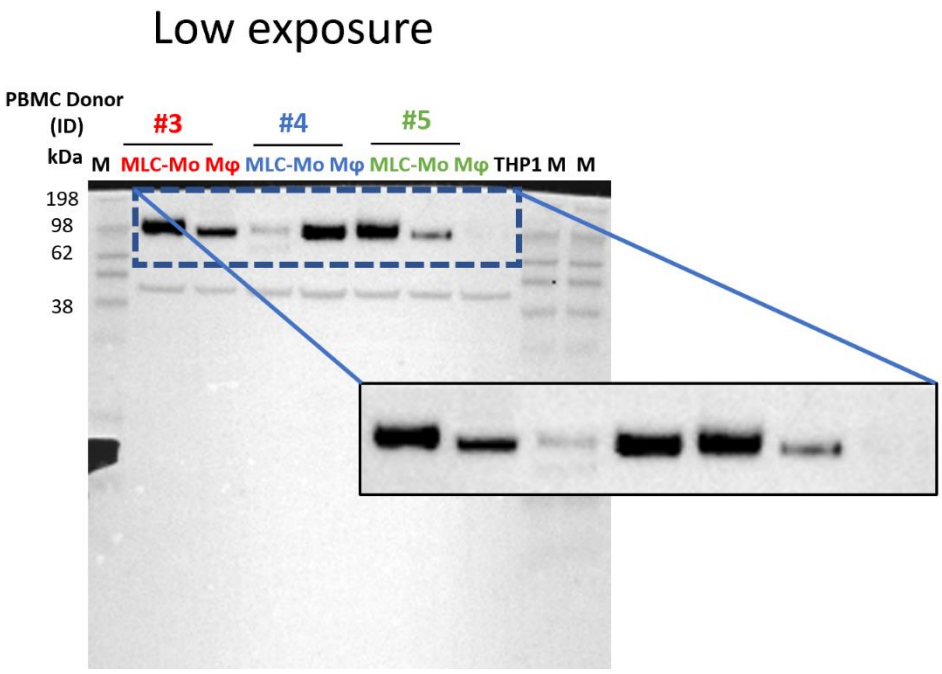

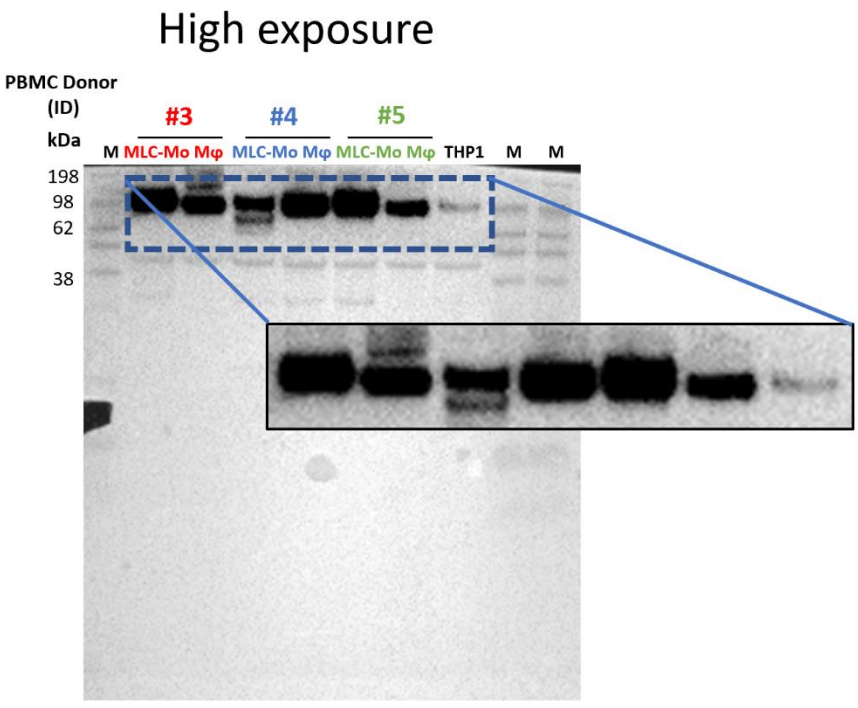

Figure S.2 - Uncropped scan of CD68 western blot of monocyte derived microglia-like cells (MLC-Mo) and macrophages (Mφ) from peripheral blood mononuclear cells (PBMC) and THP1 cell line. Ladder (M) displayed in kilodalton (kDA) units. Primary antibody: anti-cd68 from cell signalling (#D4B9C), IgG from Rabbit (Monoclonal) was used at 1:1000 dilution and incubated overnight in agitation at 4ºC. Secondary antibody: ECL Anti-Rabbit HRP-Link from GE Healthcare, IgG from Donkey was used at 1:5000 dilution. Western blot membrane was detected using Amersham ECL Select Western Blotting Detection buffer an iBright™ FL1500 Imaging System from Invitrogen.

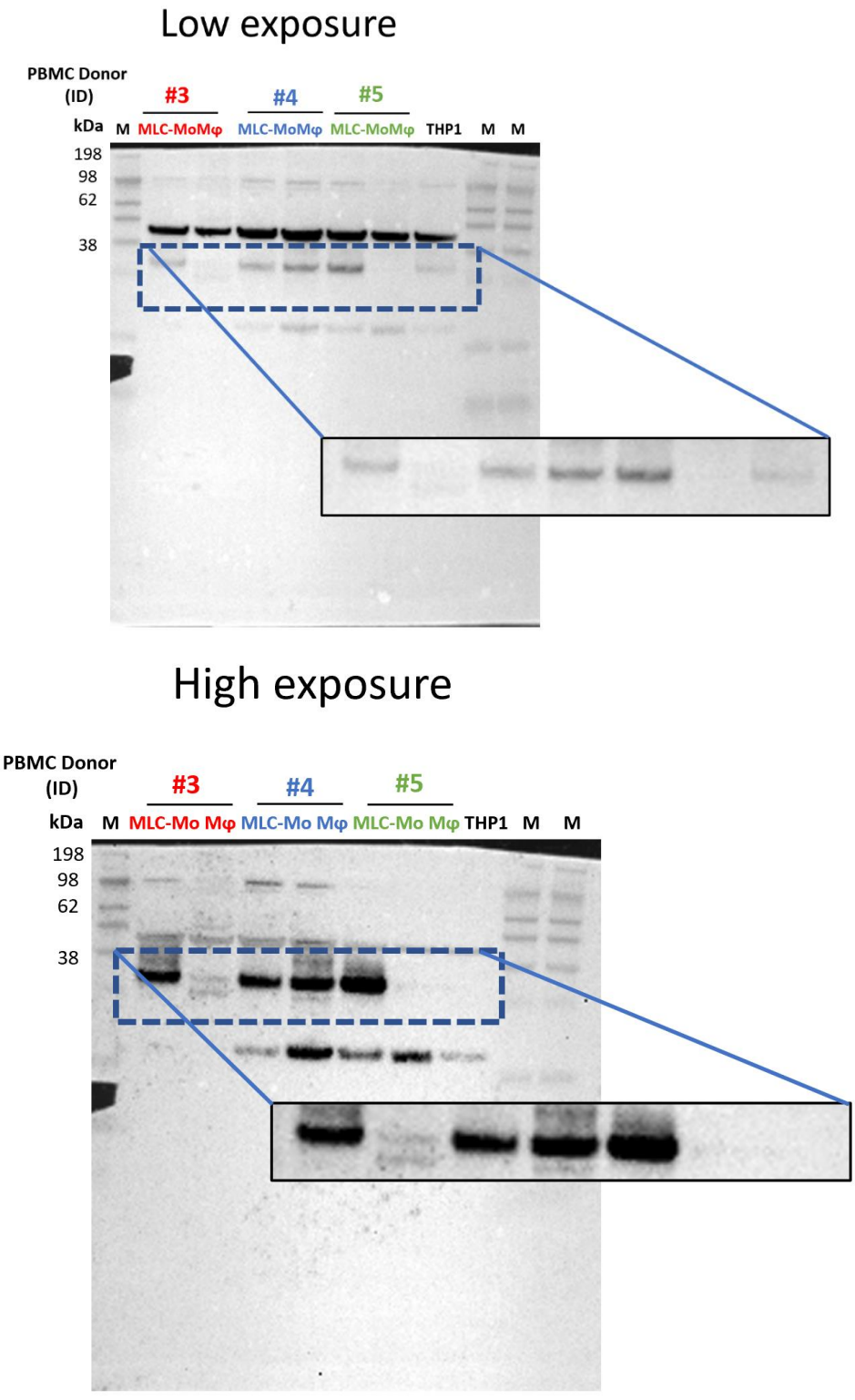

Figure S.3 - Uncropped scan of TREM2 western blot of monocyte derived microglia-like cells (MLC-Mo) and macrophages (Mφ) from peripheral blood mononuclear cells (PBMC) and THP1 cell line. Ladder (M) displayed in kilodalton (kDA) units. Primary antibody: anti-TREM2 from R&D Systems (#AF1828), IgG from Goat (Polyclonal) was used at 1:500 dilution and incubated overnight in agitation at 4ºC. Secondary antibody: ECL Anti-Goat HRP-Link from GE Invitrogen, IgG from Rabbit was used at 1:5000 dilution. Western blot membrane was detected using Amersham ECL Select Western Blotting Detection buffer an iBright™ FL1500 Imaging System from Invitrogen.

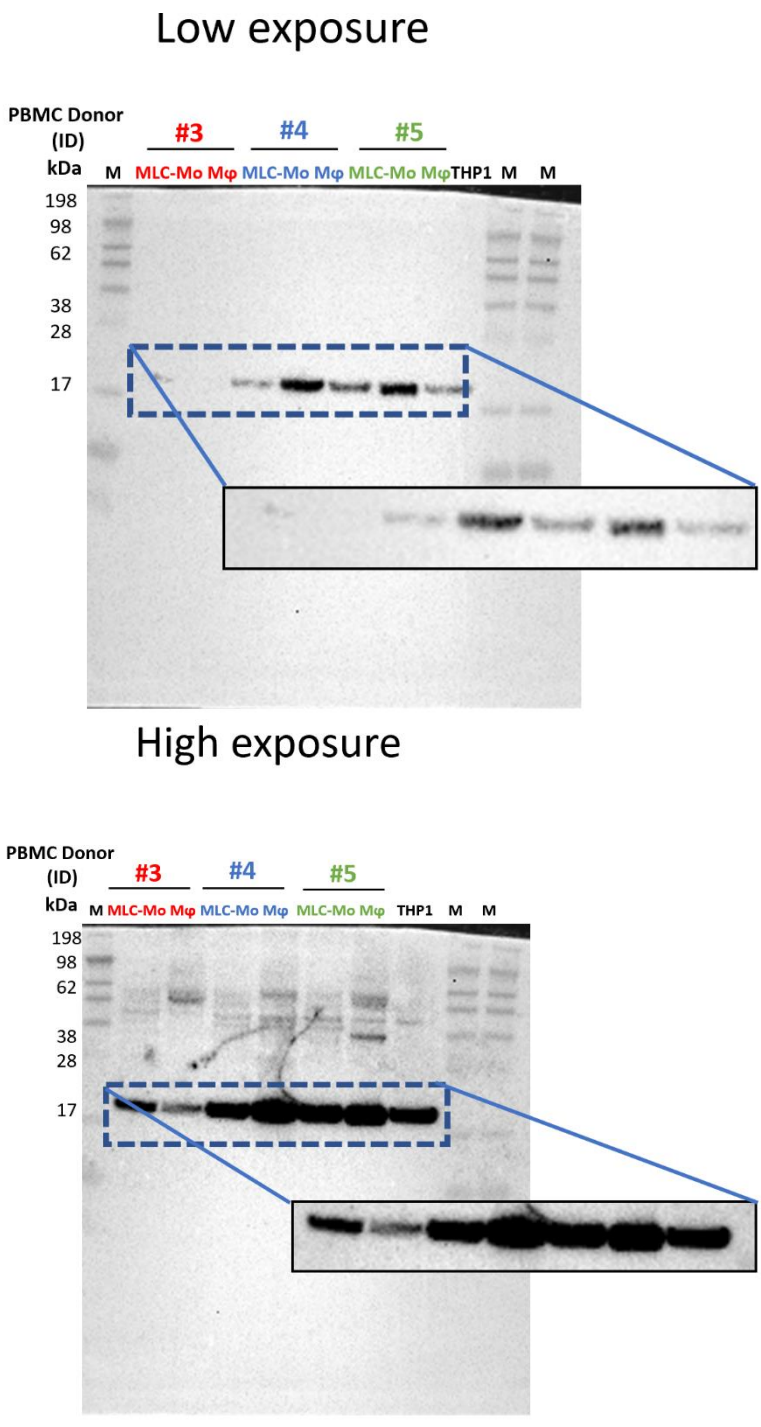

Figure S.4 - Uncropped scan of IBA1 western blot of monocyte derived microglia-like cells (MLC-Mo) and macrophages (Mφ) from peripheral blood mononuclear cells (PBMC) and THP1 cell line. Ladder (M) displayed in kilodalton (kDA) units. Primary antibody: anti-iba1 from cell signalling (#17198), IgG from Rabbit (Monoclonal) was used at 1:1000 dilution and incubated overnight in agitation at 4ºC. Secondary antibody: ECL Anti-Rabbit HRP-Link from GE Healthcare, IgG from Donkey was used at 1:5000 dilution. Western blot membrane was detected using Amersham ECL Select Western Blotting Detection buffer an iBright™ FL1500 Imaging System from Invitrogen.

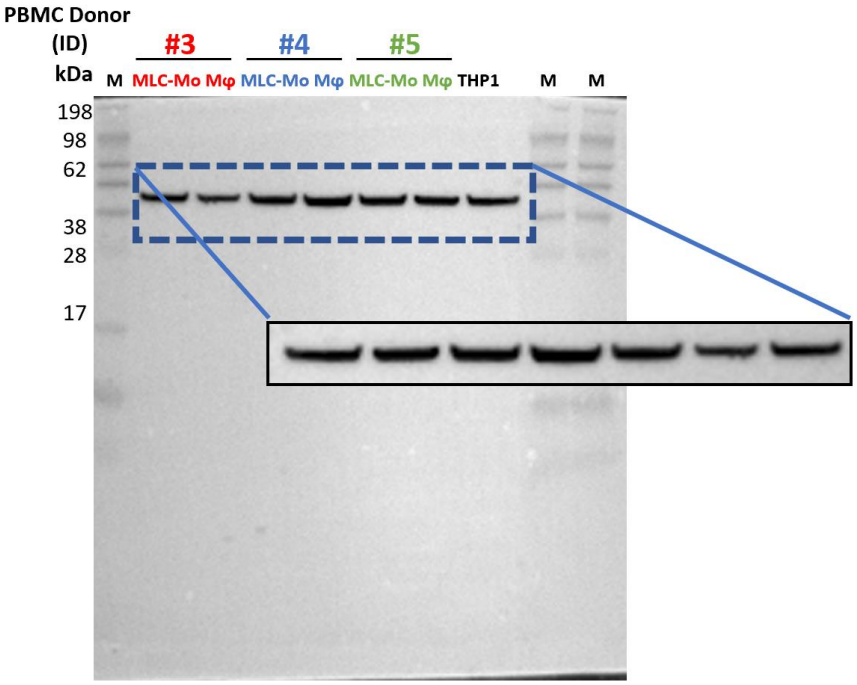

Figure S.5 - Uncropped scan of β-actin western blot membrane of monocyte derived microglia-like cells (MLC-Mo) and macrophages (Mφ) from peripheral blood mononuclear cells (PBMC) and THP1 cell line. Ladder (M) displayed in kilodalton (kDA) units**.** Primary antibody: anti-β-actin from Sigma Aldrich (#A5441), IgG from Mouse (Monoclonal) was used at 1:5000 dilution and incubated overnight in agitation at 4ºC. Secondary antibody: ECL Anti-Mouse HRP-Link from GE Healthcare, IgG from Sheep was used at 1:5000 dilution. Western blot membrane was detected using Amersham ECL Select Western Blotting Detection buffer an iBright™ FL1500 Imaging System from Invitrogen.

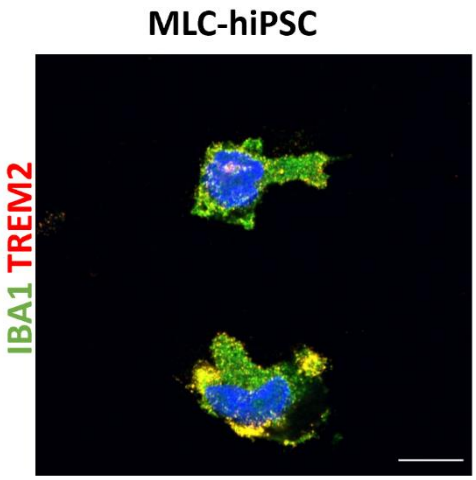

Figure S.6 - Microglia protein analysis by immunofluorescence microscopy in microglia-like cells derived from human induced pluripotent stem cells (MLC-hiPSC). A – IBA1 labelled in green (Alexa fluor ® 488*)* in TREM2 labelled in red (AlexaFluor® 594) in MLC-hiPSC. Cells were counterstained with 4',6-diamidino-2-phenylindole (DAPI, blue) for nuclei identification. Representative image from N=3 of independent Scale bar: 10 µm. Microglia markers: TREM2 – Triggering receptor expressed on myeloid cells 2; IBA1 *(AIF1)* – Allograft inflammatory factor 1.

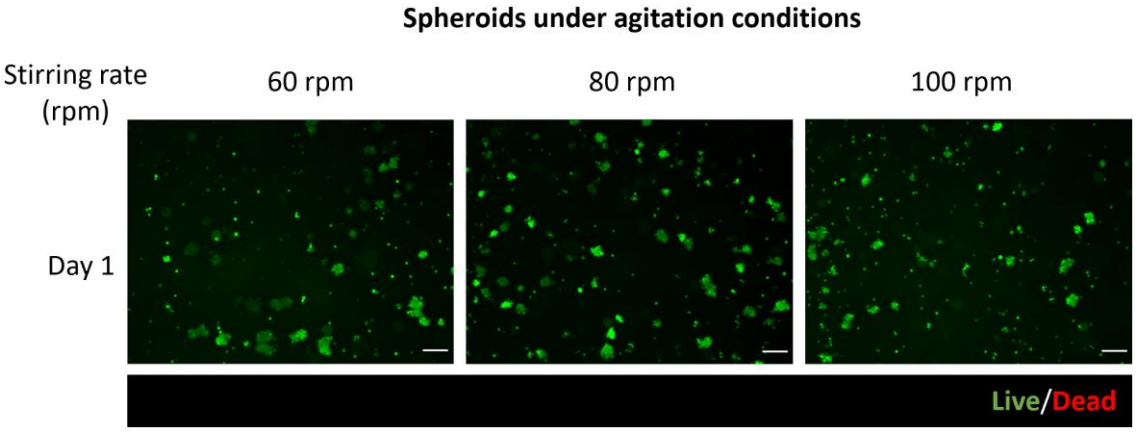

Figure S.7 –Cell viability of glioblastoma (GBM) spheroids analysed during and at the end of the culture, assessed by fluorescence microscopy. FDA, shown in green, shows live cells, while ToPro™-3 (red) shows dead cells. Representative images are shown N=3 for neurospheres and spheroids obtained under a stirring rate of 80 rotations per minute (rpm); N=2 spheroids under a stirring rate of 80 rpm, and N=1 spheroids under a stirring rate of 60 rpm Scale bar: 50 µm.

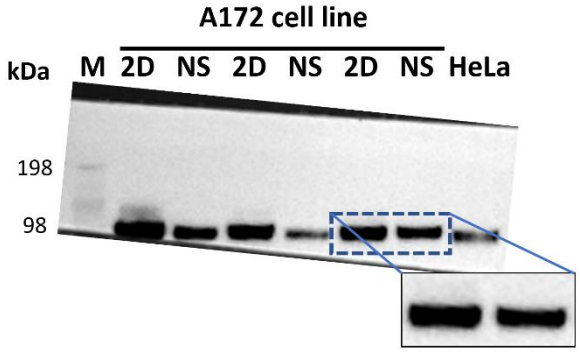

Figure S.8 - Uncropped scan of CD44 western blot membrane of A172 2D cell culture (2D), neurospheres (NS) and HeLa cell line. Ladder (M) displayed in kilodalton (kDA) units**.** Primary antibody: anti-β-actin from Cell Signalling (#8E2), IgG from Rabbit (Monoclonal) was used at 1:1000 dilution and incubated overnight in agitation at 4ºC. Secondary antibody: ECL Anti-Rabbit HRP-Link from GE Healthcare, IgG from Donkey was used at 1:5000 dilution. Western blot membrane was detected using Amersham ECL Select Western Blotting Detection buffer an iBright™ FL1500 Imaging System from Invitrogen.

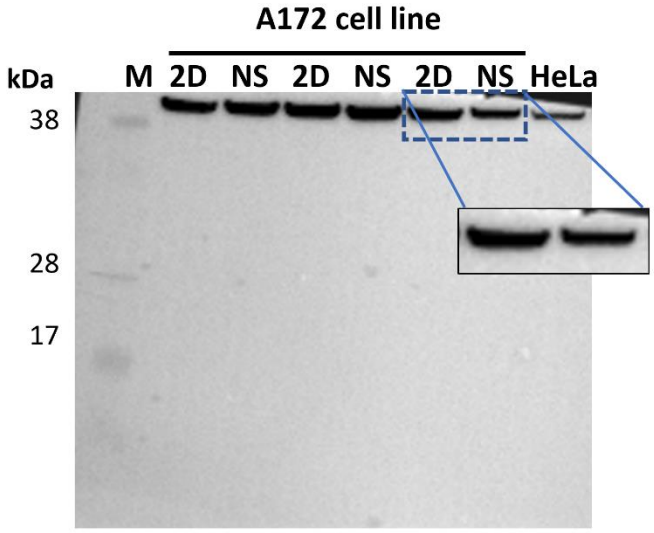

Figure S.9 - Uncropped scan of β-actin western blot membrane of A172 2D cell culture (2D), neurospheres (NS) and HeLa cell line. Primary antibody: anti-β-actin from Sigma Aldrich (#A5441), IgG from Mouse (Monoclonal) was used at 1:5000 dilution and incubated overnight in agitation at 4ºC. Secondary antibody: ECL Anti-Mouse HRP-Link from GE Healthcare, IgG from Sheep was used at 1:5000 dilution. Western blot membrane was detected using Amersham ECL Select Western Blotting Detection buffer an iBright™ FL1500 Imaging System from Invitrogen.

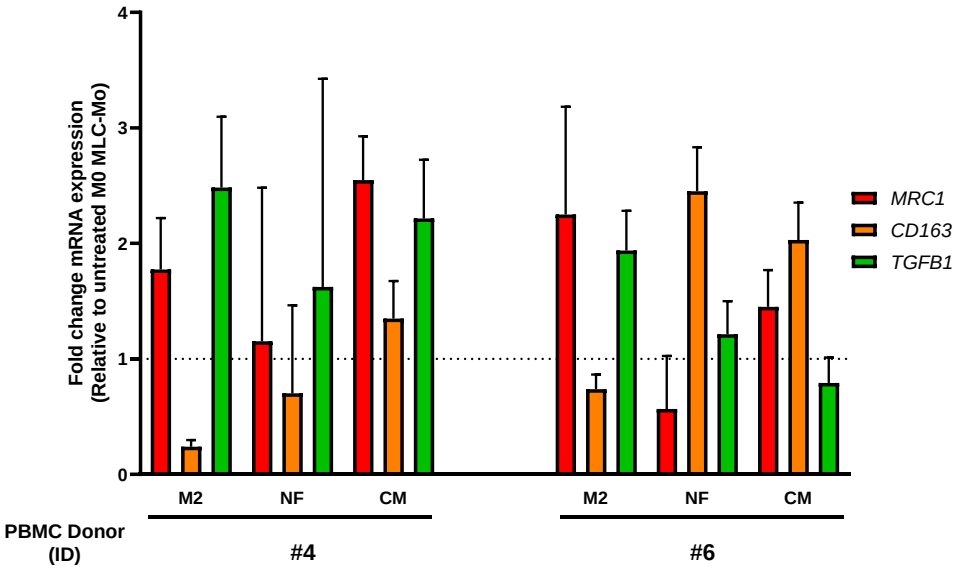

Figure S.10 - Anti-inflammatory marker expression in microglia-like cells derived from monocytes (MLC-Mo) exposed to neurosphere medium (NF) and Conditioned Medium (CM), assessed by RT-qPCR. Fold change of in gene expression of MLC-Mo from 2 different peripheral blood mononuclear cell (PBMC) donors (#4 and #5) exposed to NF and CM, determined by the $2^{-\Delta\Delta Ct}$ method. Values were normalized to the expression of the housekeeping genes *RPL22* and *36B4* represented as fold change relative to control M0 MLC-Mo mRNA expression, set as 1 (dashed line). Error bars are shown as a mean of SD of technical triplicates. Representative plot of N=2 independent experiments; Anti-inflammatory markers: *MRC1* (CD206) – Macrophage mannose receptor 1; *CD163* – Hemoglobin Scavenger Receptor; *TGFB1* – Transforming growth factor beta 1.